

# Sheffield Hallam University

*Bonding mechanisms in the application of thermal barrier coatings to turbine blades.*

HOQUE, Abdul.

Available from the Sheffield Hallam University Research Archive (SHURA) at:

<http://shura.shu.ac.uk/19825/>

## A Sheffield Hallam University thesis

This thesis is protected by copyright which belongs to the author.

The content must not be changed in any way or sold commercially in any format or medium without the formal permission of the author.

When referring to this work, full bibliographic details including the author, title, awarding institution and date of the thesis must be given.

Please visit <http://shura.shu.ac.uk/19825/> and <http://shura.shu.ac.uk/information.html> for further details about copyright and re-use permissions.

CITY OF SHEFFIELD  
SHEFFIELD S1 1WD

101 755 603 2



**REFERENCE**

ProQuest Number: 10697131

All rights reserved

INFORMATION TO ALL USERS

The quality of this reproduction is dependent upon the quality of the copy submitted.

In the unlikely event that the author did not send a complete manuscript and there are missing pages, these will be noted. Also, if material had to be removed, a note will indicate the deletion.



ProQuest 10697131

Published by ProQuest LLC (2017). Copyright of the Dissertation is held by the Author.

All rights reserved.

This work is protected against unauthorized copying under Title 17, United States Code  
Microform Edition © ProQuest LLC.

ProQuest LLC.  
789 East Eisenhower Parkway  
P.O. Box 1346  
Ann Arbor, MI 48106 – 1346

# **Bonding Mechanisms in the Application of Thermal Barrier Coatings to Turbine Blades**

**Abdul Hoque**

**A thesis submitted in partial fulfilment of the  
requirements of Sheffield Hallam University for the  
degree of Doctor of Philosophy**

**January 2004**

**Collaborating Organisation:  
Rolls-Royce plc**





## Abstract

Thermal barrier coatings (TBC's) are used to protect gas turbine blades from environmental degradation as well as to increase thermodynamic efficiency. Most TBC systems consist of a ceramic thermal barrier coating such as partially stabilized zirconia adhering to an oxidation resistant bond coat, which in turn is bonded to the turbine blade. This is required since partially stabilised zirconia will not readily bond to superalloys. However, the TBC can fail in service either by bond coat oxidation or thermal expansion mismatch between the bond coat and the TBC.

A systematic literature survey has shown that the superalloy substrate material, type of bond coat selected, with the coating application techniques i.e. thermal spray or Electron Beam PVD (EBPVD) plays a fundamental role in determining the failure mechanisms involved.

This program of work is concerned with the development of coatings with enhanced temperature capabilities for turbine blade applications by understanding the fundamental mechanisms responsible for adhesion between the nickel based turbine blade and zirconia based TBC. An understanding of the bonding mechanisms will allow the design of advanced coating systems with increased operating temperatures.

This program of work introduces the Glow Discharge Optical Emission Spectroscopy (GDOES) technique, an atomic emission technique used for both bulk and depth profile analysis, which had not previously been applied to TBC's, and SEM and TEM in order to enhance understanding of failure modes in TBC systems and adhesion process.

The results obtained from the studies indicate that the GDOES technique can be applied to depth profile bond coats and exposed TBC systems both qualitatively and semi-quantitatively. GDOES has been able to detect elements such as silicon and sodium that are in the ppm levels which are difficult / impossible to detect using EDX systems, and are very important in coating developments. In addition, as a preliminary guide GDOES has shown Ti diffusion from the superalloy substrate into the bond coat to be detrimental towards coating adhesion on most of the systems studied.

The results of SEM and cross-sectional TEM on selected bond coat systems has shown the low cost Pt bond coat microstructure system to consist of TBC,  $\text{Al}_2\text{O}_3$  bond coat and CMSX-4 superalloy substrate in all cases. The intermediate layer between the TBC and bond coat consists of  $\text{Al}_2\text{O}_3$  which has been identified as responsible for maintaining the adhesion. Also identified is evidence of Ti segregation at the  $\text{Al}_2\text{O}_3$  / bond coat interface, known to lead to decohesion in coatings. Failure in the low cost Pt bond coat system has been identified as the decohesion between the interfacial layer of  $\text{Al}_2\text{O}_3$  and the bond coat.

The program of studies has enabled failure mechanisms and factors affecting bonding to be identified in low cost Pt bond coat systems, so that in future better coating systems with enhanced properties can be designed. This should also ensure that improved reliability in engines and increased service life of turbine blades be achieved.

## Advanced Studies

As part of my research studies I have presented a number of both formal and informal research seminars at Sheffield Hallam University, Materials Research Institute and Rolls-Royce plc. In addition, I have presented my work at conferences and attended the following workshops:

- High Temperature Engineering Conference: Engineering the Surface, Sept 1997, Edinburgh Conference Centre, UK.
- The Institute of Physics Annual Congress on surface Engineering: Fundamental to Applications, March 1997, University of Leeds.
- The Third Sheffield ABS Day Congress, May 1997, Sheffield Hallam University.
- Microscopy of Internal Interfaces: Determination of Nanochemistry Poster Presentation , Feb 1998, The Institute of physics, London.
- Applied Surface Science, 14<sup>th</sup> International Vacuum Congress ( IVC –14) And 10<sup>th</sup> International Conference on Solid Surfaces, Sept 1998, The International Convention Centre, Birmingham, UK.
- Quantitative Microscopy of High Temperature Materials, Nov 1999, Sheffield Hallam University.

## Publications

The following papers and posters included have been published as a result of the studies on this thesis:

- Hoque A, Higgins J; Rickerby D; Cawley J; Ives M; 'The application of glow discharge optical emission spectroscopy to the study of thermal barrier and environmental coatings', Institute of Materials, High Temperature Surface Engineering (UK), pp. 129-140, 2000 ( appendix 1 )
- Hoque A, Cawley J, Bramhall MD, Rickerby D, Higgins J; ' Characterisation of Interfaces on Thermal Barrier Coatings', Microscopy of Internal Interfaces: Determination of Nanochemistry Poster Presentation , Feb 1998, The Institute of Physics, London ( appendix 2 )
- Hoque A, Cawley J, Bramhall MD, Rickerby D, Higgins J ; 'GDOES Analysis of Thermal Barrier Coatings for Application in Gas Turbine Blades', Applied Surface Science, 14<sup>th</sup> International Vacuum Congress ( IVC -14) And 10<sup>th</sup> International Conference on Solid Surfaces, Abstract Presentation, Sept 1998, The International Convention Centre, Birmingham, UK ( appendix 3 )
- Hoque A, Cawley J, Bramhall MD, Rickerby D; ' Electron microscopy and depth profile analysis of thermal barrier coatings for turbine blade applications', Quantitative Microscopy of High Temperature Materials, Abstract Presentation, Nov 1999, Sheffield Hallam University (appendix 4 )

## **Acknowledgements**

The author is grateful to the following people and collaborating organisations for their helpful discussion and advice, especially to the supervisors.

- Dr J. Cawley Materials Research Institute and Professor M.D.Bramhall,  
School of Engineering, Sheffield Hallam University
- Dr D Rickerby, Dr R Jones, Mr J Higgins, Rolls-Royce Plc
- Dr M Ives, Dr Q Lou, Mr P Slingsby and the research students of Materials  
Research Institute, Sheffield Hallam University
- Research Student Bursary of the Materials Research Institute, Sheffield  
Hallam University

Finally, I would like to thank my mother, father, brother and sisters for their constant encouragement and support during the research period.

# Contents

	<u>Page No.</u>
<b>Chapter 1 Introduction</b>	1
1.1 The need for Thermal Barrier Coatings	2
1.2 Temperature / Time Targets	2
1.3 Bondcoat Systems	2
1.4 Degradation Mechanisms	4
1.5 Proposed Programme of Work	6
<b>Chapter 2 Literature Review</b>	8
2.1 Substrate Materials	8
2.1.1 Superalloy Metallurgy	8
2.1.2 Superalloy Systems	10
2.1.3 The Role of individual Constituents in Superalloys	11
2.1.4 Processing ( DS, SC, CMSX-4, RR3000 Alloys)	12
2.2 Coating Systems	16
2.2.1 Aluminide Bondcoats	17
2.2.2 Overlay Bondcoats	21
2.2.3 Low Cost Bondcoats	25
2.2.4 Thermal Barrier Coatings	26
2.3 Role of Various Elements in Coating Development	30
2.3.1 Role of Platinum	30
2.3.2 Role of the Yttrium	31
2.3.3 Role of Hafnium	34
2.3.4 Summary of Hf, Y Roles	35
2.3.5 Role of Rhenium	36
2.4 Effect of Residual and Contaminants on Thermal Barrier Coatings	38
2.4.1 Effect of Sulphur	38
2.4.2 Effect of Silicon and its Oxides	40
2.4.3 Effect of Sodium and Phosphorus	43
2.5 Degradation of Thermal Barrier Coatings	44
2.5.1 Interdiffusion	44
2.5.2 Bondcoat Oxidation	47
2.5.3 Thermal Expansion Mismatch	50
2.6 Bonding Mechanisms	53

<b>Chapter 3 Experimental Development</b>	55
3.1 Coating Systems	55
3.1.1 LCBC with Additions to Substrate	56
3.1.2 LCBC with Additions to Coating	57
3.1.3 Process Parameters / Compositions	58
3.2 Analytical Characterisation	59
3.2.1 Technique Descriptions ( XRD, XRF, SEM, TEM )	59
3.2.2 TEM Cross-section – Ion Beam Thinning Process Development	62
3.3 GDOES Depth Profile Analysis to Investigate Bondcoats	66
3.3.1 General Overview and Analytical Requirements	66
<b>Chapter 4 Results: GDOES Studies</b>	68
4.1 Development of Quantitative GDOES Depth Profile Analysis to Investigate Bondcoats and TBCs	68
4.1.1 GDOES Quantification Process Route	68
4.1.2 Standards and Pre-compositional Analysis	68
4.1.3 General GDOES Analysis of Bondcoats and TBCs	69
4.2. GDOES: Investigation of the Low Cost Bondcoat System with Additions to Substrate / Coating	72
4.2.1 Standard LCBC System with Platinum – Substrate Additions	72
4.2.2 Yttrium and Hafnium- Coating Additions	76
4.3 GDOES: Investigation of the effects of residual and contaminants in LCBC systems	78
4.3.1 Effect of Silicon	78
4.3.2 Effect of Sodium	80
4.3.3 Effect of Phosphorus	81
<b>Chapter 5 Results: Thermal Cycling</b>	82
5.1 Thermal Cyclic Test Data	82
<b>Chapter 6 Results : Thermal Ageing Studies of the LCBC System</b>	85
6.1 GDOES Studies	85
6.2 SEM and Energy Dispersive X-Ray Analysis (EDX)	89
6.3 TEM / Interfacial Analysis	93

<b>Chapter 7 Discussion</b>	97
7.1 Quantitative GDOES Analysis Technique Development for Investigation of Substrate and Bondcoat Compositions	97
7.2 Factors Affecting Bonding Mechanisms	104
7.2.1 Effect of Additions to Substrate ( LCBC formation )	106
7.2.2 Effect of Additions to Coating	110
7.2.3 Effect of Silicon and Contaminants on LCBC Systems	113
7.2.4 Effect of Ageing Treatment	115
7.3 Proposed Failure Mechanisms within LCBC System	120
7.4 Proposed Improvements	123
<b>Chapter 8 Conclusion</b>	125
<b>Chapter 9 Future Work</b>	130
References	
<b>Appendix</b>	

<b><u>Figure List and Tables</u></b>	<b><u>Page No.</u></b>
Figure 1 A typical EBPVD coated turbine blade	132
Figure 2.2.4 a Plasma Spayed ZrO <sub>2</sub> Coating	133
Figure 2.2.4 b EBPVD ZrO <sub>2</sub> Coating	133
Figure 2.2.4 c Schematic illustration of a plasma spray deposition technique	134
Figure 2.2.4 d Schematic illustration of the EBPVD technique	134
Figure 2.3.2 : (a) chemical composition of the matrix phase; (b) chemical composition of the $\beta$ - phase	135
Figure 2.3.3 : (a) High temperature/ low activity pack aluminide coated specimens tested in 1180°C oxide;(b) Low temperature / high activity pack aluminide coated specimens tested in 1180°C cyclic oxidation	136
Figure 2.5.2 (a) Initiation of spalling of TBC	137
Figure 2.5.2 (b) The four propagation modes of spalling in TBC's	137
Figure 2.5.3 Thermal expansion of ZrO <sub>2</sub> .8wt%Y <sub>2</sub> O <sub>3</sub> and IN 738 Vs Temperature	138
Figure 3.1(a) Composition of CMSX-4	
Figure 3.1 (b) BSI of LCBC microstructure: (i) asprocessed condition; (ii) failed condition	138
Table 3.1.3 Enhanced Low Cost Bond Coats	
Figure 3.2.1 (a) X-ray diffraction pattern derived from the surface of low-cost Pt bond coat on alloy CMSX-4 after removal of the top coat ( as- received condition)	139
Figure 3.2.1 (b) X-ray diffraction pattern derived from the surface of low-cost Pt bond coat on alloy CMSX-4 exposed by failure (288 hours of exposure at 1150°C)	139
Figure 3.2.2 (a) The variation in ion milling rate and implantation depth as function of incident angle	140
Figure 3.2.2 (b) Specimen preparation for TEM analysis	140
Figure 3.2.2 (c) Clamp type and glue on type specimen holders	140

Figure 3.3.1: (a) Glow discharge sputtering process; (b) Glow discharge lamp (c) Light dispersion and detection; (d) Depth ranges for various surface analytical methods	141-142
Figure 3.3.1 (e) Analysis parameters	143
Figure 4.1.1 Quantitative programme set-up procedure	144
Table 4.1.2 Calibration Overview	145
Figure 4.1.3 (a) Time - Intensity trace on CMSX-4 showing Ni,Al,Co profiles	146
Figure 4.1.3 (b) Time - Intensity trace on CMSX-4 showing Co,Ti,Hf,W profiles	147
Figure 4.1.3 (c) Depth -Concentration on CMSX-4 showing Co,Ni,Al profiles	148
Figure 4.1.3(d) Depth -Concentration on CMSX-4 showing Co,Hf,Ti,W profiles	149
Figure 4.1.3(e) SEM micrograph of craters (i) at 60 sec (ii) at 1000 sec	150
Figure 4.1.3(f):(i) Laser profile of crater at 60 sec; (ii)Laser profile of crater at 1000 sec	151
Figure 4.1.3(g) Comparison of substrate/coating standards, XRF measured Vs GDOES measurements	152
Figure 4.1.3(h) Comparison of CMSX-4 substrate using XRF,EPMA and GDOES Techniques	153
Figure 4.1.3(i) TBC trace	154
Figure 4.1.3(j) Typical SEM image of TBC	154
Figure 4.1.3(k) EPMA analysis of TBC system	155
Figure 4.2.1 a,b,c,d,e,f,g,h,i: GDOES Pt depth profiles for several selected Pt plated samples studied on a CMSX-4 substrate under different plating conditions and also in the heat treated and cyclically failed conditions as supplied from Rolls Royce	156 - 164
Figure 4.2.2 a,b,c,d,e,f,g,h,i,j,k,l,m,n,o,p : GDOES qualitative plots of Y and Hf additions to coating ( i.e. signal intensity Vs time of sputtering ). All plots are between 400 and 800 seconds of sputtering time to provide sufficient information to study the chemical bonding process	165 - 180
Figure 4.3.1 (a) GDOES depth profile of as processed LCBC showing Si profile	181

Figure 4.3.1 (b) GDOES depth profile of failed LCBC showing Si profile	181
Figure 4.3.1 (c) GDOES depth profile of as processed LCBC showing Si profile ( Pink gritted -heat treated at CUK )	182
Figure 4.3.1 (d) GDOES depth profile of as processed LCBC showing Si profile ( Brown gritted -heat treated at CUK )	182
Figure 4.3.1 (e) GDOES depth profile of CMSX-4 showing no presence of Si	183
Figure 4.3.2 (a) GDOES depth profile of Pt plated CMSX-4 showing presence of sodium	184
Figure 4.3.2 (b) GDOES depth profile of standard LCBC and observed sodium peak	185
Figure 4.3.2 (c) GDOES depth profile of standard LCBC showing sodium in as plated and when heat treated(diffused)	186
Table 4.3.2 XRF analysis as plated LCBC sample showing presence of sodium	187
Figure 4.3.3 (a) GDOES depth profile of Pt standard showing P interference	188
Figure 4.3.3 (b) GDOES depth profile of Pt deposited on CMSX-4 substrate by PVD process showing P interference	189
Figure 4.3.3 (c) GDOES depth profile of LCBC for Pt plating (electrolytic) showing P interference	190
Table 5.0 Enhanced low cost bond coats- average cycles to failure	191
Fig 5.1 Enhanced low cost bond coat with additions to coatings	192
Fig 5.2 Enhanced low cost bond coats with additions to substrate	193
Fig 5.3 Pt variability studies- effect of plating tank conditions and Pt thickness variation	194
Fig 5.4 Comparison of the effect of pink and brown alumina grit on LCBC	195
Figure 6.1a(i) GDOES depth profile for base line composition with no ageing treatment ( 0 – hours)	196

Figure 6.1a(ii) GDOES selected depth (first 10 $\mu$ m) profile analysis for base line composition with no ageing treatment ( 0 – hours), showing elemental depth profiles of Ni, Cr, Al, Ti, Pt, Y, and Zr.	197
Figure 6.1b(i) GDOES depth profile for base line composition aged at 1150 $^{\circ}$ C for 4 – hours	198
Figure 6.1b(ii) GDOES selected depth (first 10 $\mu$ m) profile for base line composition aged at 1150 $^{\circ}$ C for 4 hours, showing elemental depth profiles of Ni, Cr, Al, Ti, Pt, Y, and Zr.	199
Figure 6.1c(i) GDOES depth profile for base line composition aged at 1150 $^{\circ}$ C for 16 – hours	200
Figure 6.1c(ii) GDOES selected depth (first 10 $\mu$ m) profile for base line composition aged at 1150 $^{\circ}$ C for 16 hours, showing elemental depth profiles of Ni, Cr, Al, Ti, Pt, Y, and Zr.	201
Figure 6.1d(i) GDOES depth profile for base line composition aged at 1150 $^{\circ}$ C for 25 – hours	202
Figure 6.1d(ii) GDOES selected depth (first 10 $\mu$ m) profile for base line composition aged at 1150 $^{\circ}$ C for 25 hours, showing elemental depth profiles of Ni, Cr, Al, Ti, Pt, Y, and Zr.	203
Figure 6.2(i) SEM microstructure of base line composition at X500 magnifications: (a) with no ageing treatment (0-hours); (b) with 4 hours ageing at 1150 $^{\circ}$ C; ); (c) with 16 hours ageing at 1150 $^{\circ}$ C); (d) with 25 hours ageing at 1150 $^{\circ}$ C	204
Figure 6.2(ii) SEM microstructure in Backscattered mode (BSI) and corresponding EDX of LCBC on alloy CMSX-4(a) with no ageing treatment (0-hours); (b) with 4 hours ageing at 1150 $^{\circ}$ C; ); (c) with 16 hours ageing at 1150 $^{\circ}$ C); (d) with 25 hours ageing at 1150 $^{\circ}$ C	205-208
Figure 6.2(iii) BSI and corresponding X-ray mapping images illustrating the distribution of various elements along a cross-section of low cost Pt bond coat on alloy CMSX-4; ( a) base line condion (O-hrs); (b) 4 hrs ageing; (c) 16 hrs ageing; (d) 25 hrs ageing	209-212
Table 6.2 Average oxide thickness from TEM / SEM measurement of the TGO layer and corresponding graph	213
Figure 6.3a (plate XF1-11) : BF image at 50k magnification: All 3 layers of coating with selected X-ray energy dispersive analysis of Al <sub>2</sub> O <sub>3</sub> and TBC.	214

Figure 6.3a (plate XF1-14) : A DF Image at 200K magnification of the $Al_2O_3$ layer. Detection of a possible dark phase particles in $Al_2O_3$ and corresponding EDX pattern. Two SAD patterns of this layer show typical diffuse rings corresponding to a poly crystalline material confirming its $Al_2O_3$ . Possible dark phase particles is richer in Pt,Cr,Zr and Y. EDX in standard $Al_2O_3$ is normally free from Cr,Co, although still rich in Zr.	215
Figure 6.3a (plate XF1-15): DF Image at 200k magnification with more EDX performed on $Al_2O_3$ layer on the dark phase particles.Also a DF image showing bond coat / $Al_2O_3$ interface. Bond coat EDX is richer as expected in Pt, Ni,Cr,Co and a little Al.This could be a Pt-rich $\gamma$ phase.	216
Figure 6.3a (plate XF1-16): BF image at 15k magnification in bond coat region. Several grit particles observed which have been confirmed by EDX to be Al and O rich. Also observed light and dark phases within the bond coat region.Lighter phase of bond coat composition is not rich in Ti whilst darker shows a small peak.	217
Figure 6.3b (Plate 212-11): BF Image at 11.5k magnification: Low magnification to corner all regions. There is evidence of growth in the $Al_2O_3$ region. There is mixed grains within the $Al_2O_3$ region. Finer at interface between TBC/ $Al_2O_3$ . However, coarser at BC/ $Al_2O_3$ interface.	218
Figure 6.3b (Plate 212-13): BF Image at 27.5k magnification : Interface between $Al_2O_3$ / Bond coat -very sharp interfacial region. Coarser alumina grains at the interface. Also BF Image at 50K magnification showing $Al_2O_3$ region with again precipitates present.	219
Figure 6.3b (Plate 212-15): BF Image at 150k magnification : Showing $Al_2O_3$ / TBC interface. Very sharp interfacial region without any voids indicating good adhesion.	220
Figure 6.3c (Plate 415-12): BF Image at 15k magnification : a series of images showing the analysed area of the multilayer structure. Ceramic, intermixing layer, alumina, Pt-rich substrate.	221
Figure 6.3c (Plate 415-13): BF Image at 27.5k magnification : Alumina interlayer of equiaxial microstructure. The alumina is coarse close to the substrate and becomes fine towards the ceramic layer where it presents as an intermixing layer. Also shown BF Image at 66kk : Magnified image of alumina grains and grain boundaries. No voids were involved in the microstructure.	222
Figure 6.3c (Plate 415-14): BF Image at 88k magnification : Sharp interface between the alumina and bond coat, and also a triple point.	223

Figure 6.3d (Plate 314-13): BF Image at 27.5k magnification : A series of plates showing TBC/ $\text{Al}_2\text{O}_3$  and bond coat region and analysed Edx at surface of zirconia ABD14. 224

Figure 6.3d (Plate 314-15): BF Image at 27.5k magnification:TBC/ $\text{Al}_2\text{O}_3$ /Bond coat regions. intermixing between the bond coat and alumina, EDX shows that Cr,Ni diffused through, which eventually lead to bond coat degradation. Coarse alumina is still pure, except a little Ni. 225

Figure 6.3d (plate 314-16) : Bf image at 27.5k magnification:  $\text{Al}_2\text{O}_3$  layer and pegs into bond coat ( mechanical adhesion ) 226

## **Chapter 1 - Introduction**

### **1.1 The Need for Thermal Barrier Coatings**

Turbine operating temperatures in advanced gas turbine engines will continue to increase in order to meet the need for greater performance and higher operating efficiencies [1,2].

However, longer operating lifetimes and a reduction in turbine blade degradation are also high priority requirements. As a result of these conflicting needs increasing operating temperatures will require advanced coatings .

Thermal protection required by the turbine blade can be provided by ceramic thermal barrier coatings (TBC's) [3]. The most common thermal barrier coating system currently used consists of a low thermal conductivity ceramic coating such as partially stabilized zirconia ( $ZrO_2$ ), deposited onto an oxidation and corrosion resistant Co-Ni-Cr-Al-Y bond coat on the Ni-based superalloy substrate [4,5]. Normally, the adhesion of the TBC to the Ni-based superalloy is poor , so therefore a bond coat which acts as a 'glue' to improve adhesion is provided [6]. Such TBC and bond coat systems offer good wear and corrosion resistance. The thermal barrier coatings however, have a limited life span , as it degrades allowing the ceramic to spall [7] leaving the substrate exposed to the high temperature environment [ Figures 1].

The lifetime of the thermal barrier coating is limited by two main failure mechanisms, namely (i) thermal expansion mismatch between bond coat and TBC and (ii) bond coat oxidation; both of these can cause failure of the TBC [8].

However, the main mechanisms of bonding at the interface level between the bond coat and TBC is not completely understood. This programme of work will develop knowledge to enhance the critical understanding of the bonding mechanisms, particularly at the interface level. This knowledge will then be applied to the design of turbine blades for enhanced resistance to thermal and mechanical degradation.

### **1.2 Temperature / Time Specification**

For TBC's to be certified within aeroengines, they must first reach the temperature / time specification set within Rolls-Royce. Currently, Rolls-Royce have designed their next generation of engines to run at 1150°C that equates to an interface temperature at the bondcoat / TBC interface, within the high pressure turbine section, to be 1250°C. This is the temperature to which the bondcoat / TBC will be subjected to, on take off power for a large jet airliner. Taking into account the expected life of the superalloy blade, and the time that the engine will spend at full take off power, the life of the TBC at this temperature needs to be in excess of 25 hours. This includes a 70% safety margin for the total lifetime.

[12 ]

### **1.3 Bond Coat System**

Corrosion protection coatings fall into two groups, identified by their application method, namely diffusion and overlay. In the diffusion coating application process, aluminium reacts at the surface of the substrate, forming a layer of monoaluminide. For nickel based superalloys, this is nickel aluminide ( NiAl). The coating technique hence provides a surface enrichment of aluminium ( often together with chromium and / or silicon ) which

results in the formation of protective surface oxide films of  $\text{Al}_2\text{O}_3$ ,  $\text{Cr}_2\text{O}_3$  and  $\text{SiO}_2$ . This type of coating is modified to some extent by the elements contained in the substrate as the diffusion process takes place, and may be further modified by additions of other metallic elements intentionally added during the coating application process ( for example, platinum is often added to improve corrosion resistance) . [10]

MCrAlX Overlay coatings, in which M represents a base metal Ni, Co ,Fe or some combination of these elements, and X represents either a rare earth element or some other element such as Y or Zr with a high chemical reactivity for oxygen and are widely used on superalloy turbine components. In these coating alloys, the Al provides the primary oxidation protection through formation of a slow-growing protective oxide scale; the Cr functions principally to increase the effective chemical activity of the Al; the X ( most commonly the element Y ) improves the adherence of the alumina scale. During thermal cycling, the base metal or alloy, M, provides compatibility with the substrate alloy. Overlay coatings have some significant advantage over diffusion treatments, most notably the ability to provide a larger reservoir of Al for protective scale formation and less dependence on the underlying alloy composition. [11]

Both diffusion and overlay have been tried as bond coat application methods in order to sustain higher gas temperatures. These coatings have had to be modified in order to retain TBC adhesion. The addition of Pt to these overlay coatings has extended the temperature capabilities to a point where they are now used to raise the temperature in older engines, by the fitting of TBC protected parts. A new type of coating has been developed, where Pt is

wet plated onto the superalloy substrate ( CMSX-4 ) directly. This has led to the so called low cost bondcoat system ( LCBC). Once plated, the sample is then heat treated in a vacuum furnace for 1 hour at 1150°C. Research is now underway to further improve these systems in order to reach the targets of 1250°C.[12]

### **1.3.1 Thermal Barrier Coatings**

Ceramic coatings ( TBC's ) are applied over these protective ( bond coats ) coatings with the aim of creating a barrier to the high temperature environment . Application technique includes plasma spray / EBPVD etc. These coatings rely upon the use of low thermal conductivity materials which can reduce metal operating temperatures by as much as 200°C . This leads to significant increases in the creep and thermal fatigue lives of the turbine blade component. Alternatively, it allows higher turbine entry temperatures, or reduced cooling air leading to improved efficiency. [ 13]

### **1.4 Degradation Mechanism**

The degradation processes of TBC's was fundamentally assessed by means of a comprehensive literature review [14, 15,16,17,18,19]. During varying test conditions the most significant findings have been compiled in this thesis. Failure of TBC's might arise from the thermal expansion mismatch between the components, mechanical stresses induced by thermal gradients, ceramic sintering, phase transformation, bond coat oxidation, bond coat inelasticity, corrosive and erosive attack, residual stress due to deposition and adverse component geometry. Among these the life time of the coating is limited by three main parameters:

- interdiffusion of substrate / coating ( solid – state diffusion )
- excessive bond coat oxidation
- mis-match of thermal expansion coefficient

#### **1.4.1 Interdiffusion**

Diffusion of aluminium into the base metal and base-metal elements into the coating reduce the concentration of aluminium that is available for forming alumina. A protective oxide can no longer re-form after spallation once the aluminium concentration falls below a certain level. The basic concepts of diffusion are well understood for simple systems, and the diffusion of complex, multi-element systems containing multiple phases can be formally described [15]. Obtaining actual interdiffusion coefficients and predicting the interdiffusion in these systems is a formidable task. Consequently, reliance on empirical measurements of interdiffusion is necessary and usually is sufficient for engineering purposes.

#### **1.4.2 Bondcoat Oxidation**

Oxygen can easily diffuse to the metallic bond coat owing to the high porosity, segmentation and ionic conductivity of the  $ZrO_2$  top coat. The bond coat suffers oxidation attack. An oxide layer builds up between the bond coat and top coat and the relative expansion causes internal stresses at the interface. When the oxide layer reaches a critical thickness, cracking can occur and with increasing oxidation, attack the ceramic which spalls off. Bond coat oxidation influences thermal shock resistance; with increasing oxidation, the number of thermal shock cycles to failure is reduced [16].

### **1.4.3 Thermal expansion mismatch**

The thermal shock resistance of TBC's is controlled by the thermal expansion mismatch between the zirconia top coat and the metallic substrate.

TBCs with yttria partially stabilised zirconia top coats show better thermal shock resistance than top coats with other chemical compositions [ 17] . By segmentation of the ceramic top coat or optimisation of the porosity, further improvement of the thermal shock resistance is possible [18,19].

### **1.5 Programme of Work**

The work detailed in this thesis is concerned with the development of coatings with enhanced temperature capabilities for turbine blade applications by understanding the fundamental mechanisms responsible for adhesion between the nickel based turbine blade and the zirconia-based TBC. An understanding of the bonding mechanisms will allow the design of advanced coating systems with increased operating temperatures.

This thesis reports on the development of the Glow Discharge Optical Emission Spectroscopy (GDOES) technique, which is an atomic emission technique used for both bulk and depth profile analysis, which had not previously been applied to TBC's. SEM and TEM have been used in order to enhance understanding of failure modes in TBC systems and adhesion process i.e.to understand the thermal degradation process by carrying out a “layer-by- layer” analysis of a range of bondcoats, those already in use and experimental bondcoats under development. The ability of GDOES to provide information about coating thickness, elemental distribution, elemental segregation, interfaces and interfacial

contamination, for example by Si, Na etc, all within a single technique and with such speed cannot readily be matched by any other techniques. Also the sensitivity of GDOES down to ppm levels is important in identifying contaminants that are difficult to detect using electron probe techniques ( SEM -EDX ) , which are important for coating improvements.

The overall aim of the SEM/TEM work is to supplement the GDOES work programme, in evaluating coating systems from a microstructural aspect. For example, examine the interface structure in more detail using SEM in order that the chemistry of features down to 'micron sizes' on the surfaces can be defined and how it affects bonding mechanisms. Also the use of cross-sectional TEM foils to characterise the changes in coating microstructure through the thickness of the coating, and coating microstructure from the bond coat interface to the outer surface for both as processed and specimens exposed to a high temperature service environment.

Furthermore, to use cross-sectional TEM specimens to investigate the bondcoat / ceramic interface , to search for any additional information about coating adhesion mechanisms and elemental segregation etc. Also to use EDX to carry out localised chemical analysis ( complex microchemistry ) of the interface region etc and relate to GDOES findings and cyclic performance of coatings. In addition, to establish what influences bonding quality at the substrate/ coating interface; the chemical -metallurgical interactions ( diffusion , reactions ) to help in finalising proposed failure mechanisms .

## **Chapter 2 - Literature Review**

### **2.1 Substrate Materials**

The main alloy substrate material included in this study was the single crystal CMSX-4, however other substrate materials such as the directionally solidified alloy MAR M002 and a third generation single crystal material RR3000 (CMSX-10) have been compared. It is important to understand the substrate material-coating chemistry, for example, for a given coating, the protective nature of the oxide scale development upon exposure to elevated temperatures can vary from one substrate to another depending upon its chemical composition [20]. Particularly at temperatures greater than or equal to 1000°C, elements in the substrate can diffuse into the coating, resulting in a significant effect on its behaviour [21].

In order to gain in-depth knowledge of failure involved in the coatings, a review of superalloy metallurgy, the substrate materials with their respective chemical compositions, the role of alloying elements and the respective microstructures is considered in detail.

#### **2.1.1 Superalloy Metallurgy**

A superalloy is an alloy developed for elevated temperature service, usually based on Group VIII A elements, where relatively severe mechanical stressing is encountered and where surface stability is frequently required. The term 'superalloy' was first used shortly after World War II to describe a group of alloys developed for use in turbo-chargers and aircraft turbine engines that required high performance at elevated temperatures. These

alloys usually consist of various formulations made from the following elements: Fe, Ni, Co and Cr, as well as lesser amounts of W, Mo, Ta, Nb, Ti and Al. The most important properties of the superalloys were long-term strength at temperatures above 650°C and resistance to hot corrosion and erosion [85, 28].

Superalloys consist of austenitic face-centered cubic (f.c.c.) matrix phase gamma ( $\gamma$ ) plus a variety of secondary phases.

Gamma ( $\gamma$ ): The continuous  $\gamma$  matrix is a face-centered-cubic (f.c.c.) nickel-based austenitic phase that usually contains a high percentage of solid-solution elements such as Co, Cr, Mo, and W.

Gamma Prime ( $\gamma'$ ): The primary strengthening phase in nickel-based superalloys is  $\text{Ni}_3(\text{Al}, \text{Ti})$ , and is called gamma prime ( $\gamma'$ ). It is a coherently precipitating phase (i.e., the crystal planes of the precipitate are in registry with the gamma matrix) with an ordered  $\text{L1}_2$  (f.c.c.) crystal structure. The close match in matrix / precipitate lattice parameter ( $\sim 0-1\%$ ) combined with the chemical compatibility allows the  $\gamma'$  to precipitate homogeneously throughout the matrix and have long-term stability. Interestingly, the flow stress of the increases with increasing temperature up to about 650°C. In addition,  $\gamma'$  is quite ductile and thus imparts strength to the matrix without lowering the fracture toughness of the alloy.

The secondary phases are the carbides MC,  $\text{M}_{23}\text{C}_6$ ,  $\text{M}_6\text{C}$ , and  $\text{M}_7\text{C}_3$  (rare) in all superalloy types and gamma prime  $\gamma'$  f.c.c. ordered  $\text{Ni}_3(\text{Al}, \text{Ti})$  intermetallic compound in nickel and

iron-nickel superalloys. The superalloys derive their strength from solid solution hardeners and precipitating phases. Carbides may provide limited strengthening directly ( e.g through dispersion hardening ) or more commonly , indirectly ( e.g. by stabilizing grain boundaries against excessive shear ) [ 86,87,88 ].

### **2.1.2 Superalloy systems**

The three major classes of superalloys are nickel-, iron-, and cobalt- based alloys [ 86 ].

#### **Fe-Ni Base**

The most important class of Fe-Ni base superalloys includes those alloys which are strengthened by intermetallic compound precipitation in a f.c.c matrix. The most common precipitates is  $\gamma'$ , typified by A-286, V-57 or Incoloy 901, but some alloys precipitate  $\gamma''$ , typified by Inconel 718.

#### **Co-Base**

The Co-base superalloys are invariably strengthened by a combination of carbides and solid solution hardeners. The essential distinction in these alloys is between cast and wrought structures. Cast alloys are typified by X-40 and wrought alloys by Haynes 25 .

#### **Ni-Base**

Ni - based alloys can be either solid solution or precipitation strengthened. Solid solution strengthened alloys , such as Hastelloy X , are used in applications requiring only modest

strength. In the most demanding applications, such as hot sections of gas turbine engines, a precipitation strengthened alloy is required.

The principal microstructural variables of superalloys are: (a) the precipitate amount and its morphology; (b) grain size and shape; and (c) carbide distribution [27].

### **2.1.3 The role of individual constituents in superalloys**

Superalloys contain a variety of elements in a large number of combinations to produce desired effects. Outlined here are some of the effects of the most commonly used elements .

#### **Nickel**

This element is the base constituent of blade alloys. It forms stable, high-melting-point intermetallic compounds with aluminium (NiAl, Ni<sub>3</sub>Al). It is prone to destructive interaction with sulphur with which it can form a low-melting-point eutectic system.

#### **Cobalt**

Cobalt in Ni-base alloys plays a key role in raising the  $\gamma'$  solvus temperature. As already explained earlier phase is the key factor responsible for the extraordinarily useful high temperature properties of Ni-based superalloys. Interactions of cobalt with sulphur are less destructive than they are for nickel.

## **Aluminium**

Aluminium is a major constituent of the Ni-base alloy, it forms the ( $\gamma'$ )  $\text{Ni}_3(\text{Al,Ti})$ . It provides a reservoir from which the alumina scale is repeatedly replenished. Aluminium enhances oxidation resistance.

## **Chromium**

Chromium provides good oxidation and hot corrosion resistance and solid solution strengthening in Ni-base alloys.

Other elements such as Mo, Ta, W, Re are added to provide strength within the Ni-base alloys. However, minor elements (C, B) are added to form carbides and borides; these elements plus others (Ce,Mg) are added for purposes of tramp element control [86,28].

### **2.1.4 Processing**

The material and casting technique improvements that have taken place during the last 50 years have enabled superalloys to be used first as equiaxed castings in the 1940's, then as directionally solidified (DS) materials during the 1960s and finally as single crystal (SC) in the 1970s. Each casting technique advancement has resulted in higher use temperatures. A review of each technique is outlined here with potential alloy examples.

#### **2.1.4.1 Directionally Solidified Superalloys (DS)**

In DS processing, columnar grains are formed parallel to the growth axis. In Ni-based alloys, the natural growth direction is along the  $\langle 100 \rangle$  crystallographic direction. This

morphology is accomplished by pouring liquid metal into a mould that contains a water - cooled bottom plate. Solidification first occurs at the bottom plate, after which the mould is slowly withdrawn from the furnace, allowing the metal inside to directionally solidify from bottom to top. A typical example of a DS system is MAR-M002 which is a directionally solidified alloy . A particular characteristic of this alloy is the patented addition of hafnium [24,25,26], some 2 mass % by modifying the solidification sequence. In particular, hafnium is rejected from the solidifying dendrites during casting and concentrates in the interdendritic regions thereby increasing the quantity and coarsening the form of the  $\gamma$ - $\gamma'$  eutectic. Hafnium also modifies the size, distribution, and composition of the grain boundary carbides, producing a finer dispersion, that helps to prevent the common intergranular creep failure and increase the life of turbine components.

The exceptional properties of DS alloy are due to:

1. The alignment or elimination of any weak grain boundaries oriented transverse to the eventual loading direction.
2. The low elastic modulus associated with the  $\langle 100 \rangle$  directions enhances thermal mechanical fatigue resistance in areas of constrained thermal expansion - particularly turbine vanes.

#### **2.1.4.2 Single Crystal Superalloy (SC)**

SC alloys developed during the 1970s were a spin -off from the technological advances made in the DS casting processes. SC casting are produced in a similar fashion to DS by selecting a single grain, via a grain selector. During solidification, this single grain grows to

encompass the entire part. Single crystals obtain their outstanding strength through the elimination of grain boundaries that are present in both equiaxed and directionally solidified materials [20].

The superiority of single-crystal over polycrystalline superalloys is due to:

- higher melting temperature with heat treatment for increased creep strength.
- the absence of grain boundaries which act as failure initiation site.
- low modulus  $\langle 100 \rangle$  oriented solidification texture that provides significant enhancements in thermal fatigue resistance [23].

Typical SC alloys CMSX-2, CMSX-3, and CMSX-4 (CMSX= Connor-Muskegon Single Crystal Alloys) have been developed to replace directionally solidified MAR-M002 in applications where increased creep, tensile, and fatigue strength is required. Since in the thesis CMSX-4 has been used, further particulars are discussed here.

#### **2.1.4.3 CMSX-4 Alloy**

This is a second generation nickel-base single crystal superalloy containing 3 mass % rhenium (Re) and 70% volume fraction of coherent  $\gamma'$  precipitate strengthening phase. It's finely balanced composition and offers an attractive range of properties in turbine airfoil applications. In particular the alloy's combination of high strength in relation to creep-rupture, mechanical and thermal fatigue, good phase stability following extensive high temperature, stressed exposure and oxidation, hot corrosion, and coating performance are

attractive for turbine engine applications where engine performance and turbine airfoil durability are of prime importance [22].

#### **2.1.4.4 RR3000 Alloy**

RR3000 (CMSX-10) alloy is a third generation single crystal casting material, which is used in demanding turbine engine blading applications. The flight engine certified alloy is characterized by its 6 mass % rhenium content, high additive refractory element level, and its relatively low levels of chromium employment. Based on published data, the alloy is thought to exhibit the highest creep strength and resistance to fatigue of any production Ni-base, cast single crystal superalloy.

RR3000 alloy provides an approximate 30°C improved creep strength relative to the second generation CMSX-4 alloy. Furthermore, its low cycle and high cyclic fatigue strength is as much as 2-3 times better than the best alternatives. Moreover, the alloy also develops an attractive blend of tensile and impact strengths, foundry performance, heat treatability, and environmental properties characteristics, most notably, the alloy provides surprisingly good hot corrosion resistance, despite its relatively low chromium content (2-3 mass %).

Additionally, the alloy performs extremely well in both the aluminide and Pt-aluminide coated conditions [ 89 ].

## 2.2 Coating Systems

### **Bond coats for TBC's**

The gas turbine engine provides one of the harshest environments challenging material systems today. Engine components are subject to rigorous mechanical loading conditions, high temperatures and corrosive or erosive media. Historically, engine manufactures have applied protective coatings to increase the durability and performance of superalloys. Field experience as well as the development of processing technologies has led to the evolution of many new improved coating systems for a variety of engine component applications. In the case of combustor and turbine areas, diffusion and overlay coatings such as aluminides, platinum aluminides, or MCrAlY overlay coating (where M=Co, Ni, or Fe), have been developed for oxidation and/or corrosion resistance and also are used widely as bond coats for Thermal Barriers Coatings (TBC's) [11].

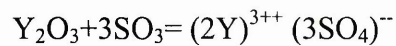
TBCs normally consisting of a low thermal conductivity zirconia stabilized by  $Y_2O_3$ , are usually produced in one of two ways, either by Air Plasma Spraying (APS) or by Electron Beam Physical Vapor Deposition (EBPVD). One over riding aspect with regard to the adoption of TBC technology is the underlying “bond coat” which establishes a thermally grown oxide at the bond-coat or ceramic interface to maintain TBC adhesion. This bond coat promotes good coating durability under thermal cycling conditions.

Continuous refining and development of the process and the coating materials has led to the extensive use of ceramic coatings in other industrial units. The movement towards higher

turbine operating temperatures and a wide range of fuels, often with significant impurity levels, has highlighted the diversity of degradation mechanisms which can contribute to coating failure and spallation.

As exposure conditions become more complex and exacting, the need to understand these mechanisms becomes more pressing as they provide the key to the successful development of new coating systems.

The bond coat contains oxide-forming elements, i.e. Al and Cr. The alumina and chromia formed at high temperatures give protection against oxidation. On the other hand, it was found that the lifetime of TBC with yttria stabilized zirconia overlay was reduced by the reaction of yttria with sulphur:



Bond-coats can be classified into two categories: diffusion and overlay coatings.

### **2.2.1 Aluminide Bond Coats**

#### **Diffusion Coating**

Diffusion coatings are deposited either by heating components to be treated in contact with the powder coating material in an inert atmosphere (solid-state diffusion) or by heating them in an atmosphere of a volatile compound of the coating material (out-contact gas-phase deposition, or chemical vapour deposition). Solid-state diffusion methods include

pack cementation, which is the most widely employed diffusion coating method. Diffusion coatings include aluminium (aluminizing), chromium (chromizing), and silicon (siliconizing). Substrate materials include nickel and cobalt-base superalloys, steels (including carbon, alloy and stainless steels), and refractory metals and alloys.

Blades and vanes made from nickel and cobalt base materials are used in the hot sections of all gas turbines and coated to enhance resistance to hot corrosion. The most widely used coatings are those based on the intermetallic compounds NiAl and CoAl, which are formed by the diffusion interaction of aluminium with surfaces of the nickel and cobalt alloys, respectively.

### **Aluminizing**

Pack diffusion coating may be considered as a CVD process carried out with the aid of a powder mixture (pack), in or near which the part to be coated (substrate) is immersed or suspended, containing the element or elements to be deposited (source), a halide salt (activator), and an inert diluent such as alumina (filler). When the mixture is heated, the activator reacts to produce an atmosphere of source element(s) halides which diffuse in the pack and transfer the source element(s) to the substrate on which the coating is formed.

Diffusion of the gaseous halides takes place across a aluminium-depleted zone that forms as a result of transport of aluminium into the coating under the action of the partial pressure gradients which exist between the pack and coating surface [31,32]. Aluminium is

transported mainly by the diffusion of AlX(g), where X signifies a halide to the coating surface where the reaction:

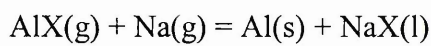


occurs. The Al(s) diffuses to form more coating while AlX<sub>3</sub>(g) diffuse back and reacts with Al(l) in the pack to regenerate AlX(g). In packs activated with NH<sub>4</sub>F (or AlF<sub>3</sub>), AlF<sub>3</sub> appears as a solid at the operating temperature, and its vapor pressure is uniform throughout the pack. The constituent therefore does not diffuse in the gas phase. Aluminum is transported primarily by the diffusion of AlF(g) to the coating surface where deposition takes place by the reaction:



The AlF<sub>3</sub>(s) that is formed deposits as crystalline solid at the surface, some of which may adhere to the coating. The supply of AlF(g) is maintained by the reverse reaction in the pack.

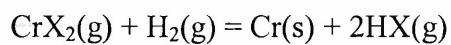
In packs activated with a sodium halide such as NaCl, NaX(l) appears as a condensed phase in the pack. Aluminium deposition occurs mainly by the diffusion of Na(g) and AlX(g) to the coating surface where a reaction of the type:



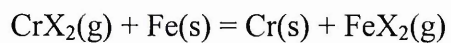
occurs with the deposition of NaX(l) at the surface [33].

## Chromizing

Although many of the same principles apply to chromizing as to aluminizing packs, the fact that chromium halides are less stable than aluminium halides introduces several new factors [34,35]. In ammonium halides activated chromizing packs,  $\text{CrX}_2(\text{l})$  appears as a condensed phase. The major constituents in the gas phase in equilibrium with chromium in the pack are  $\text{CrX}_2(\text{g})$ ,  $\text{CrX}_3(\text{g})$ ,  $\text{HX}(\text{g})$ , and  $\text{H}_2(\text{g})$ . The partial pressure of  $\text{HX}(\text{g})$  is high enough so that hydrogen reduction occurs according to the reaction:



At the coating surface there is an important mechanism for the deposition of chromium. Since the free energies of formation of  $\text{FeX}_2$  and  $\text{CrX}_2$  are comparable, if the substrate is an iron-base alloy the exchange reaction also occurs.



The  $\text{FeX}_2(\text{g})$  diffuses back into the pack where the reverse reaction leads to the deposition of  $\text{Fe}(\text{s})$  on the particles of the source alloy, thus changing its composition, while the  $\text{Cr}(\text{s})$  diffuses into the coating in this case, the weight of the substrate does not change significantly since it loses one atom of iron for every atom of chromium gained.

In summary, in the diffusion coating application process, aluminium reacts at the surface of the substrate, forming a layer of monoaluminide. For nickel based superalloys, this is nickel aluminide (NiAl). The coating technique hence provides a surface enrichment of aluminium (often together with chromium and/or silicon) which results in the formation of protective surface oxide films of  $\text{Al}_2\text{O}_3$ ,  $\text{Cr}_2\text{O}_3$ , and  $\text{SiO}_2$ . This type of coating is modified to some extent by the elements contained in the substrate as diffusion process takes place, and may be further modified by additions of other metallic elements intentionally added during the coating application process (for example, platinum is often added to improve corrosion resistance). [10]

### **2.2.2. Overlay Bondcoats**

Diffusion-type coatings, used successfully on early gas turbine, were tied to the substrate composition, microstructure and design. Later some changes were introduced:

- i) In superalloy composition, such as reduction in Cr and increase in other refractory metal.
- ii) In microstructure, by casting with more segregation.
- iii) In design, by air-cooling and with thin walls (which introduced higher thermal stress).

These changes required coating which were more independent of the substrate. Overlay coatings met this necessity.

Overlay coating also overcome the restriction encountered in diffusion coating, especially the variant, viz. Cr/Al, Ta+Cr or the Pt-aluminides all of each give better stability and oxide-hot corrosion resistance than Al alone. Nowadays, MCrAlY (where M is Ni, Co, Fe) is the more commonly overly type use in the aerospace industry. The cobalt, nickel and chromium in the intermediate coating provide a high melting point need. Also, aluminium, chromium and yttrium provide resistance to oxidation by forming a thin, tenacious oxide layer.

McrAlY overlay used in gas turbines are usually Ni and/or Co with high Cr, 5-15% Al and Y addition around less than 1% for stability during cyclic oxidation. They are multi-phase alloys with ductile matrix, e.g. gamma Co-Cr, containing a high fraction of brittle phase e.g. beta CoAl. The Cr provides oxidation hot corrosion resistance but too much Cr affects substrate phase stability. The success of most overlay coating is the presence of active elements such as Y or Hf which promote alumina layer adherence during thermal cycling, giving increased coating protectiveness at lower Al levels. Yttrium mostly appears along grain boundaries if a MCrAlY is cast but is homogeneous if plasma sprayed. Thus MCrAlY with 12% Al are more protective than the more brittle diffusion aluminides with 30% Al.

### **Influence of composition on the oxidation resistance of MCrAlY coating**

The different types of compositions as shown below will give different thermal and oxidation resistance to the overlay coating:

- I. Co-30Cr-5Al-0.5Y
- II. Co-23Cr-12Al-0.35Y
- III. Ni-40Cr-5Al-0.4Y

It has been concluded that a CoCrAlY coating of high chromium and low aluminium, content will offer protection under the engine conditions specified up to somewhat more than 30000 hours. The high chromium content of NiCrAlY overlay coating type with a nickel base should be thermochemically advantageous when compared with a cobalt base material at lower temperatures, because the  $\text{SO}_3$  partial pressure required for  $\text{Na}_2\text{SO}_4$ - $\text{NiSO}_4$  melt formation is one order of magnitude higher than that required for  $\text{Na}_2\text{SO}_4$ - $\text{CoSO}_4$  liquid. Therefore, it is not clear why the performance of the high chromium NiCrAlY overlay was worse than that of the lower chromium CoCrAlY, but the reason may be related to the greater stability of the nickel sulphides at lower temperature. Thus, the performance of the CoCrAlY overlay coatings was superior to NiCrAlY [36].

#### **Properties of MCrAlY coating which affect TBC life**

Recent studies have shown that a significant difference in TBC life can be achieved for different bond coats that exhibit little or no difference in oxidation behaviour. These data suggest that bond coat properties other than oxidation resistance can also influence TBC life.

The roughness of the bond-coat/ceramic interface is the factor which must be considered in any description of bond-coat behaviour, as the thermal cycle durability of any given bond-coat/ceramic coating system increases with increasing interfacial roughness. This has often been attributed to an improvement in interfacial adhesion based on a mechanical keying mechanism of bonding. This proposal might be valid if failure as a result of thermal cycling occurred at the bond-coat/ceramic interface, but as the failures are predominantly cohesive within the ceramic coating adjacent to the bond interface, this cannot be the correct explanation. It is far more likely that the geometrical effects on the transmission of stresses across the interface are more important in affecting durability than any alteration to the bond strength. Bond-coat powder size and spray parameters may be adjusted to produce bond-coat surfaces that have significant levels of surface roughness. However, care must be taken so that higher levels of porosity do not develop in the bond-coat which would reduce its oxidation resistance [37,38].

The bond strength of thermal barrier coatings decreases with increasing coating thickness. This is because the thicker coating causes higher tensile edge stresses and will increase the tendency for debonding. Hence it will reduce the applied stress required to cause debonding. It is also noted that this behaviour occurs without an increase in coating residual stresses for thicker coatings. Therefore, a thicker coating will be more likely to have a lower bond strength than a thinner coating with the same level of residual stress. The bond strength of the coating is important for the use of MCrAlY coating. Debonding can take place at the coating-substrate interface after a certain number of thermal cycles if the adhesive strength is poor [37].

Stress relaxation of the bond coat for plasma spray coating results in a significant increase in the out-of-plane residual stress generated at the bond coat interface. Since out-of-plane tensile stresses cause delamination of the ceramic layer, stress relaxation of the bond-coat is expected to have a deleterious effect on the TBC life [40].

Substrate material, test temperature, cycle profile, test environment, nature of top coat/bond-coat adherence, are other variables that influence the durability of thermal barrier coatings. Studies are currently underway to investigate these effects.

In summary, MCrAlX overlay coatings, in which M represents a base metal of Ni, Co, Fe or some combination of these elements, and X represents either a rare earth element or some other element such as Y or Zr with high chemical reactivity for oxygen, are widely used on superalloy turbine components. In these coating alloys, the Al provides the primary oxidation protection through formation of a slow-growing protective oxide scale. The Cr functions principally to increase the effective chemical activity of the Al, the X (most commonly the element Y) improves the adherence of the alumina scale during thermal cycling, and the base metal alloy, M, provides compatibility with the substrate alloy. Overlay coatings have some significant advantage over diffusion treatments, most notably the ability to provide a larger reservoir of Al for protective scale formation and less dependence on the underlying alloy composition [11].

### **2.2.3. Low Cost Bond-coat Systems (LCBC)**

Both diffusion and overlay bond coats were tried for TBC's, however, with today's higher temperatures these coatings have had to be modified in order to retain TBC adhesion. The

addition of Pt to these coatings has extended the temperature capabilities to a point where they are now used to raise the temperature in older engines, by the fitting of TBC protected parts. A new type of coating has been developed, where Pt is electroplated onto the superalloy substrate (CMSX-4) directly. This has led to the so called low cost bond coat system (LCBC). Once plated, the sample is then heat treated in a vacuum furnace for 1 hour at 1150°C. Research is now under way to further improve these systems in order to reach the targets now demanded (bond-coat/TBC interface, within the high pressure turbine section, to be 1250°C) [12].

#### **2.2.4. Thermal Barrier Coatings**

Ceramic coatings (TBC's) are applied over these protective bond coats. The ceramic layer is usually partially stabilized zirconium oxide, typically 250µm thick. [11,13]

Its primary function is to act as a thermal barrier between the hot combustion gas and the turbine metal surface. This is achieved by means of the very low thermal conductivity of the ceramic coating (approx. two orders of magnitude lower than that of the superalloy substrate). The result is up to a 250µm thick coating. This reduction in metal temperatures has several benefits, namely:

- Decrease in maximum tensile stress
- Decreased creep rates (i.e. increased creep rupture life)
- Increased thermal fatigue life (due to less severe transient thermal strains)
- Reduced metal oxidation rates

These benefits allow the engine designer flexibility to incorporate one or a combination of the following:

- Increase the gas temperature (turbine entry temperature), allowing the engine to operate more efficiently.
- Maintain the same operating temperature but with improvements in component life.
- The cooling air consumption can be reduced by around 30% for the same metal temperature

As mentioned above, the large majority of TBC systems are based around a partially stabilized zirconium oxide layer. In its pure form,  $ZrO_2$  undergoes a phase transformation at  $998^\circ C$ , (monoclinic→tetragonal). The result is a 9% volume increase which generates large stresses, resulting in fracture and spalling of the coating. For this reason pure  $ZrO_2$  is not used. However, additions such as magnesium oxide or yttrium oxide act to stabilize the tetragonal phase to produce the partially stabilized zirconium oxide. A typical addition of 8% yttria will stabilize the tetragonal phase at RT. The result is a material that has a superior resistance to thermal cracking.

For a given coating system, the main parameters affecting a coating's performance is the chemistry and microstructure. The coating chemistry is determined by the alloying additions required to stabilize the tetragonal phase, whilst the microstructure is primarily a function of the coating application technique.

The two commonly used techniques for the application of partially stabilised zirconia (PSZ) ceramic coatings are:

- Plasma spray deposition
- Electron beam-physical vapor deposition (EB-PVD)

The plasma spray technique has been dominant over the past 20 years; however, recent advances in technology have resulted in the EB-PVD route largely superseding the plasma spray route.

These application techniques produce markedly different microstructures; typical examples are shown in figures 2.2.4a,b.

In the plasma spray deposition technique ( figure 2.2.4c) , a plasma is generated by an electric arc in the carrier gas (usually Ar and H<sub>2</sub>). The plasma temperature is in the range of 6000-12000°C with a velocity of 200-600ms<sup>-1</sup>. The ceramic powder is injected into the plasma stream and is rapidly melted. The molten ceramic droplets impact on to the substrate and solidify allowing subsequent deposition to build up the required thickness of the layer [30,41].

The second of the commonly used application techniques is EB-PVD. Briefly, an electron beam impinges on a target ingot resulting in vapourisation of the target material. The component to be coated is suspended in the vapour and rotated to allow even coverage. The

vapour condenses on the component surface, resulting in the growth of a crystalline layer. The entire process is performed in a vacuum. A schematic illustration of the EB-PVD technique is shown in figure 2.2.4 d.

The major advantages of EB-PVD technique is the resulting strain tolerant columnar grain structure which allows accommodation and distribution of stresses resulting from thermal cycling by expansion of the loosely adhered columns into the gaps. The EB-PVD technique also produces denser coatings than the plasma spraying technique and hence has superior erosion resistance. The technique is also fast, deposition of a 200 $\mu$ m thick coating can be achieved in just 10 minutes.

Finally, the durability of a TBC system depends on not only the properties of the ceramic coating, but also the strength of the ceramic-metal and the oxidation resistance of the metallic bond coat layer.

## **2.3 The Role of Various Elements in Coating Development**

Some elements can have beneficial effects, however others can be detrimental. The role and effect of the following elements on TBC / Bondcoat will be reviewed: Pt, Re, Y, Hf.

### **2.3.1 Role of Platinum**

It has been a common industrial practice to incorporate Pt in the aluminide coating structure to improve scale adhesion [42], although the mechanism by which Pt exerts its beneficial effect is not well understood.

It has been shown that Pt modified coatings possess improved cyclic oxidation resistance because the Pt enriched zone of the coating promotes selective oxidation of aluminium with minimal effects of other elements in the coatings. The purer alumina scales have slower growth rates, which result in longer exposure times before the interlayer thickness reaches a point where spalling of the oxide occurs. Long term exposures under cyclic conditions result in substrate elements affecting oxidation behaviour.

The high affinity of Pt for Al is one of the necessary characteristics that results in the observed improved coating performances. This results in platinum aluminum phases that favour selective oxidation, exclude other elements from the coating surfaces, and may also impart some diffusional stability to the aluminide coatings. However, after long exposure substrate elements do affect coating performances and coating lives are shorter for substrates with higher concentrations of molybdenum and tungsten [99]

Additionally, it has been shown that Pt improves the protective nature of aluminide coating by eliminating chromium-rich precipitates from the outer coating layer and preventing refractory transition elements such as vanadium from diffusing into the outer coating layer [44].

### **2.3.2 Effect of Yttrium**

Yttrium is a rare earth metal and has been in use for many years. Its main application is as an active element within many ceramic structures. Thermal barrier coatings and other refractory ceramics have utilised the high melting point (i.e. 1495-1522 °C) and other attractive properties to improve the service life of many engineering applications.

Some of the principal effects of yttrium are as follows:

- Modifies oxide microstructure
- Forms intermediate oxide layer ( $Y_2O_3$ )
- Acts as a mechanical key effect
- Reduces the accumulation of oxide- alloy intervoids
- Acts as a preferential nucleation site for oxidation
- Promotes preferential cationic and anionic diffusion in the scale

#### **Modifies oxide microstructure**

The distribution of Y within a ceramic structure ( $Al_2O_3$  for example) occurs in three main areas, these being as a solid solution, an oxide layer and at grain boundaries. The percentage of Y found in solid solution is only a trace and the oxide layer ( $Y_2O_3$ ) will be

discussed later. Therefore, this section is concerned with the distribution of Y at the grain boundaries as this has a significant affect on the TBC.

Y has a tendency to segregate at the grain boundaries, this being due to the higher energy levels at these regions and therefore enabling nucleation to occur more efficiently. The Y addition acts in a similar manner to that of carbides on metallic structures. The pinning of the grain boundaries refines the microstructure, which improves mechanical properties at elevated operating temperatures. These additions of Y (usually in the order of 8-wt%) stabilize the structure, therefore maintaining a similar microstructure to that observed at room temperature and avoid phase transformation with severe conflicts of expansion / contraction.

An example of this is the addition of Y to zirconia which has favorable effects on the microstructure. The pure zirconia structure is monoclinic up to a temperature of 1100° C where upon it transforms to the tetragonal form. This phase change causes a 9% volume increase, that results in high stresses and subsequent failure of the component. The addition of Y<sub>2</sub>O<sub>3</sub>, CaO or MgO inhibits this phase transformation, therefore enabling the structure/component to operate at higher temperature with the risk of phase transformation reduced [45].

### **Forms intermediate oxide layer**

The Y reacts with oxygen during the spraying process, where the inward diffusion of oxygen forms an yttria-oxide (Y<sub>2</sub>O<sub>3</sub>) layer. A layer, that is in the region of 5µm in thickness

forms towards the outer surface of the sprayed TBC. This oxide layer acts as a diffusion barrier in preventing the penetration of heat through to the substrate.

Figures 2.3.2 a and b summarise the composition of the coating surface. As can be seen, the coating consisted of a Ni-rich  $\beta$  phase ( B2-type superlattice;  $a=0.291\text{nm}$ ) dispersed in a Co-rich solid-solution matrix phase (f.c.c;  $a=0.357\text{nm}$ ). Alloying elements present in the  $\beta$  phase included Co and Cr.

**Acts as a Mechanical key effect/ reduces oxide growth rate**

The adhesion of the TBC to the substrate is aided with the use of the bond coating, which is applied prior to spraying. However, the coating itself is required to bond strongly to prevent spallation during service. The Y additions act in several beneficial ways in forming a stronger more stable structure. The Y-rich oxide forms 'pegs' that extend into the ceramic coating ( $\text{Al}_2\text{O}_3$ ,  $\text{ZrO}_2$  etc.) and the applied bond coat enabling a far stronger bond to form, this has been shown in a number of studies [45,10,13]. It has also been proven in previous studies that  $\text{Al}_2\text{O}_3$  and  $\text{Y}_2\text{O}_3$  form an excellent adhesion between the two constituents; this therefore reduces the likelihood of disintegration of the coating during service.

Relatively new studies have revealed that the higher the initial tensile stresses prior to oxidation in the coating, the better the scale adherence. This is due to the compressive stresses formed during oxidation and therefore counteract the initial tensile stresses, i.e. reducing the bonding of the coating [7].

### 2. 3. 3 Hafnium

The oxidation of the nickel-based and cobalt-based alloys is described in some detail, from which it is clear that alloys forming  $\text{Cr}_2\text{O}_3$  scales are unlikely to be satisfactory at temperatures above  $900^\circ\text{C}$  because of volatilization of the scale. Alloys that form  $\text{Al}_2\text{O}_3$  scales are thus more oxidation-resistant, but there are problems with spalling of the scale on thermal cycling or stressing, and eventually depletion of the substrate with respect to Al will prevent re-formation of the protective scale.

The addition of reactive elements such as hafnium or its oxide improves adhesion and thus is beneficial [ 46 ].

Hafnium, is an important element for oxide scale adherence effects and is occasionally added at low levels (approximately 0.1 mass%) to superalloy compositions. It has been added to improve oxidation performance and is not intended to affect the mechanical properties of the alloy. Moreover, based on the results of the previous studies [8], hafnium derived from a superalloy substrate and present at solid solution levels in aluminide coatings was also found to strongly improve oxidation performance. However, above solid solubility levels in the coating, beneficial effects did not occur.

Hence for enhanced oxidation resistance, a strong incentive exists for including low levels of hafnium both in the superalloy substrates as well as in protective coatings. However, the optimum levels of hafnium for the greatest benefit must be identified.

To determine the optimum hafnium levels, cyclic oxidation tests have been used in the pack Aluminide coatings (high temperature/ low aluminum activity and low temperature/ high aluminum activity) [9]. The results of this cyclic oxidation testing of the pack aluminide coatings are presented in the figure 2.3.3(a) and (b). For any given substrate, the oxidation behaviour of both the low temperature/high aluminum activity and the high temperature/low aluminium activity coatings were very similar.

For both aluminide coatings, an optimal hafnium content of about 0.5wt% in the substrate was clearly indicated, in both figures 2 and 3. For hafnium contents in the alloy on either side of this level, coated substrate oxidation performance suffered. With either too little (0.1wt%) or no hafnium in the substrate alloy, oxidation resistance was significantly reduced. With too much hafnium in the alloy, i.e., 1-2wt%, oxidation resistance also suffered but not as badly as when little or no hafnium was present.

#### **2.3.4 Summary of Hf, Y Roles**

In summary additions of Y and Hf, substantially improve the bonding capability of the alumina films to the substrate. Even after extensive research the actual mechanisms by which these elements interact and suppress the S in the substrate is unknown but many theories have been put forward and include [46]:

1. Reactive elements act as vacancy sinks to suppress void formation at the alloy/oxide interface.
2. Reactive elements form oxide pegs at the alloy/oxide interface.

3. Reactive elements tie up sulphur in the alloy and prevent it from segregating to the alloy/oxide interface and weakening an otherwise strong bond.

The adherence of scale is always very important in service conditions where alloys are subjected to thermal cycles of heating and cooling. [11]. The formation of adherent slowly growing protective oxide scales is critical for high temperature applications. On the basis of low volatility, relative chemical inertness and slow growth characteristics,  $\text{Al}_2\text{O}_3$  is the scale of choice. Hence to ensure the formation of protective  $\text{Al}_2\text{O}_3$  scales, coatings enriched in aluminum are normally applied to structural hardware. However, even though protective  $\text{Al}_2\text{O}_3$  scales are formed on enriched aluminium containing coatings during elevated temperature exposure, these scales have a reputation for exfoliation on thermal cycling because the supply of aluminium in the coating layer is limited and would be rapidly depleted by exfoliation. Once significant depletion has occurred, less noble and faster-growing less protective oxide scales form, leading to the relatively rapid degradation of the hardware component. [11]. At a sufficiently high concentration of reactive element in the surface layer of the substrate, the adherence of the alumina scale to the substrate becomes excellent. In addition, the protective properties of the scale are also improved. [12]. In general, a small amount of Y addition is beneficial to scale adhesion rather than significant addition [13].

### **2. 3. 5 Role of Rhenium**

There exists very limited information on the role of Re in bond coat developments. However, in a recent paper it has been shown that the addition of Re considerably

decreased the oxidation rates of NiCoCrAlY- type overlay coatings, but even more markedly improved the thermal cyclic fatigue behaviour [47].

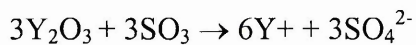
It is suggested that the improvement against oxidation and corrosion is due to the formation of a CrRe- rich alpha- phase below the oxidation layer; this phase influences the activity of Al to produce a dense Al<sub>2</sub>O<sub>3</sub> oxide layer. The additional phase in comparison to the three-phase mixture of the old MCrAlY coating is probably the reason for the improved thermal mechanical properties of MCrAlY coatings containing Re. However, further work needs to be carried out to fully understand the precise role that Re takes in improving both the microstructure and how the improvements are originated in the coating [14].

## 2.4 Effect of Residual Elements and Contaminants on Thermal Barrier Coatings

### 2.4.1 Sulphur

Sulphur and its derivatives are the most common pollutants found in high temperature application environments[48] . A thermal barrier coating which experiences this environment for example in turbines is always in contact with these corrosive additives which come from the fuel. It will associate with sodium from the turbine environment and will form very corrosive  $\text{Na}_2\text{SO}_4$  [49,50].

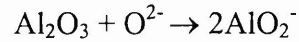
The lifetime of TBC with yttria stabilized zirconia overlay is reduced by the wear resulting from reaction of Yttria with sulphur. The reaction is shown as the following equation [4]:



The sulphur also segregates to the bond coating of the TBC, which weakens the cohesive bond between the scale and the adjacent metal and thereby increases the tendency of the scale to exfoliate under thermal condition [51]. For example in gas turbines, the corrosive  $\text{Na}_2\text{SO}_4$  that deposits will dissolve the protective oxide. It forms a sulphur phase over a wide range of  $\text{SO}_3$  and  $\text{O}_2$  in the alloy which will destroy or prevent the formation of a protective oxide scale.

The reaction between  $\text{Al}_2\text{O}_3$  (which is an important compound in the bond coat) and  $\text{Na}_2\text{SO}_4$  will form  $\text{NaAlO}_2$  or  $\text{Al}_2(\text{SO}_4)_3$  which has considerable effect on the oxidation rate

of the coating. In this reaction,  $\text{Al}_2\text{O}_3$  will either donate oxygen ions to or accept oxygen ions from the  $\text{Na}_2\text{SO}_4$  as shown in the reaction equation below:



When  $\text{Na}_2\text{SO}_4$  is present in condensed form as opposed to the vapour, it appears that the  $\text{Na}_2\text{SO}_4$  mostly serves as a barrier to oxygen and affects the equilibrium stage. Hence hot corrosion occurs as the cause of the reactions that destroy  $\text{Al}_2\text{O}_3$  that protects the substrate from corrosive substances. This condensed form can occur when the turbine temperature is increased up to  $800^\circ\text{C}$ , although the melting point of  $\text{Na}_2\text{SO}_4$  is at  $883^\circ\text{C}$  [6].

This above illustrates why sulphur is very harmful to the top coat and bond coat of the TBC for high temperature applications. The best solution to this problem is the complete removal of the sulphur and this can be achieved in many ways [52].

Repeated oxidation and polishing of for example a pure NiCrAl alloy, lowered the sulphur content from 10 to 2 parts per million by weight (ppmw), presumably by removing the segregated interfacial layer after each cycle. Total scale spallation changed to total retention after 13 such cycles, with no changes in the scale or interfacial morphology.

Another effective way of suppressing the segregation of sulphur is by hydrogen annealing . The physical processes of actually achieving an effective thermal barrier coating via the methods of sulphur removal are continuously improving as technology is continuously

advancing. If a thermal barrier coating is to perform to its maximum potential the element of sulphur has to be either fully removed, or suppressed to eliminate its detrimental effects . This therefore will ensure that the coating will last its full working life. The effect of sulphur on LCBC has not been studied. Whether it is beneficial or detrimental needs to be evaluated.

In summary sulphur is a contaminant in all metal alloys that can severely affect the strength of the material. At elevated temperatures, it can thermally diffuse to grain boundaries, coating interfaces, and ultimately, to the free surface. In the case of TBC's and in particular  $\text{Al}_2\text{O}_3$  protective coatings of Ni-based superalloys used for jet engine blades, the sulphur segregates to the coating interface and weakens the bond causing massive spallation of oxide layer.

#### **2.4.2 Silicon and its oxides**

The thermal cycling resistance of plasma sprayed zirconia –7 wt.% yttria thermal barrier coatings (TBC's) has been examined as a function of silica impurity level [54].

The properties of zirconia and other ceramic materials can be strongly affected by silica impurities [54]. From a common observation, many ceramic materials when examined by transmission electron microscopy (TEM) showed that there was a distinct amorphous grain boundary phase present as a result of sintering additives or powder impurities [55].

In bulk zirconium based ceramics, silica segregates to grain boundaries, then excessive amounts of silica is collected at the triple point [54]. One of the examples that has been found is Y-TZP (Yttria-stabilized tetragonal Zirconium polycrystal). The amorphous phase

that is present in Y-TZP is  $\text{SiO}_2$  rich and is due to contamination from two principle traditional milling media. At high sintering temperatures, a liquid phase which remains as a glass upon cooling is formed by a combination of these and other trace impurity oxides.  $\text{Y}_2\text{O}_3$  and possibly some  $\text{ZrO}_2$  from the surrounding grain have also been found in this glass phase in Y-TZP [55].

The silica content in this glass phase not only leads to a change in the size and shape of grains, but it also dissolves  $\text{Y}_2\text{O}_3$  from the  $\text{ZrO}_2$ - $\text{Y}_2\text{O}_3$  grain boundary region leading to localized destabilization. Since the concentration of the  $\text{Y}_2\text{O}_3$  in the glassy grain boundary is low, the high concentration of  $\text{Y}_2\text{O}_3$  in the  $\text{Y}_2\text{O}_3$ - $\text{ZrO}_2$  phase will diffuse to low concentration of  $\text{SiO}_2$  glassy grain boundary. This will affect the property of the structure phase since  $\text{Y}_2\text{O}_3$  is very important in stabilizing the  $\text{ZrO}_2$  for use at certain application temperatures [56]. The lower the amount of  $\text{Y}_2\text{O}_3$ , the less stable is  $\text{ZrO}_2$  at high temperature.

Silicate liquid phase acts as a sintering aid for partially stabilized zirconia. The excess liquid phase can accommodate the thermal expansion mismatch in the tetragonal phase. The faceted tetragonal  $\text{ZrO}_2$  grains with a minimum of glassy phase would be expected to have the highest toughness as well as transform to monoclinic. Rounded corners of the grains reducing stress concentration typified by shape faceted corners [54].

The high temperature flow stress can be lowered by a small addition of grain boundary glassy phase. The flow stress is most effectively lowered by the lithium silicate glass. The

tetragonal zirconia polycrystal (TZP) which contains 5 wt. % lithium silicate glass deform superplastically even at 1100°C [57].

Silica can cause dramatic increase in sintering rates [54] and decrease in electrical conductivity [58]. It may also lead to increased creep rates, as has been observed with silicon-based ceramics [59]. This is due to naturally brittle properties of glassy phase which have low creep resistance.

Silica impurities are also common in zirconia plasma spray powders and therefore may similarly influence the properties of plasma sprayed  $ZrO_2$ - $Y_2O_3$  thermal barrier coatings [60,61]. In addition to the effects observed for bulk ceramics, silica present in plasma spray powder affect the tendency of a sprayed powder particle to stick to the target, thereby affecting the as-deposited microstructure and porosity of the coating [62]. Increased sintering rates, increased creep rates, and a change in as-sprayed density all could act to increase residual stresses and decrease the thermal cycle life of the ceramic layer of a TBC.

The addition of silica also yield a small, but statistically significant, decrease in coating density and an increase in surface roughness with increasing levels of silica[54].

To summarise, silica is classed as an impurity in Zirconia based TBC's and can have a large effect on its physical properties [63]. Less than 1 mass % can drastically affect the thermal cyclic properties of the TBC, leading to a reduction in the number of thermal cycles to failure (plasma spray coatings). It is known that silica, present in small concentrations,

will tend to segregate to the grain boundaries of a bulk ceramic modifying the grain structure and orientation. Silica can dissolve Ytria and segregate to grain boundaries whilst increasing thermal creep rates [63]. In a recent paper [64] the results of an investigation on a TBC shows the complex microchemistry of the fracture surfaces, where segregation of bulk dissolved impurities such as Si, Al, Fe, and Na of the stabilizing yttrium oxide takes place from 1170K. The small area x-ray photoelectron spectroscopy (SAXPS) and small-area-x-ray-induced auger electron spectroscopy (SAXAES) results indicate that chemical composition of the segregated phase is ascribable to an infinite chain silicate of sodium with a variable presence of Fe, Y, and Al as a function of temperature. The SIMS ion images suggest, further, that the aluminium and yttrium segregate both at the silicate segregated regions as well as separately.

#### **2.4.3 Effects of Sodium and Phosphorus**

Sodium is classed as an impurity in TBC. There exists very little information regarding the effect of Na & P on the performance of bond-coats and TBC's, although it is known that Na can cause hot corrosion as a result of the potential level within fuels (0.5 ppm). Also there exists no information as regards use of GDOES to investigate sodium effects. In a recent paper [64], however, (SAXPS), (SAXAES) and secondary ion mass spectrometry (SIMS) have been used to investigate segregation phenomena at fracture surfaces of 8 mass %  $Y_2O_3$ - $ZrO_2$  plasma-spray thermal barrier coatings as a function of temperature up to 1620K.

## **2.5 Degradation of Thermal Barrier Coatings**

The degradation process of TBCs was studied by means of a comprehensive literature review [65,66,16,17,19]. During varying test conditions the most significant findings have been compiled in this thesis. Failure of TBC's may arise from the thermal expansion mismatch between the components, mechanical stresses induced by thermal gradients, ceramic sintering, phase transformation, bond-coat oxidation, bond coat in-elasticity, corrosive and erosive attack, residual stress due to deposition, and adverse component geometry.

Among these, the life time of the coating is limited by three main parameters:

- interdiffusion of substrate/coating (solid-state diffusion)
- excessive bond coat oxidation
- mismatch coefficient of thermal expansion

### **2.5.1 Interdiffusion**

Diffusion of aluminium into the base metal and base-metal elements into the coating, reduce the concentration of aluminium in the coating that is available for forming alumina. A protective oxide layer can no longer re-form after spallation once the aluminium concentration falls below a certain level. The basic concepts of diffusion are well understood for simple systems, and the diffusion of complex, multi-element systems containing multiple phases can be formally described [66]. Obtaining actual interdiffusion coefficients and predicting the interdiffusion in these systems is a formidable task.

Consequently, reliance on empirical measurements of interdiffusion is necessary and usually sufficient for engineering purposes.

## **Degradation of Diffusion Coating**

### **NiAl Alloy**

During initial exposure to an oxidizing environment, NiAl type coatings often form  $\gamma$ -Al<sub>2</sub>O<sub>3</sub> scale that tends to spall off easily. Then a more dense adherence scale of  $\alpha$ -Al<sub>2</sub>O<sub>3</sub> forms and protects the interior from further oxidation. This film will perform outstanding protection when its mechanical integrity is maintained. Unavoidable thermal cycling imposes alternate tensile and compressive stresses on the oxides, causing shearing and spalling to occur. This leads to some Al loss from the surface creating a depleted zone immediately underneath. Although the spallation, depletion, and replenishment of the original Al-rich NiAl coating gradually converts to a hypostoichiometric (Ni-rich) NiAl. Additional stresses that generate during cooling from a martensite transformation will further enhance the degradation process. At certain critical compositions, the coating is no longer a single-phase and  $\gamma'$ -Ni<sub>3</sub>Al begins to precipitate. Appearance of  $\gamma'$  in the coating is responsible for changing the oxidation mode, since it oxidizes to give NiO and/or NiO-Al<sub>2</sub>O<sub>3</sub> spinels, since mass transport is normally easier in these oxides than in Al<sub>2</sub>O<sub>3</sub> the coating begins to oxidize at an increased rate. Oxides such as NiO are often observed in porosity during growth. For this reason the appearance of  $\gamma'$  in Ni-Al based coatings marks the beginning of its demise [67].

If the coating is exposed to a further extent,  $\gamma' + \gamma$  phase will be precipitated. The  $\gamma$  phase is more susceptible to oxidation than the  $\gamma'$  phase and forms a voluminous, porous, multiphase, non-protective scale. Obviously, the coating is undergoing composition and structural changes and the substrate does not remain inactive. With the help of diffusion force, during early stage of the life of a coating, Al is expected to enter the Ni substrate from the coating, but as the coating degrades to assume a Ni-rich composition, Ni begins to enter the coating from the substrate, and leads to Kirkendall void formation immediately behind the coating-substrate interface [68].

### **Degradation of Overlay Coating**

#### **MCrAlY Alloys**

The extension of aluminized coating life with respect to degradation is rarely achieved by Al alone. In its simplest form it is a dual metal system such as Ni-Al, Co-Al, Cr-Al or Pt-Al and at most complex like MCrAl-X1 or MCrAl-X2 (overlay coating).

Chromium is an essential additive in all aluminide systems as it influences the stability, coherence and continuity of the  $\alpha$ -Al layer or as major component or minor component beneath the chromia layer. The function of MCrAl coating is to be able to form a protective barrier layer of  $\alpha$ -Al and chromia. Degradation means failure of these coatings of its coherence composition and cannot repair or sustain the barrier layer. The actual rate of the failure mechanism depends on the interaction of several parameters: the environment composition, particulate effect/velocity, and temperature [69].

The degradation pattern of NiCrAl or CoCrAl systems change very drastically when the corroding environment changes from oxide  $O_2$  to  $SO_2/NaCl$  environment coherence and subscale composition. However, in pure  $O_2$  environment the NiCrAl alloys have more protective and adherent ability than CoCrAl alloys.

### **2.5.2 Bond Coat Oxidation**

Oxygen can easily diffuse to the metallic bond coat owing to the high porosity, segmentation and ionic conductivity of the  $ZrO_2$  topcoat. The bond coat suffers oxidation attack. An oxide layer builds up between the bond coat and top coat and the relative expansion causes internal stresses at the interface. When the oxide layer reaches a critical thickness, cracks can first be observed; with increasing oxidation attack, the ceramic spalls off. Bond coat oxidation influences thermal shock resistance; with increasing oxidation, the number of thermal shock cycles to failure is reduced [70].

### **Spalling mechanism in TBC's**

The spalling mechanism of TBC's can take many forms and the major mechanisms have not as yet been identified [70,71]. However, a general mechanism has been recognised and this can be broken down into two areas - initiation and propagation.

### **Initiation of Spalling of Thermal Barrier Coatings**

Initiation of the spallation mechanism can occur in several different ways. Oxidation of thermal barrier coatings occur generally between the bond coat and the top coat. Oxygen diffuses through the TBC due to porosity, segmentation, and ionic conductivity, and

attacks the metallic bond coat. Oxide builds up at the interface and when it reaches a critical thickness it causes the top coat to crack (See fig. 2.5.2 (a) ) [16]. Oxide grains protrude into these cracks and also into imperfections such as pores in the top coat, causing the top coat to begin to split up.

Oxidation of the bond coat can have the effect of decreasing its ductility through the formation of additional oxides at the top coat/bond-coat interface [71]. This is detrimental to the TBC because in a coating that has not been oxidized, stresses caused by differences in the coefficient of thermal expansion (CTE) of bond-coat and top coat are relieved by plastic flow of the bond coat. If the ductility is reduced by oxides then the bond-coat cannot flow as freely and so cracking may occur [63].

### **Propagation and Spalling**

There are four propagation and spalling mechanisms that apply to the top-coat of a thermal barrier coating. After the initiation of spalling of the top coat at sites adjacent to protruded NiO pegs, spalling may continue to propagate via one of the following routes:

- Along lamellar splats in the top coat (route 1)
- Along the top-coat/bond-coat out-grown oxide scale interface (route 2)
- Along the bond-coat out-grown spinel oxides/ $\text{Al}_2\text{O}_3$  interface (route 3)
- Along the bond-coat out-grown  $\text{Al}_2\text{O}_3$  /metallic bond-coat interface (route 4)

All of these routes can be seen in figure 2.5.2(b) [71].

In thermally cycled specimens, spalling is hardly observed to propagate through routes three and four. Generally, spalling takes place through routes one and two, that is, along lamellar splats within the top-coat and along the top-coat/bond-coat out-grown oxide scale interface. This is due to the bond-coat being able to 'relax' after heating and negates the possibility of cracks forming at the bond-coat out-grown spinel oxides

(Ni [CrAl]<sub>2</sub>O<sub>4</sub>) / Al<sub>2</sub>O<sub>3</sub> or bond-coat out-grown Al<sub>2</sub>O<sub>3</sub> / metallic bond-coat interfaces.

However, for isothermally exposed specimens, inter-facial bond-coat oxidation induced stresses cannot be relieved by operationally induced cracks. This leads to spalling of the top-coat by propagation through the bond coat out-grown spinel oxides/Al<sub>2</sub>O<sub>3</sub> and bond-coat out-grown Al<sub>2</sub>O<sub>3</sub>/metallic bond-coat interfaces.

Nevertheless, the effects of spalling can be reduced by the application of an Al<sub>2</sub>O<sub>3</sub> diffusion barrier. This is applied to the bond-coat by a reactive sputtering process prior to the top-coat being applied. The thickness of this diffusion barrier varies from 2 to 5 µm. With this diffusion barrier the oxidation behaviour is strongly influenced. The thicker the diffusion barrier, the lower the oxidation attack of the bond-coat [16]. The diffusion barrier slows the growth rate of the oxide-layer, and after 250 operating hours the thickness of the thermally grown oxide layer can be reduced by as much as 70% [16].

This means that the volume expansion due to oxidation attack is also reduced and therefore the stresses inherent to this system are also reduced. This means that the life of the component is increased.

With the use of a diffusion barrier the oxidation resistance of the bond-coat and the adhesives strength of the ceramic top-coat are both increased. This means that failure due to spalling of the top-coat is decreased.

### **Residual Stress**

Degradation can be significantly increased by residual stresses that depend on a variety of mismatch strains and their resulting mismatch stresses. Liquid-solid volume shrinkage is often large in ceramics (not  $< 10\%$  for  $ZrO_2$ ), resulting in large tensile stresses in all coating processes. Subsequent porosity leads to stress concentrations but under normal cooling they are not a source of residual stress [10].

### **2.5.3 Thermal Expansion Mismatch**

The thermal shock resistance of TBC's is controlled by the thermal expansion mismatch between the zirconia top coat and the metallic substrate (figure 2.5.3). TBC's with yttria partially stabilized zirconia top coats show better thermal shock resistance than top coats with other chemical compositions [18]. By segmentation of the ceramic top coat or optimization of the porosity, further improvement in thermal shock resistance is possible [19,20].

## **Elastic Anisotropy**

Any textured coating, local or throughout, will have mismatch strains. These result from the elastic anisotropy that occurs in essentially all crystalline materials; they are considerably enhanced by any thermal expansion anisotropy (i.e. materials not of cubic structure). Solid deposition processes such as sputtering and chemical vapour deposition commonly produces textured coatings [10]. Cubic zirconia's elastic anisotropy is unknown. Coatings exhibiting the best adherence and resistance to thermal cycling have a random texture (elastic anisotropy effects are minimized) [16].

## **Phase transformations**

Zirconia is polymorphic, it is monoclinic from RT to 1100°C, tetragonal to 2370°C, and cubic to 2680°C. The unusually large (~ 9 vol. %) tetragonal-monoclinic expansion of unstabilized zirconia is a source of very large stresses. Transformation occurs along one crystal axis, therefore the effect is greatly increased by texturing. Partial stabilization, using 6-8 wt. % yttria, reduces the transformation temperatures and minimizes this effect. Optimum stabilizing precipitates are ~ 0.2 microns, larger particles result in microcracking. The transformation toughens the matrix via crack tip blunting therefore hindering crack propagation [16].

Transformation still partly occurs with partially stabilized zirconia, but PSZ's thermal shock resistance and linear thermal expansion coefficients are superior to fully stabilized zirconia's. Zirconia may suffer stabilizer loss during processing or thermal/corrosive exposure.  $Y_2O_3$  has higher stability in zirconia than MgO or CaO and is therefore preferred.

No  $Y_2O_3$  loss occurred in plasma sprayed zirconia coating on a turbine vane after 300 hours service with an average vane temperature of  $670^\circ C$ . Non-uniform stabilizer distribution, occurring during processing or usage, may result in formed regions of the monoclinic phase [10,16].

## 2.6 Bonding Mechanisms

The bonding mechanisms at the coating/substrate interface and between the particles making up the coating is an area which in many cases is still subject to speculation [65,72]. It generally suffices to state that both mechanical interlocking and diffusion bonding occur.

Bonding Mechanisms:

- Mechanical keying or interlocking.
- Diffusion bonding.
- Other adhesive, chemical and physical bonding mechanisms-oxide films etc.

Factors affecting bonding and subsequent build up of the coating:

- Cleanliness
- Surface area
- Surface topography or profile
- Temperature (thermal energy)
- Time (reaction rates & cooling rates etc.)
- Velocity (Kinetic energy)
- Physical & chemical properties
- Physical & chemical reactions

There exists currently no published literature on the bonding mechanisms involved in LCBC systems currently under development at Rolls Royce. However, information on other bond-coats mentioned in literature surveys exists and is reviewed below and will be used in a basis of study of bonding mechanisms for the proposed LCBC systems.

Various models have been proposed in order to predict coating performance. The two principal models for the diffusion coatings examine the roles of oxide scale spallation and interdiffusion. The diffusion model proposed by Smialek and Lowell [73] notes that in cyclic oxidation tests, significant differences are observed in the behaviour of comparable thickness of bulk NiAl and aluminide coatings on various nickel base superalloys. They concluded that as a result of interdiffusion, the aluminium level is decreased to the level where spinel oxides form, and then spallation becomes the predominant cause of the continued loss of alumina. Thus, while diffusion may not account for most of the aluminium lost in a severely degraded coating, it is responsible for the initiation of the coating degradation process.

The alternative model [73] relates spallation of the scale to the magnitude of the stresses associated with the differences in coefficients of thermal expansion between the oxide and the substrate and the weakness of the bond between the oxide and the substrate. The continuous repetition of formation and spallation leads to aluminium depletion and a resultant acceleration of oxidation. This same model is also used for overlay coating.

## **Chapter 3**

### **3.0 Experimental Development**

Low cost bond coat (LCBC) systems with additions to substrate and coatings were characterised to increase understanding of failure modes in TBC systems and adhesion process. These systems are described in detail as part of the experimental developments. The sample productions were carried out at Rolls Royce and were received in button form for characterisation using techniques such as GDOES, SEM and TEM.

### **3.1 Coating Systems**

#### **The Production of Low Cost Bond-coats**

These bond-coats have been developed specifically for TBC's. The basis of the bond-coat is a simple thin layer of Pt electroplated onto the surface of the superalloy substrate. In all cases the superalloy used was CMSX-4, the composition of which is given in figure 3.1a with a comparison to alloy RR3000.

Figure 3.1a Typical composition of alloys CMSX-4 and RR3000

Alloy	Nominal Composition mass %									
	Ni	Co	Ta	Cr	W	Al	Re	Ti	Mo	Hf
CMSX-4	Bal.	9.6	6.5	6.4	6.4	5.6	3	1	0.6	0.1
RR3000	Bal.	9.5	8.5	6.2	6.5	5.5	6	0.3	0.6	0.1

The sample is then heat treated in a vacuum furnace for 1 hour at 1150°C. A Ni based  $\gamma/\gamma'$  region is then formed at the surface of the substrate. The  $\gamma'$  phase is the bright phase that can be seen after etching ( Figure 3.1(b)). This  $\gamma'$  phase is a  $\text{Ni}_3\text{Al}(\text{Ti}, \text{Pt})$  phase with almost the same structure as the  $\gamma$  phase but has a slight misfit with the matrix.

The simple low-cost system has been tested before at Rolls-Royce but not extensively. The systems tested in this thesis include the base low-cost and several enhanced versions of this type of coatings.

### **3.1.1 LCBC with additions to substrate**

The first enhanced low-cost systems to be tested, used reactive element additions to the substrate to see what effect they had on the TBC life. Some of the compositions/systems used include:

- Pt + CMSX-4
- Pt + CMSX-4 + La
- Pt + CMSX-4 + Y + La
- Pt + CMSX-4 + Ce

The results from the isothermal soaks of the button test specimens can be seen in the thermal cycling results chapter 5.

### 3.1.2 LCBC with additions to coatings -Sputtered additions

These samples were produced by ion sputtering a thin layer of Ni ( acts as a carrier ) usually  $2\mu\text{m}$  containing different active element additions ( Ni + X where, X= active element ), directly onto the substrate before the Pt layer was applied.

For this coating process an inert gas, usually argon, will flow into the process chamber of a Physical Vapour Deposition (PVD) coating machine with a pressure below 1 Pa. By application of a DC voltage or AC voltage a glow discharge will be started within the gas environment. The chamber walls are polarized as the anode, the coating material - called target- as the cathode. The inert gas ions generated in the glow discharge are accelerated to the negative target and sputter atoms and molecules from the target primarily by momentum transmission. The sputtered particles expand within the vacuum chamber and condense on the substrates ( CMSX-4) as well as on the other surfaces in the chamber. The test samples were then subjected to a diffusion heat treatment in a vacuum furnace at  $1150^{\circ}\text{C}$  for. The aim was to form through diffusion a  $\gamma/\gamma'$  layer which should be strengthened by X. The composition/systems used are shown in page 58. The objectives were to try and answer:

- What role does the active element play in improving coating performance?
- Does it really combine with the surface?
- What would be the maximum level of active element addition?
- The diffusion process involved

### 3.1.3 Process Parameters / Compositions

Table 3.1.3 : Enhanced Low Cost Bond-coats

As Processed Sample Code	Cyclically Tested to Failure Code	Coating System
-	422.NB.100	Reference
227/1	422.GB.500	Sputtered Ni + 0.23wt% Hf
227/2	422.HA.300	Sputtered Ni + 2.27wt% Hf
227/3	422.IB.700	Sputtered Ni + 6.10wt% Y
227/7	422.PB.700	Sputtered Ni + 0.5wt% Y
227/9	422.TB.700	Sputtered Ni + 0.58wt% Y + 1.60wt% Hf
227/11	422.VB.700	Sputtered Ni + 0.43wt% Y + 1.75wt% Hf
-	422.DB.100	CMSX-4 + 22-26 ppm Ce
-	422.CB.100	CMSX-4 + 20-25 ppm La + Low cost
-	422.BB.100	CMSX-4 + 8-14 ppm Y + 12-18 ppm La
227/6	-	CMSX-4 + Y
228/1	-	CMSX-4 + 6-8 ppm Y + 11-13 ppm La
228/7	-	CMSX-4 + Pt
227/5	-	Sputtered thin MCrAlY + Pt
228/3	-	CMSX-4 + Ce + Pt
228/2	-	CMSX-4 + La + Pt
227/4	-	Sputtered thin MCrAlY

## **3.2 Analytical Characterization**

The characterization of bond-coats and TBC is essential for quality control and research and development purposes. The techniques available include; scanning electron microscopy (SEM), transmission electron microscopy (TEM), x-ray fluorescence spectroscopy (XRF), x-ray diffraction (XRD), and glow discharge optical emission spectroscopy (GDOES). It is possible to characterize the bond-coats and TBC's in terms of microstructure, phase equilibria, composition, and crystal structure, to gain a full evaluation of bonding and possible failure mechanisms.

### **3.2.1 Techniques Description**

#### **XRD**

X-ray diffraction is used to identify the types of phases present in powder, as-sprayed and heat treated coatings. XRD relies upon the diffraction of x-rays according to Bragg's law [74]. A diffraction pattern gives information about the crystal structure and lattice parameter of constituent phases. A very useful feature of XRD is to identify the preferred orientation of growth during coating manufacture. Whether this be the prominent growth direction of a single grain or to identify areas of growth occurring at different rates within the same layer. This technique is capable of analyzing each layer in multi-layered coating systems including extremely thin oxide films and interface microstructures.

X-Ray diffraction patterns were obtained on a selected bond-coat in the as processed and failed condition to determine phases present using an X-ray diffractometer Philips model PW1820 which is software controlled from a PC. The wavelength  $\lambda$  of the monochromatic

Cu  $\alpha$  radiation is  $1.54060 \times 10^{-10}$  m. The optimum voltage was found to be 12kV and the current 35mA in order to obtain peaks from the bond-coat. The peaks obtained were analyzed using computerized data processing facilities at Rolls-Royce plc. The results obtained are shown in figures 3.2.1.

### **XRF**

XRF is a method for the elemental analysis of solids and liquids. The technique involves irradiating the sample with an intense beam of x-rays, causing the emission of fluorescent x-rays, characteristic of the sample composition. The elements commonly detected range from sodium to uranium, but lighter elements from boron to fluorine may also be detected. The advantages of XRF include; quantitative analysis of bulk elemental composition, trace analysis to ppm levels, and is non-destructive [75].

### **Thermal Cyclic Testing**

The thermal cycling of bond-coats has been conducted at Rolls Royce to see how bond-coats perform at high temperatures.

Thermal cyclic test data was collected at  $1135^{\circ}\text{C}$ , each cycle being 1 hour at temperature and a 10 minute forced air cool. They represent the number of cycles required to cause the EB-PVD ceramic to spall, there is no applied external load. It is worth noting that the results can only really be compared to results from a like test and do not represent how the samples would perform at higher temperatures. Blocks with arrows attached represent the test piece is still on test and has not as yet failed (figures 5.1 & 5.2 ).

## SEM

The SEM is used primarily to study the surface, or near surface structure of bulk specimens, since the magnification and depth of field are superior, compared with optical microscopy. The SEM typically operates at 2 to 50 kV; a range of 15 to 25 kV is common for most metallurgical and ceramic applications. The electromagnetic lenses in the column are used to form a small-diameter electron probe ( $> 5\text{ nm}$  in diameter for most SEMs). A set of scan coils raster the electron probe over the specimen surface as an electron beam scans the inside of the Cathode Ray Tube (CRT) screen. At each point in the sample struck by the incident electron beam, several electron/specimen interactions occur that produce a number of different measurable signals, such as secondary electrons, back-scattered electrons, and characteristic x-rays.

The SEM can produce detailed photographs which can then be used for image analysis, producing statistical plots of the size and distribution of features on a surface.

The SEM can also be used to provide compositional information using EDX (energy dispersive X-ray analysis) analysis, to give qualitative and quantitative elemental information or WDX (wavelength dispersive) to provide more accurate quantitative elemental composition. The limitations of SEM being that analysis is restricted to the near surface, and compositional analysis is elemental, which makes distinctions between phases difficult [69].

Microstructural investigation of bond coat and also selected thermal barrier coatings (RT31) were carried out using a Philips fully computerized electron microscope -XL40.

Energy dispersive X-ray analysis was made using Oxford Instruments hardware and software.

## **TEM**

TEM typically operates at a voltage exceeding 60kV; 100, 120, or 200kV. TEM provides information about the internal structure of thin specimens. The TEM can be used to produce electron diffraction patterns, either spot or ring [76] which can provide information regarding crystal structure, lattice parameter and crystal orientation.

The main disadvantage of TEM is the thin specimen size, which makes sample preparations difficult, however, the major advantage being the possible examination of layered or zoned microstructures.

A Philips CM20 analytical microscope (200kV) equipped with EDX facilities for microanalysis, mapping and electron-diffraction facilities for selected area diffraction, convergent beam etc. was employed. Selected bond coat samples with a 2.5 $\mu$ m TBC were studied to develop a suitable method of study in terms of sample preparation, ion-beam thinning and analytical assessments.

### **3.2.2 Ion Beam Thinning Process Developments for the Study of Low Cost Bondcoats**

#### **Sample Preparations Procedure:**

The preparation of the transverse thin foil involves three sequential steps: sectioning, mechanical thinning to 20  $\mu$ m and final ion-beam thinning to electron transparency. The

various components (superalloy, bond-coat, thermal barrier top coat) thin at different rates under standard ion beam thinning conditions. A sequential step with the bond-coat thinning procedure had to be put in place in order for TEM assessment. The final technique developed that gave consistent samples is outlined below, first covering some theory which is essential in understanding this procedure.

### *Theory of Ion-Beam Thinning*

In recent years specimen preparation by ion-milling has become popular especially in dealing with composite systems and organic or inorganic regimes where other approaches to forming thin electron transparent sections are untenable. Of course any method for forming an electron transparent thin section which does not alter the regime nor create artifacts contributing to observations of the regime is acceptable. This includes smashing ceramic into flakes or shards or stripping thin layers from bulk specimens, cleaving small pieces, or other approaches. But to observe the interface between a ceramic fibre in a metal matrix or an insulating layer on a semiconductor normally precludes these approaches as well as any kind of electropolishing [77].

The principle of ion-beam thinning is extremely simple. A beam of inert gas ions or atoms is directed at the specimen from which it removes surface atoms in a process known as sputtering. If this can be achieved without the creation of artefactual damage then ion-beam thinning is an ideal method for preparation of foils from both conducting and non-conducting materials.

Sputtering will occur when ions carrying more than about 100 eV of energy hit a surface. The number of atoms ejected by each incident ion or atom is known as the sputtering yield,  $Y$ . In general,  $Y$ , and hence the thinning rate increases as the ion energy increases and as the atomic mass of the specimen decreases. The desire for high sputtering yield but no chemical change in the specimen dictates the use of argon. Lighter inert gasses (helium and neon) thin more slowly and heavier inert gases (krypton and xenon) are too expensive. Figure 3.2.2.a. shows the relationship between ion energy and sputtering yield. Initially,  $Y$  increases with ion energy but eventually at high energies the incident ion is deposited far below the surface and fewer surface atoms are ejected. The optimum energy is thus somewhere in the range 1-10 keV, and a value between 3 and 5 keV is generally used.

Automatic termination of thinning is available as above, as thinning of a single 50 $\mu$ m thick disc can take several hours, i.e. Thinning occurs at a few tenths of microns per hour [78].

### **Cross sectional preparation for transmission electron microscopy**

The coated specimen used for cross-sectional analysis had to be carefully prepared in order to get successful results reflecting the real microstructure and composition of the tested specimen [79,82].

In general the specimen preparation procedure developed is the following [79]:

- Specimens are cut into 0.5mm x 1.2mm x 3.0 mm slices as shown in figure 3.2.2.b

- Sectioned slices are mechanical ground and polished on one side to a thickness of 100 $\mu\text{m}$  and a finish of 1 $\mu\text{m}$ .
- The reverse side is further thinned and polished to make a foil with thickness of 10 to 20 $\mu\text{m}$  and a finish of 1 $\mu\text{m}$ , figure 3.2.2 ( b to h ).
- Final thinning for electron transmission is performed using argon ion-beam thinning , which basically consists of 3 thinning stages ( rough polish) performed by both guns separating with a low angle of ion incidence at starting 10° to 5°, with different keV :

#### Stage 1

Accelerating voltage of 5.5/6 keV with a current of 7-10 $\mu\text{A}$  and both guns separately with a low angle of ion incidence 10° for 30 min .This produces very quick wear, in fact reduced sample thickness from 20 $\mu\text{m}$  to 10/5 $\mu\text{m}$ .

#### Stage 2

Accelerating voltage of 5 keV with a current of 7-10 $\mu\text{A}$  and both guns separately with a low angle of ion incidence 7° for long as necessary until a hole appears in the sample.

Accelerating voltage of 4 keV with a current of 7-10 $\mu$ A and both guns separately with a low angle of ion incidence 5° for long as necessary until the hole is enlarged and thin enough for all areas to be studied: substrate, bond coat and TBC.

### Stage 3

Final polishing stage is more of a cleaning step, as follows: Use an accelerating voltage of 2.5 keV with a current of 7-10 $\mu$ A and both guns separately with a low angle of ion incidence 10° for 1.5min.

It is very important to note that the TEM sample preparation time is significantly reduced as a result of having thinned the cross section mechanically down to 15-20 $\mu$ m. Also, use of a clamp type specimen holder had the advantage shown compared to the glued on method ( see figure 3.2.2.c ).

## **3.3 GDOES Depth Profile Analysis to Investigate Bond coats and TBCs**

### **3.3.1 General Overview and Analytical Requirements**

GDOES is an analytical technique used in the study of solid surfaces and surface films. It provides chemical composition data from both the surface and sub-surface regions. GDOES is an atomic emission technique relying on the excitation of atoms within the sample being analyzed (figure 3.3.1.a & b ). The solid sample is sputtered under vacuum into the form of a low-pressure gas. The atomic species are excited by an energy source and decay by emitting characteristic light which is analysed by a Polychromator to determine chemical composition (figure 3.3.1(b) ). Sputtering rates of between one micron and tenths of

microns per minute are possible depending on the size of the sampling area and equipment parameters. Minimal sample preparation, easy operation plus rapid results enable low cost material characterization.

GDOES in addition to detecting all metals it is also capable of detecting non-metallic elements, namely O, N, H, S, P, and B, all of which have limited detectability by other analytical techniques. With respect to TBC's non-metallic are of great interest when considering oxidation/corrosion products. A major application for GDOES is depth profiling, which can provide concentration profiles down to depths of between 10nm and 100 $\mu$ m (figure 3.3.1(d) ). This process can provide both qualitative and quantitative information as follows: Chemical composition of the coating and substrate; coating thickness; layer homogeneity; interface quality; elemental diffusion at the interface and type of contamination and penetration depth at the surface and /or interface [82,83,84].

The glow discharge spectroscopy work on bond-coats was carried out on a LECO GDS-750 QDP glow discharge spectrometer.

The following optimized operating conditions shown in table 3.3.1(e) were used. Both qualitative and quantitative studies were performed, qualitative studies produced a plot of the intensity over time for a given element.

## **Chapter 4 Results: GDOES Studies**

### **4.1 Development of Quantitative GDOES Depth Profile Analysis to Investigate Bondcoats and TBCs**

#### **4.1.1 GDOES Quantification Process Route**

GDOES quantification was split into two parts: determination of the sputtered depth from the sputtering time and sputter rates of individual elements; and determination of the chemical content from the emission line intensities. The sputter rates can be calibrated from sputter depth measurements. The emission line intensities are dependent on the voltage, current and sputtering rates, as well as the chemical composition. Normally the intensity calibration is performed using certified reference materials of known chemical composition. During depth profile quantification the analyzed composition is normalized to 100%.

The steps involved in setting up a quantification program for the superalloy turbine blade assessment are shown in figure 4.1.1a and the necessary optimised condition in figure 3.3.1 (e).

#### **4.1.2 Standards and Pre-compositional Analysis**

A total of 49 calibration standards were used to calibrate the superalloy turbine blade coatings quantitative program, covering most of the elements in the coatings. In order to ensure that reliable results were obtained, the standards were selected so as to cover the

elemental concentration range in the coatings. Table 4.1.2 shows an overview of the calibration elements and analytical range with the selected standards.

EPMA using WDS was used to perform chemical analyses on both the CMSX-4 and RT31 samples to enable comparisons to be made with GDOES and XRF results.

As the substrate alloys and coatings were multi-phased systems, a straight forward single line scan would contain a lot of scatter as different phase compositions were crossed by the scanning electron beam. In order to reduce this problem a series of 'point' analyses at one micron intervals were taken. At each point the beam of the probe was 'rastered' along a 50  $\mu\text{m}$  line normal to the line produced by the series of analyses to form a 'ladder' scan. This enabled an average band (50 $\mu\text{m}$  wide) to be assessed.

#### **4.1.3 General GDOES Analysis of Bond-coat and TBCs**

The time-intensity curves and calculated quantification depth concentration profiles for CMSX-4 superalloy substrate are shown in figures 4.1.3a,b,c,d. Only elements Ni, Co, Al, (major ones) and Ti, Hf, W (minor ones) have been shown for the sake of clarity. The tendency for the lines to rise as time and depth increases is due to matrix effects resulting from differences in elemental sputtering rates at appropriate locations of isolated particular spectral wavelengths.

The crater produced during the analysis of CMSX-4 after 60 and 1000 seconds are shown in figures 4.1.3 e(i,ii) and their measurement by laser profiling is shown in figures 4.1.3 (f).

It can be seen that the bottom of the crater in figures 4.1.3 (i) is quite planar, while some re-sputtering of material has created a lip around the rim after 1000 seconds.

The laser profile depth measurement shows a good correlation to the calibrated depth values obtained from fig 4.1.3 c,d, with errors of the order of 10-15%. The roughness of the bottom of the crater normally increases linearly with time, which is one of the factors limiting the depth resolution. This necessitates a compromise between good depth resolution and high intensity spectral lines when selecting operating parameters.

The results of the GDOES and EPMA analyses are compared to the composition determined by XRF in table 4.1.3.h . Both results showed a good correlation, with the GDOES results generally closer than those of EPMA, although there were some obvious discrepancies which require investigation; the values obtained for nickel, between the spectral lines. The GDOES equipment is also not currently able to detect rhenium (Re), although Re is present in CMSX-4)

The trace obtained from the thermal barrier system (figures 4.1.3.i ) clearly distinguishes the different interfacial regions seen in the cross-sectional view (figures 4.1.3.j ). The elements identified within these regions agree with the EPMA analysis (fig 4.1.3.k ), with both techniques highlighting the yttrium concentrated at the ceramic/bond-coat and very low concentrations of elements such as sulphur, boron, carbon, and phosphorus. The results can also be obtained more rapidly with minimum sample preparation.

The current semi-quantitative program set up for turbine blade coating analysis is limited by the number of standards and calibration points used (table 4.1.2 ). For example, with a minimum of two calibration points it is thus possible to obtain a straight calibration line. It is, however, recommended to use a minimum of 5 calibration samples. The more calibration samples are used, then the easier to detect an inaccurate calibration sample, and if necessary, to make appropriate correction or deletion. In addition, extra elemental channel such as Re and additional elements need to be installed.

## **4.2 GDOES: investigation of LCBC System with Additions to Substrate / Coating**

### **4.2.1 Standard LCBC system with platinum additions – effect of Pt variability**

Addition of Pt to bondcoats such as diffusion aluminide coatings is known to improve their performance capability as surface protection systems for gas turbine blades [1]. Platinum is found to improve the coating ability to develop purer  $\alpha$ -alumina scale of a slower growth rate [2-5]. Although the underlying mechanism is not fully understood, most evidence points out that the role of Pt is to improve the diffusional stability of the coating restricting outward diffusional transport of substrate elements, particularly transition metals [2-5].

Platinum is first electrolytically plated onto the CMSX-4 superalloy substrate. Platinum plating is a complex process involving the electrochemical deposition of platinum metal onto superalloy components with complex shapes. Before plating, the turbine blades undergoes thorough cleaning and polishing cycles. This is essential to ensure binding of the platinum layer to the superalloy substrate. The blades are then mounted on a rack and checked to ensure high conductivity. As only certain parts of the turbine blades are to be plated, layers of resin are then applied to the blade root to mask it during the plating process. The parts are then rinsed in de-ionised water and further cleaned in an ultrasonic bath.

Platinum is then deposited in the plating tank. De-ionised water is first added to the tank, and the pH adjusted by the addition of ammonia. A platinum salt complex,  $\text{Pt}(\text{NH}_3)_2(\text{NO}_2)_2$ , is then dissolved in the solution. As de-ionised water is a poor conductor of electricity, several phosphate salts are added to improve electrical conductivity. These also aid pH control. Finally, the entire bath is heated to between 80 and 90°C. As a number of variables can adversely affect the plating thickness and quality, the system is stringently monitored. Temperature and pH are determined using appropriate sensors. The composition of the bath is routinely monitored using x-ray fluorescence (XRF) and atomic adsorption spectroscopy (AAS) and the required compounds replenished by addition of chemicals. Once the tank is ready and the temperature is between 80 and 90°C, the rack of blades is placed between two insoluble platinised titanium anodes. The blades act as the cathode of the electrical circuit. The platinum-based solution completes the circuit. Passing a current through the circuit leads to the decomposition of the platinum salt into platinum cations and residual anions. The positively charged platinum ions are drawn towards the negative cathode, which in this case is the turbine blade, and a thin platinum layer deposits here. Adjusting the current density, platinum concentration and the plating time allows precise control of the coating thickness. This process deposits thin, adherent, crack-free, ductile layers of platinum onto the superalloy substrate [ 39].

A diffusion heat treatment process is carried out at 1150°C for 1 hour after Pt plating in order to develop the low cost bond coat.

The objective of this work was two fold: (1) to determine whether GDOES was able to detect Pt and also distinguish between the different Pt thicknesses, because variation in bond coat performance under the same conditions and anode type could limit the application of TBC systems. (2) to determine how the cyclic performance of LCBC systems is affected by the Pt thickness variation and its overall effect on degradation mechanisms.

Presented in fig 4.2.1 are the GDOES Pt depth profiles for several selected Pt plated samples studied on a CMSX-4 substrate under different plating conditions and also in the heat treated and cyclically failed conditions as supplied from Rolls Royce. It should be noted that condition of plating has a direct affect on average number of cycles to cause failure of coating ( see chapter 5). The following plating conditions were applied: AHD 928 ( new tank containing pure plating solutions with new anode); E20 (old tank with a new anode with heavily used plating solution ); AHE63 (average plating solution tank with a new anode ).

The following comments can be deduced from the depth profiles shown in the figures 4.2.1:

(i) GDOES is able to detect and also differentiate between the different levels of Pt additions. Therefore, it is possible to highlight a failure in coating if it is due to thickness variation ( figures 4.2.1a,b,c). Also shown are the elemental profiles of Ni, Ti, Cr Al from bulk materials on each curves.

- (ii) New tank (cleaner solution) shows more tighter control in the Pt thickness than the other two E20 and AHE63 as seen from the GDOES depth profile comparisons.
- (iii) Pt thickness in all cases after 10 $\mu$ m of plating and heat treatment at 1150 $^{\circ}$ C shows a sharp drop as expected and increased diffusion into the substrate, whilst Ni shows a rise and reaches a plateau as expected, entering bulk material ( CMSX-4 substrate, fig 4.2.1 d,e,f). In addition, it will be observed that other elements such as Ti, W, Cr, Al diffused from the substrate to form the coating. Also, it is observed that the Al profile can be observed in general to be higher than that of the substrate, sufficient to selectively form the alumina scale, necessary to bond the thermal barrier coating.
- (iv) From the results of GDOES for all three different conditions studied it will be noticed that cleanliness of solution and anode type plays a key role in determining final coating thickness.
- (v) GDOES depth profiles of the failed samples (figures 4.2.1g,h,i ) shows in all cases higher levels of Ti,W,Ta diffusion at the bond coat / alumina oxide interface. These are undesirable elements which reduce the protective nature of the oxide scale. Also observed is a drop in the Al level compared to initial coating composition.

#### 4.2.2 Yttrium and Hafnium – Coating Additions

Active elements, such as yttrium and hafnium, added at low levels on alumina forming alloys have been shown to improve oxide scale adherence markedly on thermal cycling [45]. However, the actual role the active element plays has been subject to a great deal of debates as discussed in [45,10,13]. Several mechanisms proposed to account for improved cyclic performance include (1) oxide pegs which form and anchor the scale to the substrate [7], (2) increased scale plasticity produced by the alteration of the scale structure,(3) grading the mechanical property differences between the scale and the substrate, (4) modification of the scale growth mechanism and (5) elimination of pore formation by vacancy coalescence effects and improved chemical bonding between the scale and the substrate [7].

It was the objective of this study to understand the role of active elements on the cyclic performance of various low cost bond coat systems with different levels of additions to the coating ( see table 3.1 ), using the GDOES technique.

The procedure briefly involves the ion sputtering of a thin layer of Ni each containing the different active elements directly to the substrate prior to Pt plating and heat treatment to develop the coating.

GDOES was employed to study the chemistry of these coating systems i.e. the elemental depth profiles clearly demonstrate differences after the improved chemical bonding between substrate and scale ( see figures: 4.2.2.a,b,c,d,e,f,g,h,I,j,k,l,m,n,o,p ). The

plots are qualitative (i.e. signal intensity versus time of sputtering). All plots are between 400 and 800 seconds of sputtering time to provide sufficient necessary information to study the chemical bonding.

GDOES was able to clearly distinguish between the different levels of Hf additions (0.23mass% -sample 422GB500 and a combination of 0.58mass%Y and 1.6mass%Hf in sample 422TB700). However, GDOES was not able to detect Y < 0.5 mass % but was detectable only when concentrated to higher levels, for example 6 mass % (sample 422IB700).

It was evident that a higher level addition of Y ( 6 mass % ) to the bond coat, was not generally beneficial in terms of thermal cyclic test results ( see table 5.1 ) as compared to minimal addition of ( 0.5 mass % ). However, it will be observed that there is a slight shift of Y concentration towards the bond coat / alumina interface progressing from as processed to failed sample in these cases.

Comparisons of the GDOES curves for samples 422IB700 ( 285 cycles ) and 422PB700 (375) cycles showed the effect of Ta , Ti and W diffusion on failure. These elements are thought to be detrimental when diffused through the bondcoat [11 ], they tend segregate at the oxide scale and reduce the protective nature of the oxide scale.

### **4.3 GDOES : Investigation of the effects of residual and contaminants in LCBC**

#### **Systems**

##### **4.3.1 Effect of Silicon**

It has been shown in reference [63 ] that silica content has a direct effect on the life and performance of TBC. TBC life increases with decreasing silica level. Silica based impurities tend to segregate to grain boundaries with excessive amounts collecting at triple points. Silica at the grain boundaries leads to changes in the size and shape of grains, [56] and it may dissolve  $Y_2O_3$  from the  $ZrO_2$ - $Y_2O_3$  grain boundary regions leading to localized destabilization . Silica can also cause  $ZrO_2$  polycrystal superplasticity dramatic increases in sintering rates and decreases in electrical conductivity . It may also lead to increased creep rates, as has been observed with silicon -based ceramics [62].

The surface of the CMSX-4 superalloy is normally grit blasted prior to Pt plating in order to free the surface from grease and oxides and any other contaminants. The objective is to ensure that increased mechanical and chemical bonding is obtained, for the bond coat formation [45]. In addition for the final ceramic deposition another grit operation is performed.

The grit blasting process is carried out using mainly two types of alumina grit: brown and pink alumina. The window parameter for the gritting stage was wide and movement within this resulting in the part to part variation observed. The parameters are set at: 20-30psi and 220  $Al_2O_3$  grit ( brown or pink type). This allows considerable variation especially on the distance the component was held away from the gritting nozzle which remained undefined.

Under the worse conditions of high pressure and short working distance there was a real danger of removing the Pt layer.

Considerable variation in the development of LCBC has been observed in the past during Pt addition to the base alloy CMSX-4 and it has been thought that after analysis of the process route, the most likely cause of the variability was silicon contamination. The objective of this work is to assess whether silicon has any effect on the adhesion of the thermal barrier coating (TBC).

Work at Rolls Royce using EPMA has been unable to detect silicon, because it is below the detection limit of the instrument. GDOES results presented in figure 4.3.1a shows Si present in the as processed samples at the coating substrate interface. It should be noted these samples heat treated at Chromalloy (CUK), however in the failed samples the Si flattened (fig 4.3.1b). Initial thoughts were that the Si was coming from the gritting stage / heat treatment atmosphere. To eliminate the gritting effect, samples of both the pink and brown alumina gritted coatings were depth profiled. It is known that from certification pink which is more pure alumina grit contains less Si than brown. Results of GDOES traces as shown in fig 4.3.1c,d clearly showed Si to be present in both, at similar levels. This proved that the Si must be coming from either the processing or the actual CMSX-4 substrate material. Substrate material depth profiled results are shown in fig 4.3.1e and indicate little or no presence of Si.

In order, to understand the effect of silicon during cyclic testing for example, whether there is any diffusion of silicon taking place, results are shown on a failed LCBC ( fig 4.3.1b ). The results show the silicon to be leveling off towards the substrate in the GDOES trace, suggesting that diffusion was taking place. However, results obtained from similar LCBC samples that were heat treated at Rolls-Royce and CUK and then cyclic tested showed no difference in cyclic performance.

#### **4.3.2 Effect of Sodium**

Sodium has already been mentioned in the literature section and is regarded as an impurity. The presence of sodium has been shown both in the as processed and heat treated state by both GDOES and XRF techniques ( fig4.3.2a and b and table 4.3.2.d) on LCBC. Results show that sodium is present on the surface and as depth increases it does not follow the platinum profile as observed for phosphorous rather the sodium level decreased.

The sodium is most likely to originate from the salt used in the electroplating process. This salt contains Na, N,O and potentially P, C, S and Si.

Accepting that the GDOES results are correct, then it correlates with sodium already mentioned in reference 64, where it was demonstrated that the chemical composition of a segregated phase of TBC is ascribable to an infinite chain silicate of sodium. The actual quantity present is unknown, it must be above 50 ppm ( GDOES detection capability ).

Also it can be observed from fig 4.3.2(c) that sodium diffuses inwards i.e towards substrate from high to low concentration after heat treatment.

### **4.3.3 Effect of Phosphorus**

The aim was to check LCBC for presence of phosphorus, which is an impurity in bond coats, and understand its role in the degradation process. However, during the investigation the GDOES traces showed phosphorus interference i.e. there was an overlap between the platinum and the phosphorus line observed.

To confirm that it was a true interference pure Pt and Pt deposited by PVD process on a stainless steel substrate and a variety of LCBC samples were depth profiled and GDOES traces ( figs 4.3.3a,b,c) examined. In all cases the phosphorus signal followed the Pt trace.

## **Chapter 5**

### **Thermal Cycling Test Results**

Thermal cyclic test data was collected at 1135°C, each cycle being 1 hour at temperature and a 10 minute forced air cool. This isothermal test condition selection was based on a laboratory simulation of the high temperature period likely to be experienced by a typical engine. The test cycle is continued until the number of cycles required to cause the EB-PVD ceramic to spall is reached. The test is conducted with no applied external load. It is worth noting that the results can only really be compared to results from a like test and do not represent how the samples would perform at higher temperatures. Data points as seen in figures 5.1 and 5.2 with arrows attached represent test pieces that are still on test and have not as yet failed.

Test data are shown for: Enhanced LCBCs with; additions to coatings, additions to substrate, Pt variability samples and data for the effect of different types of alumina grit.

Table 5.0 Enhanced LCBCs average cycles to failure

Fig 5.1 Enhanced LCBC with additions to coatings

Fig 5.2 Enhanced LCBC with additions to substrate

Fig 5.3 Pt variability studies- effect of plating tank conditions and Pt thickness variation

Fig 5.4 Comparison of the effect of pink and brown alumina grit on LCBC

Table 5.0 Shows the LCBC systems studied with the calculated average cycles to failure.

Data were collected at Rolls Royce over a period of few months using the specifically designed quench rig. Test samples were removed from the hot zone of the cyclic furnace

and forced cooled, in order to attain as high thermal transients as possible during testing. For reproducibility samples had to be placed into the same region of the furnace during heating and to the same position for optimal cooling. Also shown is a reference standard low cost sample (422NB100) without any additions either to the coating or to the substrate.

Best performances in terms of average cycles to failure was shown by samples 422PB700 (sputtered Ni+0.5mass% Y); 422TB700 (sputtered Ni+ 0.58%Y+1.60mass%Hf) and 422VB700 (sputtered Ni+0.43mass%Y+1.75mass%Hf). These results show that it is critical to have the right amount of yttrium or yttrium and hafnium combination additions for improved performance.

Fig 5.1 Shows the data for selected sample each with an active elements addition to the coating. Note in all cases the 'enhancement' was added prior to the LCBC being applied over the top. Comparing the four systems shown it will be noticed that in the Ni+low Hf system, two out of the six samples were surviving indicating better performance than the others. It will be noticed that in ranking terms of cyclic performance Ni+low Hf system shows the best performance and Pt+Y is the lowest.

Fig 5.2 illustrates four systems studied with additions of La, Ce and La+Y to the substrate (CMSX-4) with a standard LCBC coating. Two of the systems were similar except one was a disc and the other a pin system. Arrows indicate test that have not failed

for the La and La+Y systems. The results show that La had better results than Ce additions.

Fig 5.3 illustrates a comparison of electroplated Pt variability plated under differing conditions at Rolls Royce. It has been established at Rolls Royce that plating conditions had a direct affect on the performance of the coatings. New tank and old anodes show better results than the rest. It will be demonstrated later that the variation in cycles to failure is linked directly to the Pt plating thickness as correlated by the GDOES studies.

Fig 5.4 Shows two types of grit that were studied: brown and pink alumina that were used to clean the substrate surface. From the data shown there was no major differences between the pink and brown grits. Also there was no major differences between samples that were gritted at Rolls Royce and CUK.

## **Chapter 6 Results: Thermal Ageing Studies of the LCBC System**

A key feature for expanding the use of TBC is increased spallation life and reduced spallation life variability. In order to understand the degradation process a common technique used is to thermally expose the coating at a temperature in excess of the working temperature to accelerate the degradation process. Degradation is measured by the degree of inter-diffusion, the growth of spinel oxides and general spallation. This experiment has been designed to expose the as-manufactured bond coat base line composition shown below to a series of thermal exposures of 4hrs, 16hrs and 25 hrs at 1150°C.

Base line composition: ( CMSX-4 +Y+La) + 10 $\mu$ m Pt bondcoat + 2.5 $\mu$ m CN33 (TBC)

The precise experimental details are given in chapter 3. The chemical inter-diffusion process is described in section 6.1, with GDOES studies displaying the depth concentration profiles from the TBC to the substrate .The macroscopic description of the coatings is given in section 6.2. The sub-microscopical details afforded by the TEM technique, especially understanding of the thermally grown oxide (TGO) and its interaction with the TBC and bond coat are given in 6.3.

### **6.1 GDOES studies**

GDOES depth profile analyses showed the coating composition and evolution of the different layers for ageing times of 0, 4, 16, 25 hours at 1150°C ( figures 6.1(a) to 6.1 (d) . This technique reveals any heterogeneity in the coatings and elemental migration at

the interface. It will also detect segregation of defects to interfaces that result in changes to local properties of the interfaces such as chemical composition structure and diffusion processes involved. It was the objective of this work to examine the way in which segregation occurs with time at temperature during the ageing treatment, and also to assess the capability of using a direct current source rather than radio frequency during GDOES depth profile analysis, such that quantitative assessment could be performed on those samples with non conducting layers. However, it was proven that the direct current source was capable of depth profiling through the approximate 2.5  $\mu\text{m}$  thick CN33 ceramic TBC layer without the need for the radio frequency source.

The Zr/Y concentration profiles (fig 6.1(a)ii to fig 6.1(d)ii) were clearly shown for all the samples at the TBC /  $\text{Al}_2\text{O}_3$  interface as expected. However, some initial general observations showed that diffusion of other important elements had taken place progressing from 0 to 25 hours.

The  $\text{Al}_2\text{O}_3$  ( TGO) layer that forms beneath the TBC plays an important role in determining the performance of the TBC. The GDOES traces were enlarged in the TGO region to establish improved understanding of the degradation process.

#### General Observation: 0- 25 hours

Observations for a semi-quantitative GDOES approach are reported here because qualitative analysis limits the absolute comparability of the results. Comparability is a general problem, especially for investigations over a long time period, but also for

different sensitivity settings. Contamination of the Glow Discharge Lamp, the optical system and a drift of the spectrometer also lead to drifts in signal intensities. Therefore, it was necessary to implement quantitative analysis to produce absolute comparable results [ 84 ].

It is evident from the as received sample (fig 6.1a(i) ), that the Pt had diffused into the CMSX-4 substrate after heat treatment at 1150°C to form  $\gamma/\gamma'$  structure ( low cost bond coat). Also observed was the diffusion of Ti from the substrate into the bond coat, showing a double peak. However, it is rather difficult to predict what is happening within the bond coat / alumina / TBC interfaces . Ta is behaving similarly to Ti, however there are no double peaks. W is substantially lower in composition and is again showing diffusion towards the bond coat Zr/ Y interface and so is Mo.

Exposing for 4, 16 and 25 hours ( figs 6.1b(i), 6.1c(i), 6.1d(i) ) results in diffusion of Ni, Al, Cr outward from the substrate towards the bond coat , whilst Zr, Y and Pt diffuses inwards. Examination of individual profiles reveals that Pt, Al, Ni, profiles stabilize after 16, 25 hours, whilst most of the inter-diffusion appeared to occur within the first 4 hours of exposure, as indicated by the change in concentration of both Ni and Pt. However, with continued exposure there is no real change to the Pt and Ni depth profiles.

The Pt average bond coat coverage is 35  $\mu\text{m}$  in the as received sample with a peak concentration of 60 -70 wt %; this is due to the initial deposition. However, when aged there is evidence of diffusion further into the substrate as shown in figs 6.1b, 6.1c to

65 - 85  $\mu\text{m}$  and also flattens out to peak concentration of 40-50%. The outward diffusion of Al is a sign of weakness. Depletion of Al from substrate will cause imbalance, i.e. oxide thickness growth; imbalance in coating will lead to spallation. There is a large concentration of Al at the bondcoat after continued exposures but it is difficult to predict the exact concentration level. In addition, there is a continuous build up of Ti with continued exposure of the bond coat.

From all of the general observations it is very difficult to predict what exactly happens within the first 10  $\mu\text{m}$ , in all cases. This region of the TBC/  $\text{Al}_2\text{O}_3$  is obviously of real interest in understanding the bonding mechanism within TBCs.

#### Specific Depth Analysis ( First 10 $\mu\text{m}$ in all samples)

Figures 6.1a(ii), 6.1b(ii), 6.1c(ii), 6.1d(ii) shows the elemental depth profiles of Ni, Cr, Al, Ti, Pt, Y,Zr with continued exposure for the first 10  $\mu\text{m}$  layer of all the samples.

Interestingly Ti has diffused through from the substrate towards the bond coat into the  $\text{Al}_2\text{O}_3$  region and with continued thermal exposure there is Ti ( which is degrading to bond coat adhesion as confirmed in reference [12]) enrichment at the bond coat /  $\text{Al}_2\text{O}_3$  interface affecting the purity of alumina layer. Pt, however, diffused through as indicated by a fall in concentration increasing towards the bond coat. Ni diffusion increased with exposure towards the bond coat /  $\text{Al}_2\text{O}_3$  interface. A marked growth in the Al thickness is observed at the TBC /  $\text{Al}_2\text{O}_3$  interface from 0 to 4 hours. Then with continued exposure upto 25 hours there was a decrease in thickness. Both the Zr / Y diffused with exposure, however there is quite a difference in the level of diffusion between 4, 16 and 25 hour profiles.

## 6.2 Scanning Electron Microscopy (SEM) and Energy Dispersive X-Ray Analysis

### (EDX) studies

#### Coating Morphology and Thickness

The first sample represents the base condition ( as received ) without extended thermal exposure and represents the coating as manufactured . The coating substrate consisted of three layers, TBC, alumina, bondcoat, as illustrated in the backscattered electron SEM images of Fig 6.2 (a)i at 500 and 1000 magnification. The initial coating was developed by interaction with the superalloy substrate material i.e. 10  $\mu\text{m}$  Pt plated onto the surface of CMSX-4 +Y+La by electroplating. Thereafter a diffusion heat treatment step was carried out at approximately 1150°C for 1 hour so as to cause the platinum layer to diffuse into the substrate. Platinum diffusion and the subsequent structural changes that forms the bond coat consists of two different phases, a bright phase rich in platinum, and the dark phase depleted in platinum as indicated by the EDX analysis, with also Ni and Al present. Both phases have been identified as Pt-rich  $\gamma'$  and Pt depleted  $\gamma$  [1]

Once formed the bond coat was subjected to vacuum heat treatment, for example a temperature of 1080°C, to form an alumina layer that provides both a resistance to further oxidation and a bonding surface for the TBC.

The ceramic thermal barrier layer in this particular case 2.5  $\mu\text{m}$  to enable GDOES study is applied by electron beam PVD and as a result , has a columnar grained microstructure. The columnar grains or columns as can be seen are oriented approximately normal to the surface of the substrate. Between the individual columns are micron sized gaps ( dark regions )extending from the outer surface of the ceramic layer toward ( within a few microns) the alumina layer.

The presence of inter-columnar gaps reduces the effective modulus (increase compliance ) of the stabilized zirconia layers in the plane of the coating. Increased compliance provided by the gaps enhances coating durability by eliminating or minimizing stresses associated with thermal gradient and superalloy / zirconia thermal expansion mismatch strains in the stabilized zirconia layer [1].

However, after 4, 16 and 25 (figures 6.2(b)i, 6.2(c)i and 6.2(d)i ) hours exposure at 1150°C, there was evidence of clear differences between the samples. The bond coat thickness increased as shown in the microstructures for 4, 16 and 25 hrs soak indicating coating growth by inter-diffusion . There, was however, a marked increase in coating thickness after 4 hours of aging thermal treatment, and then the coating thickness remained unchanged with continued aging to 25 hours.

#### Coating Composition

Figure 6.2(a)ii , 6.2(b)ii, 6.2(c)ii and 6.2(d)ii shows EDX spectra of phase compositions from the baseline composition and 4, 16, 25 hrs aged samples. From the EDX spectra it

will be noticed that there was outward diffusion of nickel during exposure, shown by the increase in concentration at the outermost coating layer ( bond coat ). In the as received condition, most of the platinum was concentrated in the bond coat. However, after thermal exposure the platinum diffused inwards, as indicated by the increase in concentration in the EDX spectra. In contrast there was no significant change in Al. Whilst the Cr concentration in the outer coating layer increased, it decreased in the matrix of the inter-diffusion zone.

Observation from the EDX spectra shows several other elements that were found to diffuse into the bond coat during thermal exposure. For example in the as received condition the outer most coating layer was relatively free of W and Ti. However, after thermal exposure for 4, 16 and 25 hrs both elements were detected in the outer most coating layer as shown in the EDX and SEM microstructures. Although it was possible that Hf and Ta had diffused into the coating, their concentrations were too low to be detected by EDX.

### X-Ray Mapping

Figures 6.2(a)iii to 6.2(d)iii shows the backscattered electron images(BSI) and corresponding x-ray mapping images illustrating the initial and progressive ageing (4, 16 and 25 hours ) distribution of various elements along a cross-section of low cost Pt bond coat on alloy CMSX-4.

From figure 6.2(a)iii, as indicated by the mapping images of O and Al, the average thickness of the interfacial oxide layer is about 0.3 -0.5 microns. However, the oxide thickness does far exceed this value at localised positions. From the Al map it will be noticed that two areas of major Al concentrations, one at the alumina /TBC interface and another within the bond coat area. Within the bond coat the Al is in a grit particle form. These grits are most likely remaining after the gritting process completion, prior to electroplating with Pt to form the bond coat. These grit particles could lead to an imbalance in the Al concentration. The material below is depleted in Al and will have a modified composition. The elements Ni, Cr and Co are concentrated mainly within the substrate, as expected. The Pt, however is concentrated within the bond coat as expected. The Zr/Pt peaks are difficult to separate, however, if the L-line of Pt is subtracted, the Zr layer is obtained as expected within the outer surface. The degrading elements Ti, Ta, W are concentrated within the bond coat and substrate, without any enrichment within the Al layer.

Figure 6.2(b)iii shows the elemental maps after 4 hours ageing at 1150°C. There has been an increase in the thickness of the Al<sub>2</sub>O<sub>3</sub> at the alumina /TBC interface. The bond coat is more defined with the 'finger formation' rich in Pt as expected but however, depleted in Cr, Co. There however seems to be some Co, Cr concentration in the Alumina layer, possibility of spinel formation. The Ni has homogenised within the substrate and bond coat. Ti is very finely dispersed at very low concentration throughout the substrate, bondcoat and alumina layer. The Zr layer is concentrated within the outer surface as expected. W/Ta concentration is very low and unable to be detected.

Progressing from figure 6.2(c)iii – 16 hours ageing to figure 6.2(d)iii - 25 hours , there is little change in the maps except more Ni diffusion towards the bondcoat and alumina layer, which can form unwanted spinels that are degrading to bond coats.

#### Characterization of surface scale ( $\text{Al}_2\text{O}_3$ )

In all the samples studied an alumina layer was detected. However, following thermal exposure for 4,16 and 25 hours soak it did reveal changes in the thickness. During the very short 4 hours exposure period there is a rapid growth in the alumina layer from  $0.3\mu\text{m}$  to  $2.2\mu\text{m}$  followed by a slight decrease to 25 hours (table 6.2).

The presence of other elements such as Ti, Cr, Ni, Co that may be damaging to the adhesion of the TBC were shown in the EDX analysis for each sample.

### **6.3 TEM / Interfacial Analysis**

At higher magnifications, microstructural details within the TGO interfacial region can be resolved, which will increase understanding of the degradation process, in order to improve thermal cyclic resistance. Presented are results for 0, 4, 16 and 25 hrs ageing treatment.

The as received sample (0 hrs) with no ageing treatment figure 6.3a [plate xf1-11] consisted of TBC , alumina, bond coat and superalloy, as observed using SEM. There is variation in the thickness of  $\text{Al}_2\text{O}_3$  across the coating. The ceramic coating exhibits a columnar structure. The  $\text{Al}_2\text{O}_3$  scale, which was about 0.3 -0.5 microns thick and observed in fig6.3a [plate xf1-14], with the selected area diffraction pattern (SAD)

showing typical diffuse rings corresponding to a poly-crystalline material. A number of finely dispersed dark phase particles were scattered throughout the  $\text{Al}_2\text{O}_3$  layer (Thermally Grown Oxide- TGO). EDX analysis of the dark particles showed it to be rich in Pt, Cr, Zr and Y than pure  $\text{Al}_2\text{O}_3$ , and also present was Cu which originated from the Cu grid used in TEM specimen preparation, with the major peak being Al. No other elements were detected through the TGO layer. The Cu is most likely sputtered from the ion beam thinning process, as it is not present within the bond coat.

Extending into the bond coat present were  $\text{Al}_2\text{O}_3$  pegs, suggesting mechanical interlocking [ fig6.3a -plate xf1-15]. On EDX analysis the bond coat was as expected richer in Pt, Ni, Cr, Co and a little Al. This could be a Pt-rich  $\gamma'$ -phase. Similar observations in SEM investigations within the bond coat shows a possible two different phases that have been identified with varying elemental compositions: dark and light [fig 6.3a plates xf1-16 ], dark phase of the bond coat , EDX shows Cr, Co, peaks which are known to be degrading to the bond coat. The lighter phase of the bond coat composition was depleted in Ti. Also identified were grit particles with composition rich in Al. These were particles left embedded after initial grit blasting the superalloy prior to Pt plating to create the bond coat.

After 4 hours the  $\text{Al}_2\text{O}_3$  scale had grown to a thickness of 2.35 microns [ fig6.3b -plate 212-11]. It is most likely that aluminium is diffusing out from the bond coat /substrate. The  $\text{Al}_2\text{O}_3$  was comprised of a mixed grain size that were fine and equiaxed at the TBC/  $\text{Al}_2\text{O}_3$  interface, with columnar at the  $\text{Al}_2\text{O}_3$  / bond coat interface. This two zoned

structure is in agreement with earlier studies [4,5]. Interfacial regions of the microstructure between  $\text{Al}_2\text{O}_3$  / bond coat was very sharp [ fig 6.3b -plate 212-13], without any voids present, indicating good adhesion. Otherwise interfacial voids can weaken the alumina – bond coat interface and lead to scale spallation upon cooling. Also, the interfacial region between TBC /  $\text{Al}_2\text{O}_3$  was sharp again [fig 6.3c -plate 212-15] without any voids, and a triple point bonding indicating good adhesion.

After 16 hrs ageing the top ceramic coating exhibited a columnar morphology, not a fully dense structure, and a rough surface profile [ fig 6.3c -plate 415-12]. There were no voids present at the ceramic-alumina interfacial region. The  $\text{Al}_2\text{O}_3$  interlayer again shows a mixed two zoned structure [ fig 6.3c-plate 415-13]. The measured  $\text{Al}_2\text{O}_3$  layer thickness is 2.2 micron. The  $\text{Al}_2\text{O}_3$  layer is coarse close to the bond  $\text{Al}_2\text{O}_3$  / bond coat interface and becomes fine towards the surface ceramic layer where it forms as an intermixing layer [ fig 6.3c- plate 415-13]. Bright field imaging of the alumina grains and grain boundaries show no void present in the microstructure. Dark phase precipitate particles observed in as received and 4 hours samples were increasing. Within the bond coat alumina grit particles were also observed. The interfacial region between  $\text{Al}_2\text{O}_3$  / bond coat was very sharp without any voids, again indicating good adhesion [ fig 6.3c -plate 415-14].

Finally, after 25 hrs of ageing the measured thickness of the  $\text{Al}_2\text{O}_3$  layer is 1.45 – 2.2 microns. Again similar to 4 and 16 hours ageing treatment the  $\text{Al}_2\text{O}_3$  region shows a mixed grained structure with coarser and fine grains present [ fig 6.3d -plate 314-13]. The intermixing  $\text{Al}_2\text{O}_3$  layer present at the  $\text{Al}_2\text{O}_3$  / bond coat interface shows that Ti, W, Ni, Cr diffused through into  $\text{Al}_2\text{O}_3$ , which eventually would lead to bond coat degradation

because of the formation of spinels [ fig 6.3d -plate 314-15]. However, the coarse  $\text{Al}_2\text{O}_3$  towards the  $\text{Al}_2\text{O}_3$  / ceramic interface is still free from Ti, except for a little Ni. Also observed were  $\text{Al}_2\text{O}_3$  pegs projecting into the bond coat , suggesting mechanical interlocking of the coating.

## **Chapter 7 : Discussion**

### **7.1 Quantitative GDOES analysis technique development for investigation of substrate and bond coat compositions**

#### **Technique selection**

In the field of TBC characterisation, surface analysis plays a key role in explaining oxide bonding mechanisms and degradation modes for thermal barrier and environmental protection coating systems.

To describe the process it is necessary, through basic considerations to choose the proper analysis techniques. These considerations include [91] :

- the expected homogeneity of the TBC
- selection of representative sample positions
- the technological range of interest for lateral and depth resolution
- the appropriate number of analyses to get representative results
- the expected accuracy for the analytical result
- efficiency and economy of the analytical work

Several surface analysis techniques such as electron spectroscopy for chemical analysis (ESCA) , auger electron spectroscopy and secondary ion mass spectroscopy are currently

available to accurately determine coating composition. Unfortunately, investigations via these techniques are time consuming, expensive and require highly skilled operators.

However, GDOES is a fast, easy to operate analytical procedure, which produces detailed information at a lower cost than the other methods, with sensitivity down to approximately 50 ppm; the technique is also capable of quantitative depth profile analysis [92].

In this section the GDOES results of both qualitative and quantitative analysis of bond coats under development are discussed, with issues raised on calibrations, quantitative technique developments, interfacial segregation study and an ensuing explanation of the global bonding mechanism.

### **Qualitative analysis**

Several new bond coat compositions with rare earth additions such as yttrium, hafnium, and combinations of yttrium and hafnium are shown in chapter 4, designed to deliver higher temperature requirements in aero-blade applications. The GDOES technique has been able to successfully detect both yttrium and hafnium additions. However, there are detection capability limitations. The minimum detection capability established in this work was approximately 0.5 mass % addition. The detection capability was dependant on the instrument setting parameters, set-up sequence, available Glow Discharge Lamp control settings, such as pre-pumping time and argon float time. GDOES, however, as already shown in chapter 4, clearly shows diffusion of the detrimental elements Ti, Ta, W

from the substrate and subsequent enrichment at the interface between bondcoat / alumina for failed samples containing both Y, Hf and a combination of Y and Hf. This is in agreement with Sprague and Cocking findings [11] where Ti and W were shown to diffuse from the substrate into the coating, reducing the protective nature of the oxide scale on M-Cr-Al-X coatings for superalloys. Furthermore, there was diffusion of other substrate elements Cr, Al, Co, Mo, Mn, Ni in various quantities towards the interface, which could form spinels, that are known to be detrimental to the bond coat [11]. It should be noted that, in order to develop a relationship between depth and quantity, a quantitative programme needed to be established. This would also enable location of elements accurately for compositional improvements, in order to predict a coating chemistry that minimizes interdiffusion.

### **Quantitative analysis**

The absolute comparability of the bond coat results was limited by the use of qualitative GDOES depth profile analysis. Comparability can be a problem, especially for investigations over a long time period and large depths, but also different sensitivity settings. In addition a drift of the spectrometer also leads to drifts in signal intensities. Therefore, it is essential to set up quantitative analysis for comparability.

The quantitative analysis approach developed for the bond coat using multi-matrix calibration is explained in chapter 3 and neglects Re and does not deal with interferences from phosphorus, as will be explained in the calibration section. The semi-quantitative

analysis program developed here can be used to explain structural and chemical transformation as follows:

It is evident from the results presented in chapter 6 figure 6.1a(ii),6.1b(ii),6.1c(ii),6.1d(ii) on the as-received and aged samples that most of the interesting interaction in explaining a failure mechanism was taking place within the first 10  $\mu\text{m}$  analyzed volume. If the four samples were compared: 0, 4,16, and 25 hours exposure, it will be noticed that there was a gradual enrichment of Ti at the bond coat/ alumina interface with ageing treatment. In addition there was a build up of other elements such as Ni,Cr,Co also as shown in reference [11] which leads to the formation of spinels, which can degrade the alumina leading to coating spallation. This is the first time to the authors knowledge this has been shown from a global perspective using the GDOES depth profile characterization technique on a LCBC system.

### **Calibration of technique**

For GDOES depth profiling of the bondcoat, it has been shown that the depth resolution depends mainly on the form of the erosion crater [94]. The crater produced during the analysis of CMSX-4 is shown in fig 4.1.3(e)i, 4.1.3(e)ii and its measurement using Dektak laser profiling is shown in fig 4.1.3(f)i and 4.1.3(f)ii. It can be seen that the bottom of the crater is quite planar, while some re-sputtering of material has created a lip around the rim. The laser profile depth measurement shows a good correlation to the calibrated depth value obtained from fig 4.1.3(e)i and fig 4.1.3(e)ii, with errors of the order of 10-15%. The roughness of the bottom of the crater normally increases linearly

with time, which is one of the factors limiting the depth resolution. This necessitates a compromise between good depth resolution and high intensity spectral lines when selecting operating parameters.

The results of the GDOES and Electron Probe Micro Analysis (EPMA) analyses are compared to the composition determined by XRF in table 4.1.3(h). Both results showed a good correlation, with the GDOES results generally closer than those of EPMA, although there were some obvious discrepancies which require investigation; the value obtained for Ni, Ta, Hf and Pt are inaccurate and may be due to interference between the spectral lines.

The current semi-quantitative programme used in this analysis is limited by the number of reference calibration standards available; a greater number of standards would increase the accuracy. Also, in addition installation of an extra elemental channel such as rhenium would enable improvements in the semi-quantitative programme. It was observed that there was an interference of Pt on the P line (i.e. we see a P signal when analysing pure Pt). Since P is a lower spectral resolution in the spectrometer and Pt with higher concentration, generally the interference is severe. Measurement of Pt however, with EDX as shown in chapter 4 is in agreement with that of the GDOES depth profile. In order to resolve the interference of Pt/P it would be necessary to select suitable wavelengths and re-calibrate the spectrometer. This was not deemed possible due to practical constraints.

## Technique Novelty

The current semi-quantitative program developed can be used in order to explain bonding mechanisms globally within LCBC systems. The technique as it currently stands is able to determine coating thickness, rough composition, show segregant presence of contamination at the interface, which may result in poor surface cleaning or migration of elements during the coating process, as already shown in chapter 4 and 6. The technique is fast, reliable, and cost effective compared to EDX, which can be very time consuming. Also it has been proven that a direct current source can be used for depth profiling thin 2.5  $\mu\text{m}$  TBC coated samples, instead of the need for radio frequency, which is very time consuming.

## Global Bonding Mechanism

Growth of the TGO (alumina) is a dominant phenomenon controlling bonding mechanisms in low cost Pt bond coats. The bond coat, in the low cost bond coat system comprises a relatively large local Al reservoir provided by the substrate, such that alumina forms in preference to other oxides. The formation of alumina at high temperature has been studied [118-120] and it has been shown that growth proceeds through  $\gamma, \delta, \theta$  and finally  $\alpha$ -alumina. The growth rates of the metastable phases are generally faster than the stable high temperature  $\alpha$ -alumina phase. It is generally agreed that the  $\theta$ -alumina transforms to  $\alpha$ -alumina in a few hours at 1,000°C. Although if Y or Ti ions are present then the  $\theta$ -form can transform to  $\alpha$ -alumina more quickly [118] or, when larger ions such as Y, Zr, Hf or La are present be stabilised for longer periods [120]. The alumina layer for the LCBC system was formed during a vacuum heat treatment at 1080°C. A protective scale of  $\text{Al}_2\text{O}_3$  cannot be

maintained when the aluminium concentration falls below a critical level, usually cited as approximately 4 to 5 mass percent aluminium[11,66]. The preference for alumina relates to its low growth rate and superior adherence. The chemistry and microstructure of the bond coat are crucial, because of their influence on the structure and morphology of the TGO [90].

Characteristic elemental compositions for the as processed bond coat and bond coat surface exposed by the failure are summarized in chapter 4.

This work has contributed to knowledge by showing evidence from the GDOES depth profiles that failure was accompanied by significant inter-diffusion between the substrate and bond coat as indicated by a marked increase in Ni concentration and decrease in Pt concentration. Inter-diffusion resulting in a change in chemical composition of the bond coat surface resulted in phase changes as indicated in the SEM microstructures of aged samples figures 6.2b(i),6.2c(i),6.2c(i),6.2d(i). For all the low cost Pt bond coat systems studied, the bond coat surface at failure showed increased Ti, Cr and Co concentration. This outward diffusion of transition metals led to the formation of non protective oxides degrading the adherence of  $\text{Al}_2\text{O}_3$ . This is in agreement with work reported by John E.Schilbe [95]. Also, since the CMSX-4 alloy is essentially free of C, strong carbide forming elements potentially Ta and Ti, are available to diffuse as described into the bond coat and be oxidized. This leads to nucleation of voids at the oxide/bond coat interface causing decohesion of the oxide.

## **Chapter 7.2 Bonding Mechanism Factors**

The performance of LCBC systems is determined by the TGO ( $\text{Al}_2\text{O}_3$ ) scale that forms beneath the TBC. The oxide scale adherence is an important key factors that distinguishes the coating performances. There are many numerous factors involved in determining the adhesion process between the  $\alpha$  -  $\text{Al}_2\text{O}_3$  and the alloy substrate and the bond coat. The following factors outlined below are important, however only a select few that would be helpful towards understanding bonding mechanism have been studied:

- substrate composition
- rare earth additions to coating
- ageing treatment
- minor elements
- role of silicon
- role of interdiffusion
- stress generation in the scale
- metal-oxide thermal expansion mismatch
- growth stresses generated isothermally

It is shown from chapters 4,5,6 results that from the above main factors that are contributing in the formation of 'ideal scale ' and adhesion to substrate there are mainly three important ones: (i) no major redistribution of alloying elements within the metal

substrate . (ii) segregation of Zr to the metal-scale interface and the scale grain boundaries, and (iii) ability to tolerate stresses generated in the scale.

In order to develop predictive failure modelling to suggest improvements in coating composition such that improved performance is achieved, the following selected factors: substrate composition, rare earth addition to bond coats, ageing treatment, role of silicon, minor element roles from above were studied in-depth using analytical characterisation techniques such as GDOES, SEM, XRD, and TEM and the findings are outlined in the following sections.

## **7.2.1 Effect of Additions to Substrate (LCBC formation )**

### **Additions of Platinum**

The addition of Pt to the aluminide coating is recognized as being beneficial to scale adhesion (9, 10). However, the role of Pt in improving scale adhesion is not well understood. In this case, the outer coating layer contains intermetallic phases such as  $PtAl_2$ ,  $Pt_2Al_3$  or  $PtAl$  depending on the type of coating [97]. Earlier studies suggest that platinum excludes refractory transition elements such as molybdenum, vanadium and tungsten from the outer coating layer [98], which promotes selective oxidation of aluminum [99]. A number of other Pt-related mechanisms have been proposed, including : mechanical keying of the scale [100], rapid self-healing of  $Al_2O_3$  [101], modification of aluminide Al content [44], and suppression of void formation along the oxide-metal interface. In order, to explain this in detail for LCBC systems, the initial microstructure of the as received LCBC will be described, followed by thermal stability effects and a study of localised variations within bond coats and comparison to literature review with present findings.

### **Microstructure of the as received condition**

Low Cost Pt bond coats are developed by a reaction between Pt and the alloy substrate ( in this case CMSX-4) which results in a mixture of Pt-rich  $\gamma'$ - phase and a Ni –rich solid solution containing Pt (  $\gamma$ - phase) [12]. A typical microstructure of the low cost Pt bond coat in the backscattered electron image from an as received sample is shown in figure 6.2. It is observed that the coating layer of about  $28\mu m$  in thickness is separated from the alloy substrate by an alloy depleted zone free from the cuboidal  $\gamma'$  - phase. Evidently as can be

seen from figure 6.1a(i), GDOES result show that, this zone had resulted from depletion in Al during the coating cycle involving formation of  $\gamma'$ - phase within the coating layer. The bond coat generally consisted of a rather continuous layer of  $\gamma'$ - phase containing islands of  $\gamma$ - phase nearer the surface. However, nearer the alloy substrate ( CMSX-4), the  $\gamma'$ - phase became discontinuous and assumed a lamellar morphology. This interdiffusion process between Pt and the CMSX-4 substrate leads to a significant change, as already shown here in the coating composition and structure, which has been observed similarly in a platinum aluminized nickel -base superalloy system [102].

### **Thermal Stability of the Bond coat**

A typical microstructure of a low cost Pt bond coat cross section is shown in figure 3.1(b)(ii) at the time of failure and GDOES depth profiles figures 4.2.2 b and 4.2.2 d. It was evident from both microstructures and GDOES depth profiles that interdiffusion had taken place, as was also shown in a platinum aluminized nickel -base superalloy system [102]. Thermal cyclic exposure results are shown in figure 5.3 which shows a typical link between the manufacturing process and cycles to failure of a typical average 10  $\mu\text{m}$  Pt plated bond coat specimens with TBC. The thermal exposure caused the coating layer to grow prior to spallation and the  $\gamma/\gamma'$  structure to coarsen relative to the as – received condition.

It is evident from the GDOES results, however that the cause of variation in the bond coat thermal stability results is a direct result of the variation in Pt plating thickness. Also it is an indication a thinner coating can reform alumina scale for longer periods compared to less thickness ones. From a manufacturing perspective the most promising source of tighter

control in Pt thickness providing good thermal stability performance seems to be the use of a combination of new tank and new anodes.

In view of coating performance it seems that longer life is achievable with a thicker Pt-rich layered coating, because it would be more likely to provide better diffusional stability.

### **Localised variation in Bond coat**

It has been observed during the SEM study of bond coats that there is a localized variation within the bond coat due to Pt -thickness variation as already shown in chapter 4 . The thickness of the bond coat varies across the coating region. The thickness of the alumina layer was about 2-3 $\mu\text{m}$ . Normally, however, the thickness of this alumina oxide layer developed to act as a glue between the TBC and bond coat is about 1  $\mu\text{m}$ . This localized variation could lead to surface structure variation and compositional differences of the bond coat leading to differences in oxidation rate from one region to another. In addition this would cause variations in the movement of transition metals from the CMSX-4 substrate to the alumina layer, which is an important source of variability in bond coat performance. So, during exposure the adhesion of TBC to the alumina would vary from one location to another in accordance with the local thickness and volume fraction of Pt-rich  $\gamma$ - phase in the bond coat.

### **Summarized effects of addition to substrate**

Variation in the manufacturing process can lead to variation in the Pt thickness which in turn can lead to bond coat variations as was shown from the thermal cyclic data and also by GDOES assessment.

Pt variation can lead to changes in diffusivities, as observed in the GDOES elemental depth profiles figures 4.2.1 which in turn can affect movements of transition elements from the substrate. From an oxidation standpoint, these transition elements have the potential to accelerate the growth and degrade the adherence of the protective alumina scale [11]. So therefore, maintaining the purity of the alumina oxide layer is essential to obtaining good interface bond strengths and preventing spallation of the ceramic layer.

### **7.2.2 Effect of additions to coating**

The effects of yttrium and hafnium concentration in low cost bond coats on the cyclic furnace life of thermal barrier coatings were studied. It is claimed that minor but critical additions of rare earth (Y,Hf) active elements, either individually or in combinations to  $\text{Al}_2\text{O}_3$  forming alloys and coating systems, improve the protective nature of the scale [103,104]. That would prevent the diffusion of detrimental elements such as Ti, W. The underlying operating mechanisms have been subject to a great deal of debate as discussed in the literature review section [103,104,105,106].

It is the objective of this discussion section to clarify the role of Y,Hf in coating developments. Also to ascertain the location and amount present, in order to help build a knowledge basis for correct addition levels to optimise LCBC systems.

The evaluations carried out were on disc specimens in cyclic furnace tests at  $1135^\circ\text{C}$ , each cycle being 1 hour at temperature and a 10 minute forced air cool. The test cycle continued until the number of cycles required to cause the TBC to spall is reached.

On the basis of the data obtained in this study, it was established that the presence of and concentration of yttrium and hafnium in the bond coating is very critical. Without yttrium and hafnium in the low cost bond coat, the thermal barrier systems failed very rapidly. The optimization of yttrium and hafnium concentrations in low cost bond coats led to a very significant improvement of the low cost bond coat system.

It is evident from the thermal cyclic results described in chapter 5 , table 5 -average cycles to failure, that a 0.5 mass % Y addition to LCBC shows a higher resistance to spallation, than 6.10 mass % addition and also when compared to the reference low cost bond coat sample without any additions. However, the Hf addition did not seem to make a great difference. Detailed examination of the qualitative GDOES curves for the above samples in terms of the elemental diffusion revealed that there was a change in diffusion chemistry i.e. transport of elements from the coating to substrate and vice versa via Y, Hf additions. The right addition level is critical in improving the cyclic performance.

Comparison of 0.5 mass% Y with that of the 6.0 mass% Y addition, the major difference as observed from the GDOES curve is the increased Ti diffusion from the substrate to coating in the 6.0 mass% sample. This suggests that a significant increase in either the yttrium concentration in the bond coatings or the yttria concentration in zirconia results in a significant decrease in the life of the TBC. Although a large yttrium peak is observed in the 6.0 mass% sample the GDOES technique is incapable of detecting below 0.5mass% Y; a global picture emerges of the bonding mechanisms in terms of diffusion chemistry as already described in section 7.1.

The SEM microstructural studies combined with GDOES of the tested specimens showed the microscopic location of Y to be located at the bondcoat / alumina interface and also within the  $\alpha$  -  $\text{Al}_2\text{O}_3$  scale. It was also visually observed that the coated specimen having the yttrium free bond coat failed at the substrate- bond coating interface. The coating scale consists of  $\alpha$  -  $\text{Al}_2\text{O}_3$  ( rhombedral );  $a= 0.476\text{nm}$  and  $c= 1.299\text{nm}$  as shown from

XRD of the failed specimen. Observed are regions of a less protective spinel -type oxide isomorphous with  $\text{NiAl}_2\text{O}_4$  ( cubic  $a = 0.794\text{nm}$  ) and expected to be of the type ( Co, Ni ) ( Al, Cr) $_2\text{O}_4$  [12].

It is evident from the experimental results presented here that for LCBC, yttrium and hafnium additions could with the correct addition improve the protective nature of the scale by more than one mechanism as described below.

Formation of Y-rich oxide pegs could improve the mechanical adherence of the scale to the coating as proposed in a number of studies[107]. It is possible that oxidation of Y into Y-rich oxide could occur by inward diffusion of O. Both outward diffusion of Al and inward diffusion of O are believed to contribute to growth of  $\alpha\text{-Al}_2\text{O}_3$  scale [8,21].

The presence of a small Y concentration within  $\alpha\text{-Al}_2\text{O}_3$  scale in solid solution could decelerate the kinetics of Al lattice diffusion reducing the scale growth rate [108]. In the meantime, segregation of Y to grain boundaries of  $\alpha\text{-Al}_2\text{O}_3$  scale could have a number of beneficial effects on its protective nature. For example this could maintain a scale of a fine-grained structure improving its elevated mechanical strength.

Another possible effect of this segregation could be filling voids or pores along grain boundaries of the scale improving its cohesion [109,110]. Diffusional transport along grain boundaries influencing scale, growth rate[111,112] could also be modified by the presence of Y reducing the scale growth rate and in turn the extent of growth stresses [105,109].

### **7.2.3 Effect of Silicon and contaminants on LCBC systems**

The effects of silicon concentration in low cost bond coats on the cyclic furnace life of thermal barrier coatings were studied. The effect of silicon on LCBC has been shown to be negligible, as illustrated from the results of chapter 5 for thermal cyclic performance results for both pink and brown alumina. This is in contradiction with what has been shown in the literature section 2.3, where it has been shown that silica content has a direct effect on the life and performance of TBC. TBC life increases with decreasing silica level [54]. In addition, there were no observed differences in the optical microstructures for both pink and brown alumina grit.

Silicon was initially thought to have originated from the alumina grit. However, it has been demonstrated by both pink and brown alumina grit GDOES depth profiles that it rather originates as a contamination from the heat treatment process, perhaps most likely from the silica bricks or from the heat treatment atmosphere. Although silicon does diffuse through during heat treatment when forming the low cost bond coat, silicon is thought to be in the ppm range and EPMA has been unable to detect silicon, because it is below the detection limit of the SEM instrument. The silicon tended to concentrate at the coating / substrate interface as shown by GDOES, possibly leading to a loss in interfacial adhesion. From the results in chapter 4 and figures 5.4 it has not been possible to see any real effect of silicon, so therefore, the variation within bond coats cyclic performance could be due to the other observed factors such as Pt thickness variation or Y,Hf addition levels as mentioned in the earlier discussion parts. The programme of work carried out using GDOES / SEM and

thermal cyclic results has eliminated silicon as a potential variable contaminant source, as initially thought, although silicon is at the ppm level.

The role of silicon needs to be established from an in-depth microstructural aspect using TEM, so that additional information on understanding the degradation process can be established with the current GDOES data, such that a minimal acceptable level can be set.

In order to set-up acceptable levels of silicon, the current quantitative GDOES programme set-up would have to be re-calibrated with new silicon containing standards having variable levels of silicon used. This would truly be a faster technique than EPMA, where further development work needs to be done. Also work needs to be done in order to identify using XRD whether silicon occurs as an element or as silica and what roles it plays.

Sodium, a residual from the Pt - electroplating process, has successfully been identified using GDOES depth profiling to be present in the LCBC system. This is in confirmation with previous findings using XPS and other techniques mentioned [64]. It is known to cause hot corrosion, however the level present, which must be above the 50ppm GDOES limitation is perhaps not sufficient to show any effects. Also, the GDOES results would have to be quantified with correct standards similar to Si, in order to show any real effects. The results of GDOES shows that Na diffused through from the surface into the bond coating. This is likely to cause poisoning of the TGO layer where maintenance of the purity of the TGO layer is essential for good adhesion of TBC and also improved thermal cyclic resistance.

#### 7.2.4 Effect of ageing treatment on Low Cost bond Coat

The effect of ageing the LCBC at 1150°C has not been studied in the past. Therefore, this study was undertaken in order to enable development of a basic understanding of the mechanisms governing durability, such that a technical base could be established for further improvements in bond coat technology. Initially a technique had to be perfected for the production of thin foil films for TEM examination of the aged samples, as demonstrated in chapter 3. Such evidence and determination of various phases present, plays an important role in determining bonding mechanisms in LCBC systems. Also TEM enables the direct imaging of the TGO to search for further information on bonding mechanisms.

During the ageing treatment at 1150°C for 4, 16 and 25 hours inter-diffusion processes occurred progressively within the LCBC system. It is observed that the aging treatment caused the coating layer to grow in thickness, and the  $\gamma/\gamma'$  structure to coarsen relative to the as-received condition (figures 6.2a,b,c,d backscattered electron images), which could be explained in terms of inter-diffusion between the coating and alloy substrate as shown in the SEM microstructures and also confirmed by GDOES and TEM results. This is in agreement with findings shown in references [73,113] in a bond coat and superalloy system. There is also observed an increase in the Ni concentration during ageing towards the  $\text{Al}_2\text{O}_3$  interface which can lead to a phase transformation within the bond coat.

However, the Pt located initially in the outer layer of the coating diffuses inwards, and as shown in the SEM mappings figures 6.2(ii), is homogeneously distributed. However, as the ageing progresses there is a large decrease in the Pt at the outer surface, whilst increased

within the bond coat. This would affect the phases formed, ultimately affecting bonding mechanisms.

After TBC deposition on superalloys, the coating is subjected to vacuum heat treatment at, for example a temperature of 1080°C, to form a thin  $\alpha$ -Al<sub>2</sub>O<sub>3</sub> - based film on the metal / ceramic interface. This so called thermally grown oxide (TGO) provides a high adhesion bond (chemical bond) between the TBC (YSZ) layer and the bond coat. Thus, development of advanced TBC systems requires design of improved bond coatings that form virgin Al<sub>2</sub>O<sub>3</sub> scales with optimized adhesion and minimized growth rates [117].

The rapid growth of the Al<sub>2</sub>O<sub>3</sub> layer after 4 hours of ageing which is aided by oxygen diffusion and aluminium consumption, leads to changes in the bond coat composition and microstructure as illustrated in the GDOES, SEM and TEM results. This is caused by depletion of Al in the bond coat, which therefore allows the less active elements, Cr, Ni and Co, to form  $\alpha$ -Cr<sub>2</sub>O<sub>3</sub> and (Ni,Co)(Cr,Al)<sub>2</sub>O<sub>4</sub> spinel, which would increase the stress in TBCs and induce cracking in the Al<sub>2</sub>O<sub>3</sub> layer [114]. However, after 16 and 25 hours there is a slight decrease in the Al<sub>2</sub>O<sub>3</sub> layer which could be due to a number of reasons. In the early stages of oxidation, demand for oxygen cannot be met and the rate of growth of alumina layer is determined by oxygen transport through the ceramic topcoat. As a consequence, the alumina thickens more slowly than it would under conditions of unconstrained access but its growth rate will be constant ( 4 hours ageing ). However, at some longer time the balance of supply and demand switches such that sufficient oxygen becomes available to permit alumina growth at its intrinsic rate. Over this later period, the growth rate will

decrease with time. The net effect is that the final alumina thickness will be less than in the absence of a topcoat and that, over the entire period of oxidation, the rate of growth will appear to decrease with increasing ageing time ( 16 and 25 hours ageing) [116].

In some cases, the outward growth component incorporates some of the TBC into the TGO-spallation at interfaces or inside the zirconia. This is where some of the spalled Al is likely disappearing. The depletion of aluminum results in phase changes in the bond coats. The ability of the bond coat to continue to support the growth of an  $\text{Al}_2\text{O}_3$  scale depends on the activity and the total amount of Al available in the coating. When the Al concentration in the bond coat falls below the level at which  $\text{Al}_2\text{O}_3$  can be formed, other faster growing oxides of the elements in the bond coat will form preferentially [11].

Measurement of the growth in alumina as shown in the table 6.3 is debatable. Deciding the correct interface within quantitative GDOES is limited by GDOES resolution, as already mentioned in chapter 3 and 4. However, the measurement of the depth using TEM microstructure has assisted in the process as well as an estimation of growth layer using SEM.

The alumina present has been shown in LCBC , just like other systems, to be amorphous in nature. This is directly evident from the selected area diffraction pattern, which gives rise to a series of faint rings fig 6.3a plate XF1-14. However, a continuous and dense  $\text{Al}_2\text{O}_3$  layer formed by the selective oxidation would suppress the transport of oxygen through the  $\text{Al}_2\text{O}_3$  layer, resulting in the outward diffusion of metal ions (such as  $\text{Cr}^{3+}$ ,  $\text{Ni}^{2+}$  and  $\text{Co}^{2++}$ )

through the  $\text{Al}_2\text{O}_3$ . The metal ion would form the oxides within the pre-existing  $\text{Al}_2\text{O}_3$  near the ceramic coating [68]. This would ensure better adhesion of TBC.

It is evident from the results illustrated that the coarse  $\text{Al}_2\text{O}_3$  towards the  $\text{Al}_2\text{O}_3$  / ceramic interface is still free from Ti, except a little Ni. Also observed are  $\text{Al}_2\text{O}_3$  pegs projecting into the bond coat, suggesting mechanical interlocking of the coating, hence improving adhesion.

In summary, cross-sectional TEM, along with GDOES and SEM were used to support findings, to characterize the coating microstructurally and chemically in details from the bond coat interface to the outer surface (TBC). Important observations include an alumina interfacial region between the bond coat and the ceramic layer, which is believed to provide a strong adhesion between the two layers. This has been observed in references [42,114,117] in both EBPVD and also Plasma sprayed TBC with other types of bondcoat systems. Therefore, this work has found that low cost bond coats must have a similar type of bonding mechanism operating.

The metallic coating must also form an adherent, slow -growing external  $\text{Al}_2\text{O}_3$  layer beneath the overlying low thermal conductivity ceramic top coat. The ability of the coating to reform a protective TGO or scale in the event of spallation is no longer the key. It is much more important that the scale be developed with a minimum of transient oxides and that it have near -perfect adhesion to limit spallation of the ceramic top coat, thereby achieving a long TBC lifetime [96].

Also it has been shown from the experimental observations suggesting that one failure mode is associated with a compositional change in the TGO from  $\text{Al}_2\text{O}_3$  to a mixture of chromia and spinel and that this in turn is associated with depletion of Al from the Bondcoat and concurrent enrichment of Co, Ni, and Cr in the oxide [115].

### **7.3 Proposed failure mechanisms within LCBC systems**

The research work conducted on LCBC systems so far has identified potential factors, such as the variation in Pt thickness, rare earth content (Y, Hf content) and residual elements. Ageing treatments have a pivotal role in explaining the degradation process using various analytical characterisation techniques, including the expansion of the novel GDOES technique giving the ability to analyze in ppm. This section will focus on developing possible failure prediction models. The failure mechanisms involve the thermally grown oxide (TGO), the TGO / bond coat (BC) interface and / or the thermal barrier coating (TBC). Current understanding is that these mechanisms are activated primarily by the stress state caused by the residual compressive stress in the TGO.

In LCBC systems it has been demonstrated both by using the quantitative GDOES, SEM and TEM techniques, that there is considerable diffusion taking place at the thermally cycled test temperature of 1150°C. This can allow chemical damage at the TGO / Bond coat interface, leading to a loss of interfacial adhesion. It was observed that the  $\gamma$ - phase of the bond coat on alloy CMSX-4 seems to provide an active source of Ti to diffuse into the alumina surface and be oxidised to  $\text{TiO}_2$ , degrading the adherence of the  $\text{Al}_2\text{O}_3$  scale (SEM / TEM microstructure and EDX data in chapter 6). This has been observed in several references [42,11], and the effect is critically dependent upon the exact Ti content. Also, during thermal exposure at 1150°C, the  $\gamma'$ -phase of the bond coat on alloy CMSX-4 was converted from Pt-rich into Ni-rich (mass % basis) as a result of interdiffusion between the coating and substrate. However, here in this LCBC system it has been shown

(chapter 6.3) that after 25hrs of ageing that the bonding is still intact, although considerable substrate elements have diffused through, suggesting the bond coat to be quite good. Also almost zero sulphur was observed using GDOES. This could be due to the fact that grit blasting of the bond coat surface had a significant impact, in terms of removal of surface impurities (especially S), as well as acceleration of  $\alpha$  - alumina nucleation.

During high temperature ageing treatments, it has been shown that there is an increase in the oxide thickness, initially followed by stabilisation (see table 6.3), which elevates the elastic energy available to drive debonding. Control of the TGO thickness is vital in maintaining the adhesion of the TBC.

Oxide pegging clearly indicates how important mechanical keying effect can be in improving thermal cyclic resistance. Extending into the bond coat present were  $Al_2O_3$  pegs, suggesting mechanical interlocking [ fig6.3a -plate xf1-15].

Failure mechanisms operating in LCBC can be summarized as follows:

Firstly, as the growth mechanism for TGO is from exposure of surface aluminium at temperature, the movement of aluminium to the surface will continue until sufficient depletion ( see GDOES results in figure 6.1) of the aluminium within the base material has occurred to stop any formation, at this point failure of the oxide layer will occur. The spallation of the oxide coating can occur on cooling and thermal cycling advances the process, but is dependent on the process used.

Secondly, during screening of candidate LCBC bond coats for TBC (see table 5.0) and referenced GDOES depth profiles in chapter 4 for characterisation of enhanced LCBC systems, it has been shown that there is considerable diffusion of Ti and other transition elements, leading to formation of degrading oxides at the TGO/bond coat interface. This leads to decohesion between the interfacial layer of  $\text{Al}_2\text{O}_3$  scale and the bond coat.

Thirdly, given initial variation in Pt content of the LCBC, the results from chapter 4 and 5 suggest that during thermal exposure at  $1150^\circ\text{C}$ , the  $\gamma'$ -phase of the bond coat on alloys CMSX-4 continued to lose Pt and gain Ni at the same rate. This adding variation in diffusion rates leads to eventual degradation.

Fourthly, the performance capability of the low-cost Pt bond coat is a sensitive function of the base material in this case CMSX-4 alloy substrate chemistry with regards to diffusion of elements from the base. Also phases present within the bond coat play a key role in determining diffusion of elements from the substrate and vice versa. They are responsible for retaining or blocking elemental movement. Therefore, increasing the life of the bond coat.

## **7.4 Proposed Improvements**

The research work has identified several key factors for improving the adhesion of the TBC to the turbine blade as mentioned in the discussion section. Some potential strategies to form more adherent alumina scale in LCBC systems that would enable increased cyclic performance would be:

### **Alternate Substrate ( RR3000)**

It has been shown that the higher Ti content of alloy CMSX-4 caused the  $\gamma$ - phase to act as an active source of Ti to diffuse into the bond coat surface and be oxidized hence degrading the adherence of  $Al_2O_3$  scale and in turn accelerating failure of the coating system. However, if for example RR3000, which is a third generation single crystal casting material, which as can be seen from table 3.1 (a) has a lower Ti content than CMSX-4 is used as an alternative, the Ti would most likely be partitioned to the  $\gamma'$ -phases with its lower content.

### **Modification to bond coat composition**

The best bond coat identified was 0.5mass% addition Y on a CMSX-4 substrate. This bond coat in combination with RR3000 may result in great improvements in thermal cyclic resistance. The Ti would be held in the  $\gamma'$  and the Y would be available to form pegs to increase thermal cyclic resistance, therefore also, maintaining the purity of the alumina scale, that is preventing the formation of spinels. Further, investigation of the bond coat microstructures or phases which may inhibit diffusion of elements from the substrate into

the alumina scale or identification of roles of elements such as Hf ( alone or in combination Y ) which is detrimental to scale adhesion from a microstructural aspect.

### **Alternate Pt-deposition techniques**

The Pt-plating of the substrate (CMSX-4) has disadvantages in terms of possible contamination from the platinum salt,  $\text{Pt}(\text{NH}_3)_2(\text{NO}_2)_2$ , which is added for plating. Also as de-ionised water is a poor conductor of electricity, several phosphate salts are added to improve electrical conductivity within the bath. This may lead to contamination from the plating salt, and also thickness variations as already shown, which has been shown to cause variability in LCBC systems. Physical Vapour Deposition ( PVD), would perhaps be an alternative means of Pt deposition, where there is better control of the thickness.

### **Control of alumina growth**

Simulated ageing treatment studies has shown there to be growth in the alumina grains, due to oxygen and Al diffusion. Control of the growth is vital in improving the thermal cyclic resistance. Also design of a LCBC system with an alumina based on a natural limitation that alumina scales thicker than approximately 5-8  $\mu\text{m}$  will not remain ideally adherent and thus cannot support the TBC. The approach would be to set a barrier layer below the TBC against diffusion of oxygen toward the bond coat and substrate. In such case, the tendency of formation of the TGO to grow would be minimized, thus increasing cyclic resistance. Therefore, ceramics with a lower oxygen diffusivity than Ytria Stabilised Zirconia (YSZ) would be a good candidate. The other alternative would be to have a plentiful supply of Al, thus when alumina spalls it is readily formed again, thus maintaining TBC adhesion.

## **Chapter 8**

### **Conclusions**

The following conclusions may be drawn from the research work completed within this thesis:

#### **GDOES Analysis**

- The work conducted in the investigation of bondcoats and ageing treatment of low cost platinum bond coats on TBC's has shown GDOES, which had not been previously applied to be a useful analytical tool for characterisation.
- Comparing GDOES to other analytical techniques such as WDX, EDX, it has the following advantages: little or no sample preparation required; it reduces matrix effects and normalises sample to sample inconsistencies; because successive surface layers are removed offers compositional depth profiling; due to the small cathode to anode distance, sputtering occurs over a narrow volume resulting in uniform sample erosion over analysed area giving good resolution when used for depth profiling; sensitivity down to approximately 50 ppm. However GDOES has limitations: need a solid relatively flat sample that will make a vacuum tight seal; liquids are not possible to analyse and powders are difficult; range of elements that can be analysed by one spectrometer is limited to a maximum of 44; a dc supply is used so samples must be electrically conductive; RF sources are available , but qualitative depth profiling is not yet possible.

- GDOES can clearly distinguish between the various bond coat systems studied.
- Our GDOES system is unable to detect La, Ce and Re and also cannot detect yttrium less than 0.5% by mass.
- GDOES has helped to identify Ti, Ta, W elements diffusing from the substrate towards bond coats as the damaging elements in bond coat development.
- GDOES is able to detect other contaminant elements O, C and S which will lead to process improvements.
- GDOES has shown that the presence of Si which comes from the gritting process in bond coats which is very difficult to detect using an EPMA technique. However, cyclic performance data has shown it not to be detrimental, as there is no change in cycles to failure for two potential systems under consideration.
- GDOES has shown the presence of sodium in bond coats and also possible sodium diffusion.
- GDOES has shown variability in Pt levels within Low cost bond coats. Variability plays a key role in determining the thermal cyclic performance of this type of coating.

- GDOES has been proven to be very successful in depth profiling the low cost bondcoat with a thin layer of TBC deposit, with a dc source, rather than the need for a RF. It has been possible to investigate segregation of elements at interfaces using this method.
- Segregation of the following damaging elements are evident on the aged sample's interfaces TBC / Al<sub>2</sub>O<sub>3</sub> and Al<sub>2</sub>O<sub>3</sub> / Bond coat: Ti, W, Ta. As the ageing treatment increases there is evidence of increasing diffusion of those elements towards the interfaces.

#### Thermal Cycling Tests

- Thermal cycling testing has been shown to be a very useful way of ranking bond coats.
- The best bond coats identified from the thermal cycling test were the ones with La present in the substrate and yttrium present in the bond coats. These coatings can typically maintain adhesion of TBC for 250 hours at a temperature of 1150°C on a CMSX-4 superalloy substrate.

#### Morphological Analysis

- The intermediate layer between the TBC and the bond coat consists of Al<sub>2</sub>O<sub>3</sub> which is responsible for maintaining the adhesion. In the sample with no age treatment (0-hours) the structure of Al<sub>2</sub>O<sub>3</sub> is very fine. However, there is a variation in the thickness across the coating. Also evident is a Ti peak, which grows with ageing. Ti present is known to degrade bonding at the interfaces.

- There is evidence of growth in the  $\text{Al}_2\text{O}_3$  layer with ageing time.
- There is evidence of diffusion of Zr into the  $\text{Al}_2\text{O}_3$  and so adhesion between TBC /  $\text{Al}_2\text{O}_3$  must be chemical. Also there is evidence of pegging from the bond coat into the  $\text{Al}_2\text{O}_3$ , which is good for maintaining mechanical adhesion of the coating.
- At 25 hour aging treatment, the coating is still intact, although there is growth in the  $\text{Al}_2\text{O}_3$  layer.
- There is evidence of grit particles in the  $\text{Al}_2\text{O}_3$  layer, which can lead to stress cracking of the coating.
- Evidence of Ti/W segregation at the  $\text{Al}_2\text{O}_3$  / bond coat interface is known to lead to decohesion of the coating.

#### Failure Mechanisms / Bonding Factors

- From the thermal cycling / GDOES / SEM and TEM studies it has been shown that failure in low cost Pt bond coat systems is decohesion between the interfacial layer of  $\text{Al}_2\text{O}_3$  and the bond coat.
- Outward diffusion of Ti, W, Ta into the bond coat, leads to the formation of oxides which degrade the adherences of  $\text{Al}_2\text{O}_3$  and the bond coat.

- Surface condition of alloy substrate and variation in the thickness of Pt layer , as shown from GDOES / SEM studies, are identified as important sources of variability in TBC bonding.
- Performance of low cost bond coat systems can be concluded to be a function of alloy substrate chemistry.

### Overall Conclusion

- This study has been very successful in developing GDOES and Thin foil TEM as a characterisation tool in the study of bond coat systems.
- The program of studies has enabled failure mechanisms and bonding factors to be identified in low cost Pt bond coat systems , such that in the future coating systems with enhanced properties can be designed. This should also ensure in future that improved reliability in engines and increased service life of turbine blades is achieved.

## **Chapter 9**

### **Further Work**

Suggestion for further work in this area of research are as follows:

- GDOES analysis: Re /Rh channel installation: There is a need for GDOES to be able to detect these elements, as they can be of benefit for coating developments. The main problem is that there is no channel currently available on the rowland circle, because it is to its full capacity ( 48 elements ) and Re can only be installed as a filter channel instead of fluorine. The possibilities should be assessed in conjunction with LECO, the equipment supplier.
- GDMS Studies: Detection and quantification of very low level elements such as S, O, C, Y , impossible to detect in very low concentrations using GDOES. This will help in coating process improvements.
- XRD Studies: Identify and quantify compound formations within low cost Pt bond coats using the XRD technique before and after thermal age treatment to help increase understanding and also support current research.

- Substrate Chemistry: As already shown in low cost Pt bond coats the performance is dependent on the substrate chemistry, it would be very appropriate to investigate alternative available substrates such as RR3000, as potentials with currently available low cost Pt bond coats. This is to help slow down the diffusion process and prevent spinel formation, in order to make the coating more stable. Thus higher life expectancy would be obtained.
- TEM Investigation: Determine EDX on sample 212 to help in comparative process.
- TEM Investigations: Determine by point analysis the elemental composition across coatings on all aged samples, so that a full comparison may be made with GDOES findings.
- TEM Investigations: Characterise in more detail the Al<sub>2</sub>O<sub>3</sub> scale in new and current compositions in order to help identify phases and spinels. This should help in developing more cyclic resistant coatings.
- Interface Engineering: Overall, future work should concentrate on the interfaces engineering in greater detail using current techniques developed and techniques currently not utilised such as GDMS, SIMS, FEG. This will enable a better understanding of impurity segregation, its relationship to cyclic performance on new compositions and current compositions, so that real improvements can be gained.

Figure 1. A typical EBPVD coated turbine blade [122]

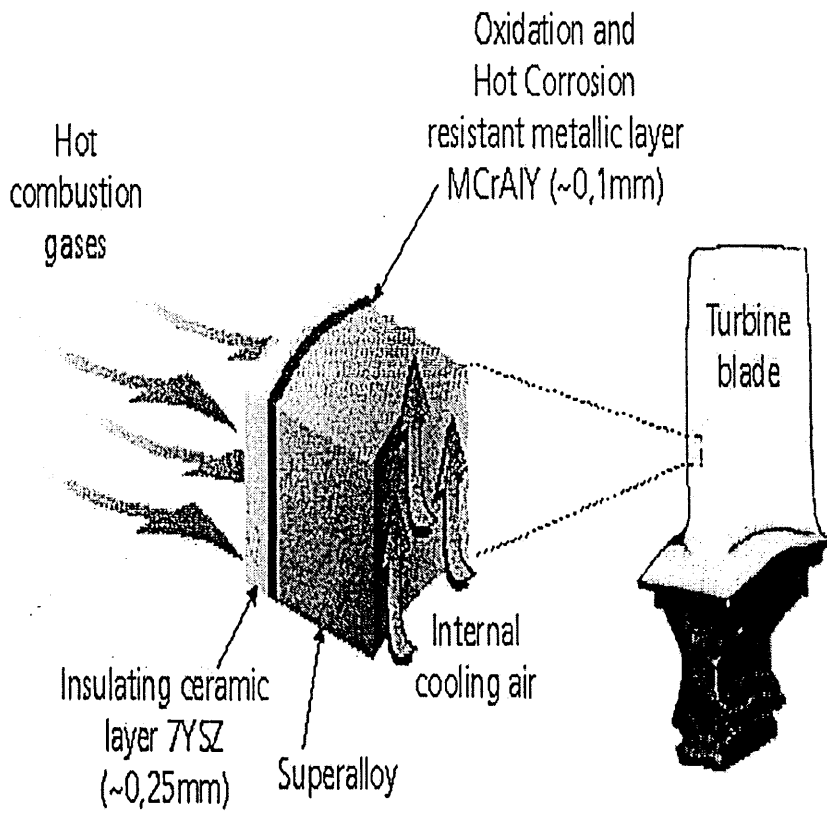


Figure 2.2.4 (a) Plasma sprayed  $ZrO_2$  coating [123]

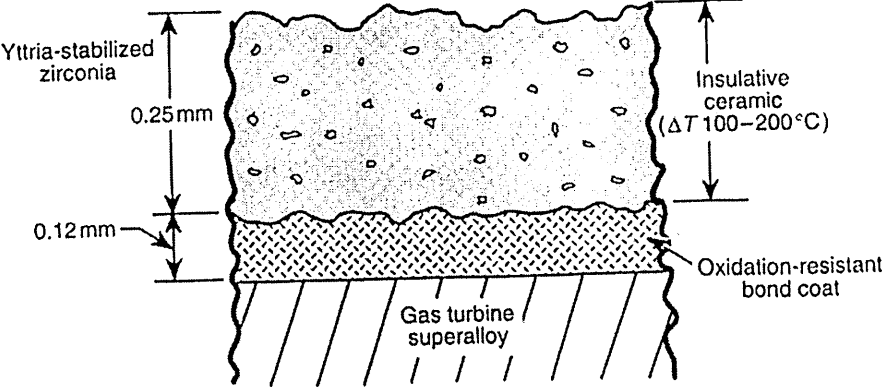


Figure 2.2.4 (b) EBPVD  $ZrO_2$  Coating [123]

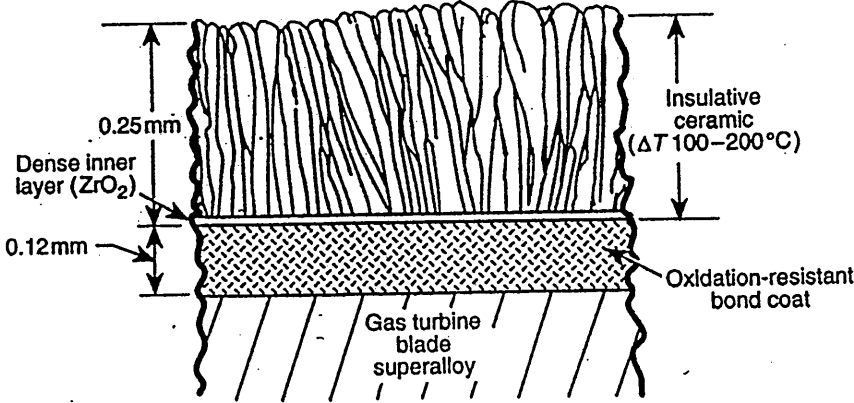


Figure 2.2.4 (c) Schematic illustration of the plasma spray deposition technique [123]

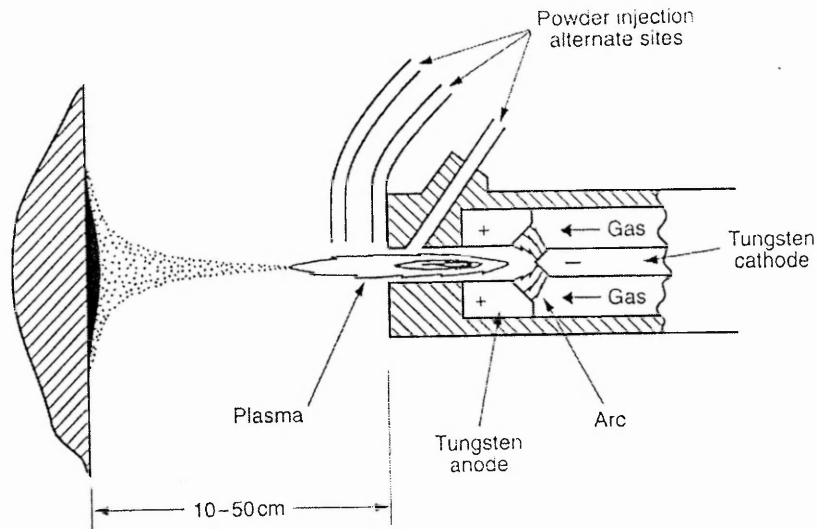


Figure 2.2.4 (d) Schematic illustration of the EBPVD technique [124]

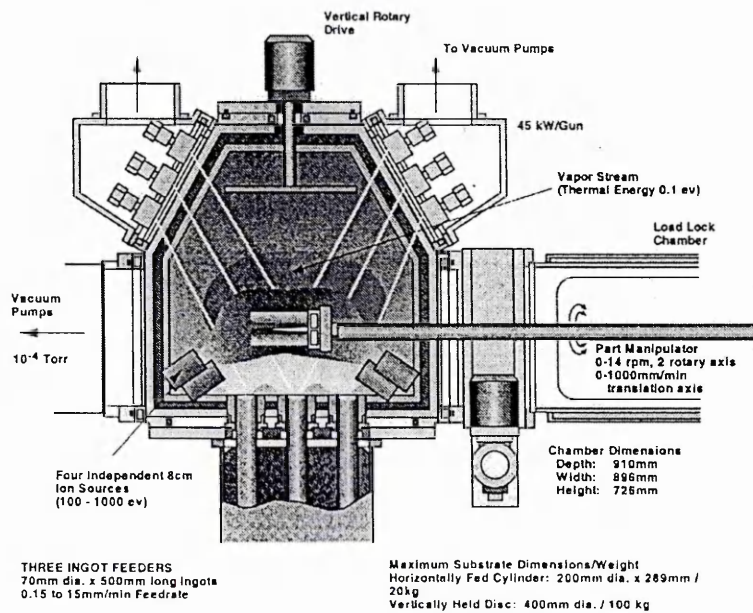
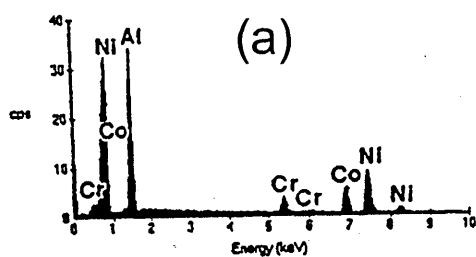
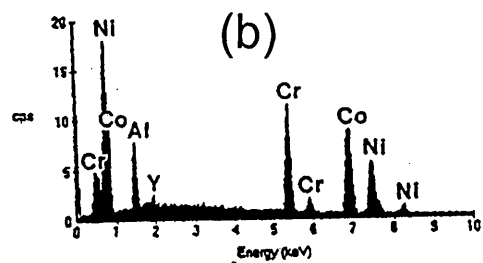


Figure 2.3.2 : (a) chemical composition of the matrix phase; (b) chemical composition of the  $\beta$  – phase [93]



Chemical Composition of the  $\beta$ -Phase

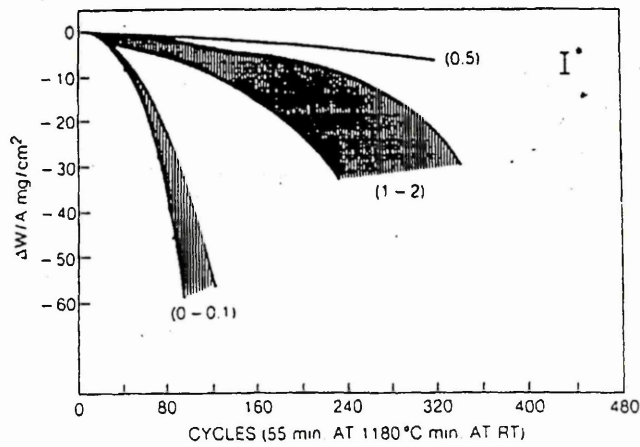
	<u>Atomic %</u>	<u>Weight %</u>
Ni	41.00	51.19
Co	18.02	22.48
Al	35.42	20.22
Cr	5.56	6.12



Chemical Composition of the Matrix Phase

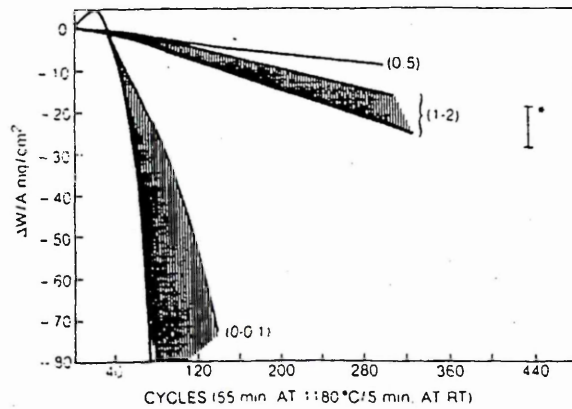
	<u>Atomic %</u>	<u>Weight %</u>
Co	38.47	41.52
Ni	29.38	31.59
Cr	22.44	21.37
Al	9.05	4.47
Y	0.65	1.06

Figure 2.3.3 (a) High temperature/Low activity pack aluminide coated specimens tested in 1180°C cyclic oxidation.



\*CORRESPONDS TO WEIGHT CHANGE FOR THE CONVERSION OF ALL A: IN COATING TO  $\text{Al}_2\text{O}_3$ , i.e. COMPLETE COATING FAILURE

Figure 2.3.3 (b) Low temperature / High activity pack aluminide coated specimens tested in 1180°C cyclic oxidation.



\*CORRESPONDS TO WEIGHT CHANGE FOR THE CONVERSION OF ALL A: IN COATING TO  $\text{Al}_2\text{O}_3$ , i.e. COMPLETE COATING FAILURE)

( ) INDICATES NOMINAL w/o HI CONTENT IN SUBSTRATE ALLOY

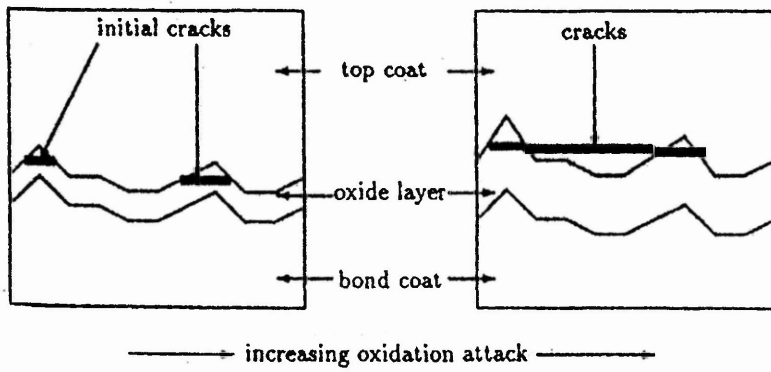


Figure 2.5.2 (a) Initiation of spalling of TBC [8]

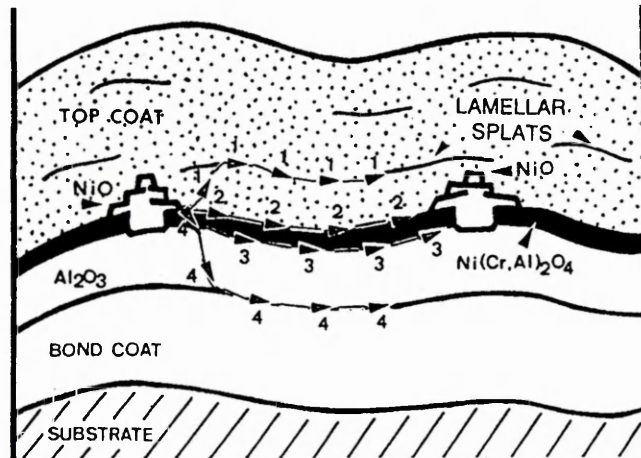


Figure 2.5.2 (b) The four propagation modes of spalling in TBC's [127]

Figure 2.5.3. Thermal expansion of  $ZrO_2$  8wt%  $Y_2O_3$  and IN 738 Vs Temperature [8]

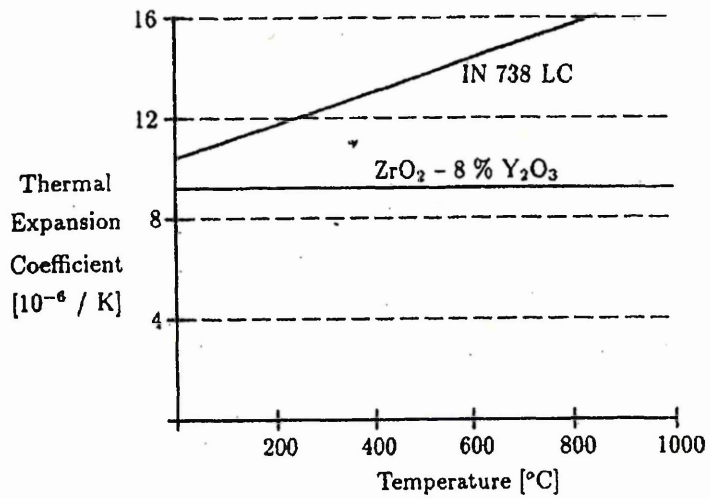


Figure 3.1(b) Back scattered images of LCBC microstructures:

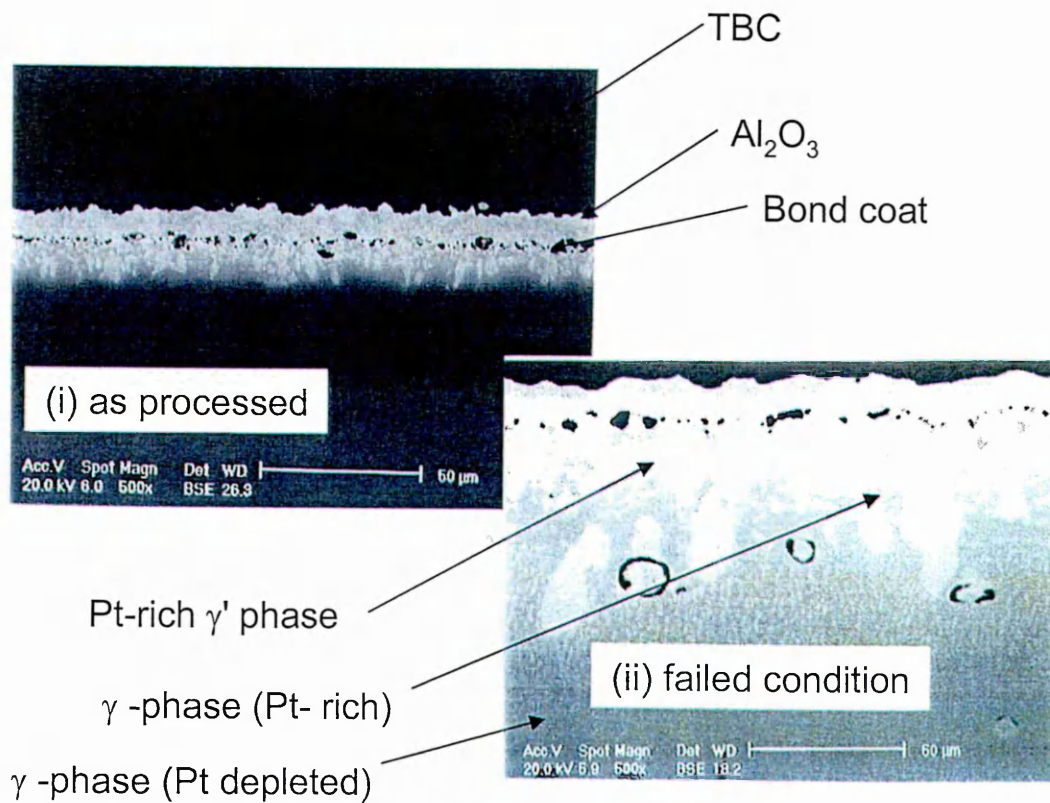


Figure 3.2.1(a) X-ray diffraction pattern derived from the surface of a LCBC after removal of the top coat (as received condition)

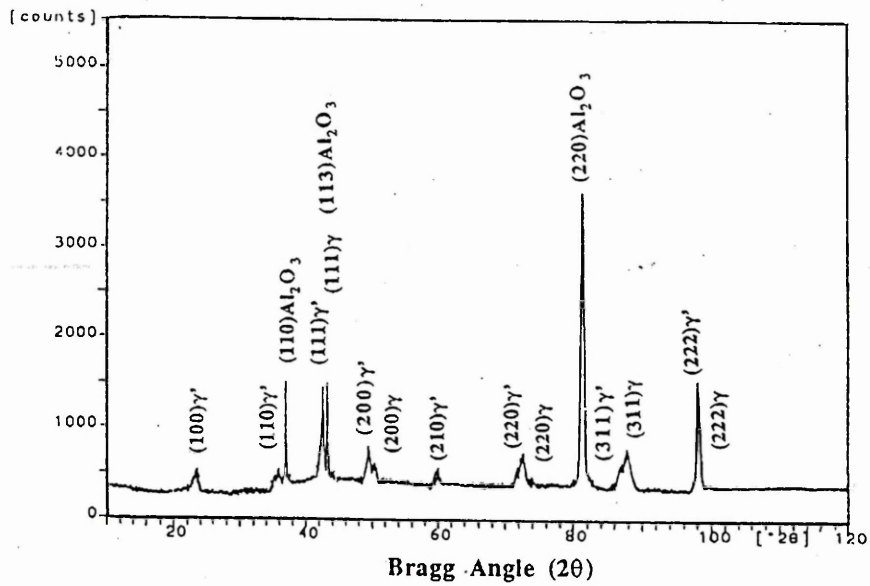


Figure 3.2.1(b) X-ray diffraction pattern derived from the surface of a LCBC exposed by failure (288 hours of exposure at 1150°C).

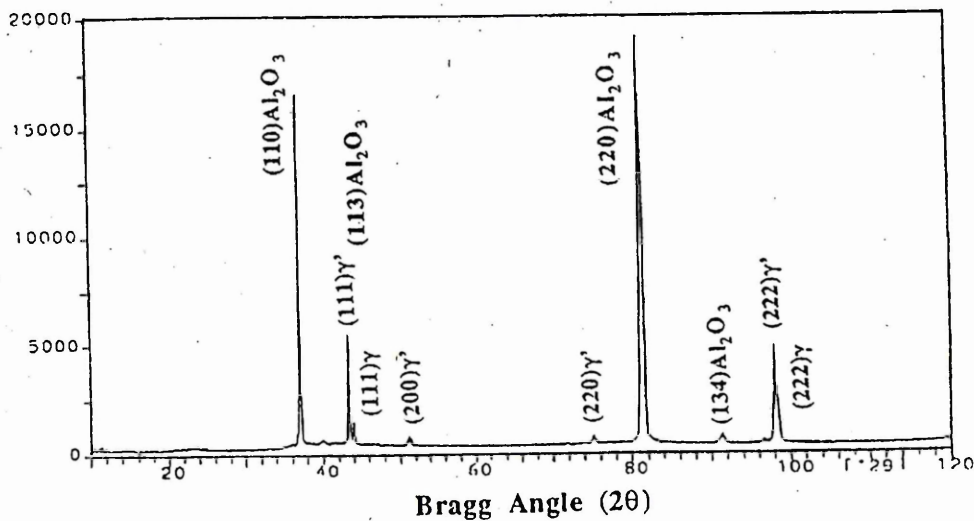


Figure 3.2.2 (a) The variation in ion milling rate and implantation depth as a function of incident angle [78]

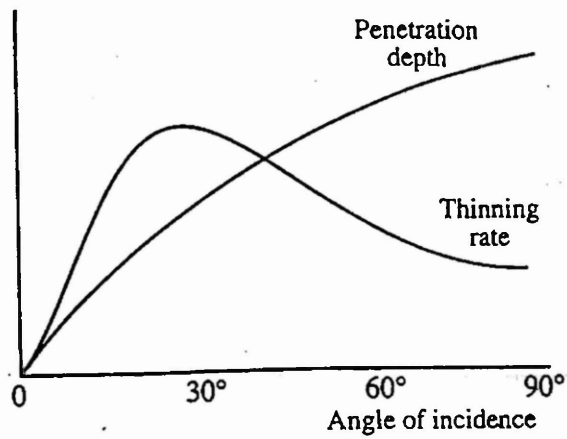


Figure 3.2.2 (b) Specimen preparation for TEM analysis [80]

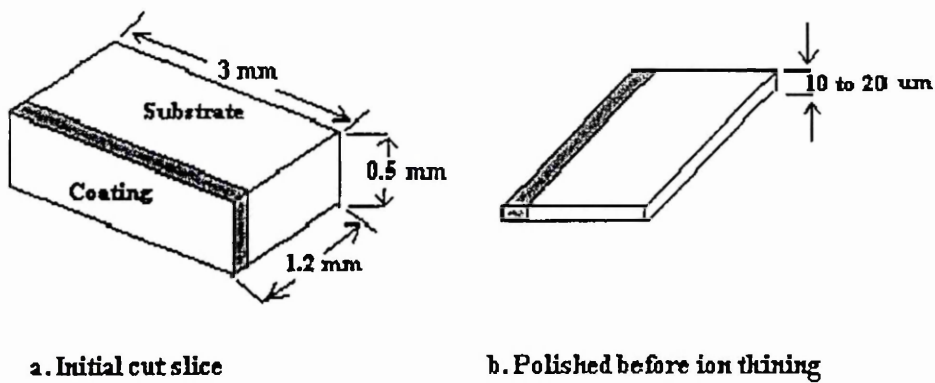


Figure 3.2.2 (c) Clamp type and glue-on-type specimen holders [82]

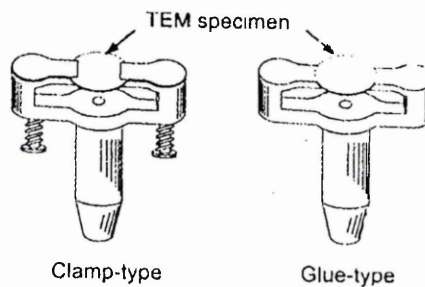


Figure 3.3.1 (a) Glow discharge sputtering process

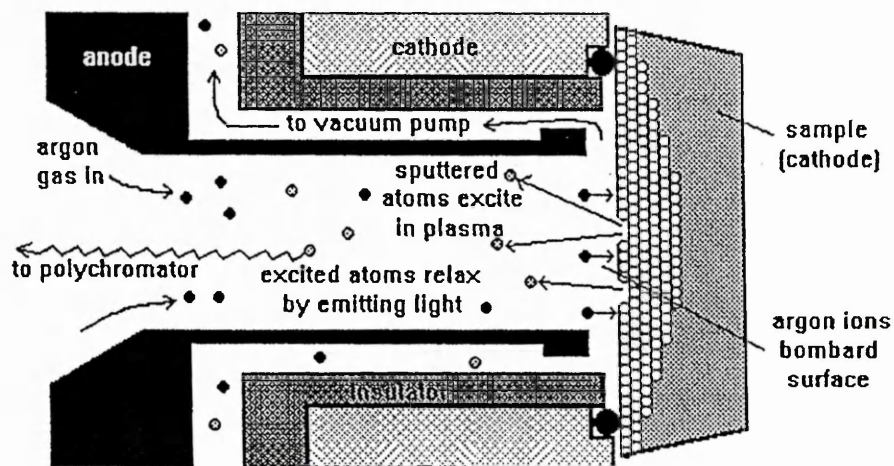


Figure 3.3.1 (b) Glow discharge lamp

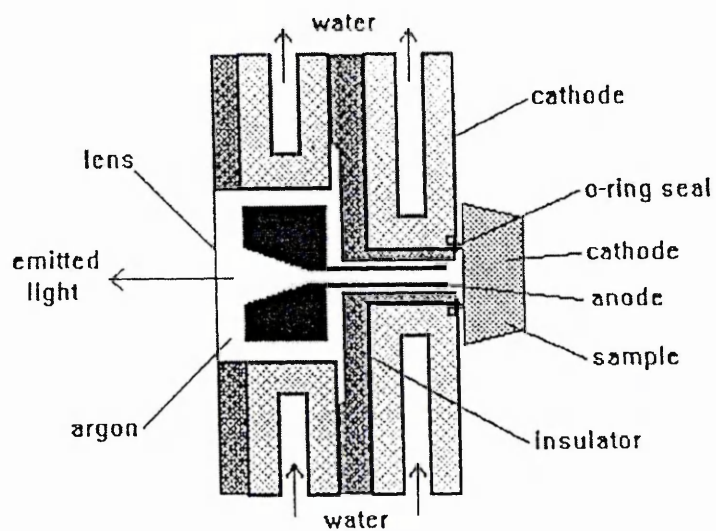


Figure 3.3.1 (c) Light dispersion and detection

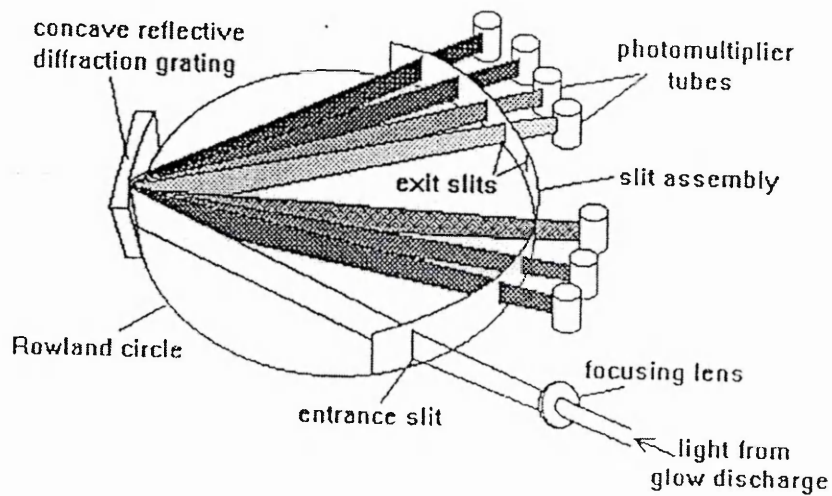


Figure 3.3.1 (d) Depth ranges for various surface analytical methods

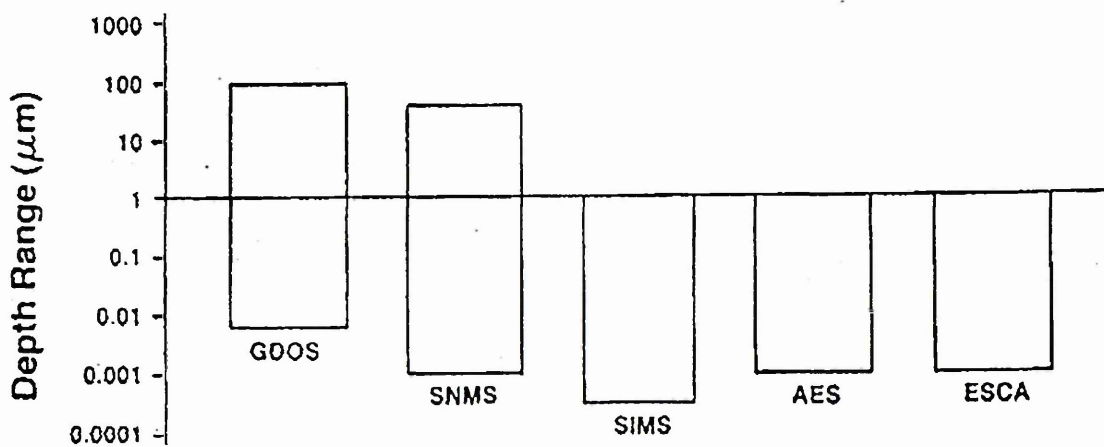


Table 3.3.1 (e) Analysis parameters used

Evacuation time	10 sec
Argon flushing time	20 sec
Preburn time	60 sec
Interval delay	0
Burn time	0
Numner of repititions	0
Compensation	5 sec
Integration time	10 sec
GDL operating time	11
Preburn excitation	700 V
Integration excitation	700 V; 30 mA
Flow rate in digits	400
Evacuate until	10E-3 mBar
Anode diameter	4 mm
Profile duration (depends on sample)	300–1000 sec

Figure 4.1.1 Quantitative program set-up procedure

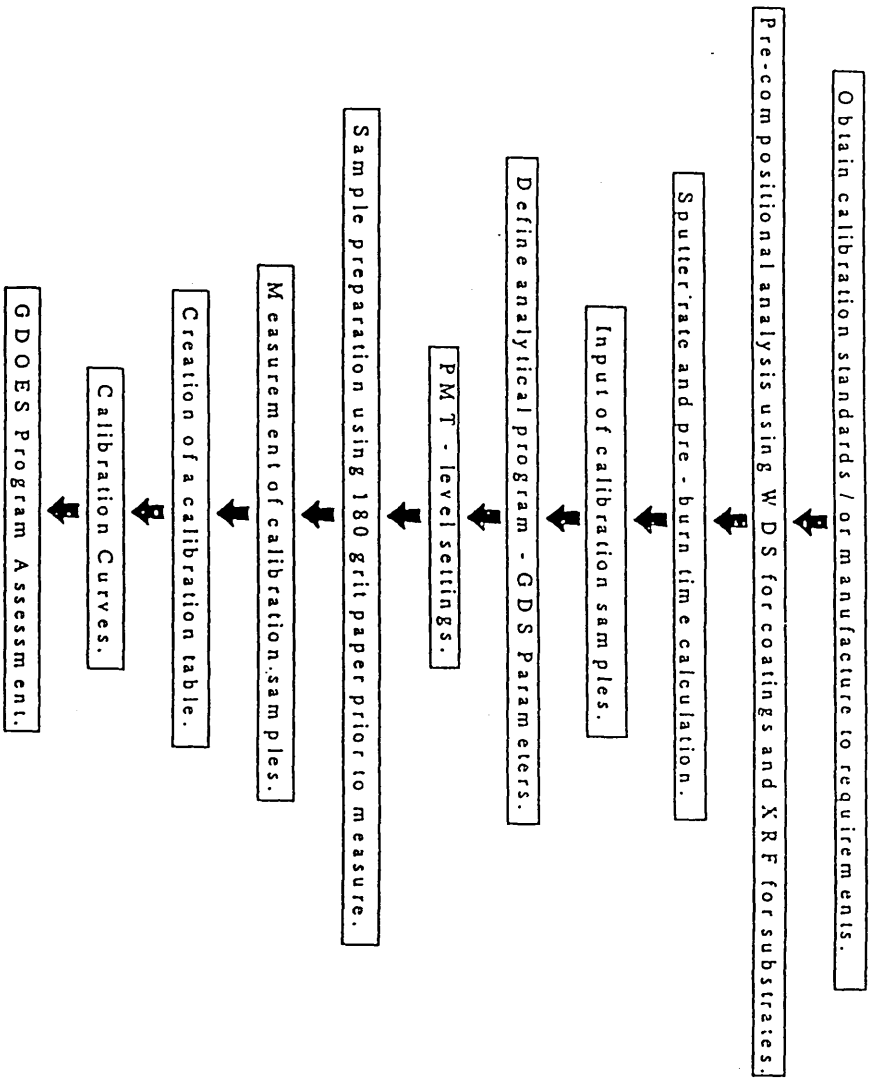


Table 4.1.2 Calibration Overview

Analyte	Analytical range	Matrix Element in	Calibration points used
Ni	1.99–64.69%	Ni Fe grades; Aluminide coatings; Pure Ni; MCrAlY	29
Cr	0.23–8.78%	Superalloy: Marmoo2, CMSX-4 Low alloy steel; Pure Co	7
Al	0.00–17.91%	Aluminide coating; Superalloys Pure Al	16
Ti	0.11–1.44%	Superalloys; Aluminide coatings Pure Ti	10
Pt	0.00–99.99%	Pure Pt; Aluminide coatings	4
Y	0.00–99.99%	Pure Y MCrAlY coating	2
Co	0.38–9.42%	Pure Co; High alloy steel; Aluminide coating	19
Mo	0.30–9.41%	Low alloy steel grades High alloy steel grades	11
W	0.20–9.65%	Superalloys Aluminide coatings	9
Ta	1.13–6.48%	Superalloys Aluminide coatings	4
Hf	0.07–1.27%	Superalloy grades	2
Zr	0.00–97.67%	Pure Zirconia	1
Si	0.05–2.69%	Cast iron; High alloy steel Superalloy grades	17
P	45.2–225.8 ppm	Low alloy steel grades High alloy steel grades	13
B	4.27–27.12%	BTiAlN Ni–B	2
S	30.1–378.6 ppm	High alloy steel grades Low alloy steel grades	8
C	0.00–3.35%	Cast iron grades; High alloy grades; Low alloy steel grades	14
O	0.00–26.60%	FeO	1

Figure 4.1.3 (a) Time – Intensity Trace on CMSX-4 showing Ni,Al,Co profiles

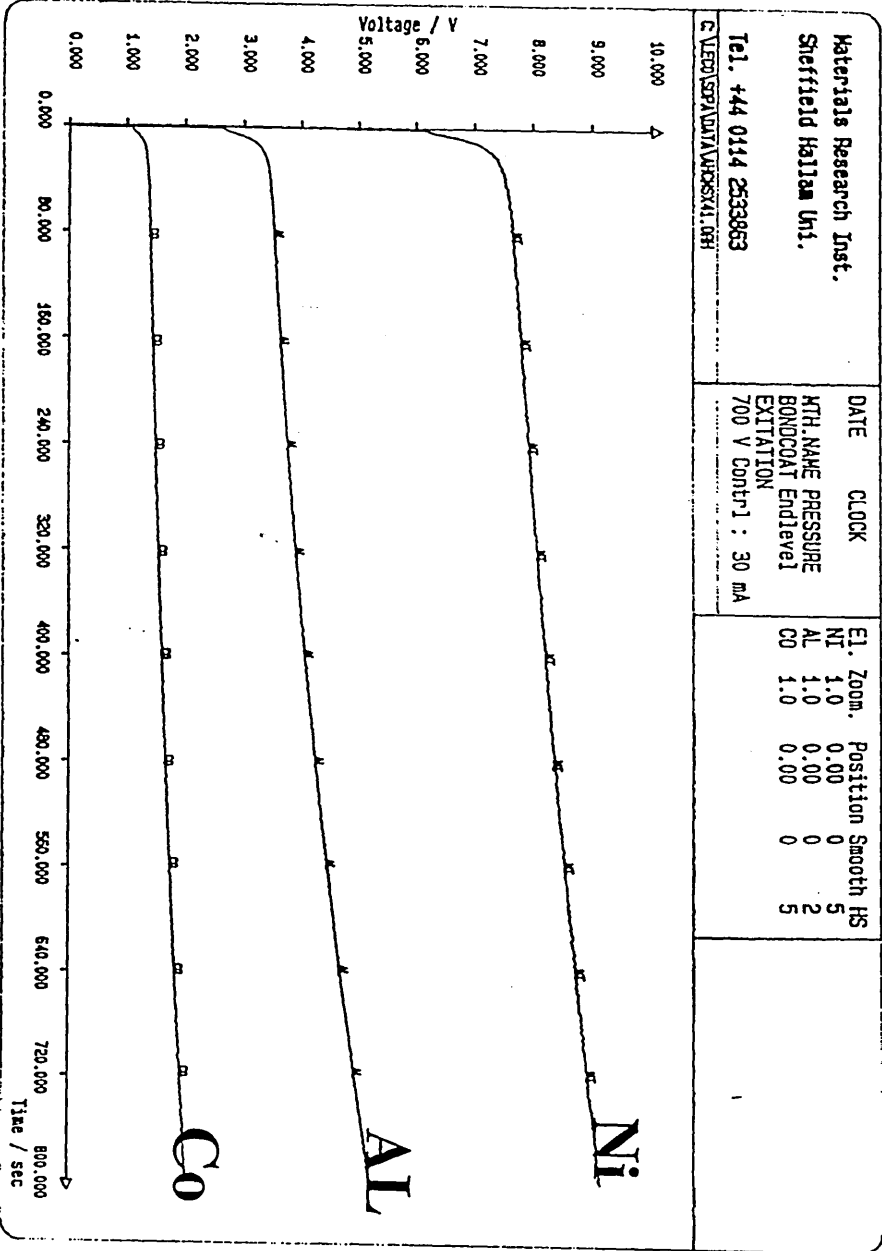


Figure 4.1,3 (b) Time – Intensity Trace on CMSX-4 showing Co,Ti,Hf,W profiles

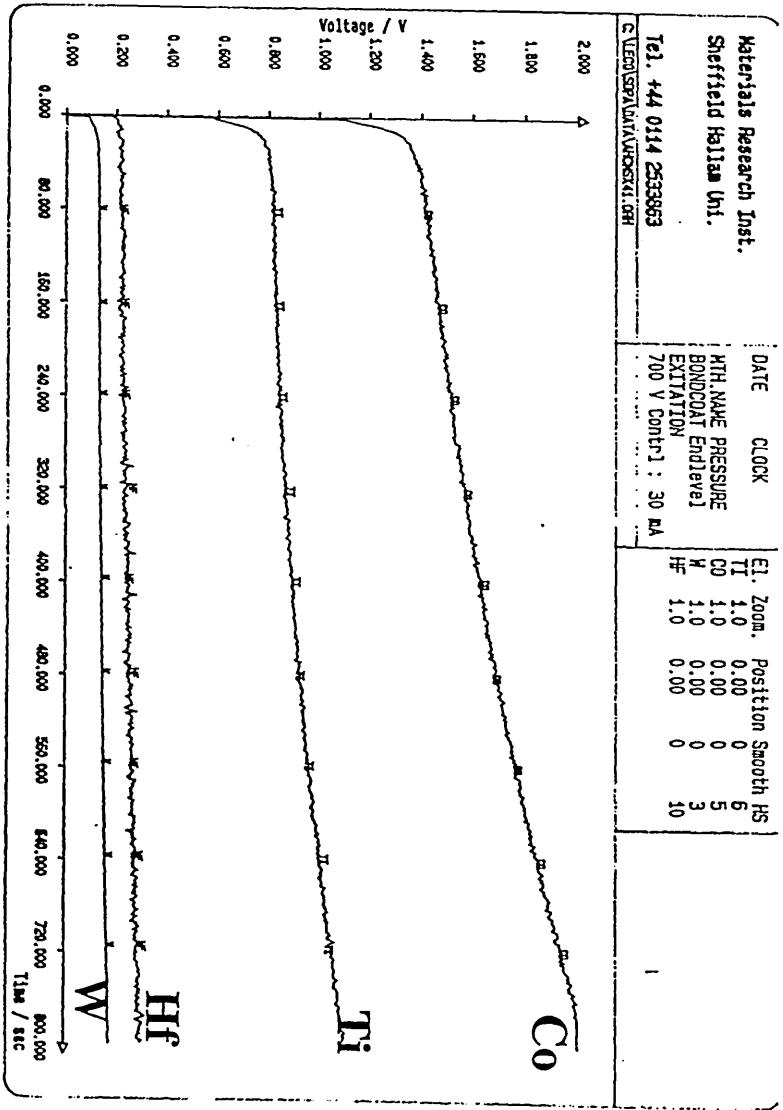


Figure 4.1.3 (c) Depth – concentration profile on CMSX-4 showing Ni,Al,Co profiles

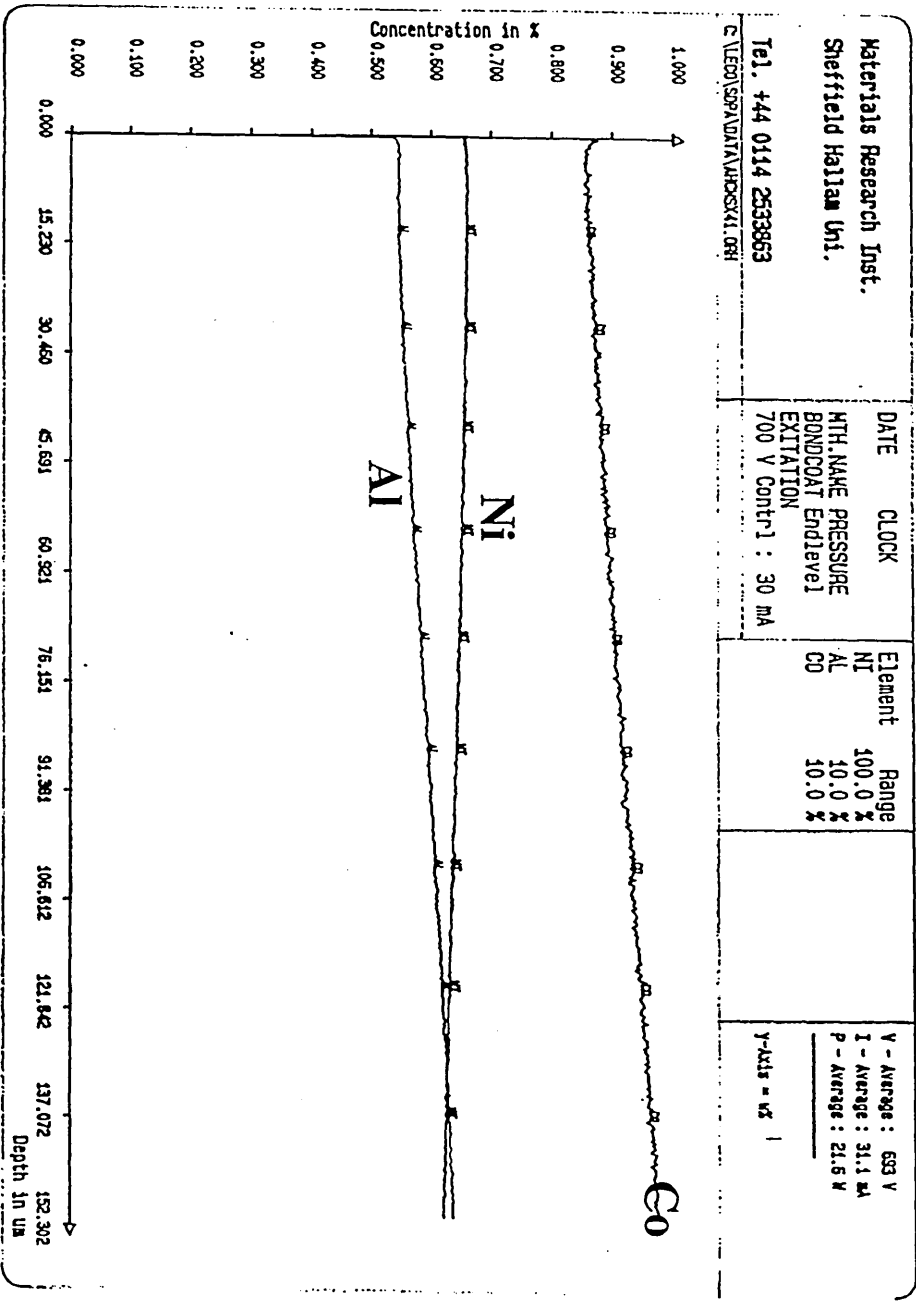


Figure 4.1.3 (d) Depth-concentration profiles on CMSX-4 showing Co,Hf,Ti, W profiles

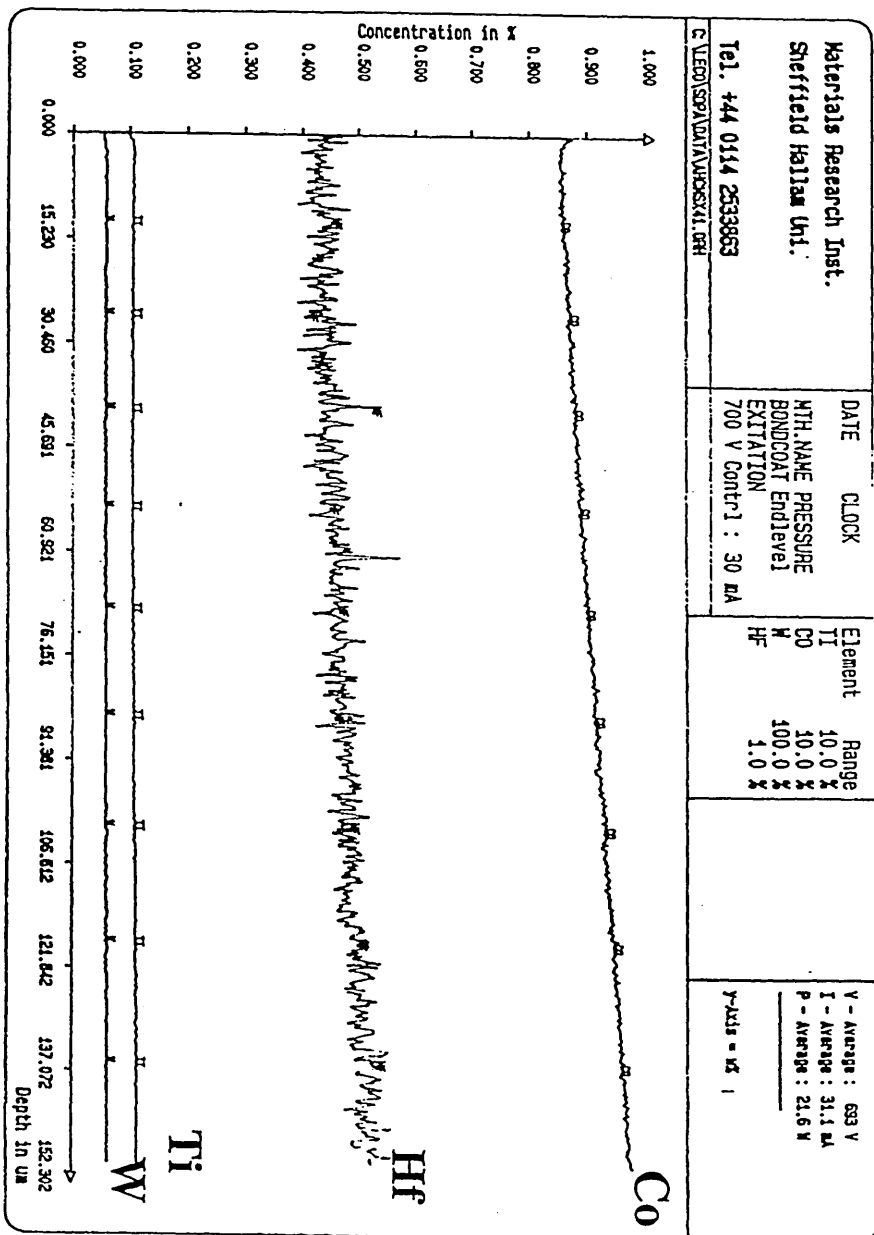


Figure 4.1.3 (e) (i) SEM micrograph of crater at 60 sec

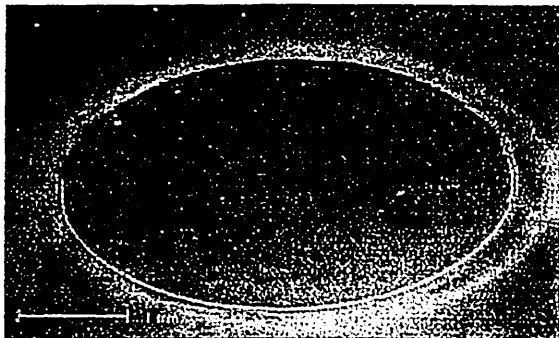


Figure 4.1.3 (e) (ii) SEM micrograph of crater at 1000 sec

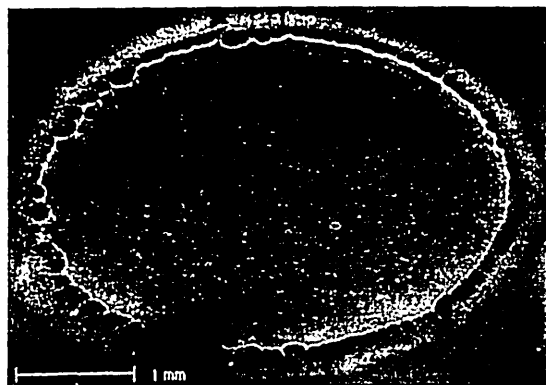


Figure 4.1.3 (f) (i') Laser profile of crater at 60 sec

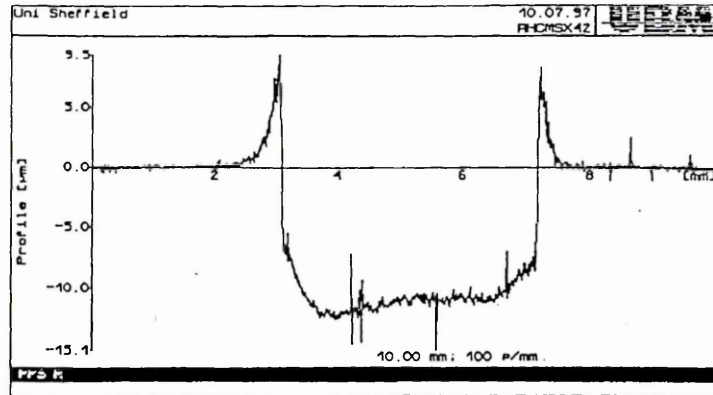


Figure 4.1.3 (f) (ii') Laser profile of crater at 1000 sec

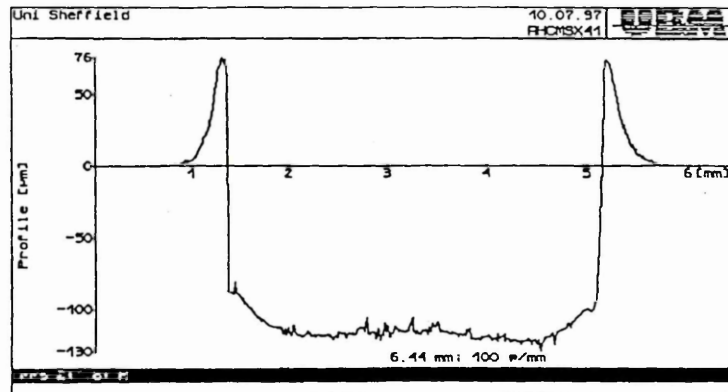


Figure 4.1.3 (g) Comparison of substrate/coating standards, XRF measured vs GDOES

ELEMENT (mass %)	NI	CR	AL	TI	PT	CO	MO	W	TA	HR	ZR	SI	Y	P
SUBSTRATE & COATINGS														
CMSX-4 Substrate XRF measured	60.82	6.3	5.83	0.98	0.012	9.46	0.60	6.32	6.52	0.1	0.005	0.03		-0.001
CMSX-4 Substrate GDOES measured	65.04	6.35	5.48	1.04	0.48	9.20	0.54	5.91	5.46	0.46	0.007	0.04		0.009
MARM002 Substrate XRF measured	59.74	9.01	5.6	1.49	0.001	9.92	0	9.95	2.73	1.24	0.039	0.14		0.009
MARM002 Substrate GDOES measured	61.05	8.88	5.39	1.56	0.38	9.49	0.007	8.56	2.84	1.76	0.029	0.05		0.012
MCRALY Coating XRF measured	30.9	23.7	7.7			37.7							0.5	
MCRALY Coating GDOES measured	29.43	25.50	8.89			35.64							0.54	

Figure 4.1.3 (h) ii Comparison of substrate using XRF, EPMA and GDOES Techniques

Element (mass %) / Technique	Ni	Cr	Al	Ti	Pt	Co	Mo	W	Ta	Hf	Zr	Si	Y	B	O	RE	C	P
XRF Analysis	60.82	6.30	5.83	0.98	0.012	9.46	0.60	6.32	6.52	0.10	0.005	0.03	0.00	0.00	0.00	2.71	0.00	0.00
EPMA Analysis	59.90	6.70	6.30	1.10	0.00	9.60	0.60	6.10	6.40	0.10	0.00	0.00	0.00	0.00	0.00	3.70	0.00	0.00
GDOES Analysis	64.51	6.39	5.89	1.09	0.431	9.11	0.55	6.07	5.40	0.47	0.009	0.029	0.020	0.00	0.00	0.00	0.001	0.007

Figure 4.1.3 (i) TBC trace

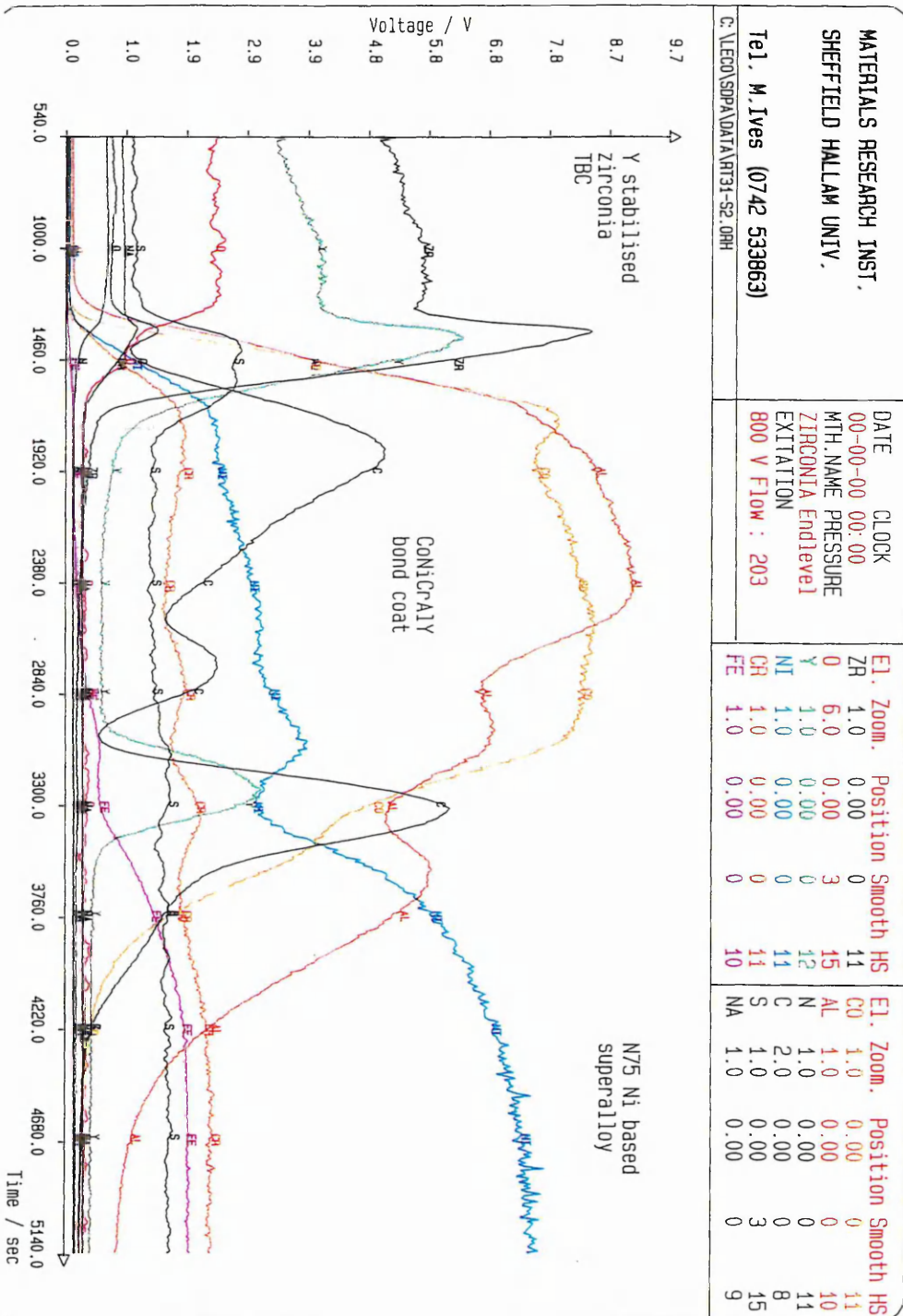


Figure 4.1.3 (k) EPMA analysis of a TBC system

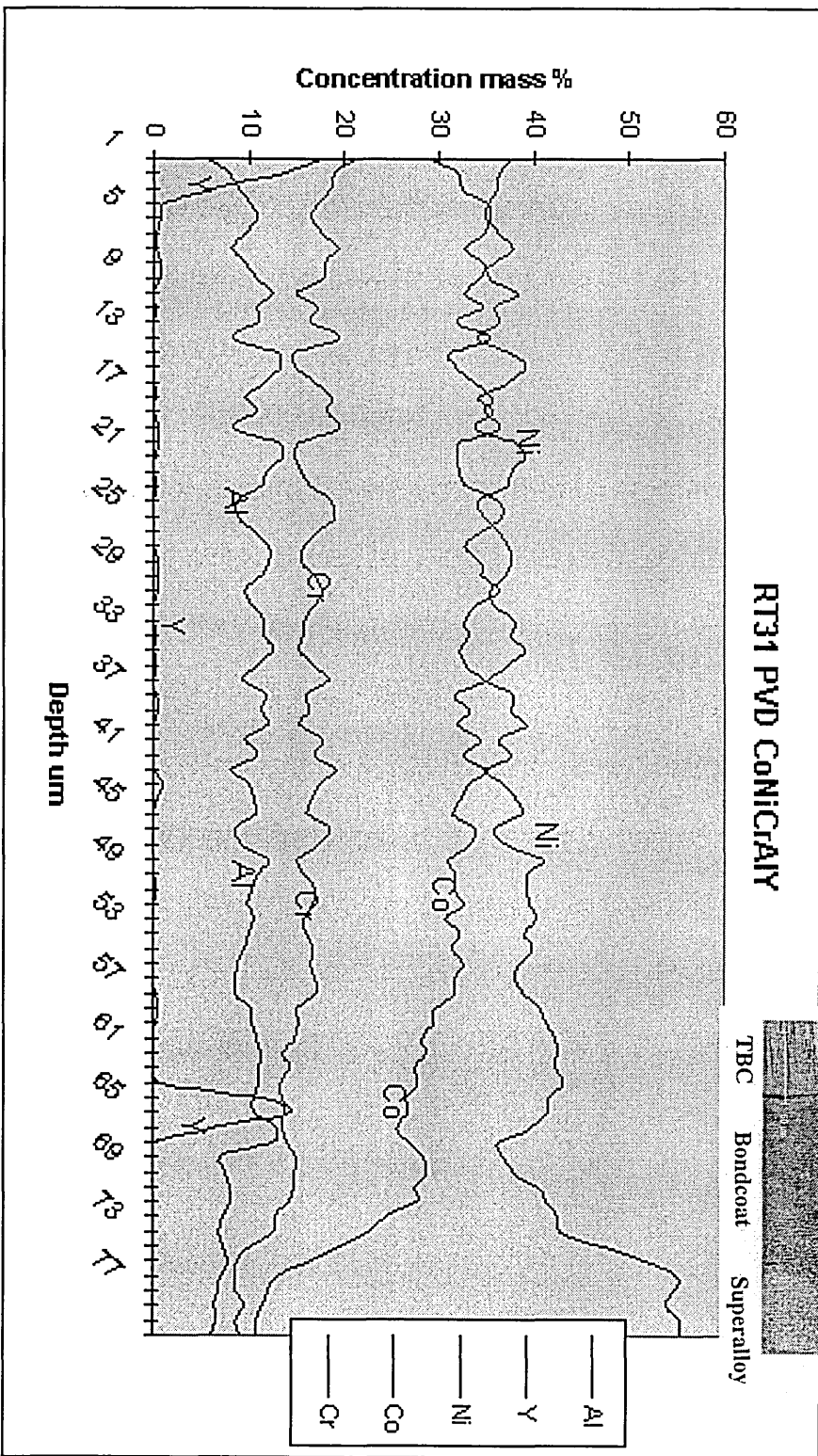


Figure 4.1.3 (j) Typical SEM image of TBC

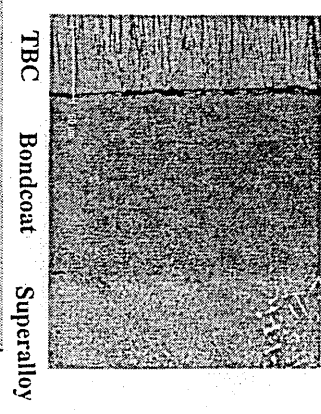


Figure 4.2.1 a: GDOES Pt depth profile for sample AHD 982 as plated

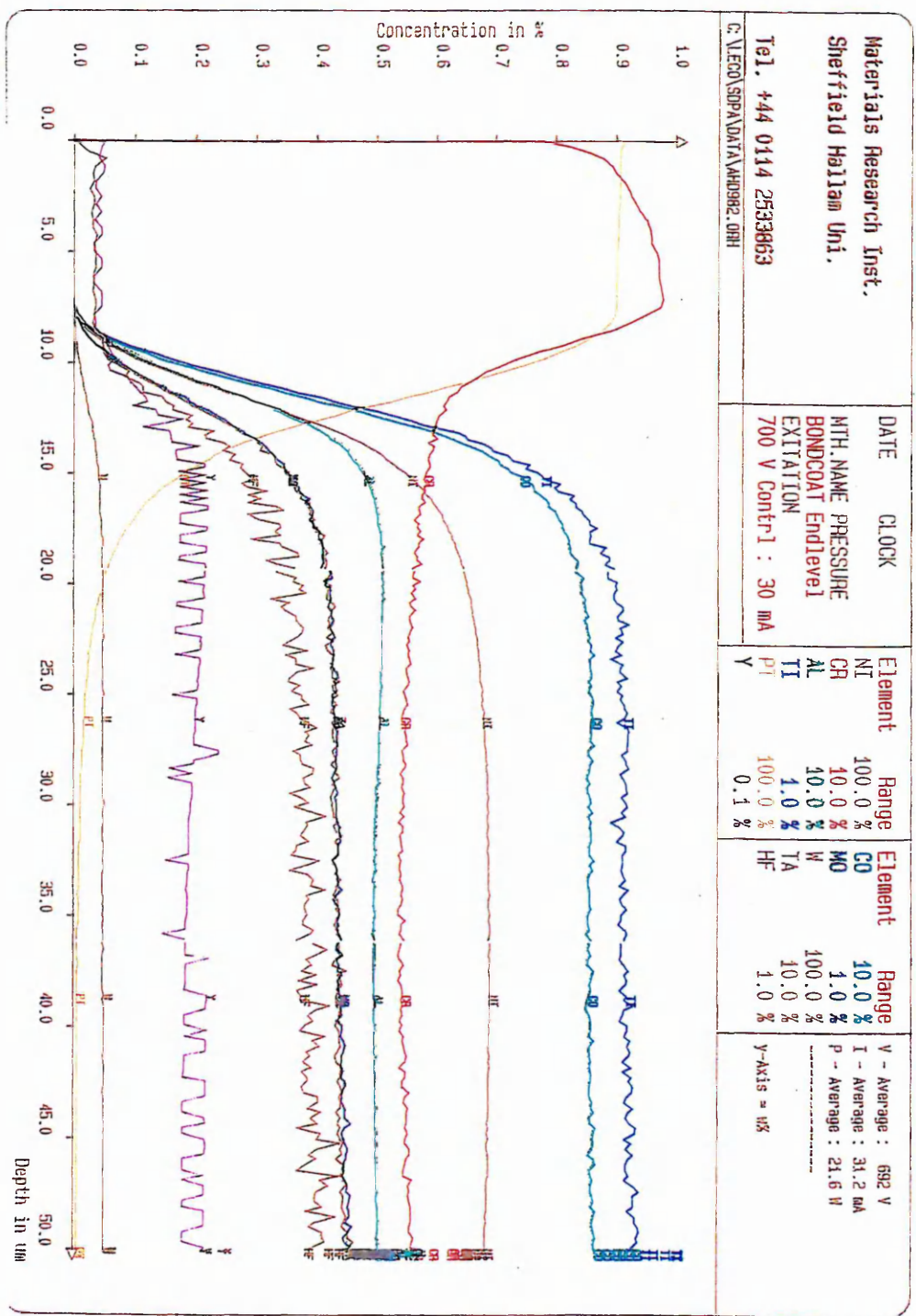


Figure 4.2.1 b: GDOES Pt depth profiles for sample E20 as plated

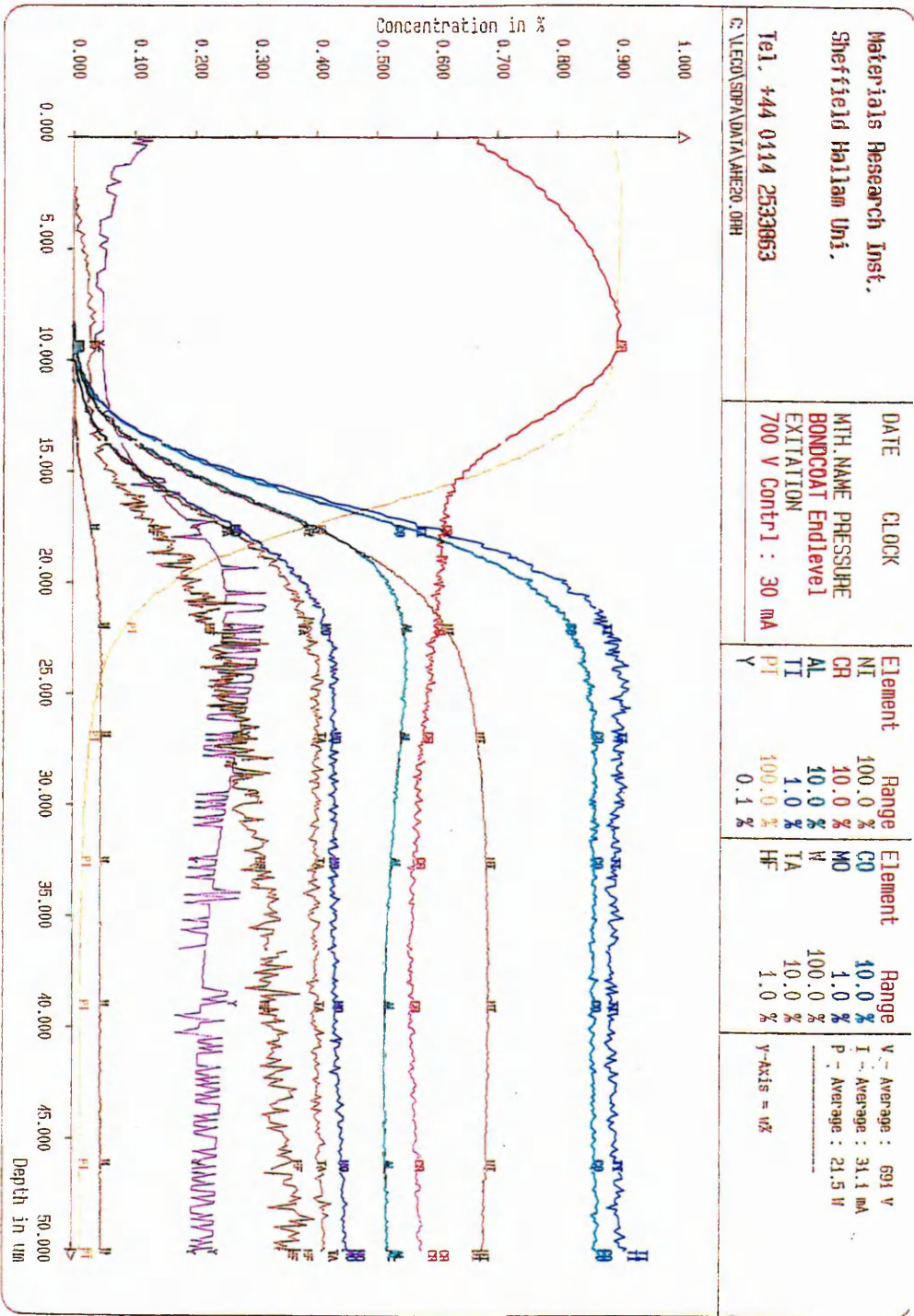


Figure 4.2.1 c: GDOES Pt depth profiles for sample AHE63 as plated

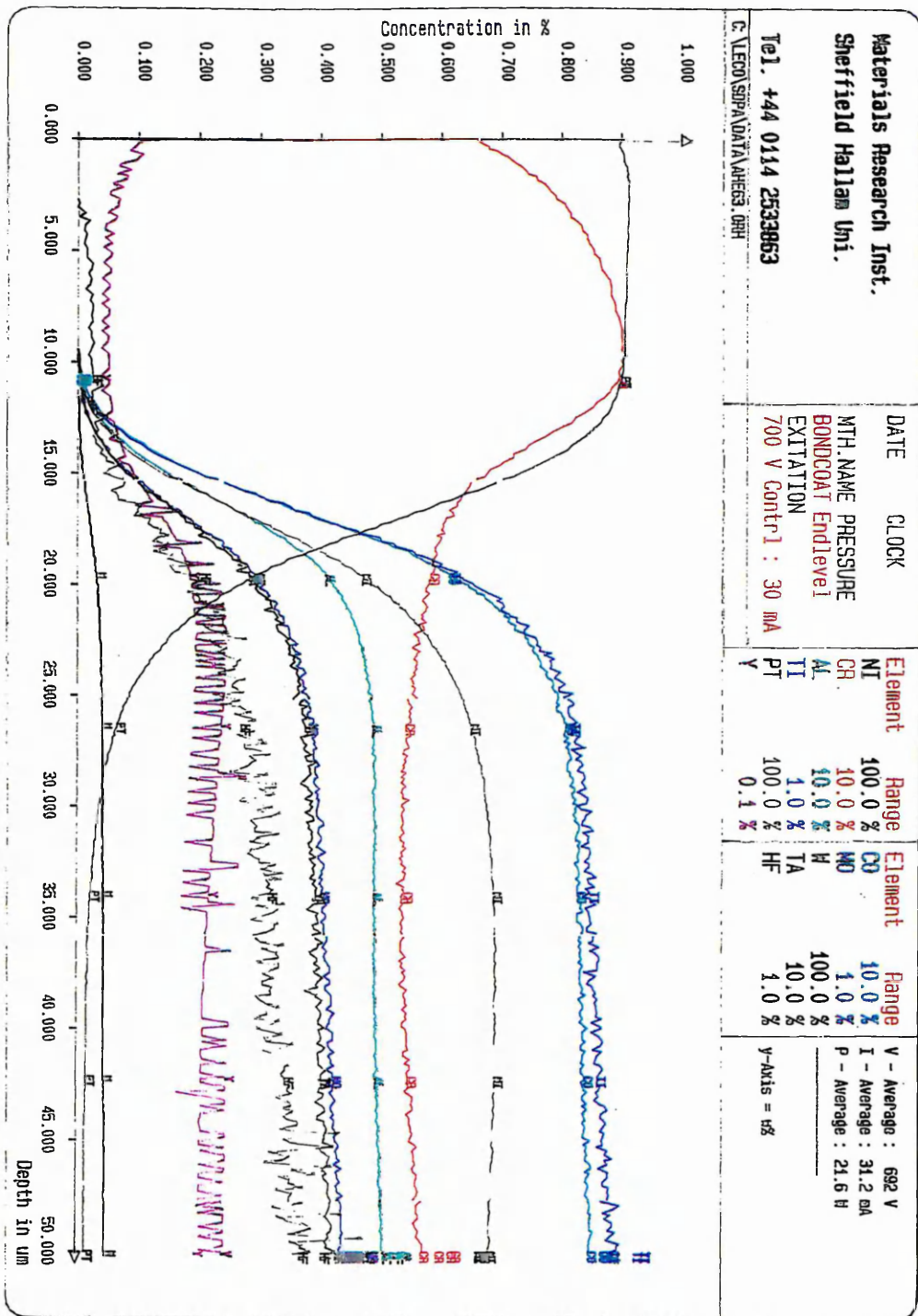


Figure 4.2.1 d: GDOES Pt depth profiles for sample AHD928 in the Heat treated condition

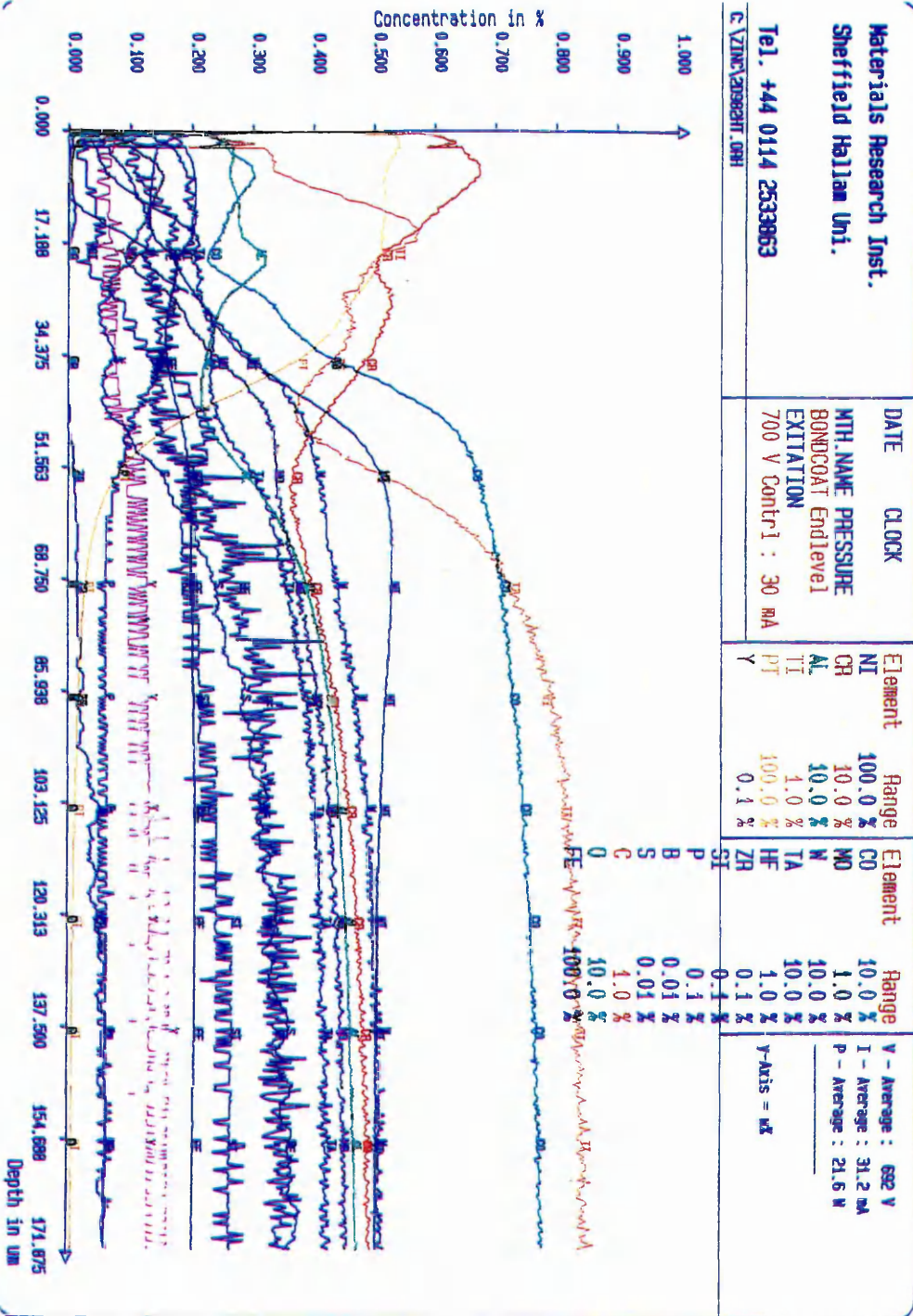


Figure 4.2.1 e: GDOES Pt depth profiles for sample E20 in the Heat treated condition

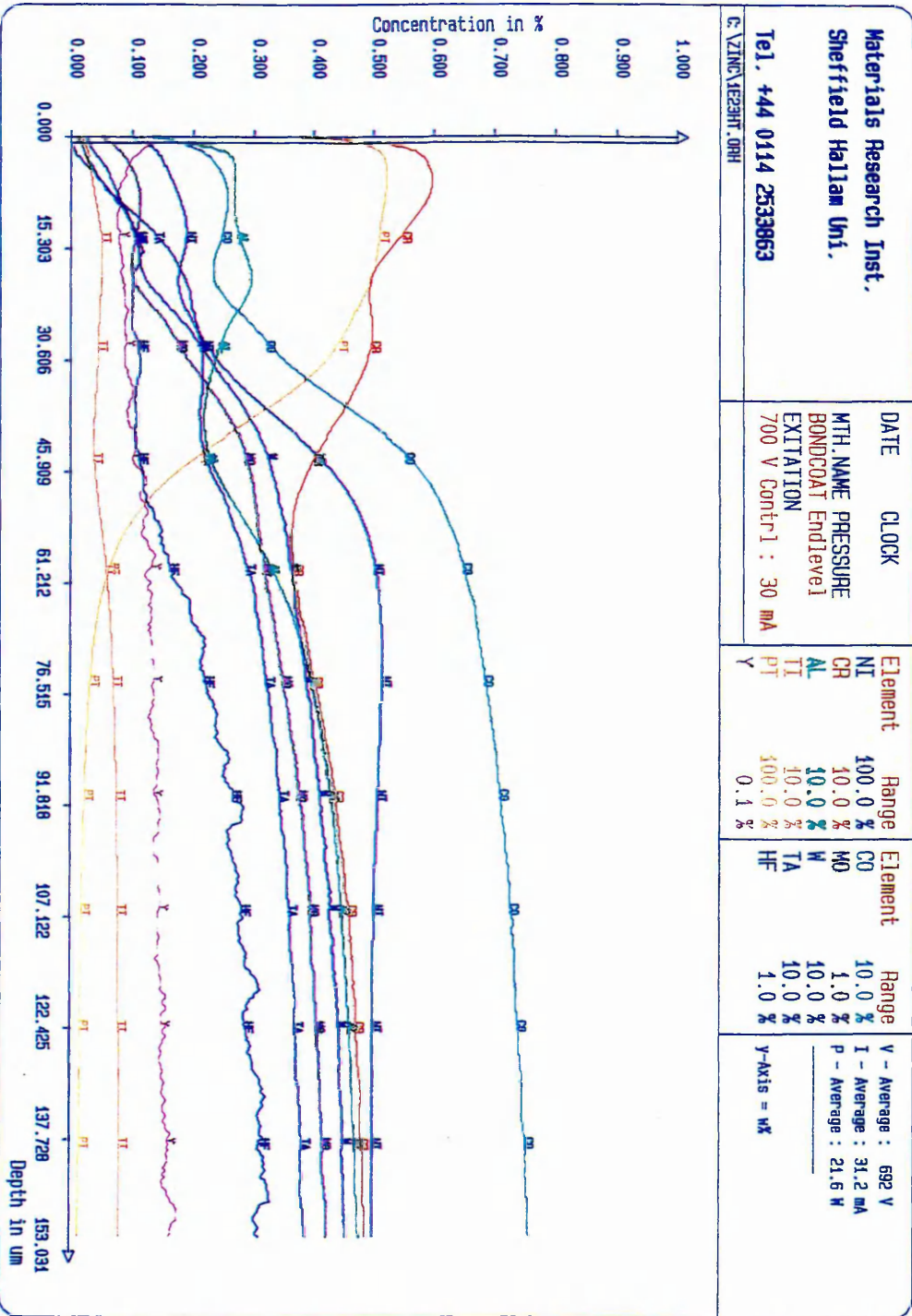


Figure 4.2.1 f: GDOES Pt depth profiles for sample AHE63 in the Heat treated condition

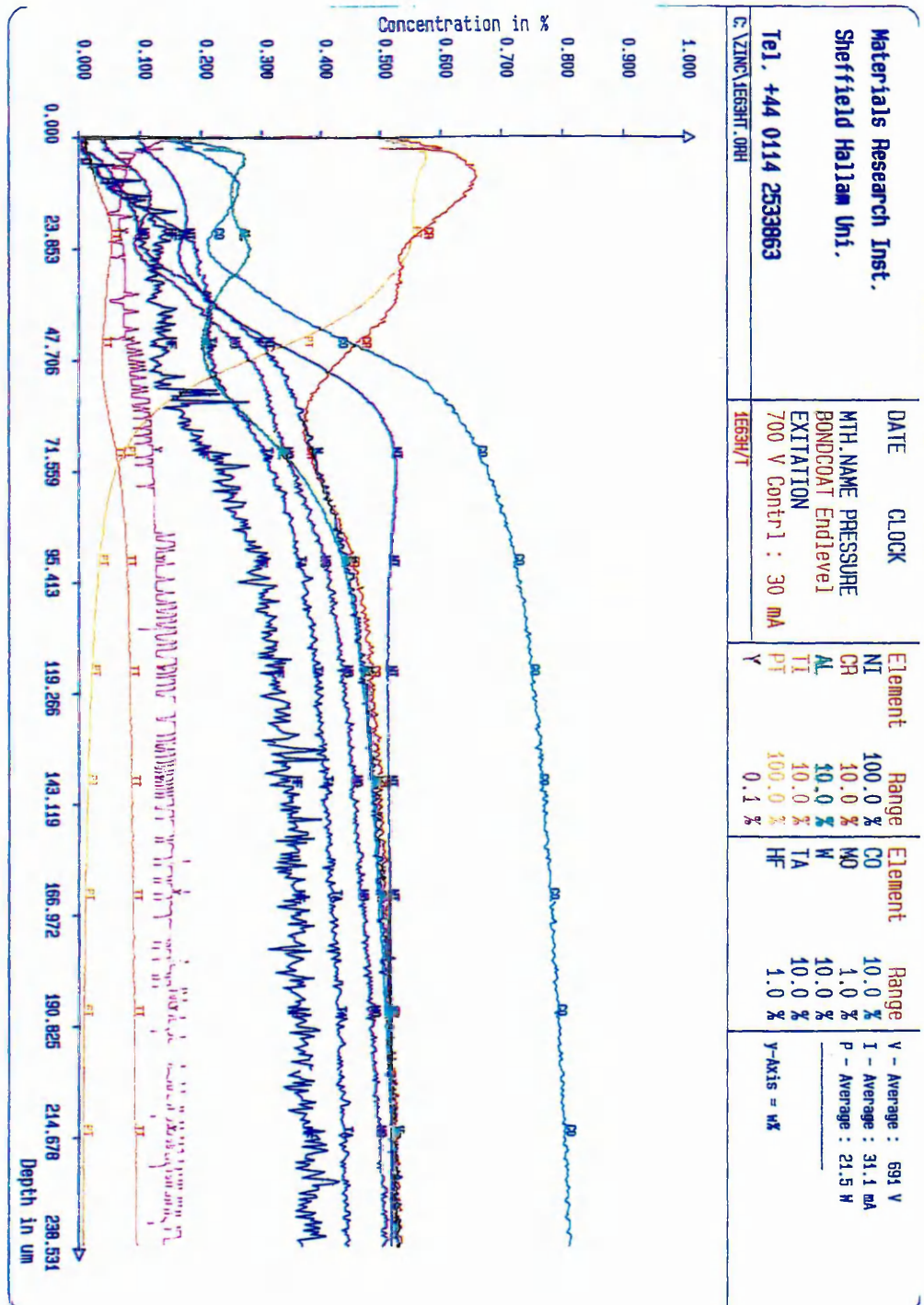


Figure 4.2.1 g: GDOES Pt depth profiles for sample AHD928 in the failed condition

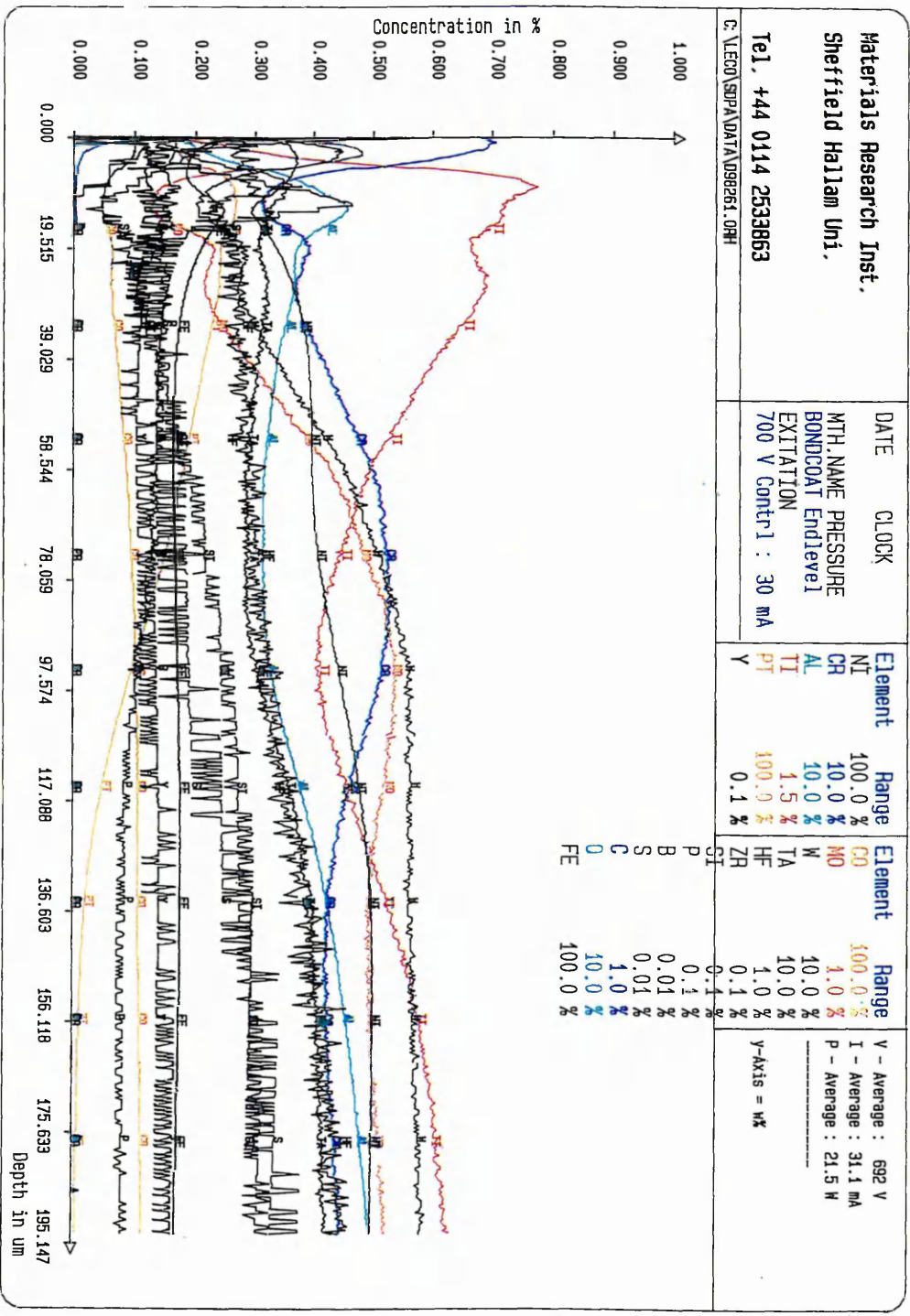


Figure 4.2.1 h: GDOES Pt depth profiles for sample E20 in the failed condition

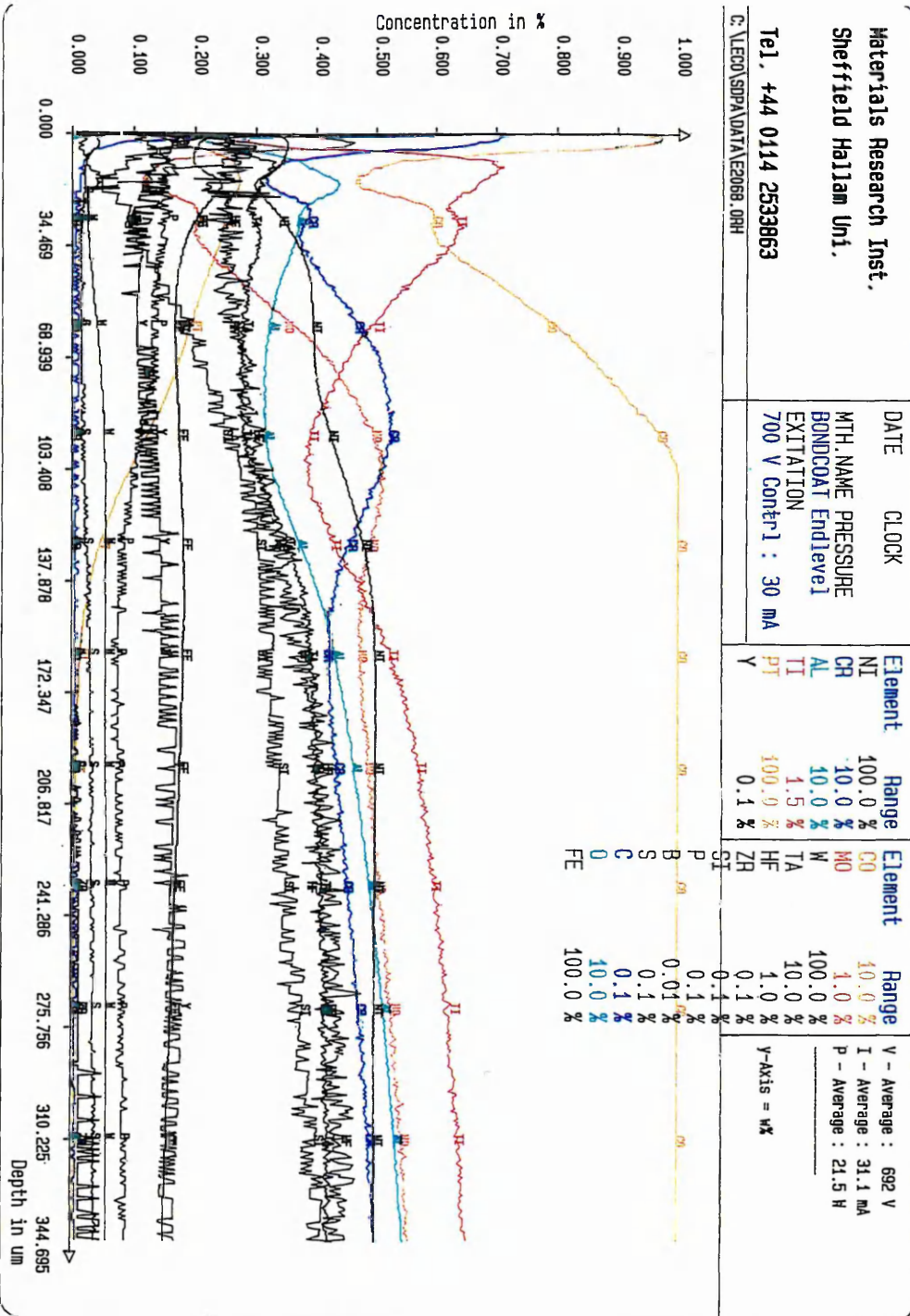


Figure 4.2. 1 i: GDOES Pt depth profiles for sample AHE63 in the failed condition

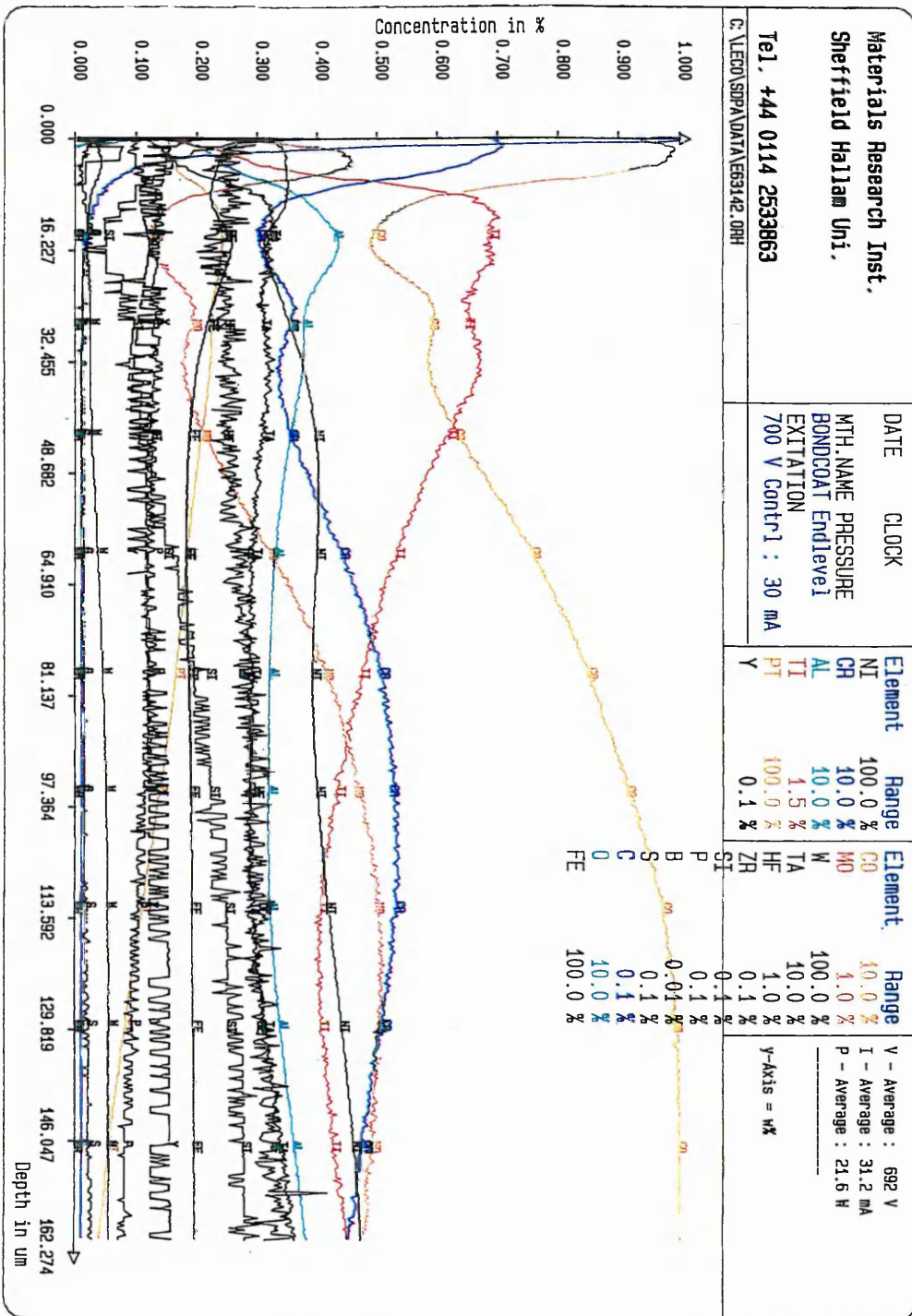


Figure 4.2.2 a: GDOES depth profile of as processed (Sputtered Ni+0.23mass% Hf LCBC showing elemental profiles for Cr, Al, Co, Mo, Mn and Ni

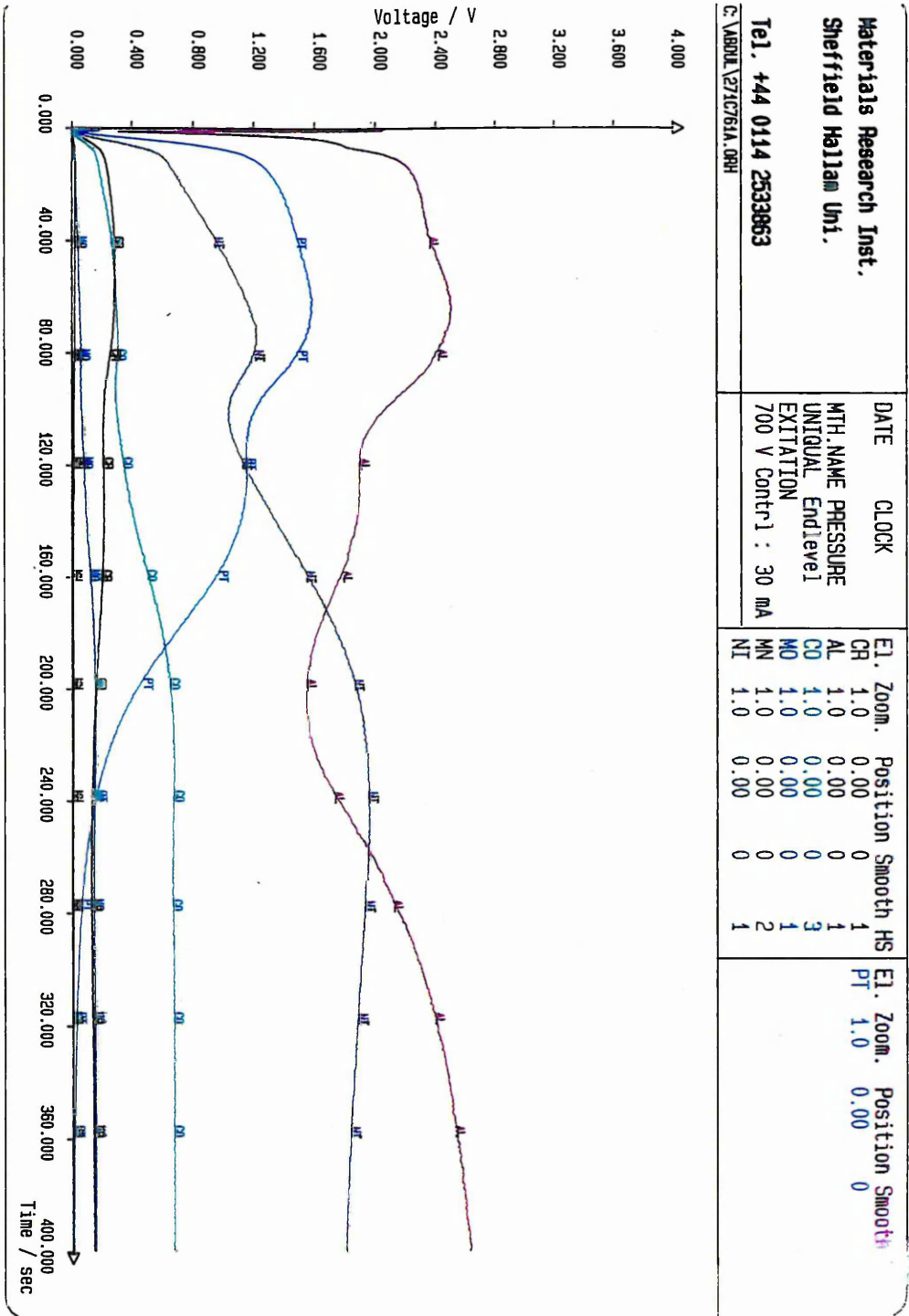


Figure 4.2.2 b: GDOES depth profile of as processed (Sputtered Ni+0.23mass% Hf LCBC showing elemental profiles for Ti, Hf, w, Ta, Y and Pt

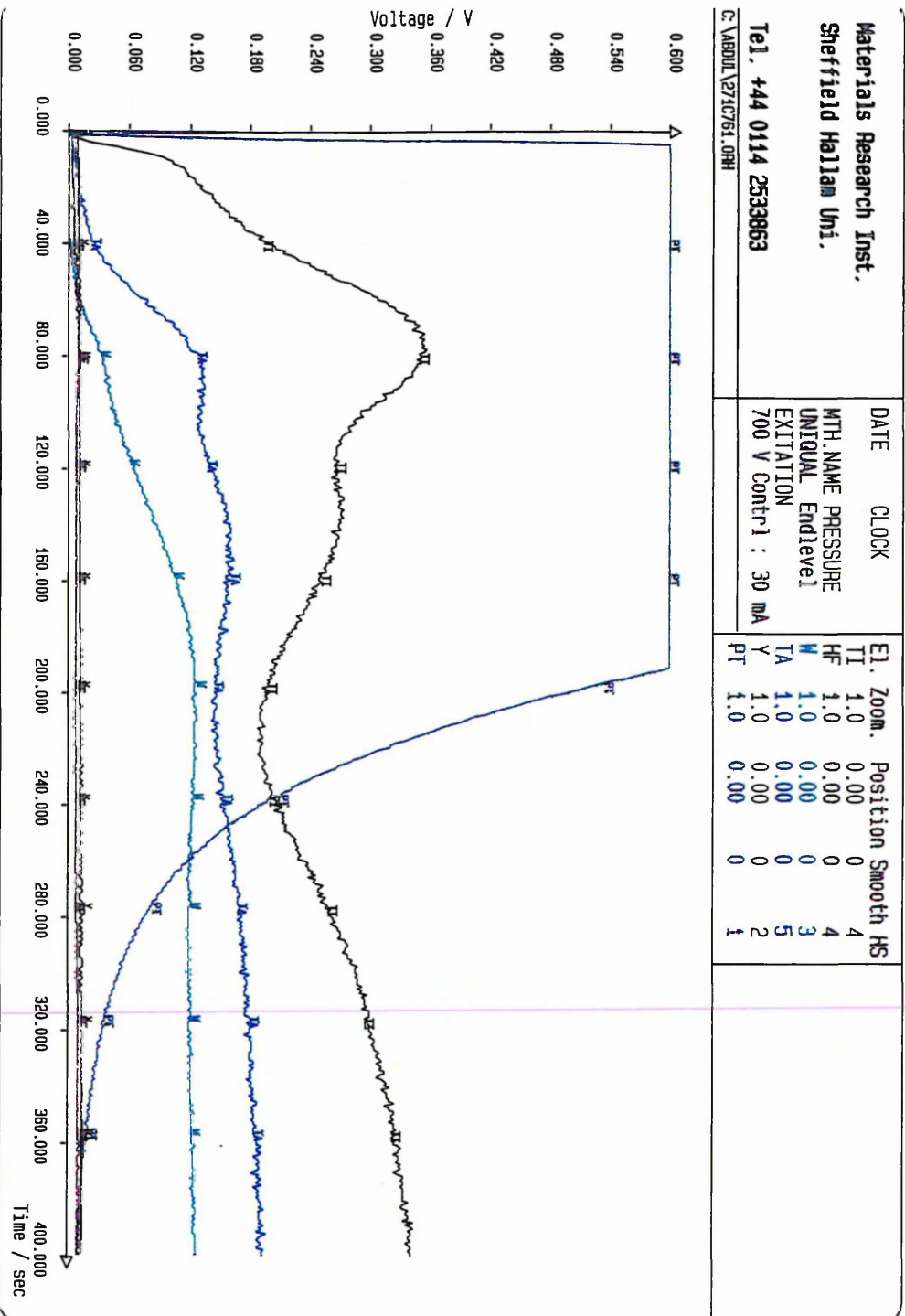


Figure 4.2.2 c: GDOES depth profile of as failed (Sputtered Ni+0.23mass% Hf LCBC showing elemental profiles for Cr, Al, Co, Mo, Mn and Ni

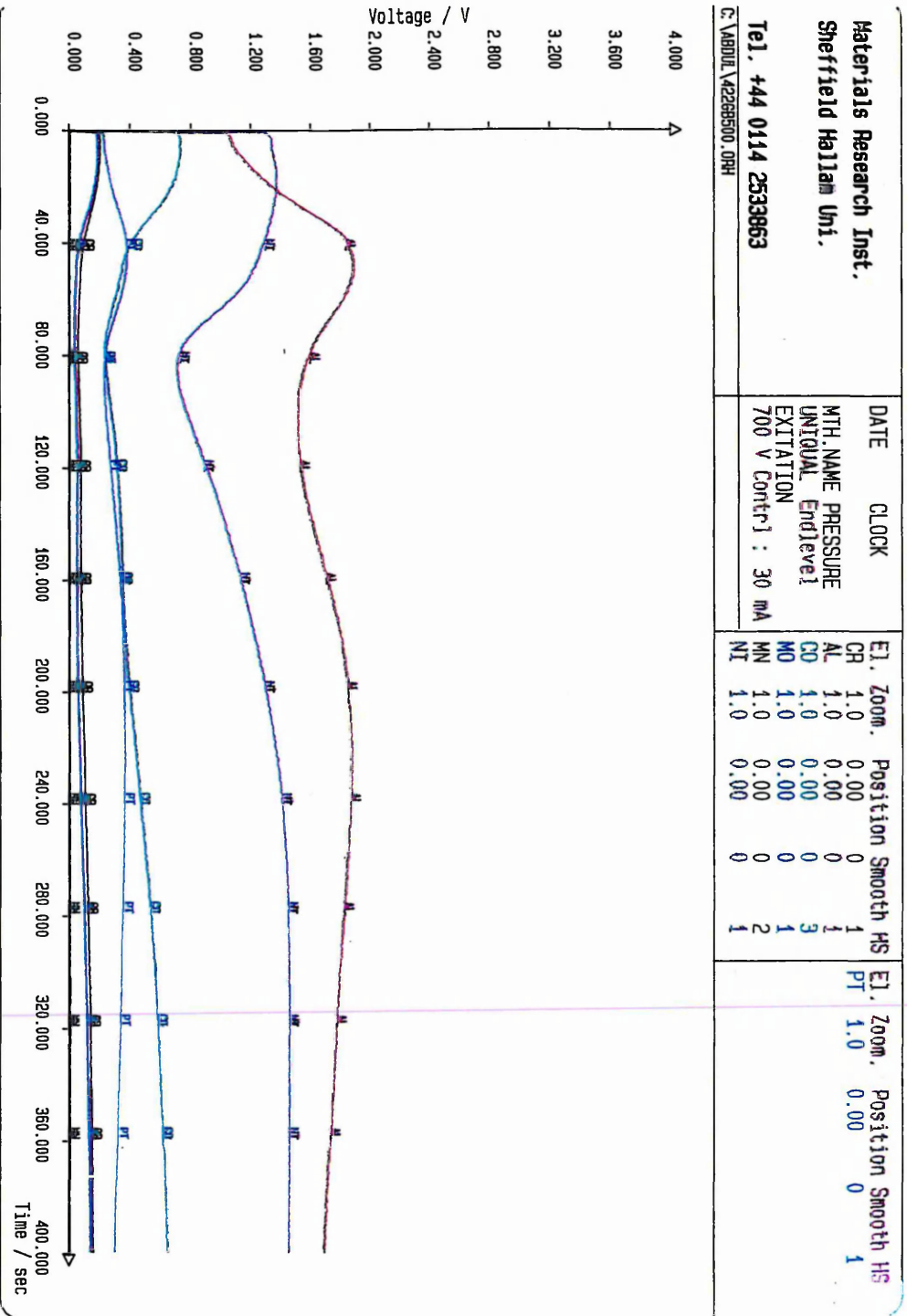


Figure 4.2.2 d: GDOES depth profile of as failed (Sputtered Ni+0.23mass% Hf LCBC showing elemental profiles for Ti, Hf, w, Ta, Y and Pt

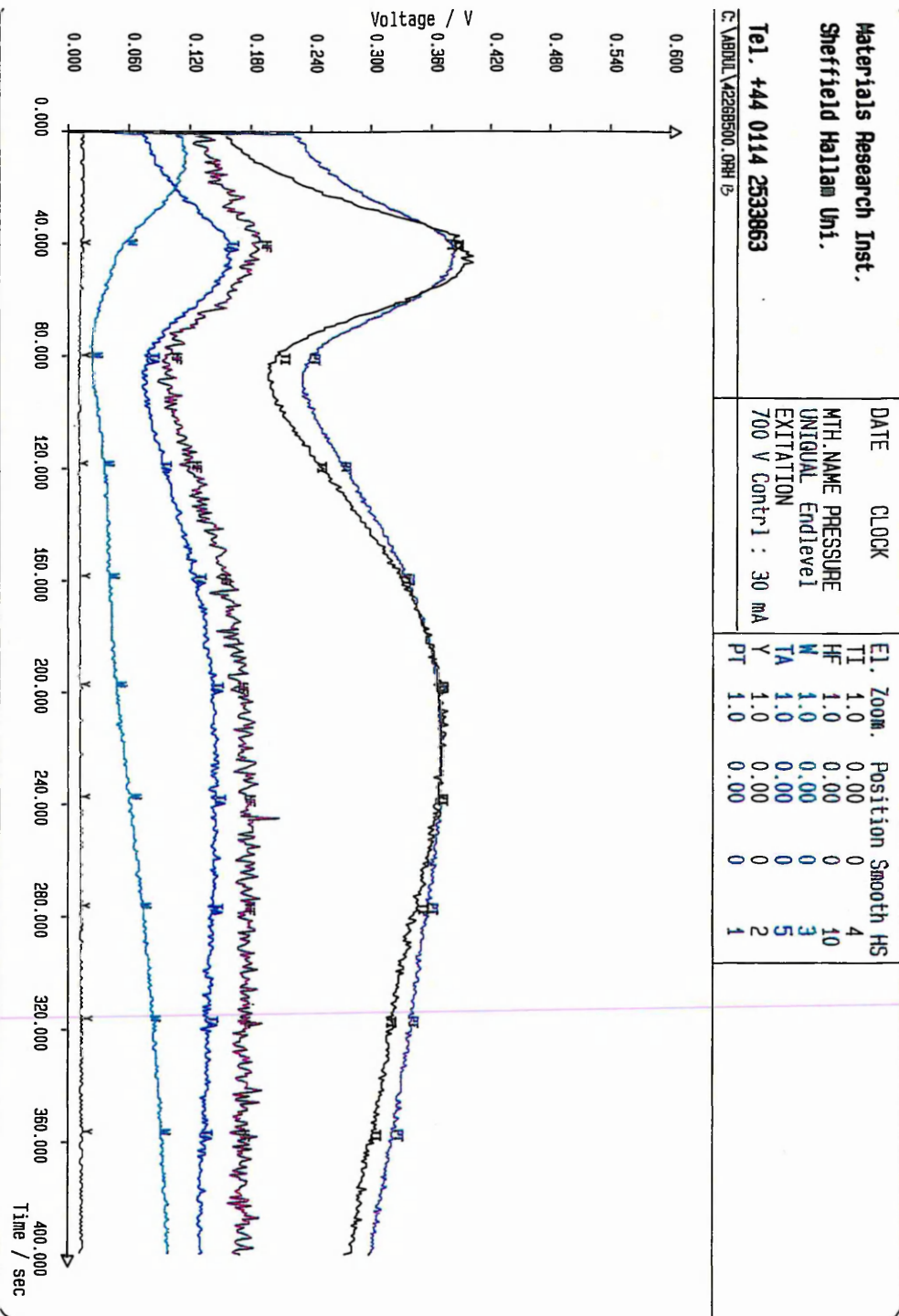


Figure 4.2.2 f: GDOES depth profile of as processed (Ni+0.58mass% Y+1.6 mass% Hf) LCBC showing elemental profiles for Ti, Hf, w, Ta, Y and Pt

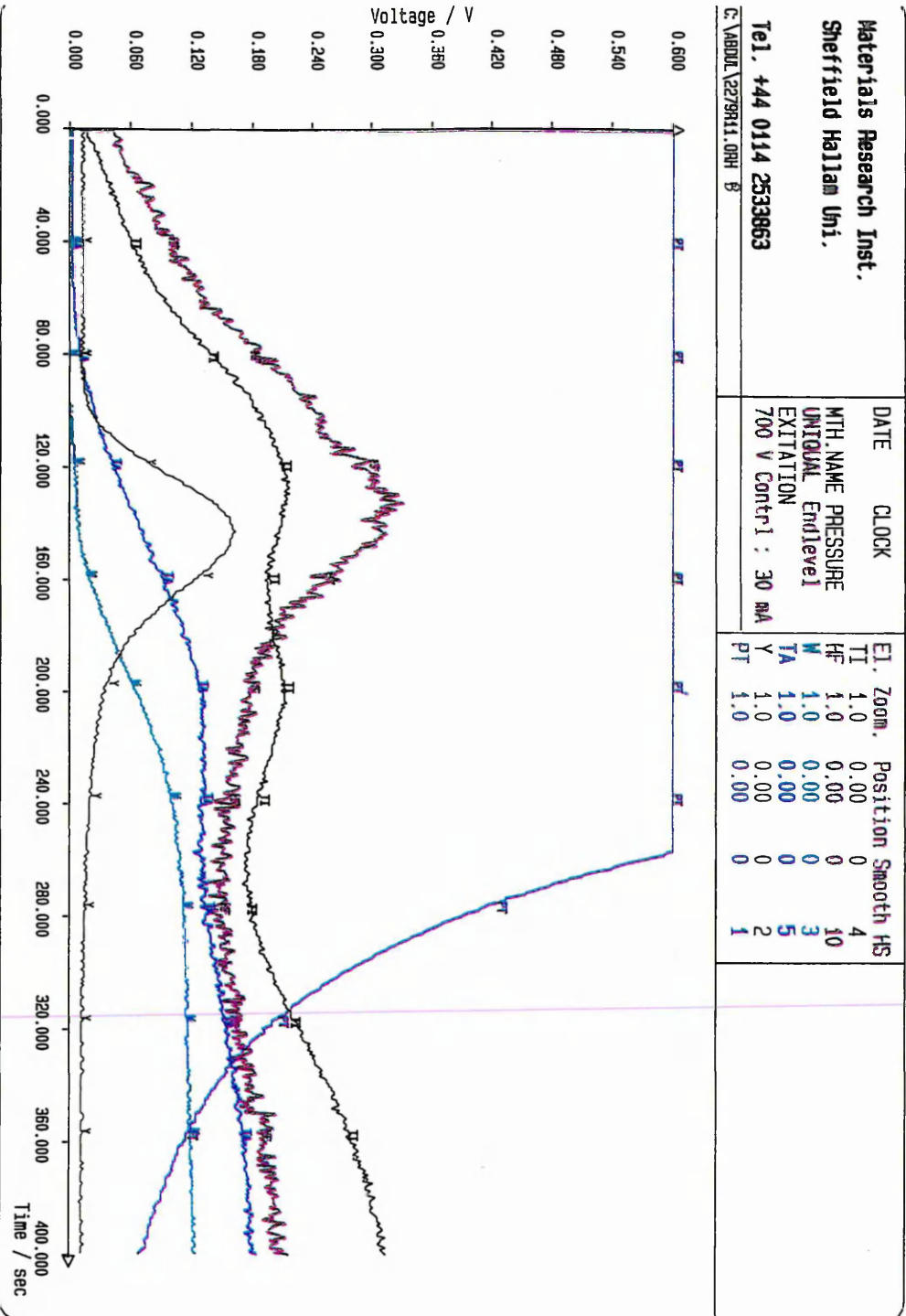


Figure 4.2.2 g: GDOES depth profile of as failed (Ni+0.58mass% Y+1.6 mass% Hf) LCBC showing elemental profiles for Cr, Al, Co, Mo, Mn and Ni

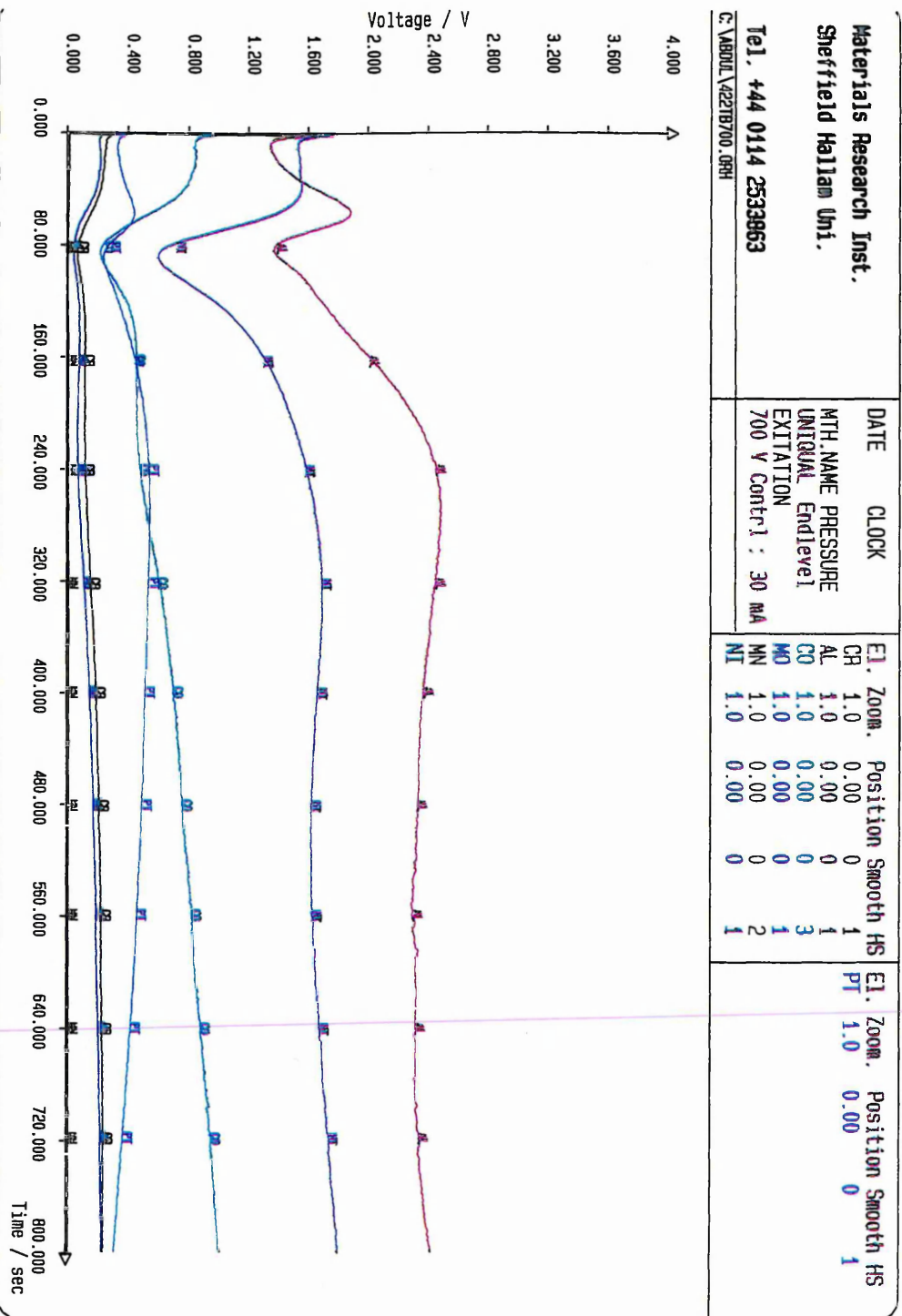


Figure 4.2.2 h: GDOES depth profile of as failed (Ni+0.58mass% Y+1.6 mass% Hf) LCBC showing elemental profiles for Ti, Hf, w, Ta, Y and Pt

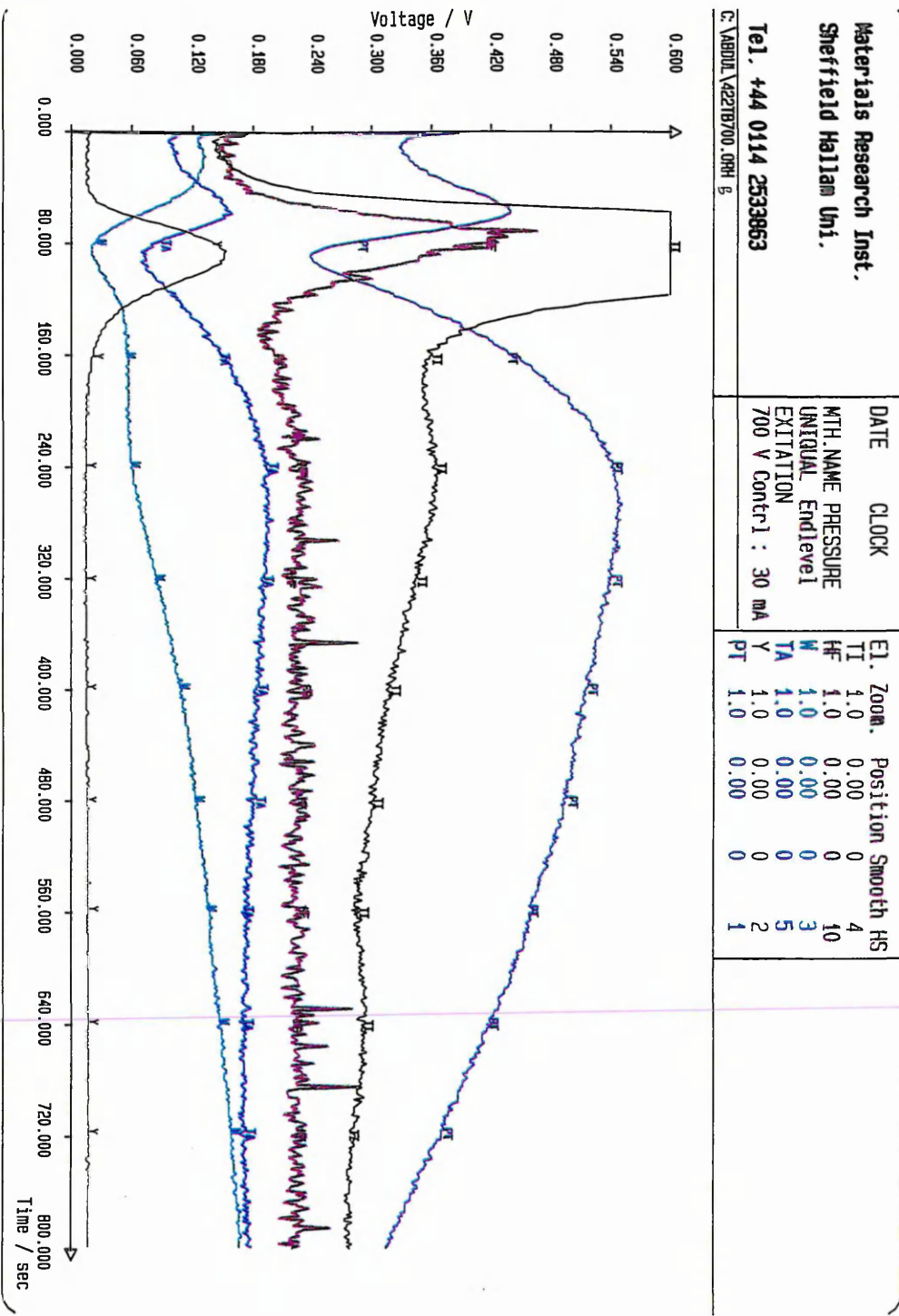


Figure 4.2.2 i: GDOES depth profile of as processed (Ni+0.5mass% Y) LCBC showing elemental profiles for Cr, Al, Co, Mo, Mn and Ni

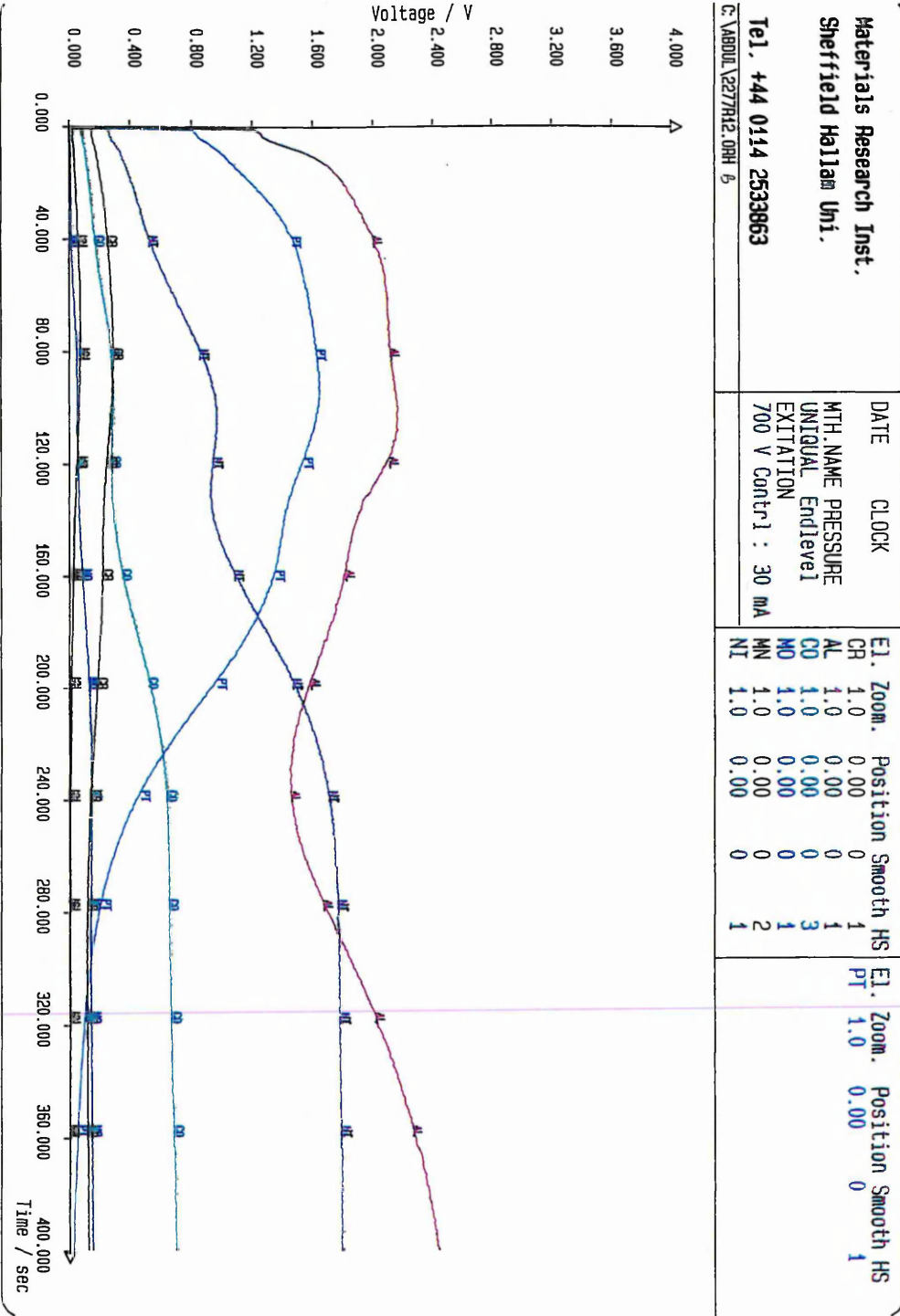


Figure 4.2.2 j: GDOES depth profile of as processed ( Ni+0.5mass% Y )  
 LCBC showing elemental profiles for Ti, Hf, w, Ta, Y and Pt

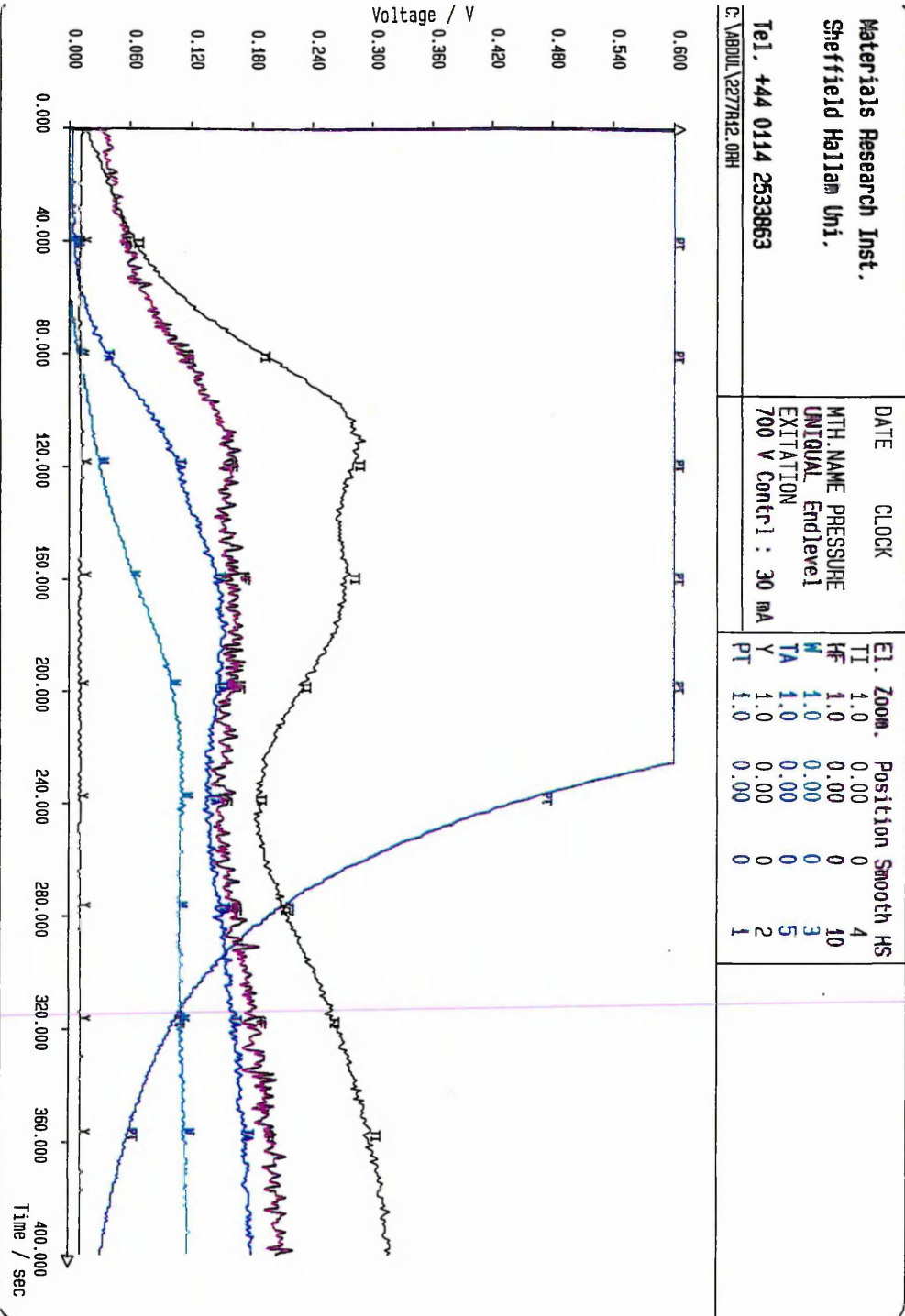


Figure 4.2.2 k: GDOES depth profile of as failed (Ni+0.5mass% Y)  
 LCBC showing elemental profiles for Cr, Al, Co, Mo, Mn and Ni

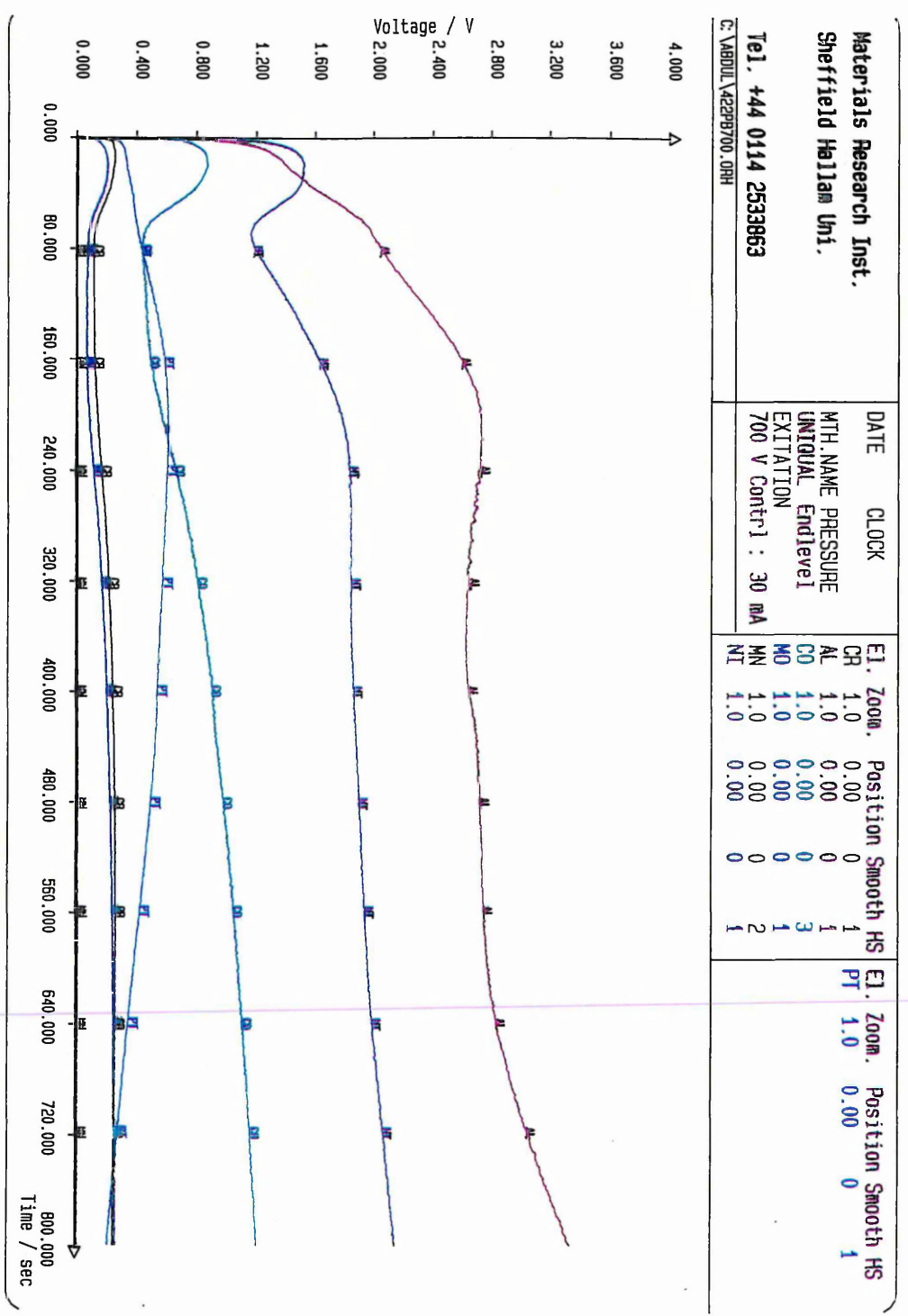


Figure 4.2.2: GDOES depth profile of as failed (Ni+0.5mass% Y) LCBC showing elemental profiles for Ti, Hf, w, Ta, Y and Pt

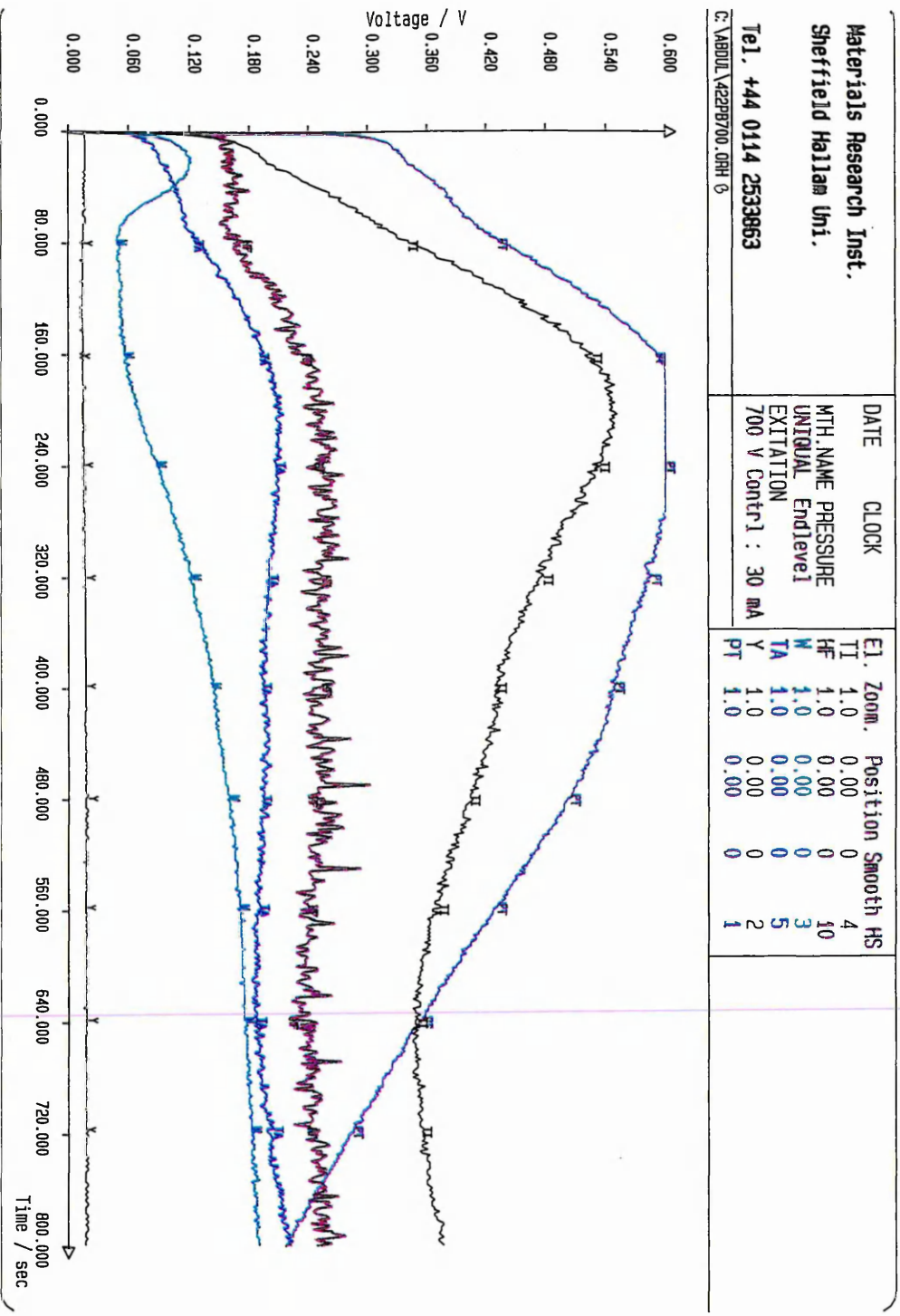


Figure 4.2.2 m: GDOES depth profile of as processed (Ni+6.1mass% Y) LCBC showing elemental profiles for Cr, Al, Co, Mo, Mn and Ni

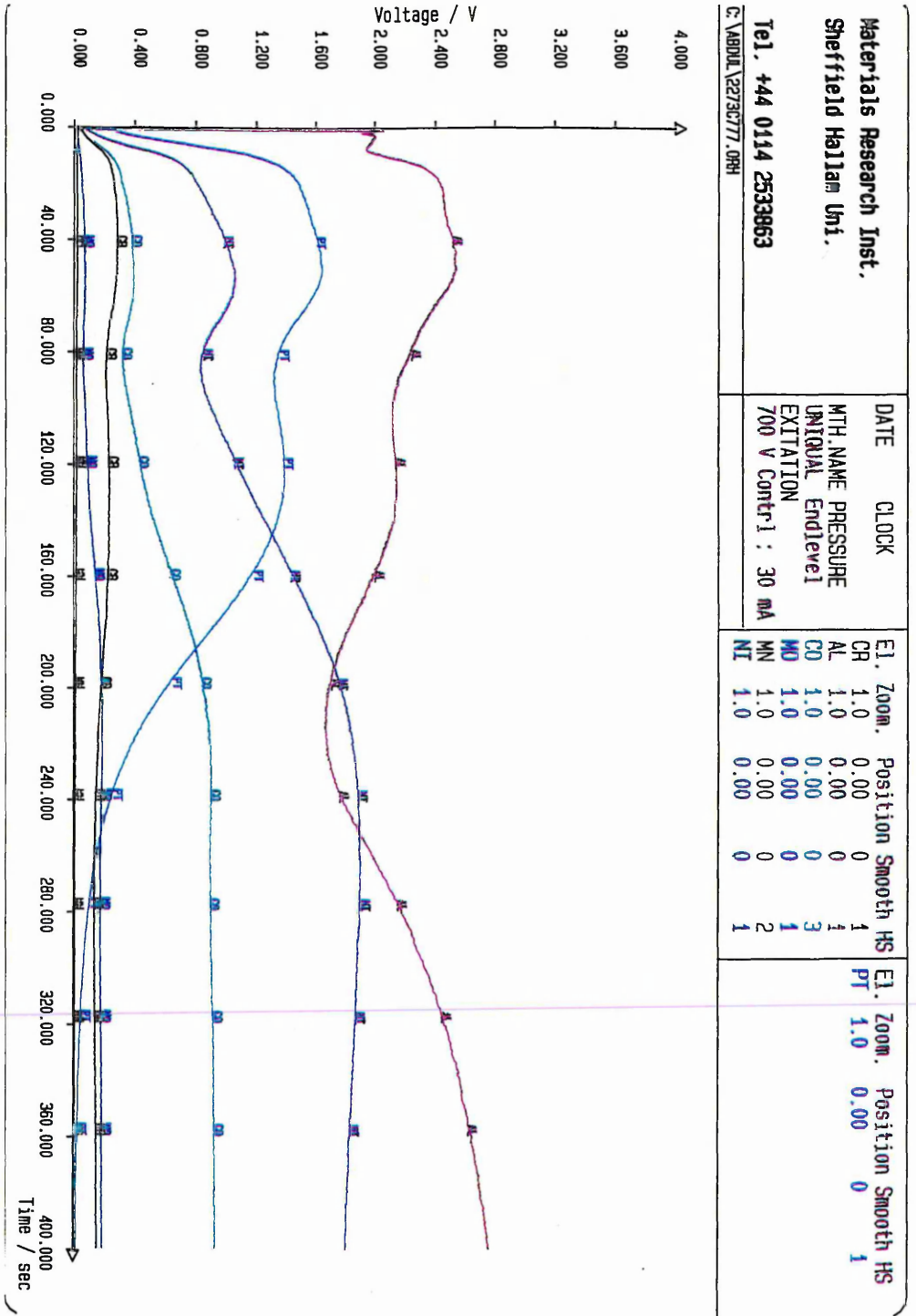


Figure 4.2.2 n: GDOES depth profile of as processed ( Ni+6.1mass% Y )  
 LCBC showing elemental profiles for Ti, Hf, w, Ta, Y and Pt

<b>Materials Research Inst.</b> <b>Sheffield Hallam Uni.</b> <b>Tel. +44 0114 2533863</b> <small>C:\ABDUL\2273C777.ORN 0</small>		DATE MTH, NAME PRESSURE UNIT/VAL End[level] EXITATION 700 V Contn1 : 30 mA	E1, Zoom, Position Smooth HS TI 1.0 0.00 0 4 HF 1.0 0.00 0 10 W 1.0 0.00 0 3 TA 1.0 0.00 0 5 Y 1.0 0.00 0 2 PT 1.0 0.00 0 1
---	--	--	---

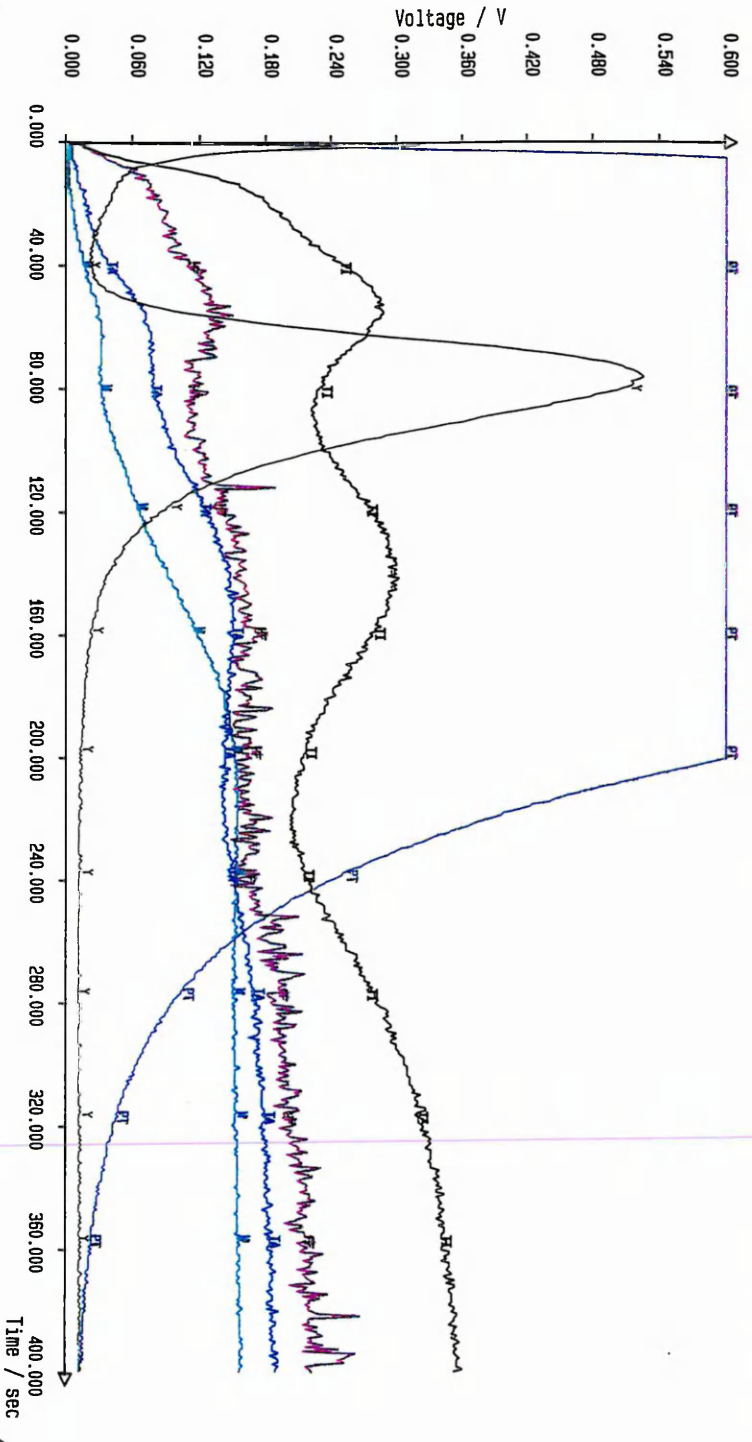


Figure 4.2.2 o: GDOES depth profile of as failed ( Ni+6.1mass% Y )  
 LCBC showing elemental profiles for Cr, Al, Co, Mo , Mn and Ni

<b>Materials Research Inst.</b> <b>Sheffield Hallam Uni.</b> <b>Tel. +44 0114 2533653</b> <b>C:\ABDUL\A2218700.DPH</b>		DATE MTH.NAME UNIFORMAL EXITATION 700 V Contr1 : 30 mA	CLOCK PRESSURE Endlevel1	E1. Zoom. CR 1.0 AL 1.0 CO 1.0 MO 1.0 MN 1.0 NI 1.0	Position 0.00 0.00 0.00 0.00 0.00 0.00	Smooth 0 0 0 0 0	HS 1 1 3 1 2 1	E1. Zoom. PT 1.0	Position 0.00	Smooth 0	HS 1
---	--	--	--------------------------------	---	--	---------------------------------	----------------------------------	---------------------	------------------	-------------	---------

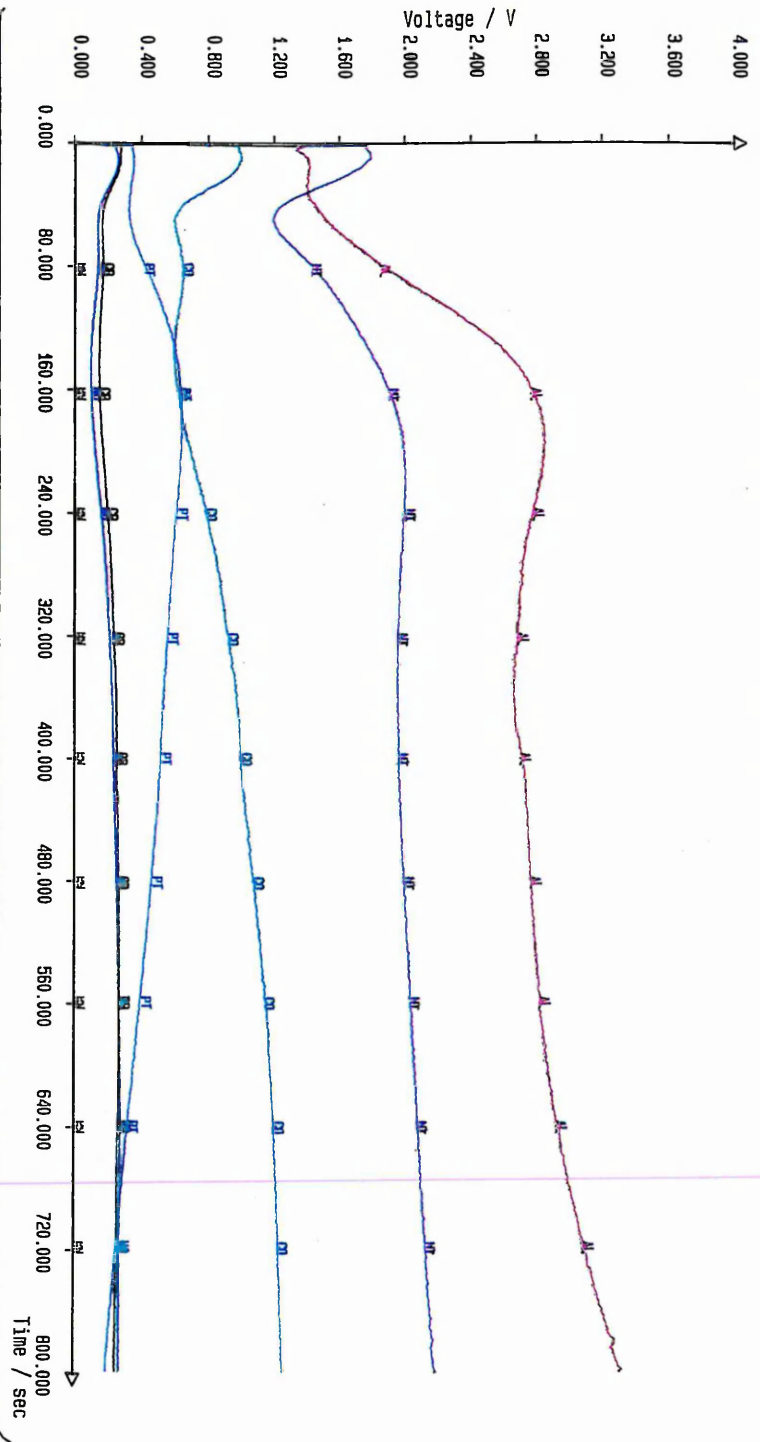


Figure 4.2.2 p: GDOES depth profile of as failed (Ni+6.1 mass% Y) LCBC showing elemental profiles for Ti, Hf, W, Ta, Y and Pt

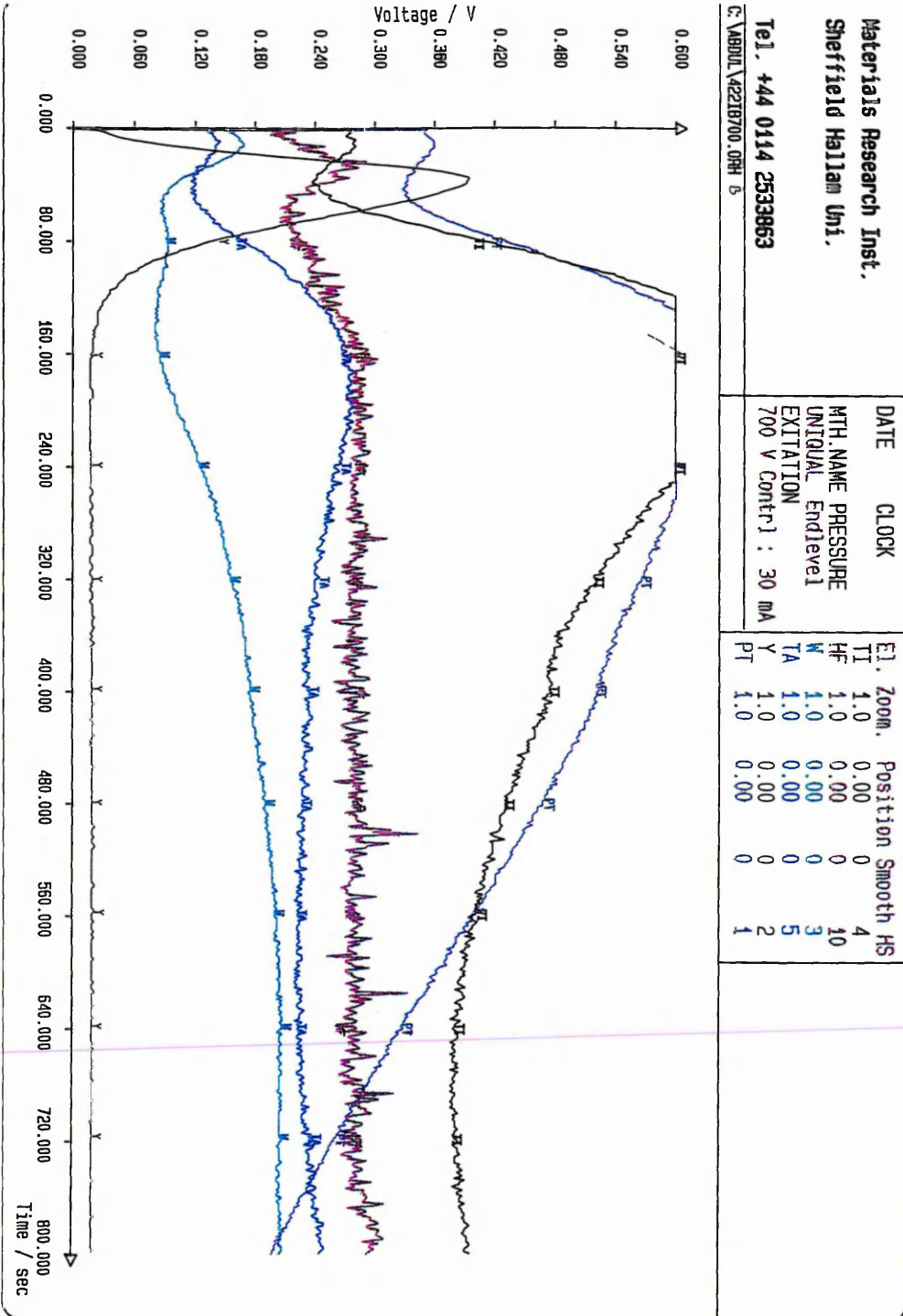


Figure 4.3.1 (a) GDOES depth profile of as processed LCBC showing Si profile

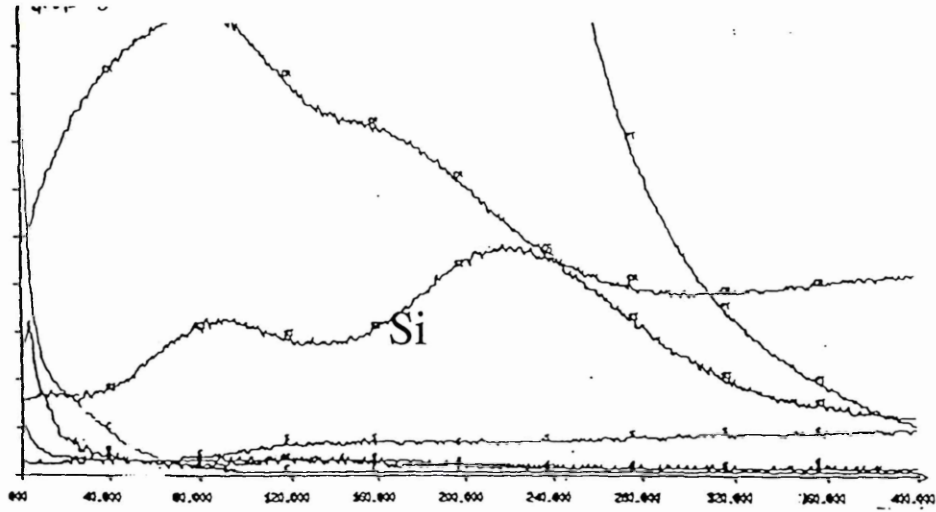


Figure 4.3.1 (b) GDOES depth profile of as failed LCBC showing Si profile

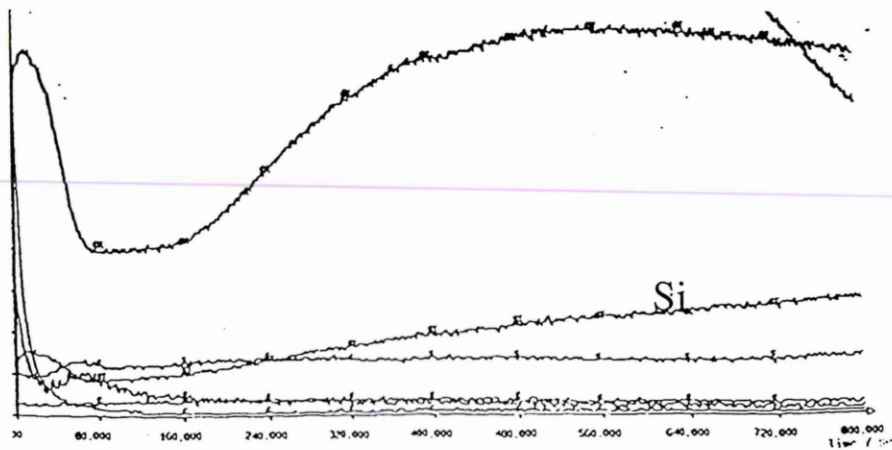


Figure 4.3.1 (c) GDOES depth profile of as processed LCBC showing Si profile ( pink gritted – heat treated at CUK)

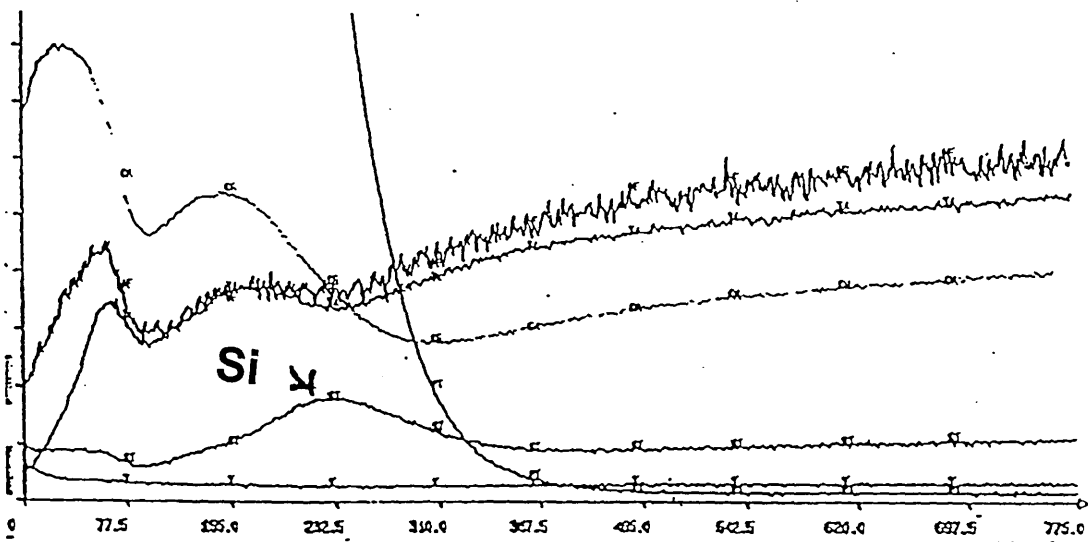


Figure 4.3.1 (d) GDOES depth profile of as processed LCBC showing Si profile ( Brown gritted – heat treated at CUK)

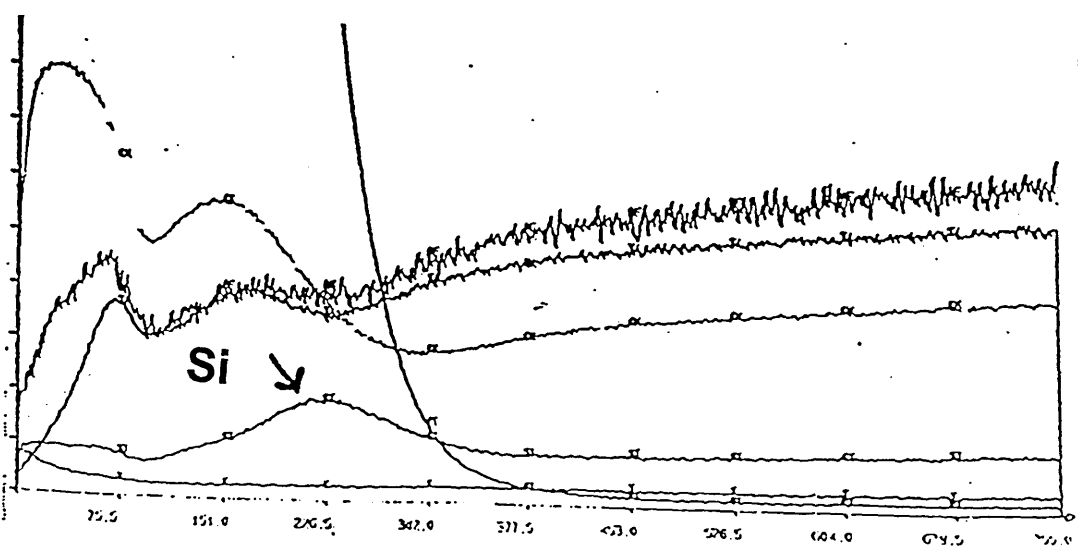


Figure 4.3.1 (e) GDOES depth profile of CMSX-4 showing no presence of Si

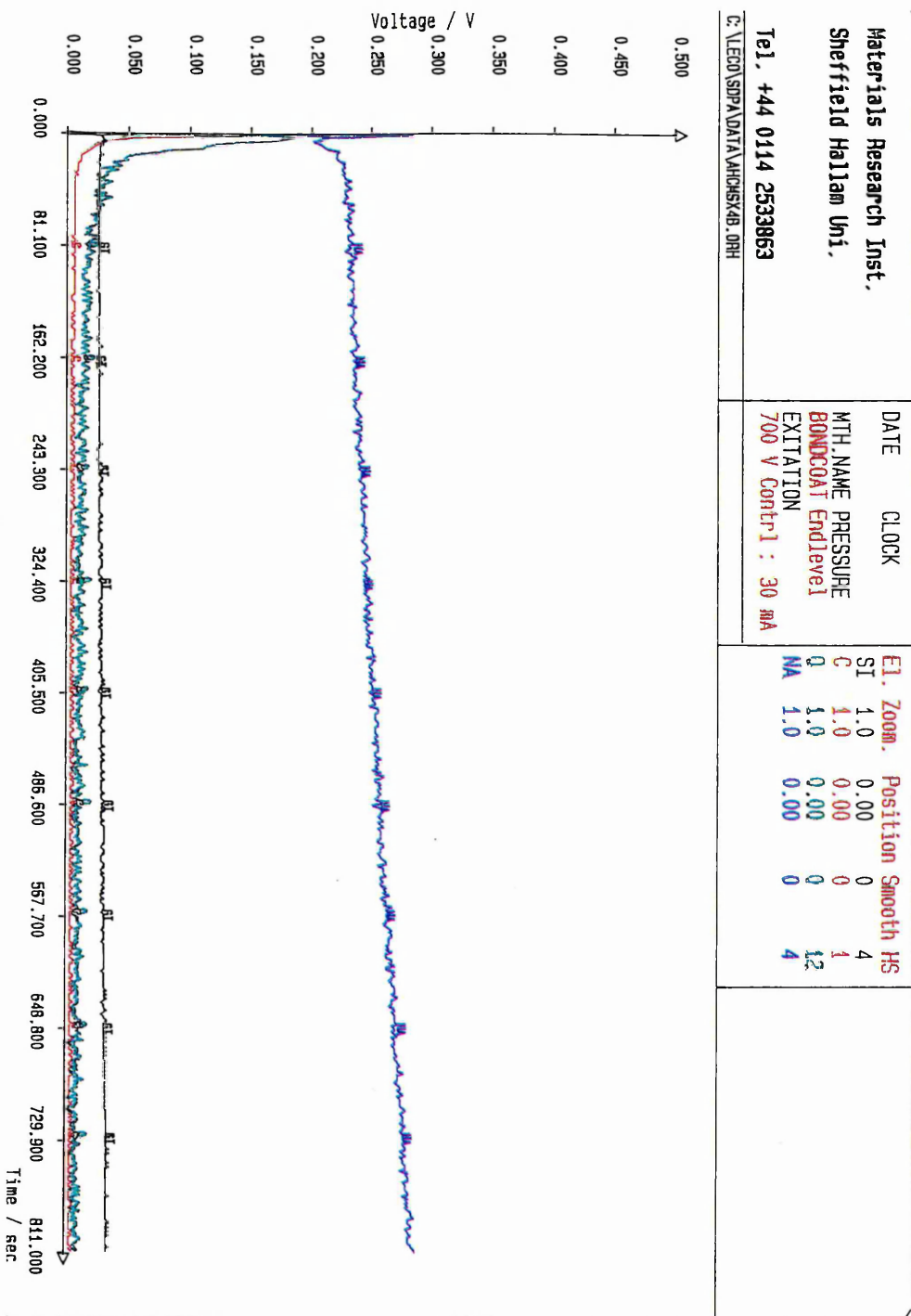


Figure 4.3.2 (a) GDOES depth profile of Pt plated CMSX-4 showing presence of sodium

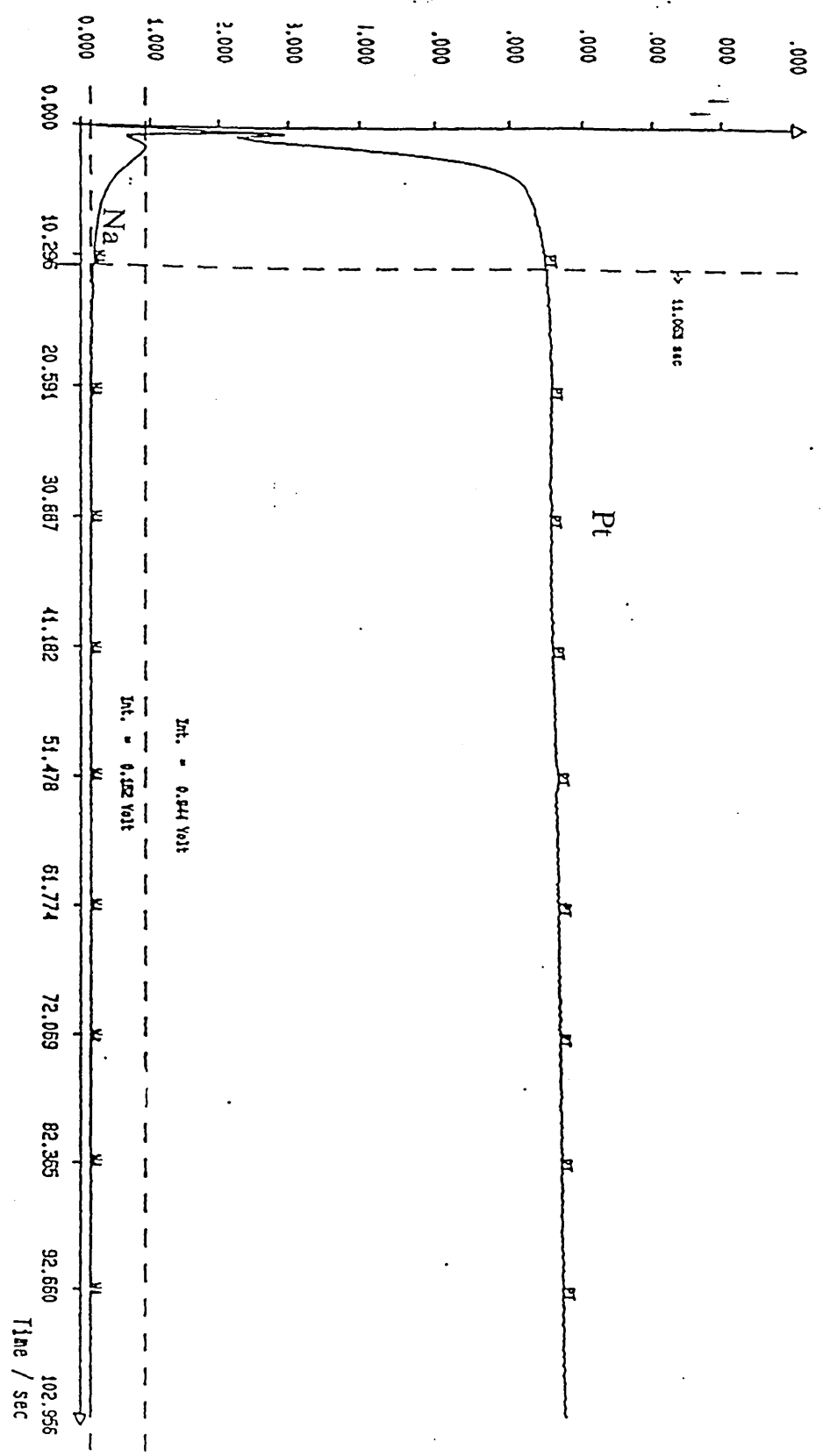


Figure 4.3.2 (b) GDOES depth profile of standard LCBC and observed sodium peak

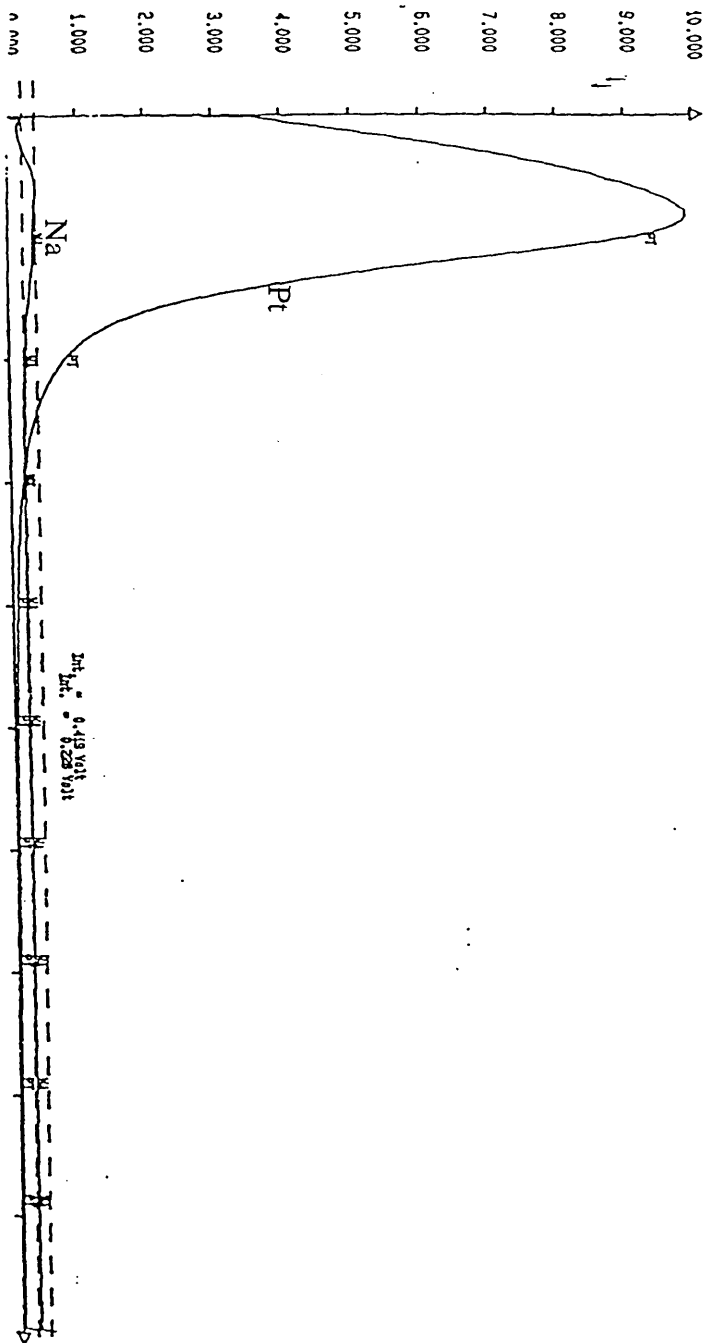


Figure 4.3.2 (c) GDOES depth profile of standard LCBC showing sodium in as plated and when heat treated

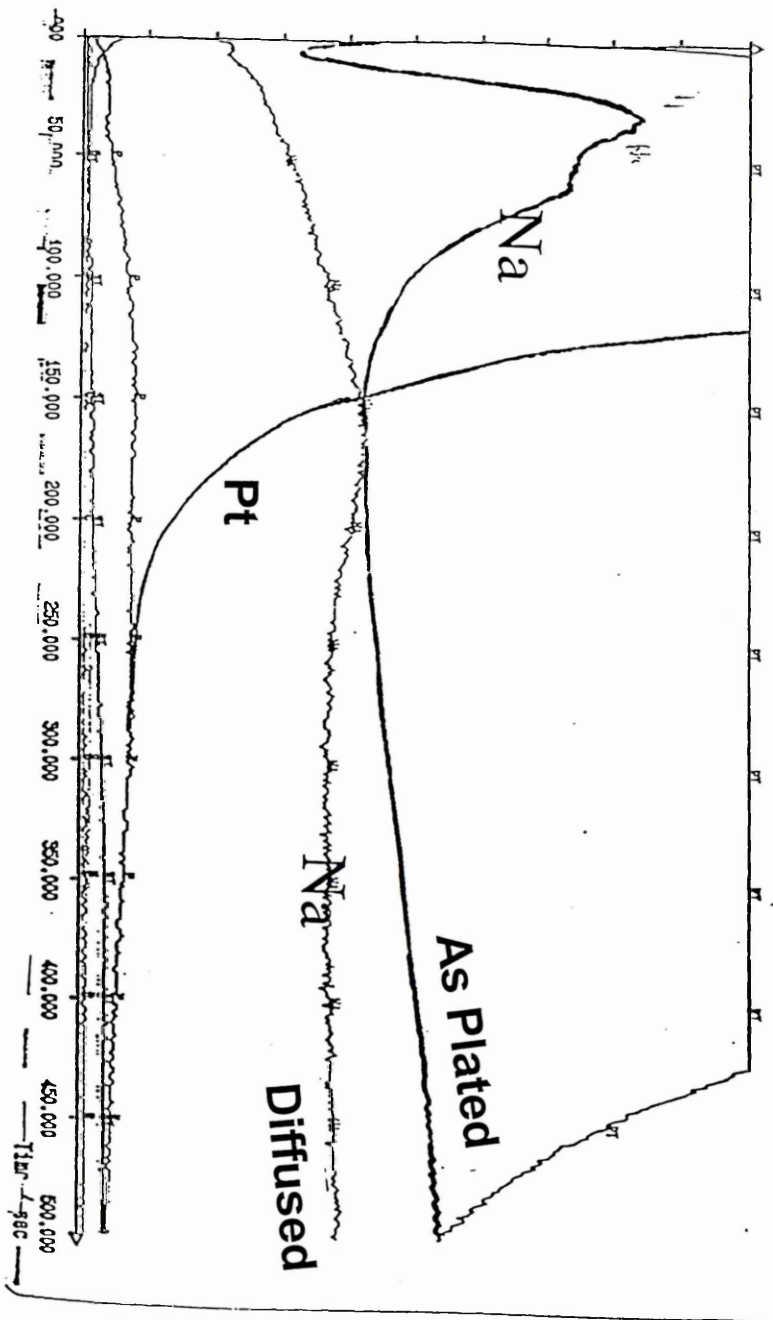


Table 4.3.2 XRF analysis as plated LCBC sample showing presence of sodium

```

JOB: 563 of 11-NOV-94
Spectrometer: PH2400 Rh 60KV LiF220 Ge111 TIAP
Sample ident = E84
Further info =
Kepps list = 17-Jan-96 Channel list = 22-Dec-94
Calculated as : Elements Spectral purity data : Teflon-----
X-ray path = Vacuum Film type = No supporting film
Case number = 0 Known Area, %Rest, Diluent/Sample and Mass/Area
Eff.Diam = 11.35 mm Eff.Area = 101.1 mm2
KnownConc = 0 %
Rest = 0 %
Dil/Sample = 0
Viewed mass = 10000 mg
Sample height = 5 mm
< means that the concentration is < 100 ppm
<2e means that Conc < 2 x StdErr
=====
Z      wt%   StdErr   Z      wt%   StdErr   Z      wt%   StdE
=====
SumRe...F 0      1.05    29 Cu   <
11 Na    0.15   0.02    30 Zn   0.034  0.004   51 Sb   <
12 Mg   <
13 Al   0.034  0.006   31 Ga   <
14 Si   0.046  0.006   32 Ge   <
15 P    0.042  0.004   33 As   <2e    55 Cs   <
16 S    0.15   0.01    34 Se   <2e    56 Ba   <
17 Cl   0.14   0.01    35 Br   <
18 Ar   <
19 K    0.067  0.008   36 Kr   <
20 Ca   0.059  0.007   37 Rb   <
21 Sc   <
22 Ti   <
23 V    <
24 Cr   <
25 Mn   <
26 Fe   0.049  0.007   38 Sr   <
27 Co   0.029  0.005   39 Y    <
28 Ni   0.24   0.02    40 Zr   <
29 Cu   <
30 Zn   0.034  0.004   41 Nb   <
31 Ga   <
32 Ge   <
33 As   <2e    42 Mo   0.078  0.023   72 Hf   <
34 Se   <2e    43 Tc   <
35 Br   <
36 Kr   <
37 Rb   <
38 Sr   <
39 Y    <
40 Zr   <
41 Nb   <
42 Mo   0.078  0.023   73 Ta   0.034  0.0
43 Tc   <
44 Ru   <
45 Rh   <
46 Pd   <
47 Ag   <
48 Cd   <
49 In   <
50 Sn   <2e    52 Te   <
51 Sb   <
52 Te   <
53 I    <
54 Xe   <
55 Cs   <
56 Ba   <
57 La   <
58 Ce   <
59 Pr   <2e
60 Nd   <
61 Pm   <
62 Sm   <
63 Eu   <
64 Gd   <2e
65 Tb   <
66 Dy   <
67 Ho   <
68 Er   <
69 Tm   <
70 Yb   <
71 Lu   <
72 Hf   <
73 Ta   0.034  0.0
74 W    0.061  0.0
75 Re   <
76 Os   <
77 Ir   <
78 Pt   98.60  0.0
79 Au   <
80 Hg   <2e
81 Tl   <
82 Pb   <
83 Bi   <2e
84 Po   <
85 At   <
86 Rn   <
87 Fr   <
88 Ra   <
89 Ac   <
90 Th   <
91 Pa   <
92 U    0.031  0.1

==== Light Elements =====
4 Be
5 B
6 C
7 N
8 O
9 F

==== Noble Elements =====
44 Ru
45 Rh
46 Pd
47 Ag
75 Re
76 Os
77 Ir
78 Pt  98.60  0.08
79 Au

==== Lanthanides =====
57 La
58 Ce
59 Pr  <2e
60 Nd
61 Pm
62 Sm
63 Eu
64 Gd  <2e
65 Tb
66 Dy
67 Ho
68 Er
69 Tm
70 Yb
71 Lu

KnownConc= 0 REST= 0 O/S= 0
Sum Conc's before normalisation to 100% : 224.0 %

```

Figure 4.3.3 (a) GDOES depth profile of Pt standard showing P interference

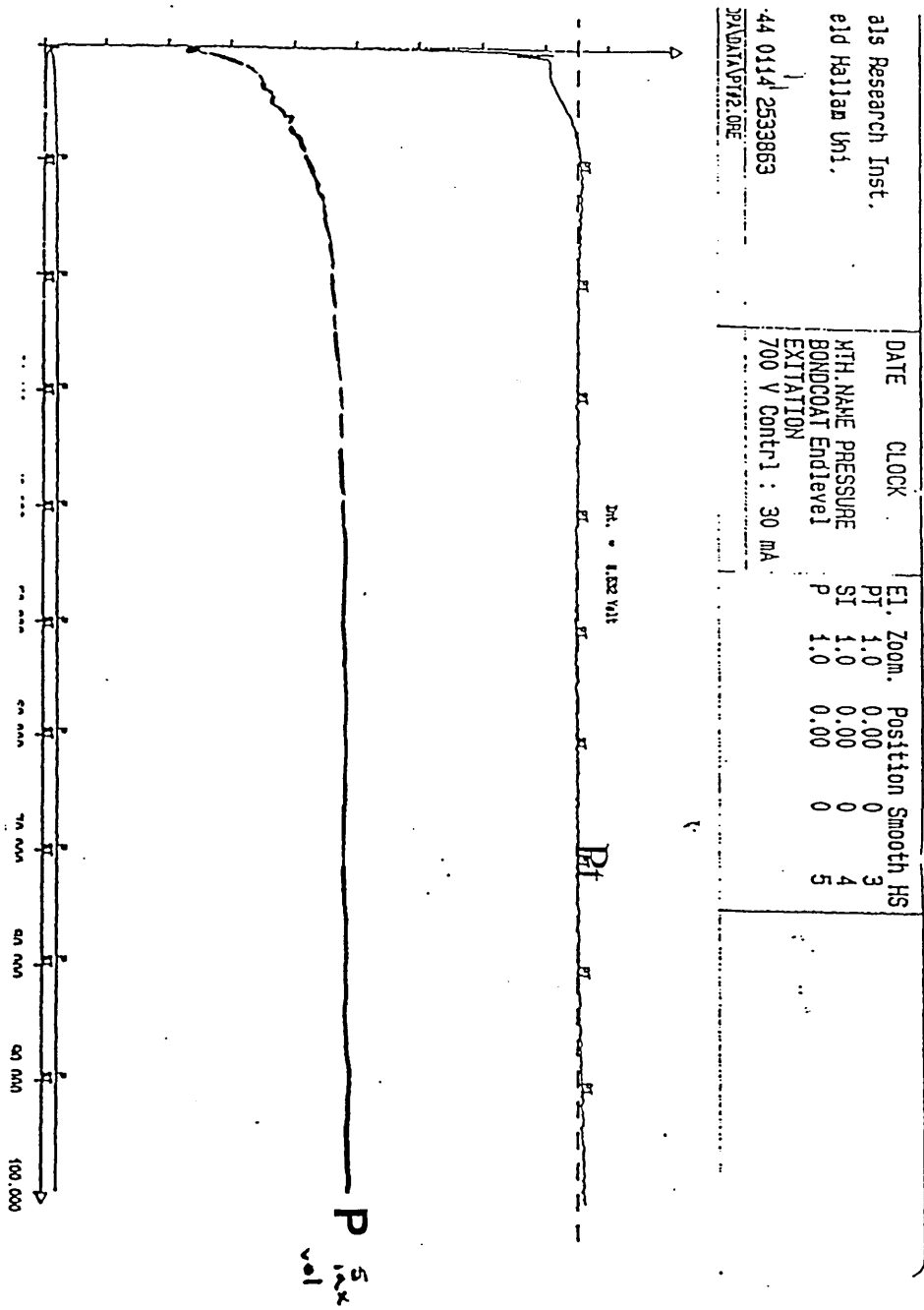


Figure 4.3.3 (b) GDOES depth profile of Pt deposited on CMSX-4 substrate by PVD process showing P interference

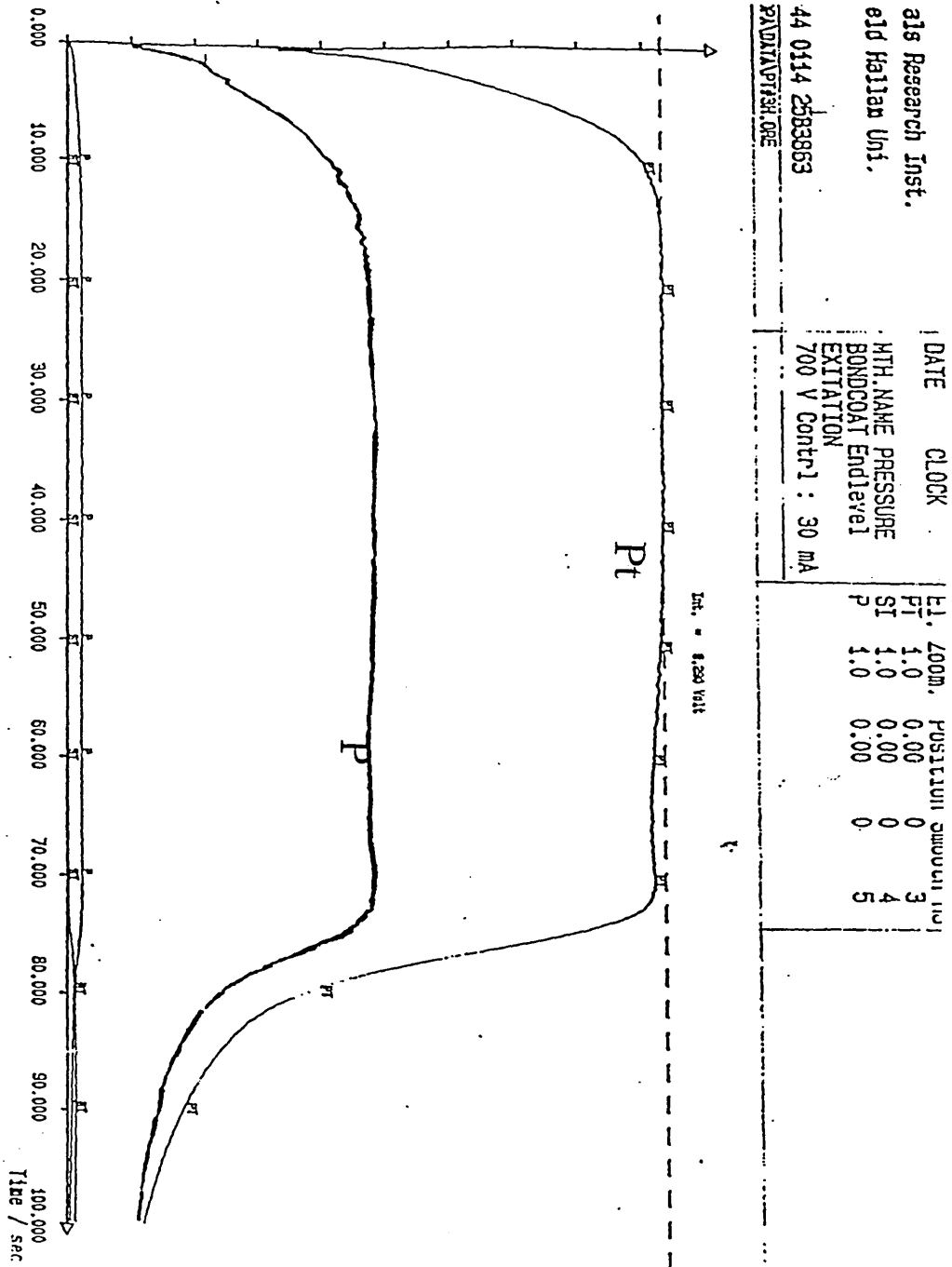


Figure 4.3.3 (c) GDOES depth profile of LCBC for Pt plating (electrolytic technique ) showing P interference

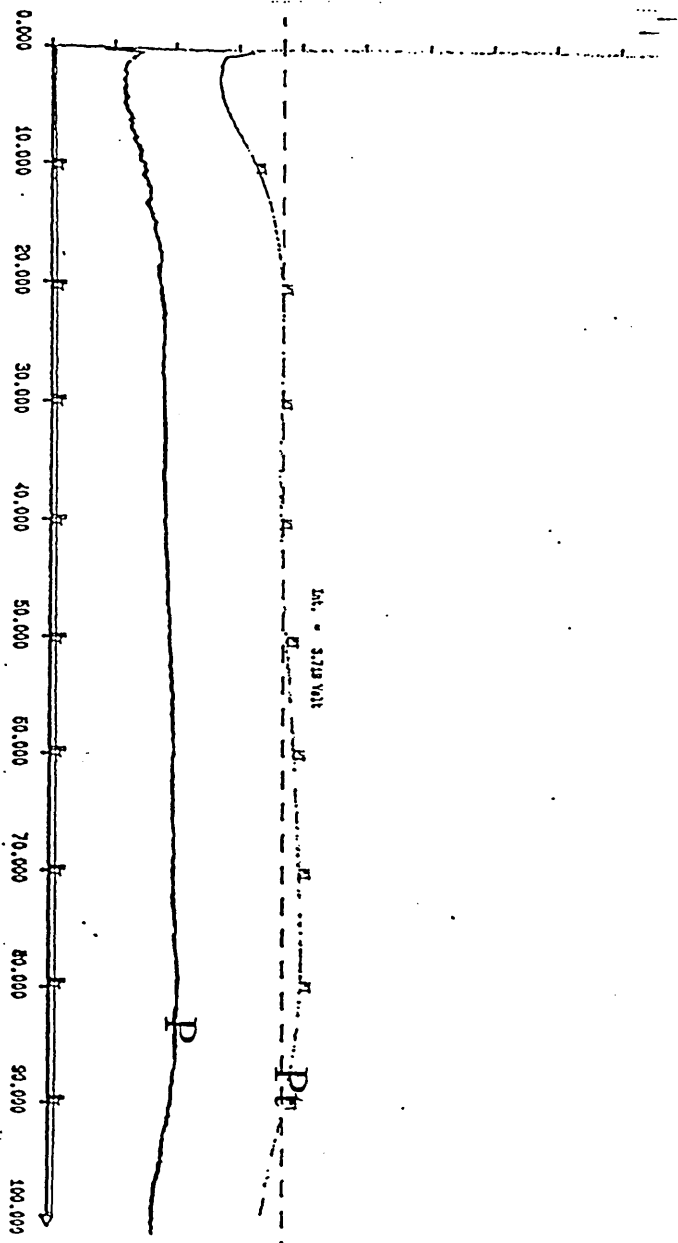


Table 5.0 Enhanced low cost bond coats- average cycles to failure

Original Code	JDP Code	System	Cycles to Failure
	422.NB100	Reference	249
227/1	422.GB.500	Sputtered Ni + 0.23wt% Hf	226
227/2	422.HA.300	Sputtered Ni + 2.27wt% Hf	242
227/3	422.IB.700	Sputtered Ni + 6.10wt% Y	285
227/7	422.PB.700	Sputtered Ni+ 0.5wt% Y	375
227/9	422.TB.700	Sputtered Ni + 0.58wt% Y + 1.60wt% Hf	300
227/11	422.VB.700	Sputtered Ni + 0.43wt% Y + 1.75wt% Hf	330
-	422.DB.100	CMSX-4 + 22-26 ppm Ce	211
-	422.CB.100	CMSX-4 + 20-25 ppm La + Low cost	244
-	422.BB.100	CMSX-4 + 8-14 ppm Y + 12-18ppm La	244

Fig 5.1 Enhanced low cost bond coat with additions to coatings. Comparing the four systems shown it will be noticed that in the Ni+low Hf system, two out of the six samples were surviving indicating better performance than the others. It will be noticed that in ranking terms of cyclic performance Ni+low Hf system shows the best performance and Pt+Y is the lowest.

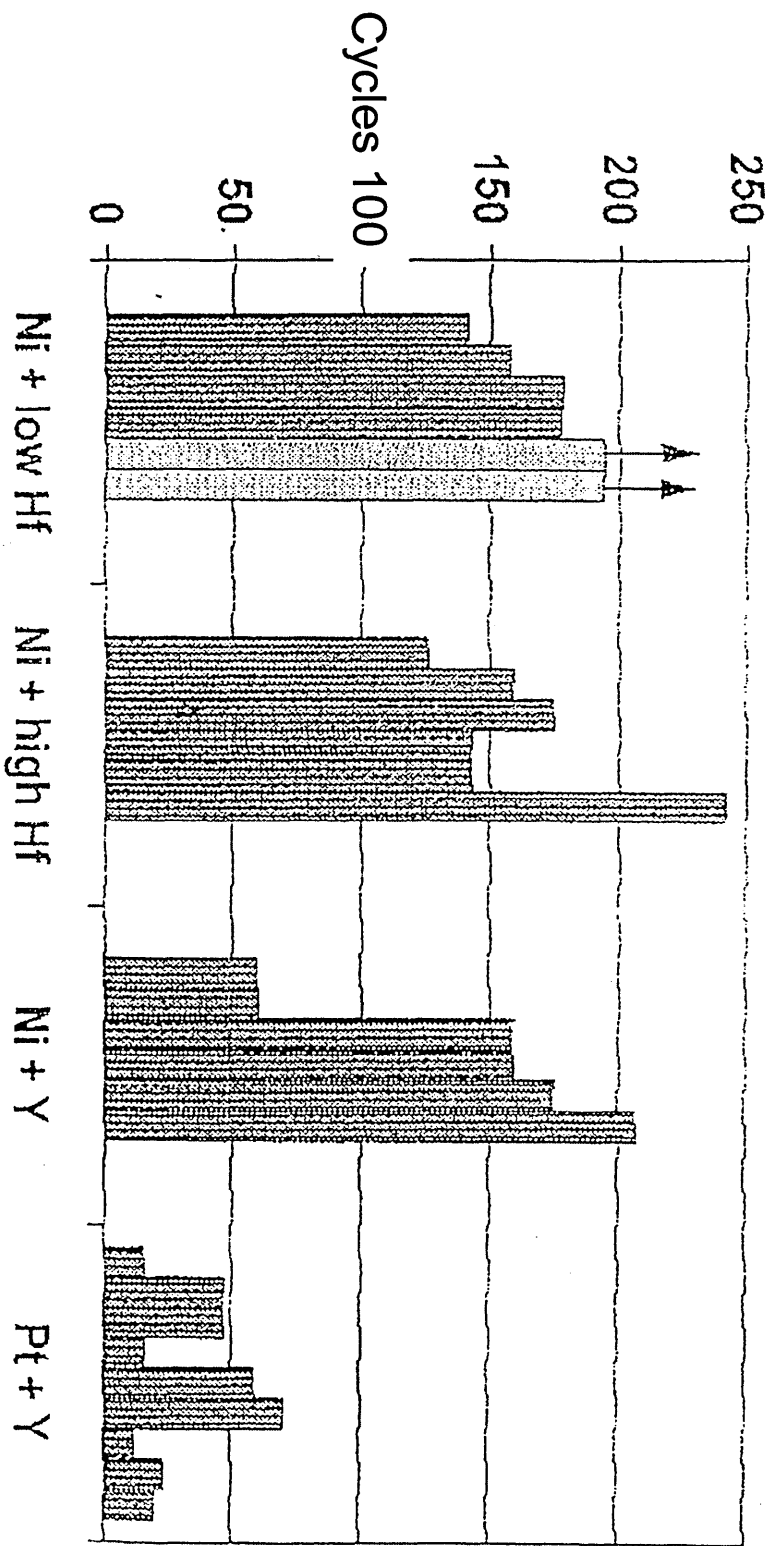




Fig 5.3 Pt variability studies- effect of plating tank conditions and Pt thickness variation. Illustrates a comparison of electroplated Pt variability plated under differing conditions at Rolls Royce. It has been established at Rolls Royce that plating conditions had a direct affect on the performance of the coatings. New tank and old anodes show better results than the rest.

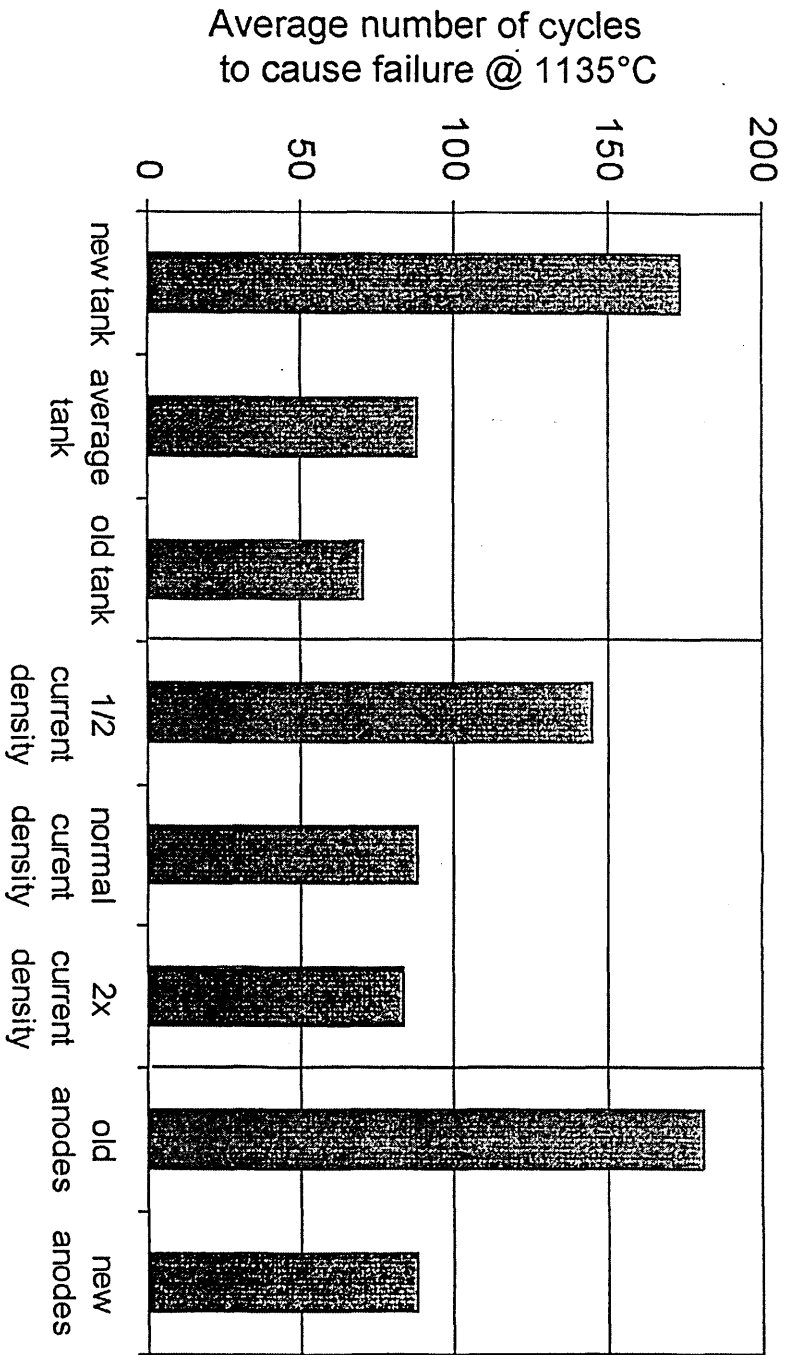


Fig 5.4 Comparison of the effect of pink and brown alumina grit on LCBC. From the data shown there was no major differences between the pink and brown grits. Also there was no major differences between samples that were grit blasted at Rolls Royce and CUK.

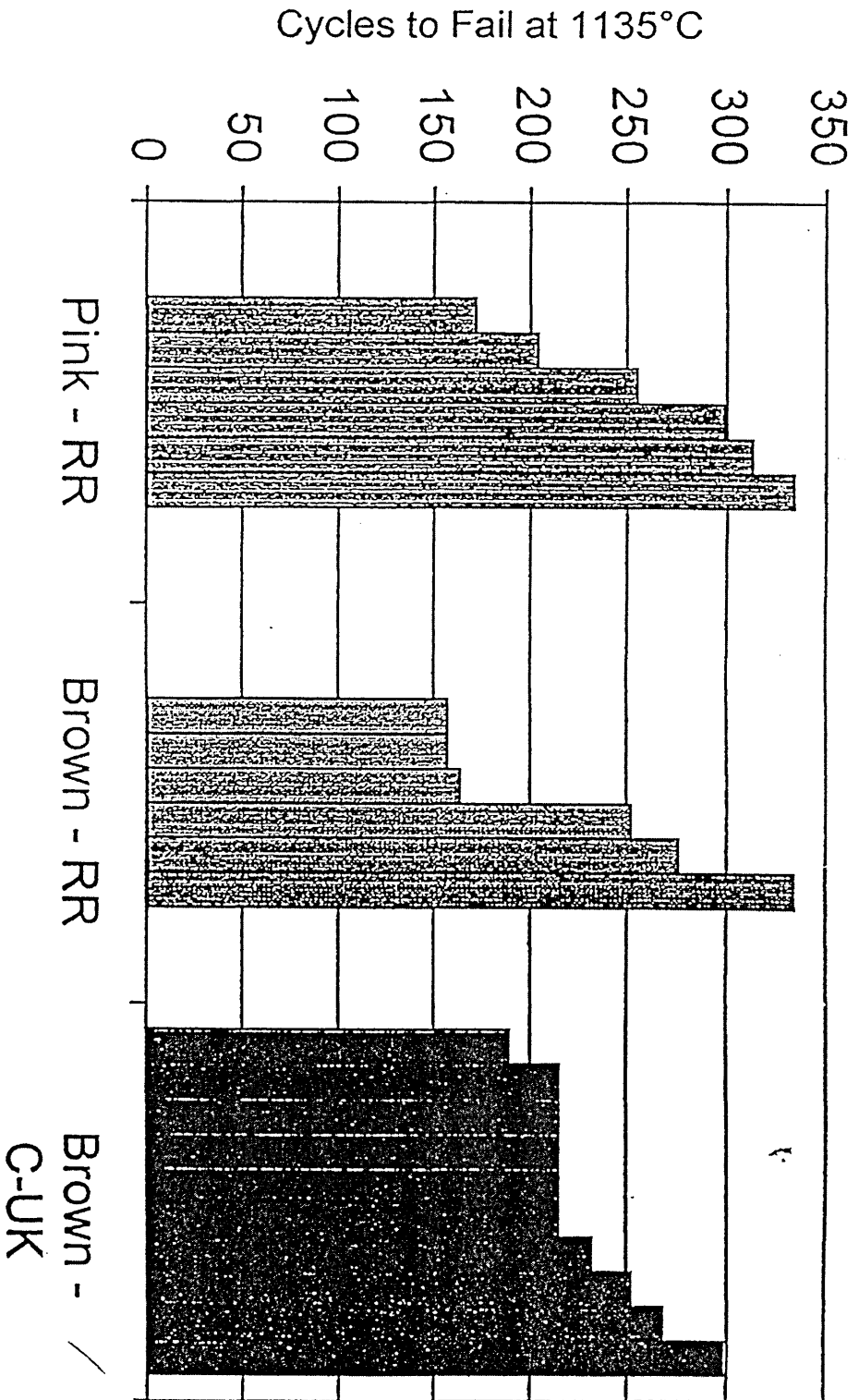


Figure 6.1a(i) GDOES depth profile for base line composition with no ageing treatment ( 0 – hours)

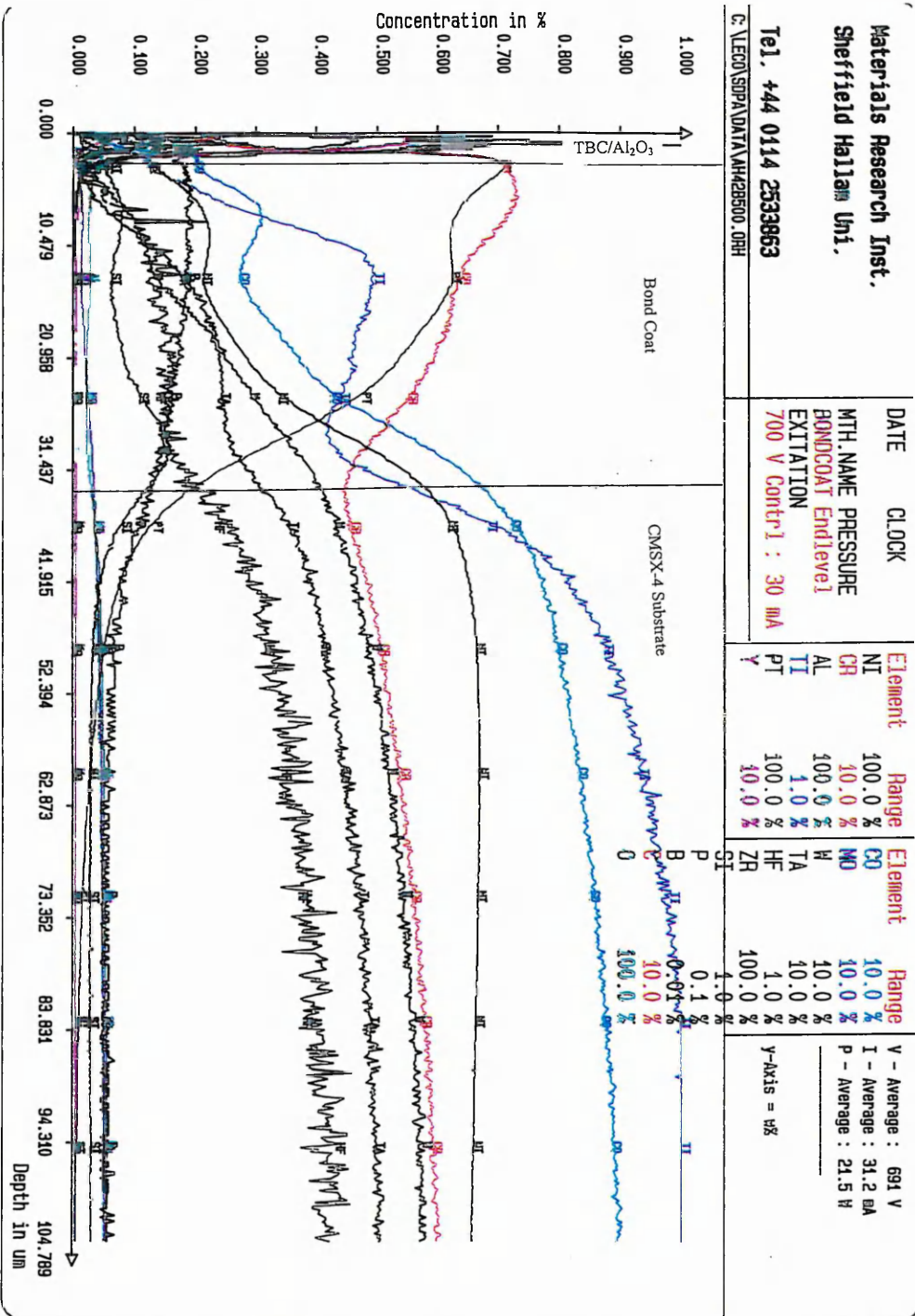


Figure 6. 1a(ii) GDOES selected depth (first 10µm) profile analysis for base line composition with no ageing treatment ( 0 – hours), showing elemental depth profiles of Ni, Cr, Al, Ti, Pt, Y, and Zr

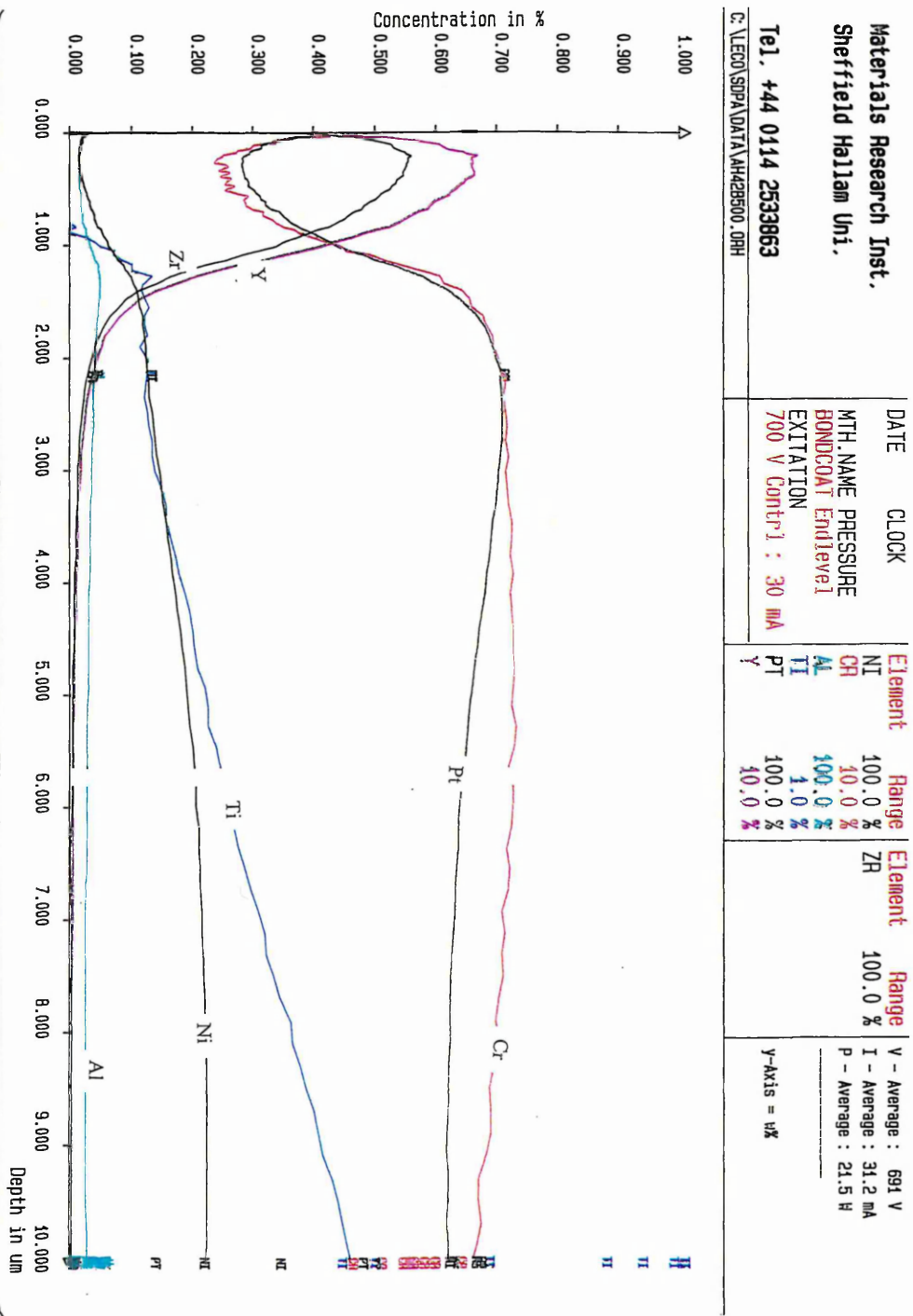


Figure 6. 1b(i) GDOES depth profile for base line composition aged at 1150°C for 4 – hours

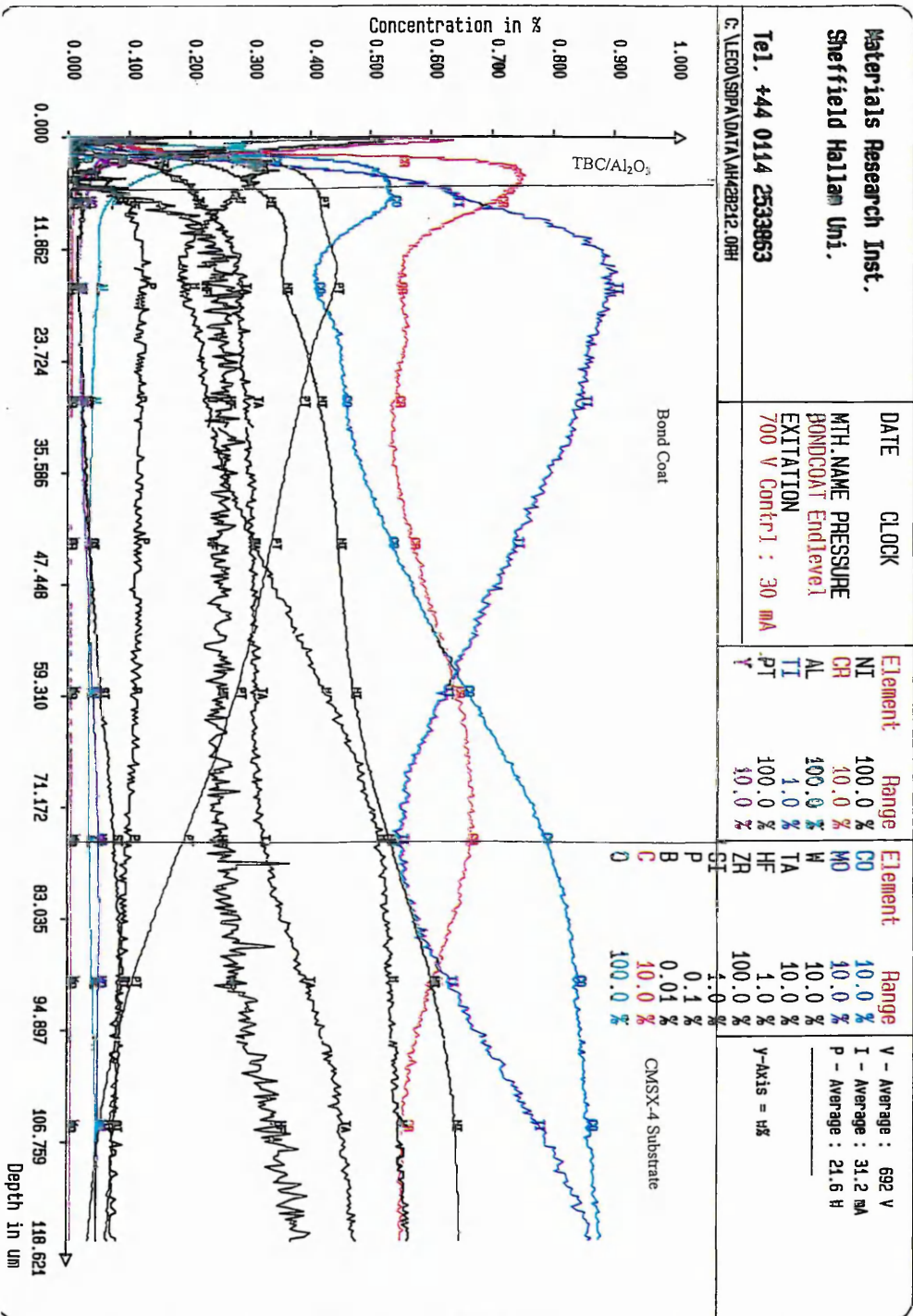


Figure 6. 1b(ii) GDOES selected depth (first 10 μm) profile for base line composition aged at 1150°C for 4 hours, showing elemental depth profiles of Ni, Cr, Al, Ti, Pt, Y, and Zr.

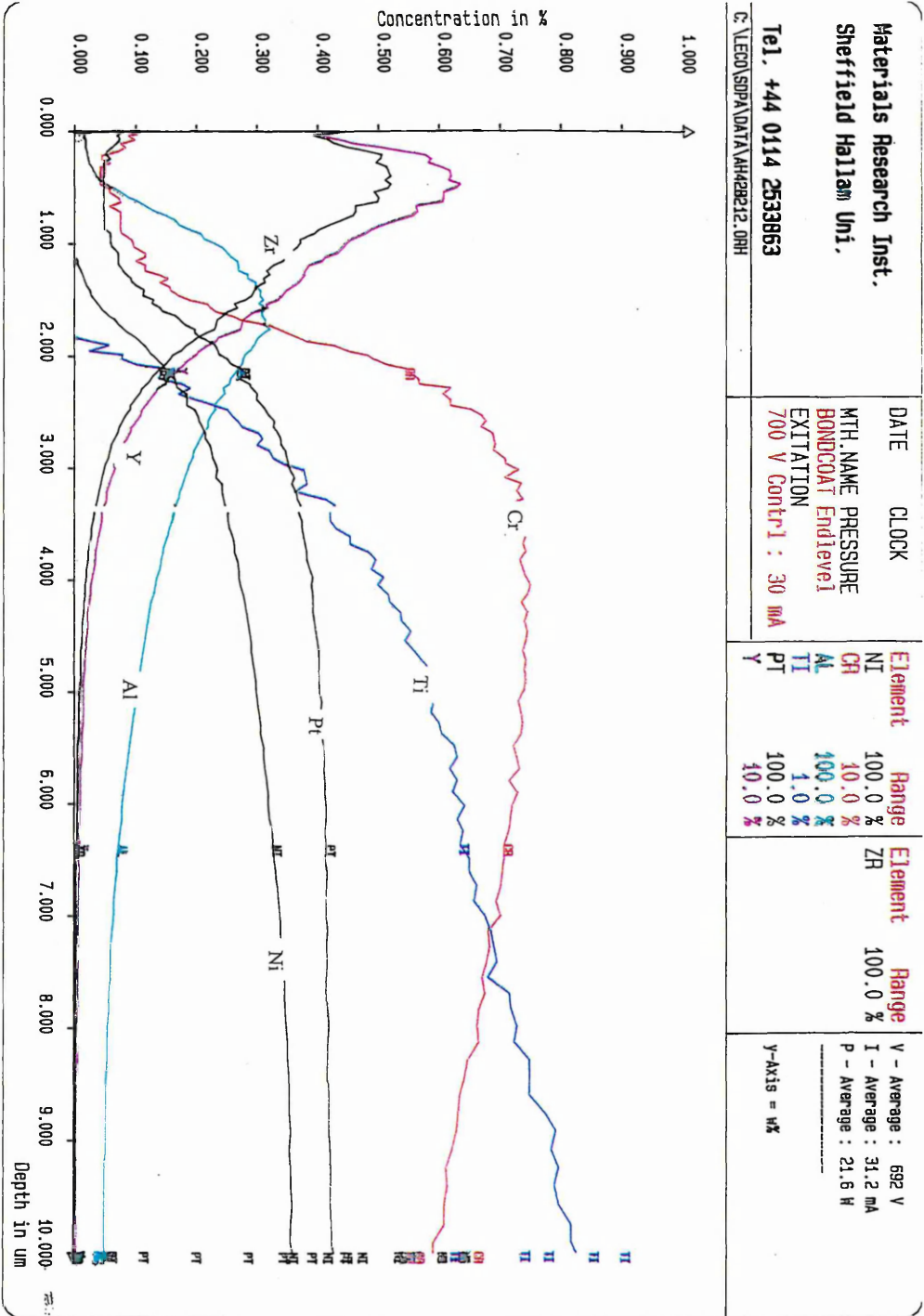


Figure 6.1c(i) GDOES depth profile for base line composition aged at 1150°C for 16 – hours

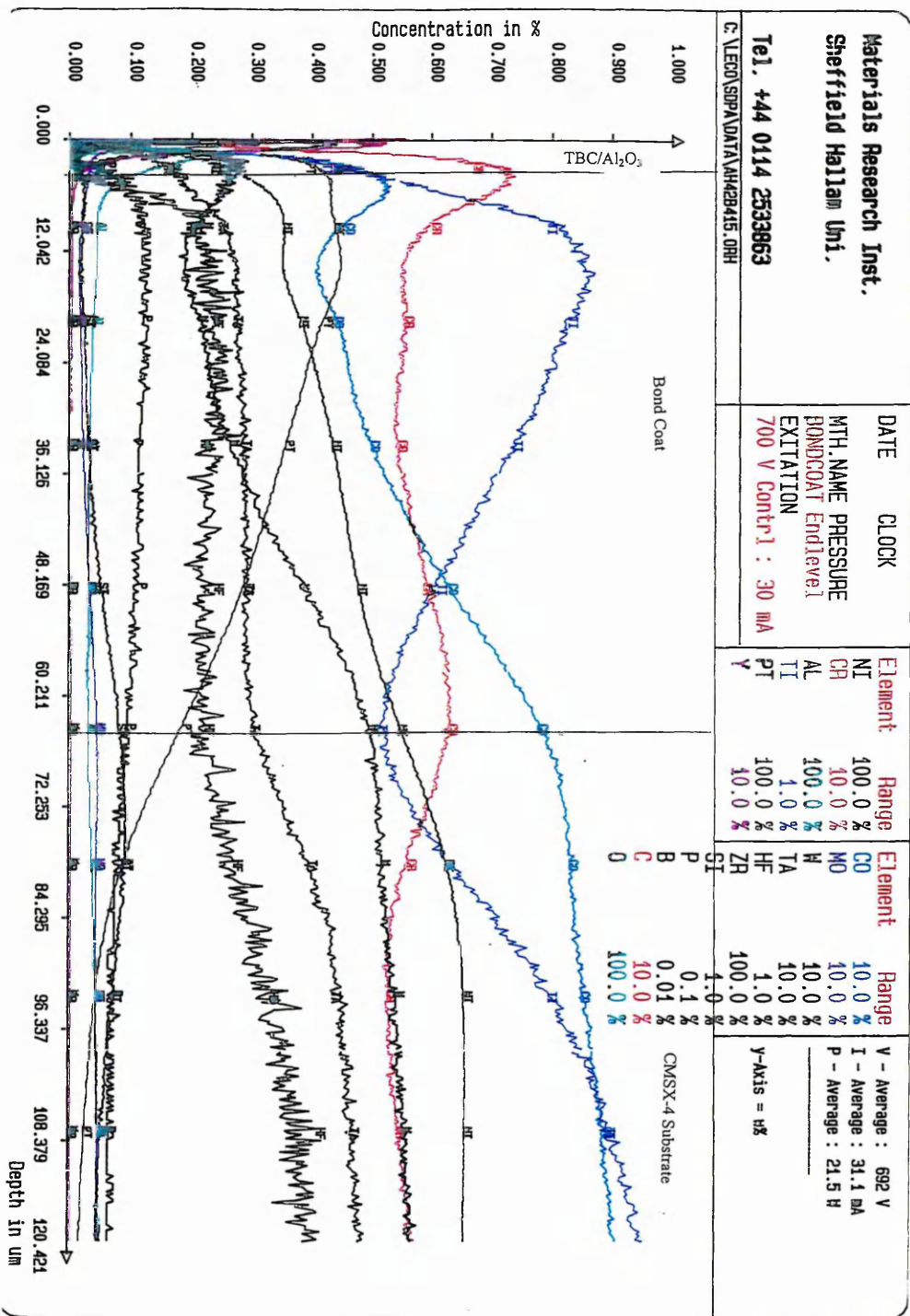


Figure 6. 1c(ii) GDOES selected depth profile (first 10 μm) profile for base line composition aged at 1150°C for 16hours, showing elemental depth profiles of Ni, Cr, Al, Ti, Pt, Y, and Zr.

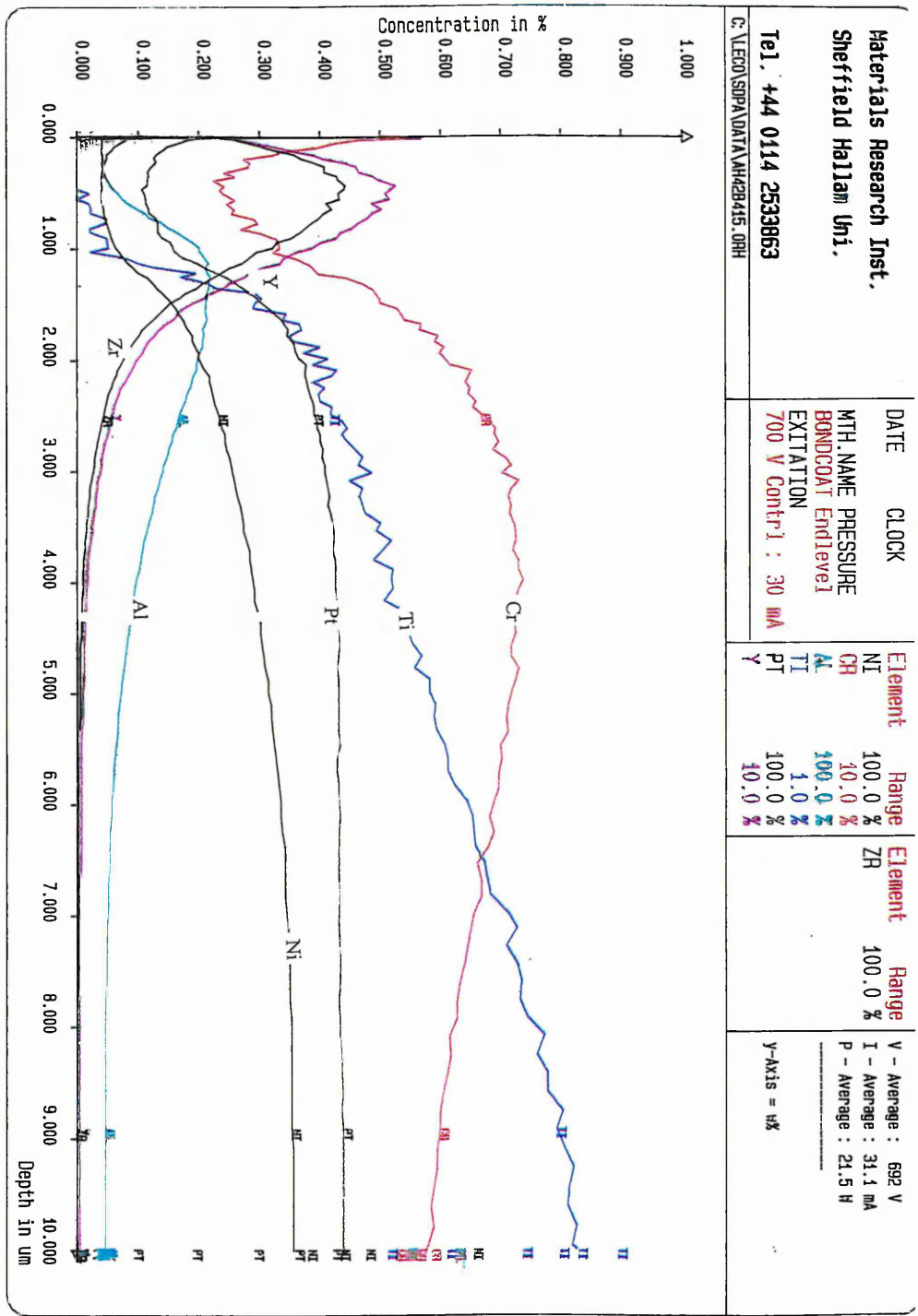


Figure 6. 1d(i) GDOES depth profile for base line composition aged at 1150°C for 25 – hours

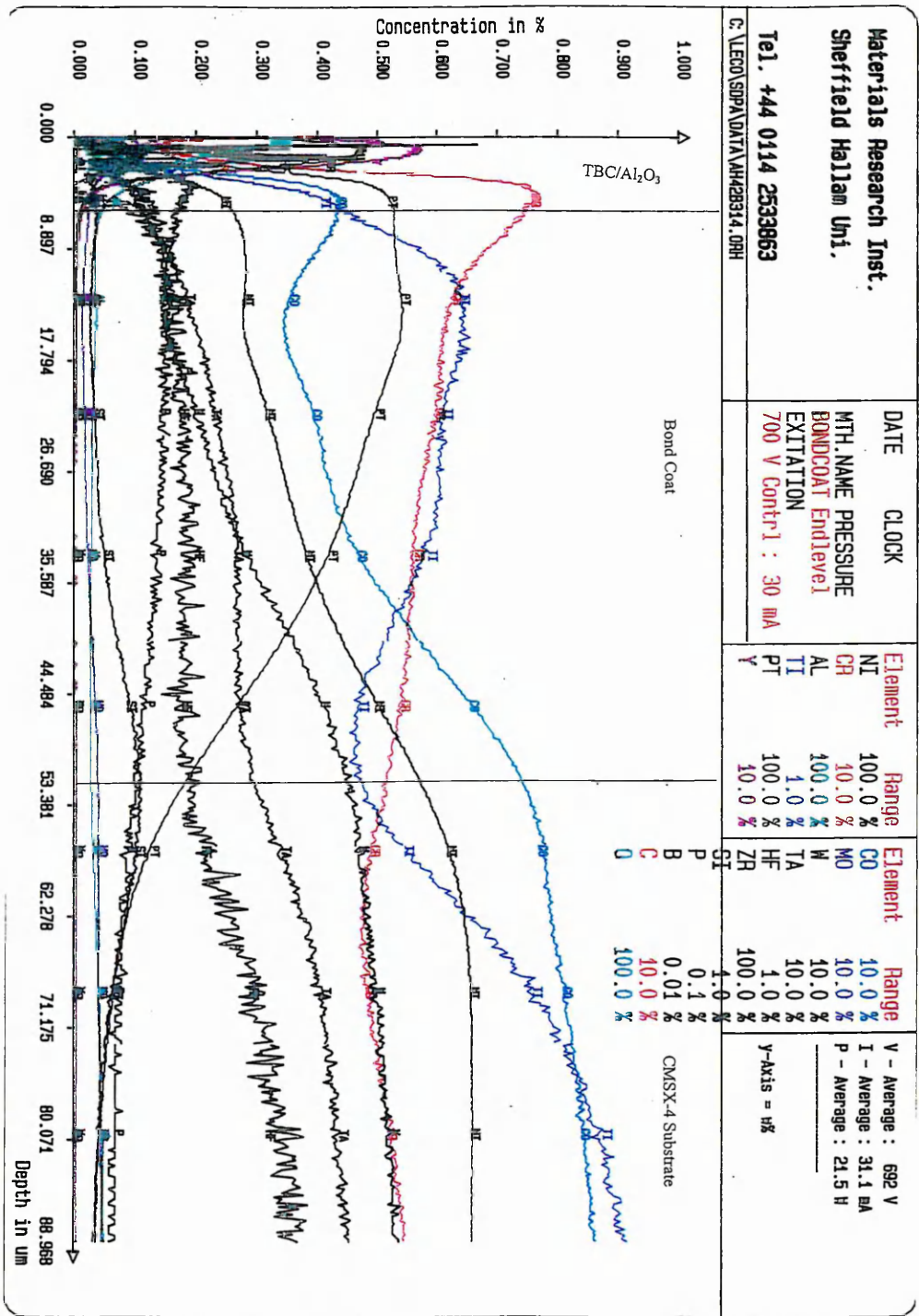


Figure 6. 1d(ii) GDOES selected depth (first 10 μm) profile for base line composition aged at 1150°C for 25 hours, showing elemental depth profiles of Ni, Cr, Al, Ti, Pt, Y, and Zr.

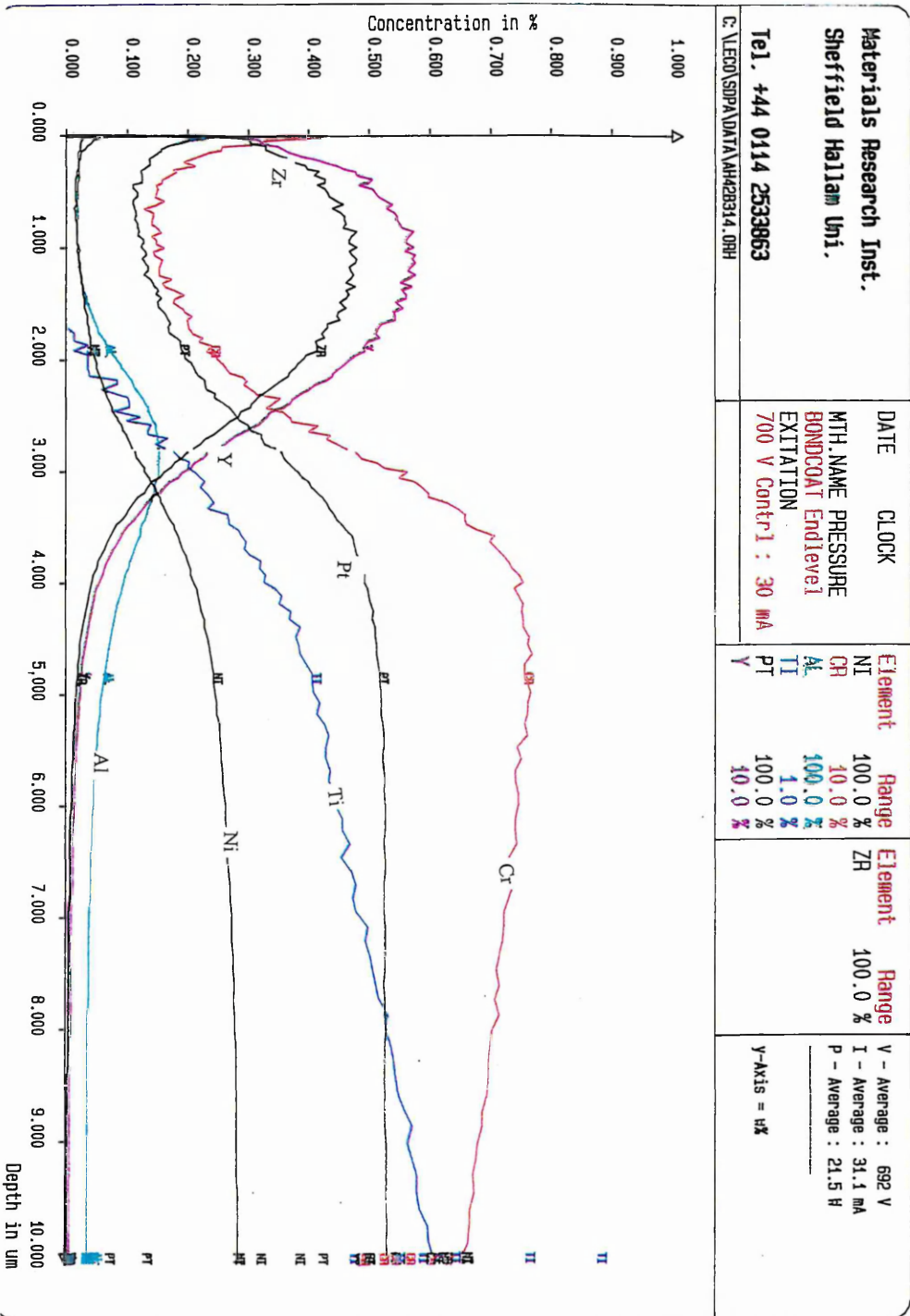
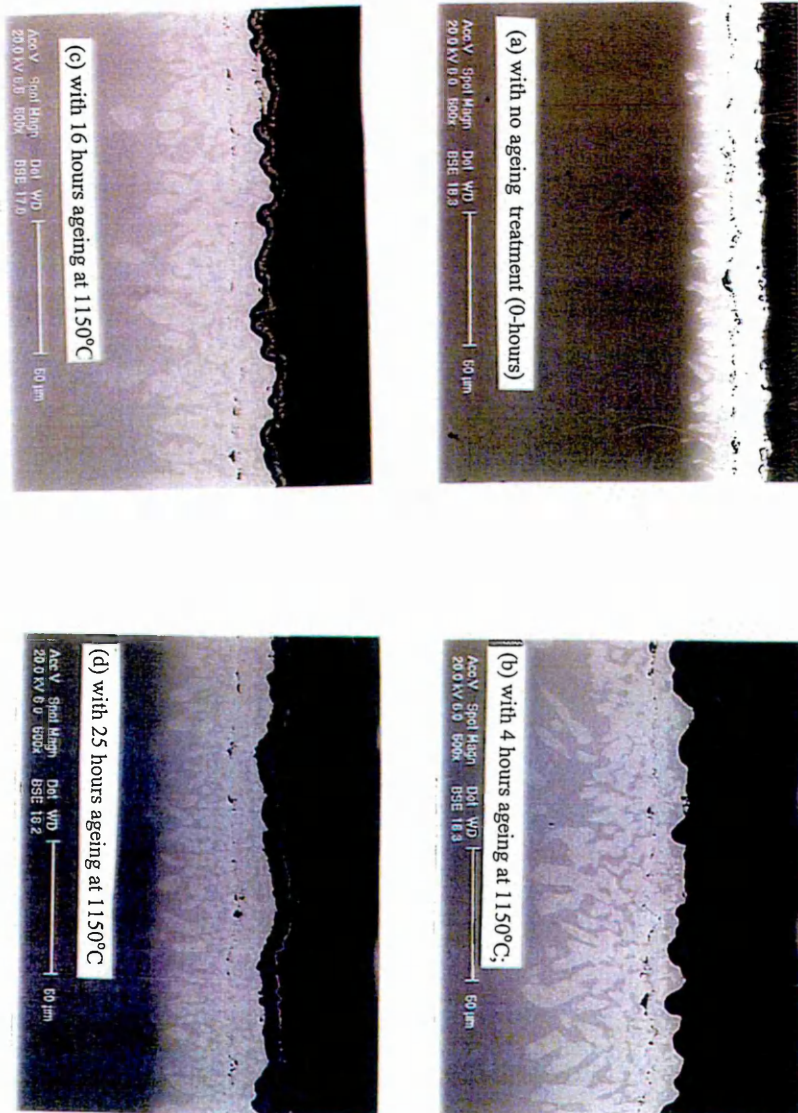


Figure 6.2 SEM microstructure of base line composition at X500 magnifications: (a) with no ageing treatment (0-hours); (b) with 4 hours ageing at 1150°C; (c) with 16 hours ageing at 1150°C; (d) with 25 hours ageing at 1150°C



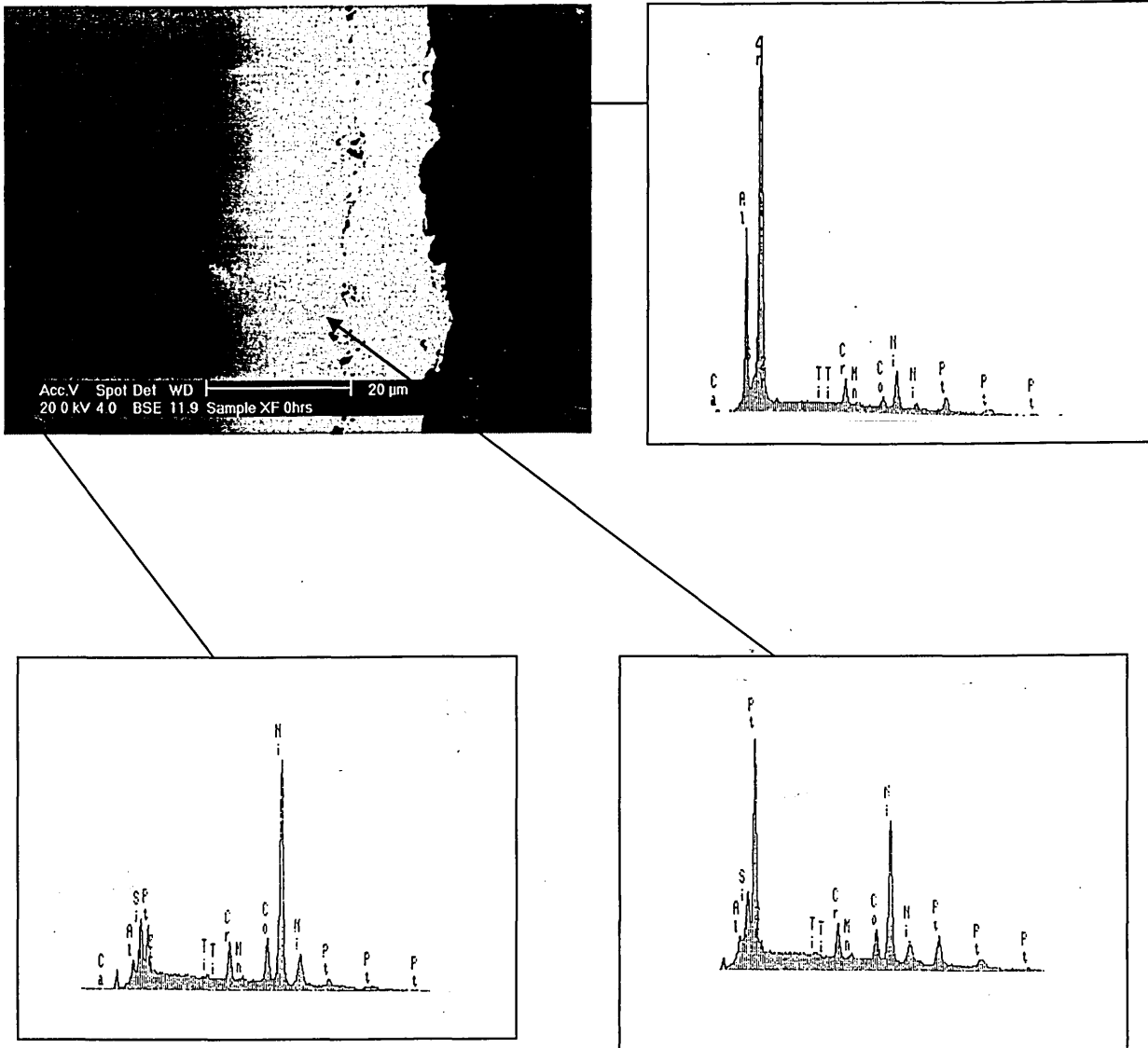


Figure 6.2(ii) SEM BSE and corresponding EDX of LCBC on alloy CMSX-4 ; (a) base line condition

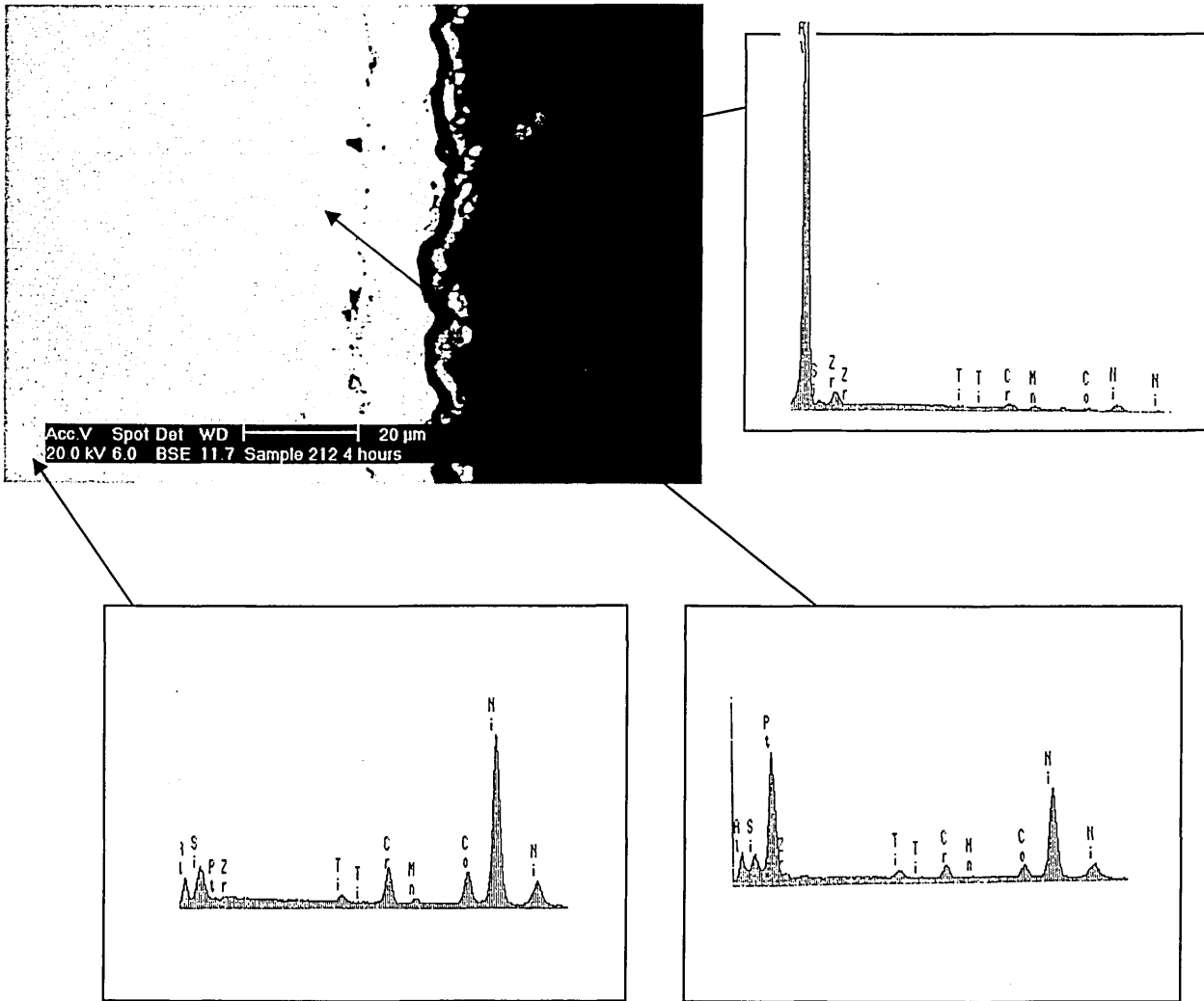


Figure 6.2(ii) SEM BSI and corresponding EDX of LCBC on alloy CMSX-4 ; (a) 4 hours ageing

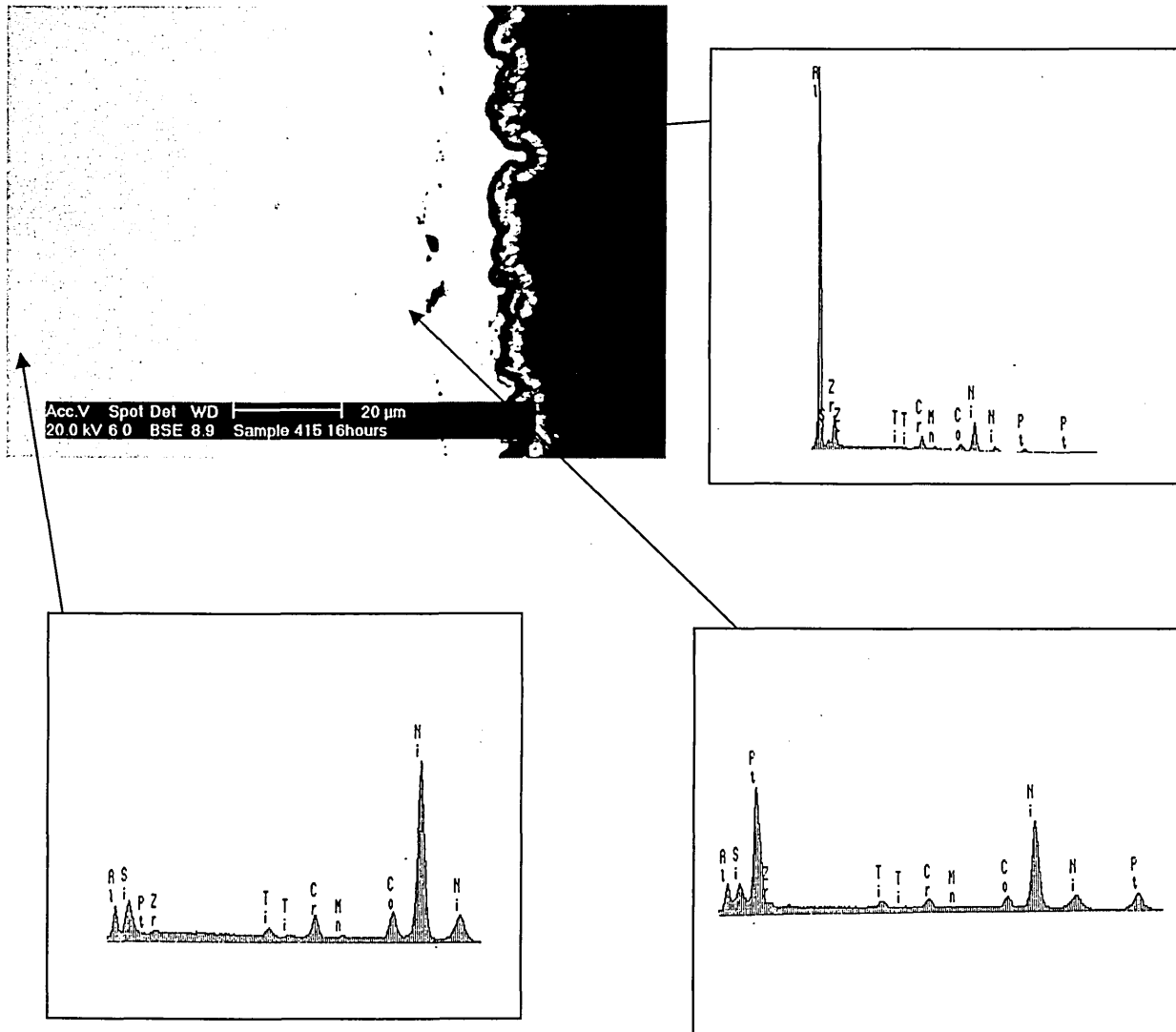


Figure 6.2(ii) SEM BSE and corresponding EDX of LCBC on alloy CMSX-4 ; (a) 16 hours ageing

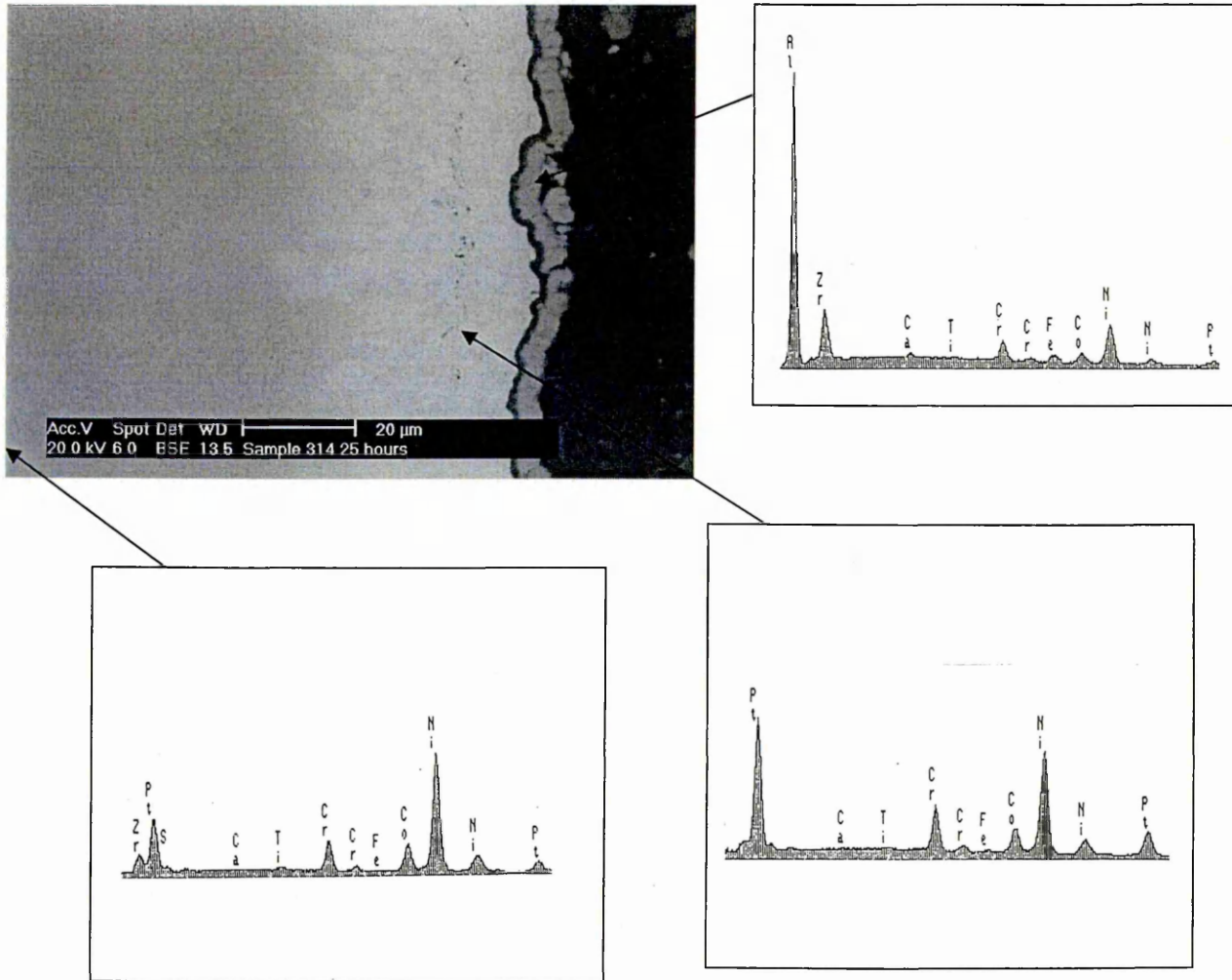


Figure 6.2(ii) SEM BSI and corresponding EDX of LCBC on alloy CMSX-4 ; (a) 25 hours ageing

Figure 6.2(iii) BSI and corresponding X-ray mapping images illustrating the distribution of various elements along a cross-section of low cost Pt bond coat on alloy CMSX-4; ( a ) base line condition

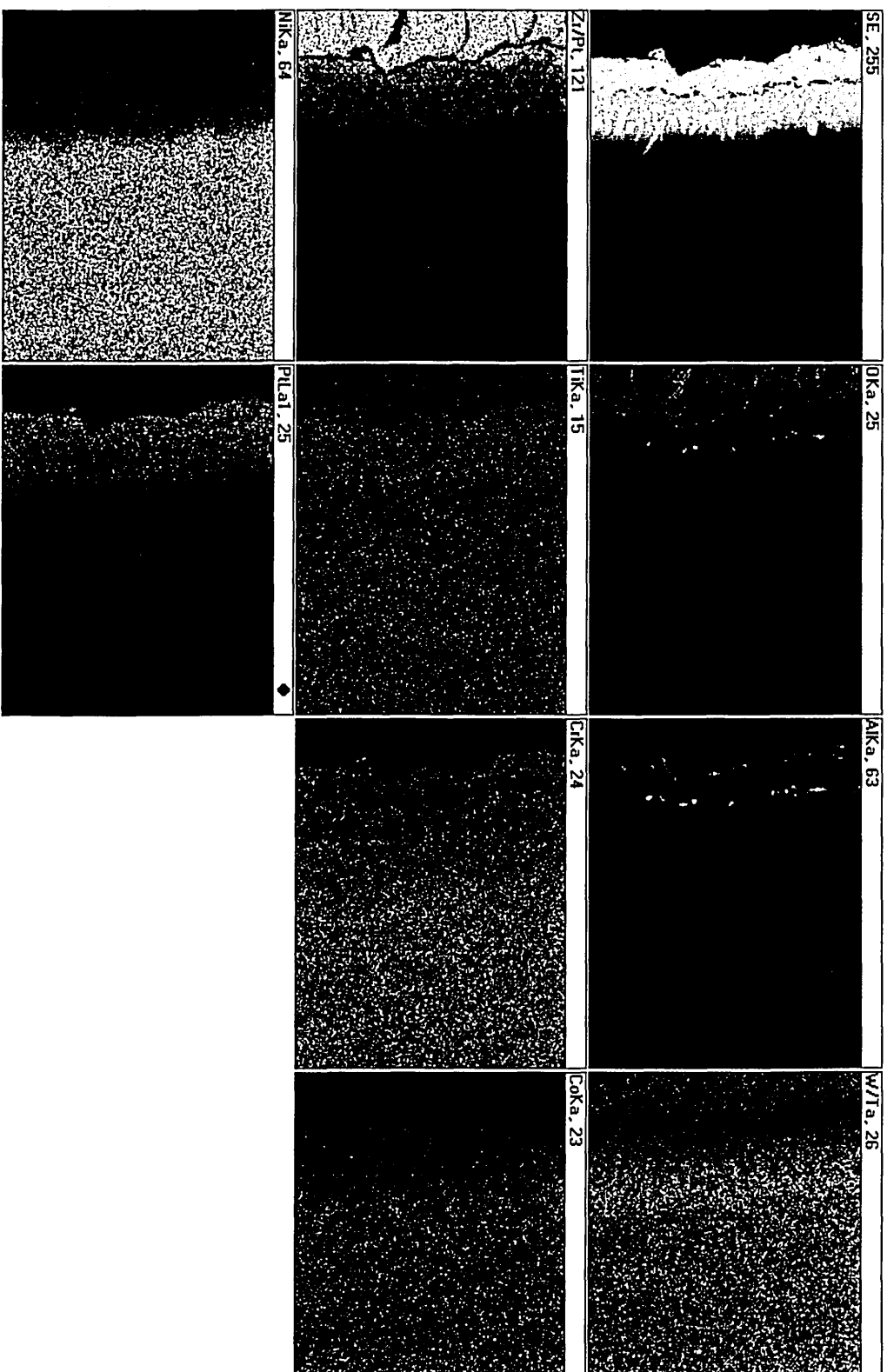


Figure 6.2(iii) BSI and corresponding X-ray mapping images illustrating the distribution of various elements along a cross-section of low cost Pt bond coat on alloy CMSX-4;(b) 4 hrs ageing

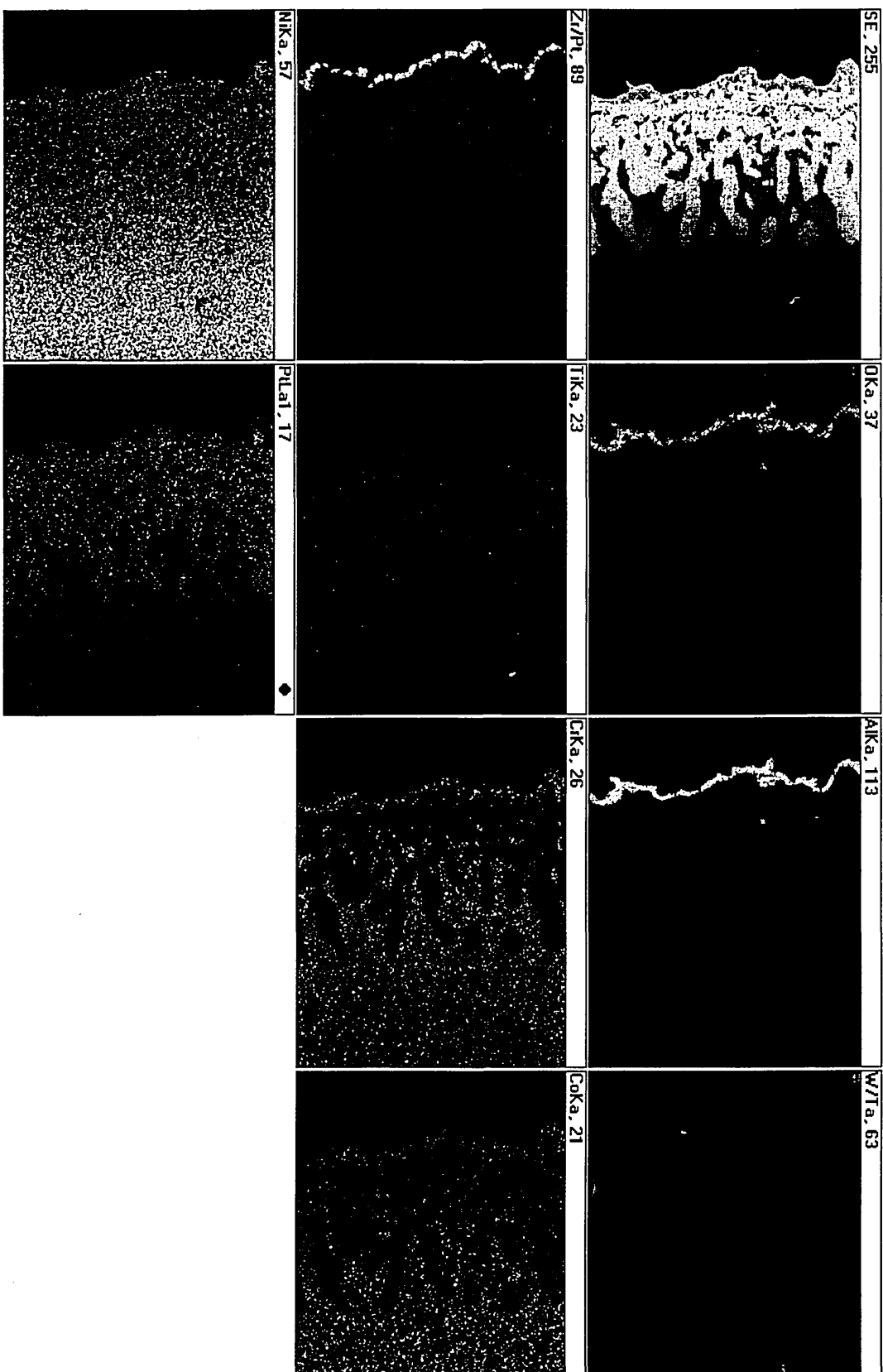


Figure 6.2(iii) BSI and corresponding X-ray mapping images illustrating the distribution of various elements along a cross-section of low cost Pt bond coat on alloy CMSX-4;(c) 16 hrs ageing

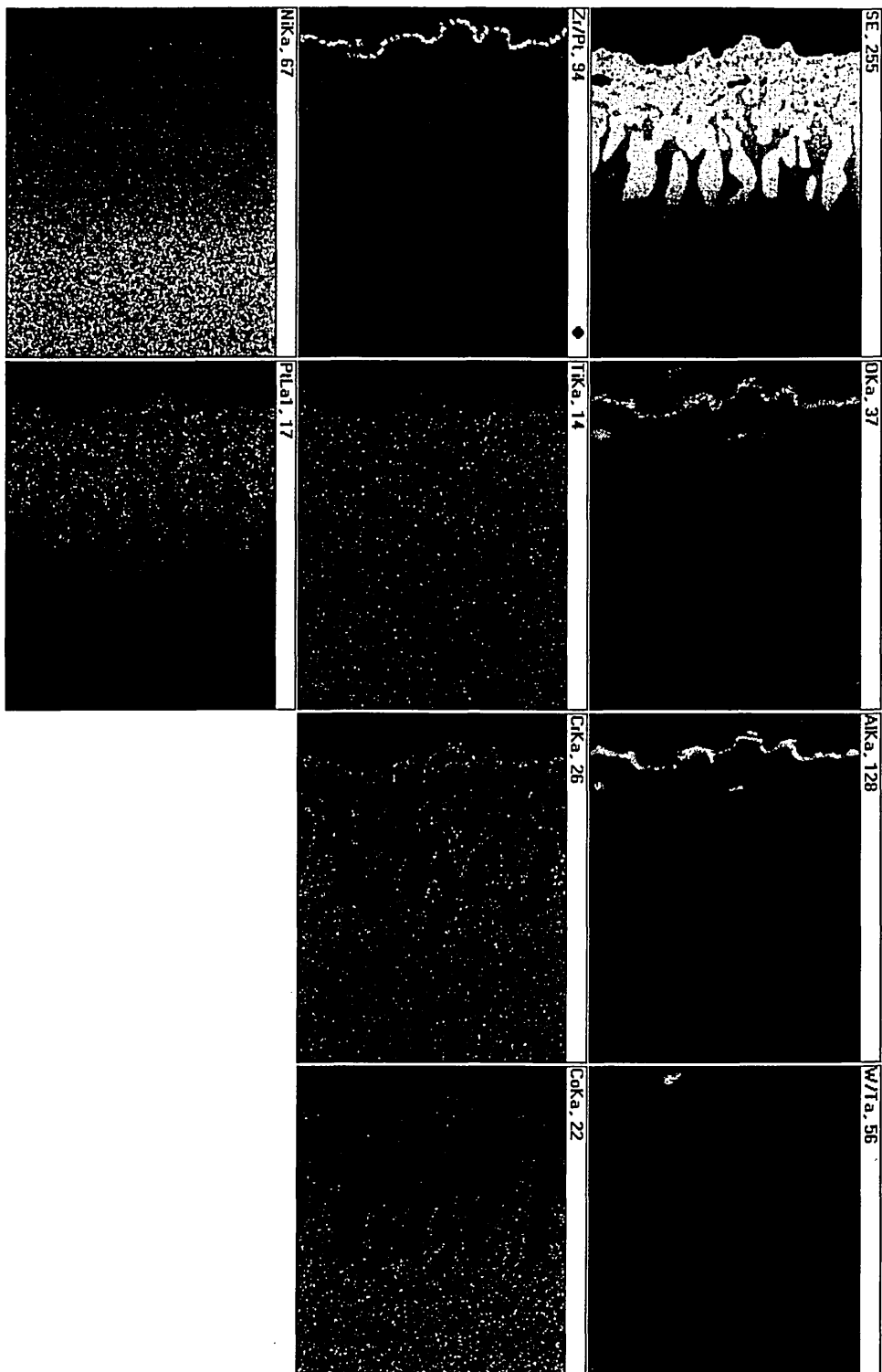


Figure 6.2(iii) BSI and corresponding X-ray mapping images illustrating the distribution of various elements along a cross-section of low cost Pt bond coat on alloy CMSX-4;(d) 25 hrs ageing

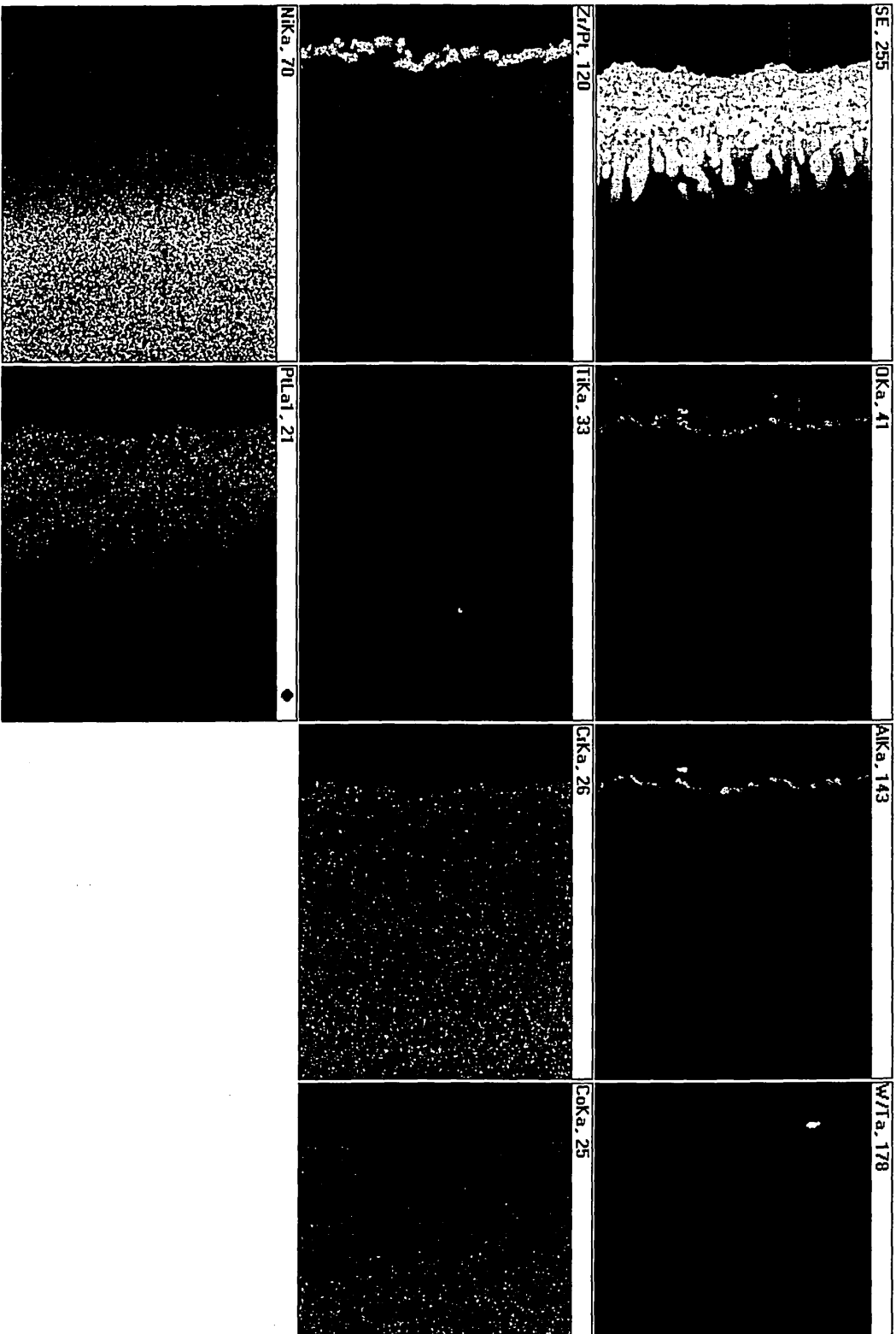


Table 6.2 Average oxide thickness from TEM/SEM measurement of TGO layer and corresponding graph

Ageing (hours)	TGO (microns)
0	0.3
4	2.25
16	1.75
25	1.5

**Aluminium oxide thickness vs ageing times**

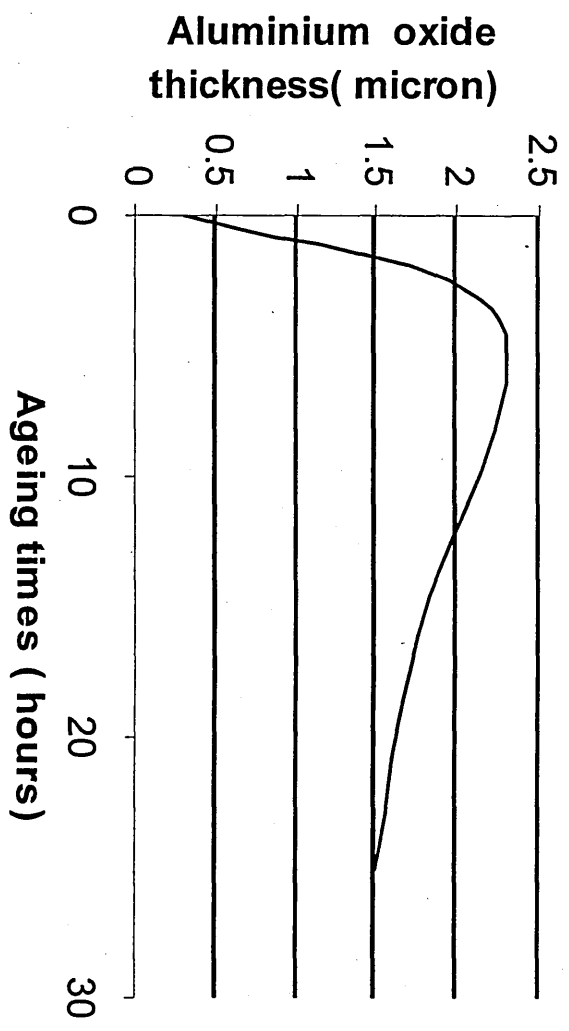


Figure 6.3a (plate XF-1-11) : BF image at 50K magnification: All 3 layers of coating with selected X-ray energy dispersive analysis of Al<sub>2</sub>O<sub>3</sub> and TBC

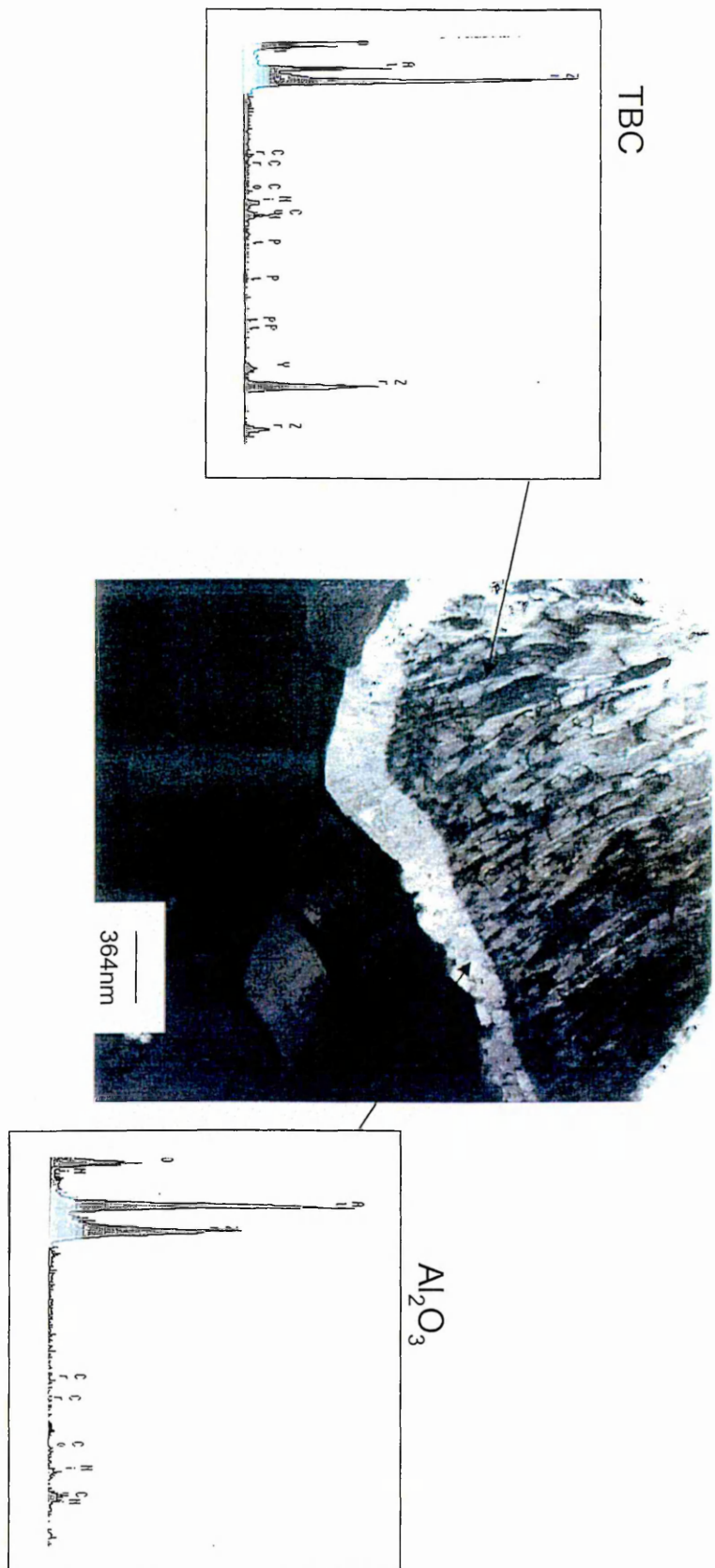


Figure 6.3a (plate XF1-14) : A DF Image at 200K magnification of the  $Al_2O_3$  layer. Detection of a possible dark phase particles in  $Al_2O_3$  and corresponding EDX pattern. A SAD pattern of this layer shows typical diffuse rings corresponding to a poly crystalline material confirming its  $Al_2O_3$ . Possible dark phase particles is richer in Pt,Cr,Zr and Y. EDX in standard  $Al_2O_3$  is normally free from Cr, Co, although still rich in Zr.

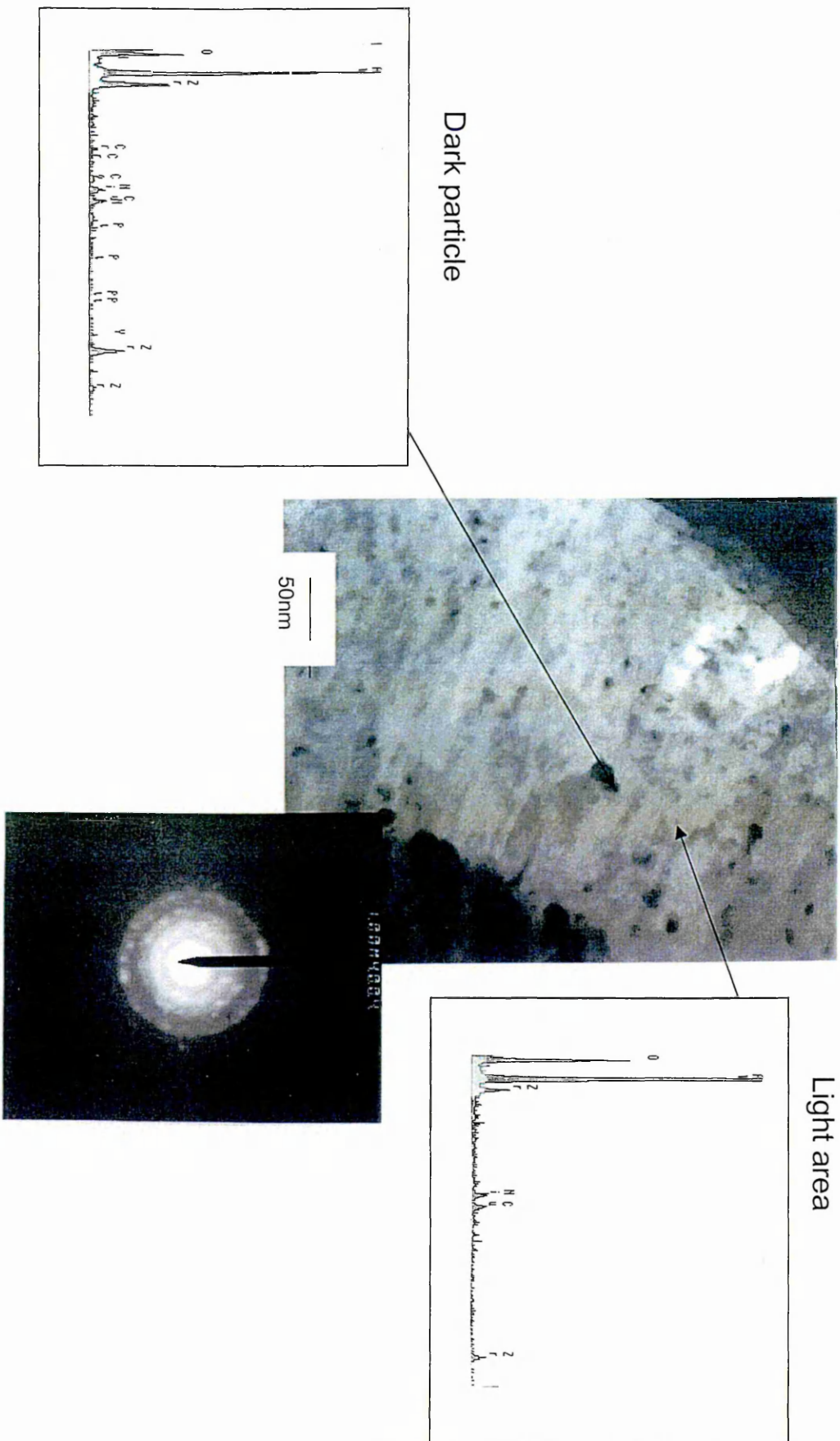


Figure 6.3a (Plate XF-1-15): DF image at 200K magnification with more EDX performed on Al<sub>2</sub>O<sub>3</sub> layer on the dark phase particles. Also a DF image at 250K magnification showing possible peg at bond coat / Al<sub>2</sub>O<sub>3</sub> interface. Bond coat EDX is richer as expected in Pt, Ni, Cr, Co and a little Al. This could be a Pt-rich  $\gamma'$  phase.

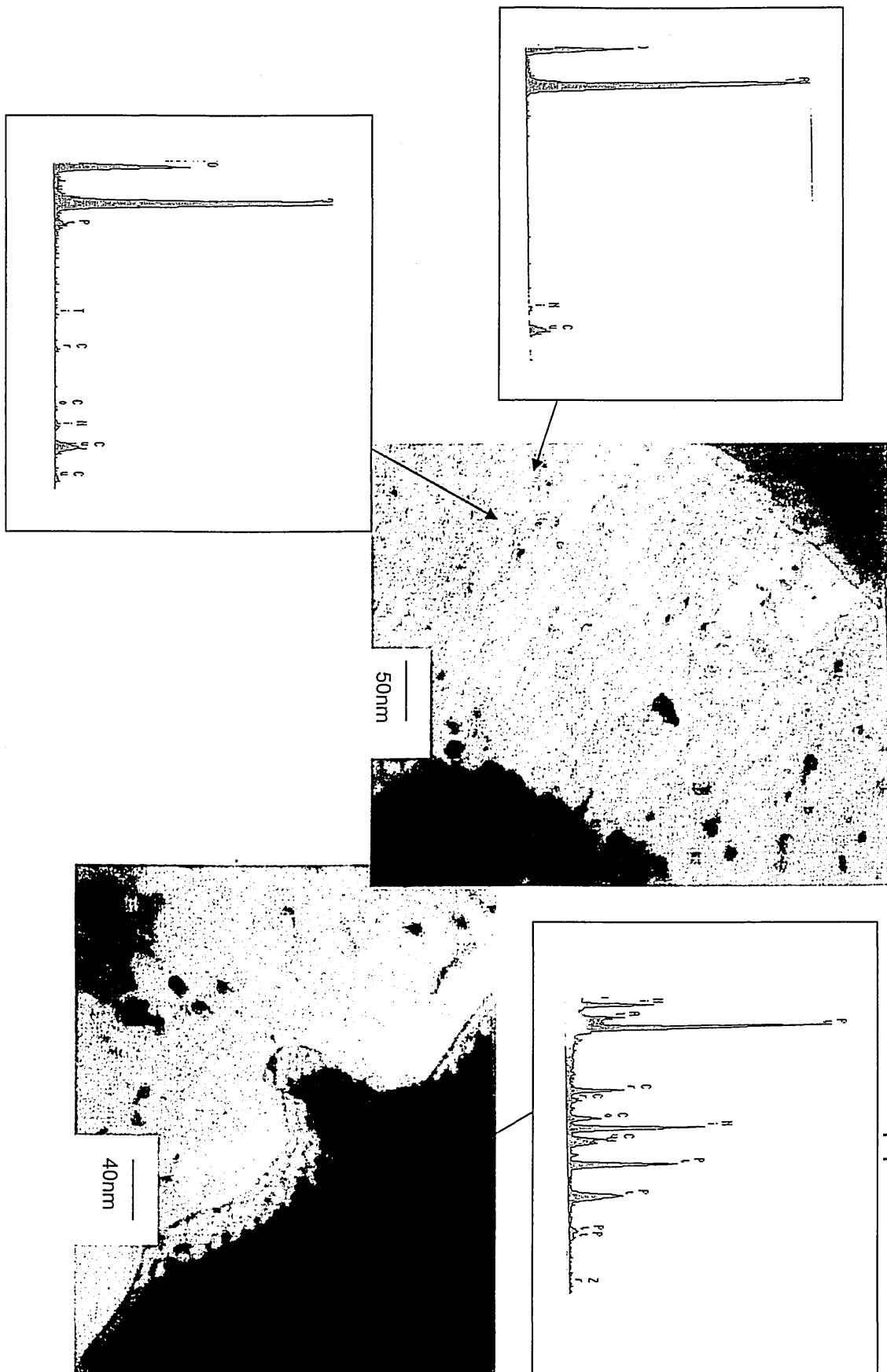


Figure 6.3a (plate XF1-16): BF image at 15k magnification in bond coat region. Several grit particles observed which have been confirmed by EDX to be Al and O rich. Also observed light and dark phases within the bond coat region. Lighter phase of bond coat composition is not rich in Ti whilst darker shows a small peak.

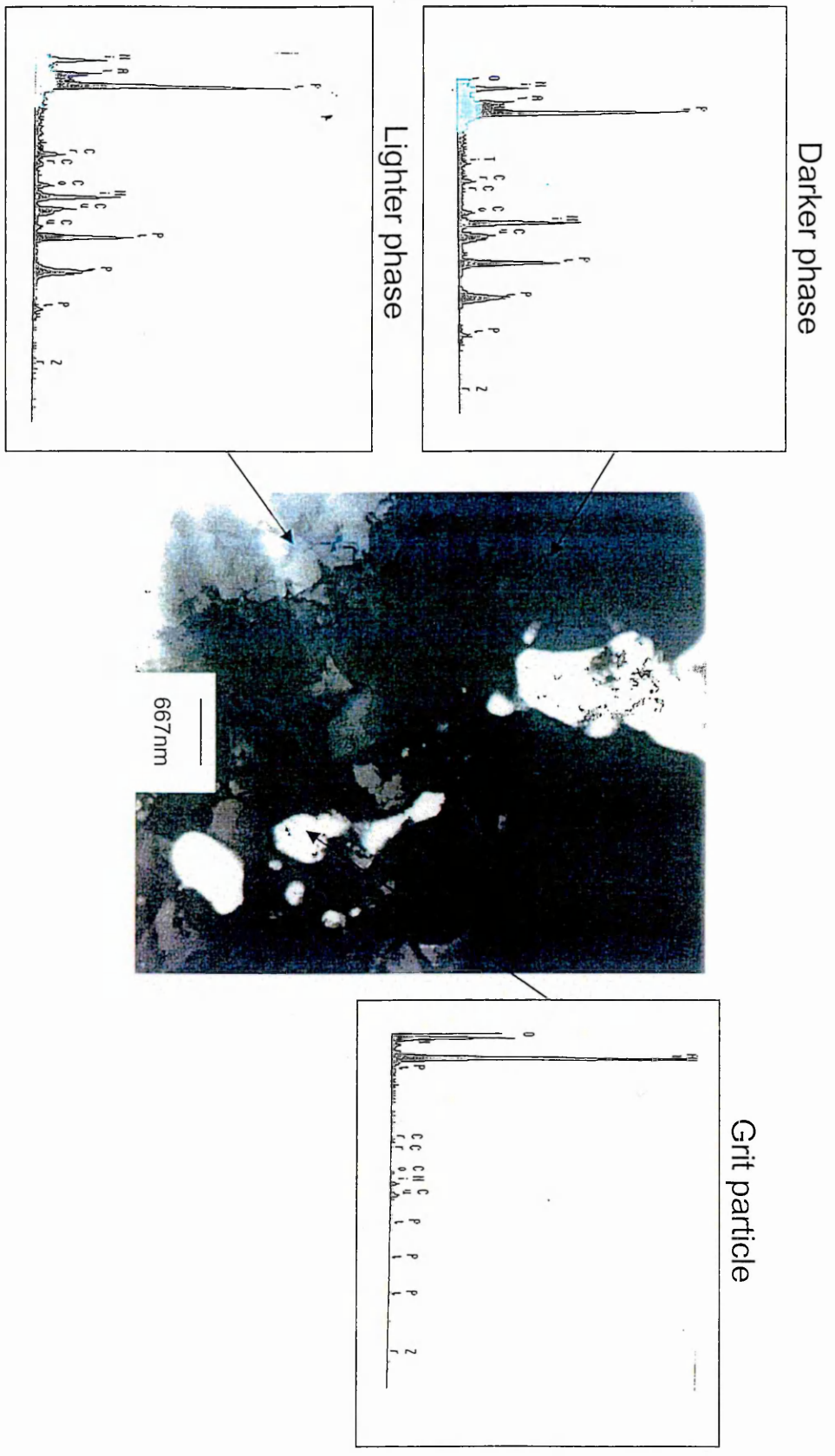


Figure 6.3b: 4 hours ageing (Plate 212-11): BF Image at 11.5K magnification: Low magnification to corner all regions. There is evidence of growth in the  $Al_2O_3$  region. There is mixed grain size within the  $Al_2O_3$  region with finer at interface between TBC/ $Al_2O_3$ . However, coarser at BC/ $Al_2O_3$  interface.

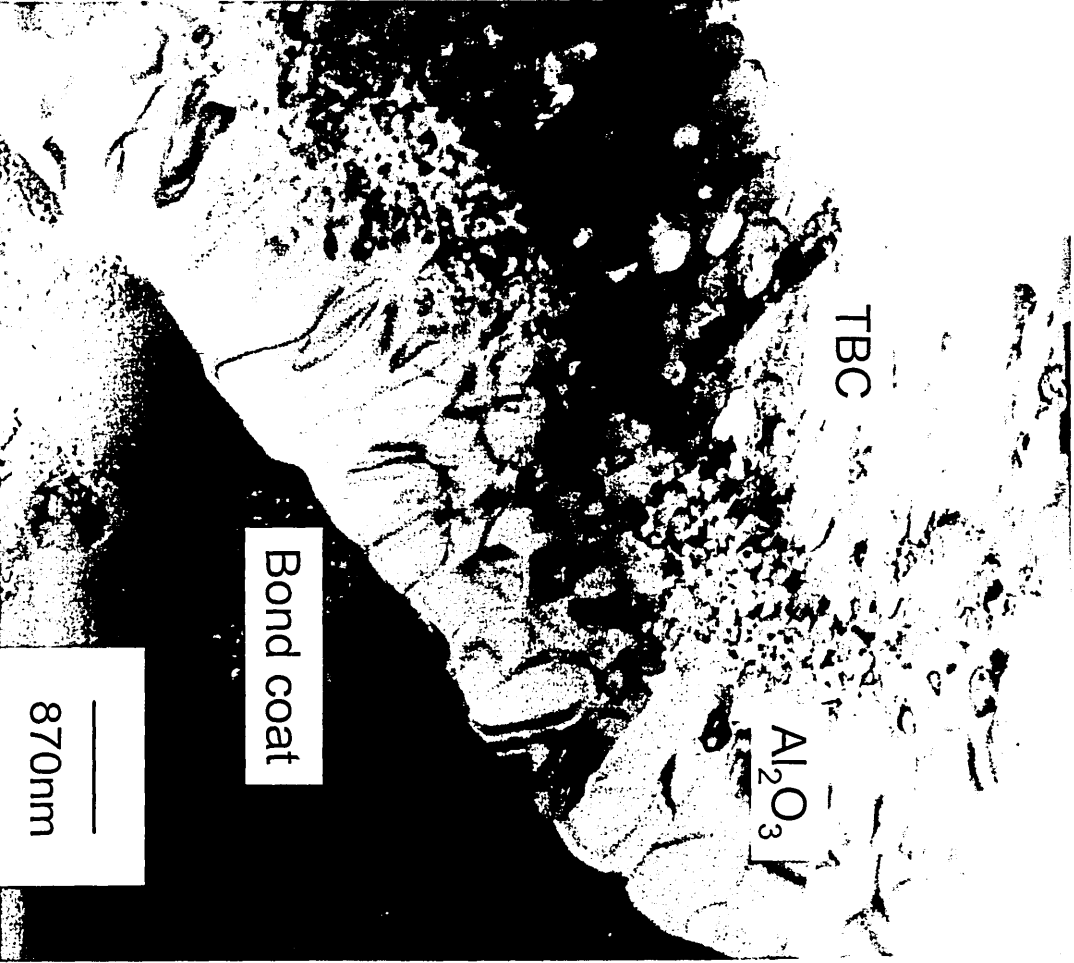


Figure 6.3b: 4 hours ageing (Plate 212-13): (i) BF image at 27.5K magnification : Interface between  $\text{Al}_2\text{O}_3$  / Bond coat -very sharp interfacial region. Coarser alumina grains at the interface. (ii) Also BF image at 150K magnification showing  $\text{Al}_2\text{O}_3$  region with again precipitates present.

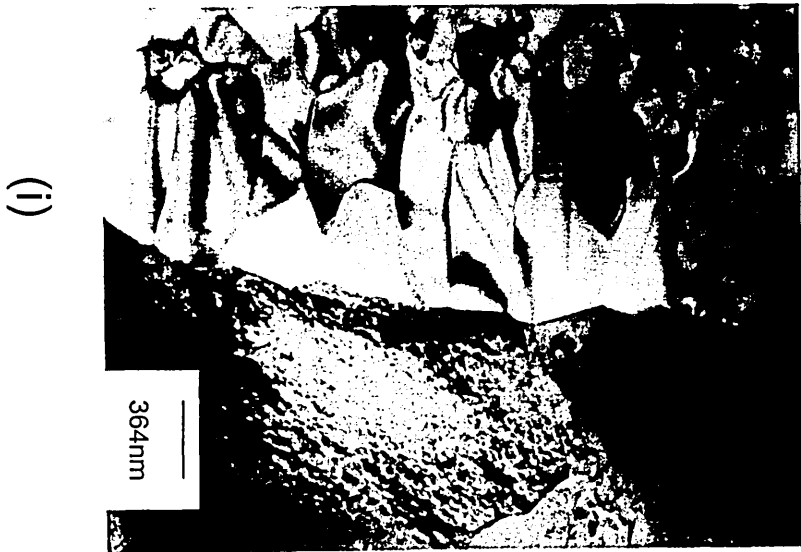
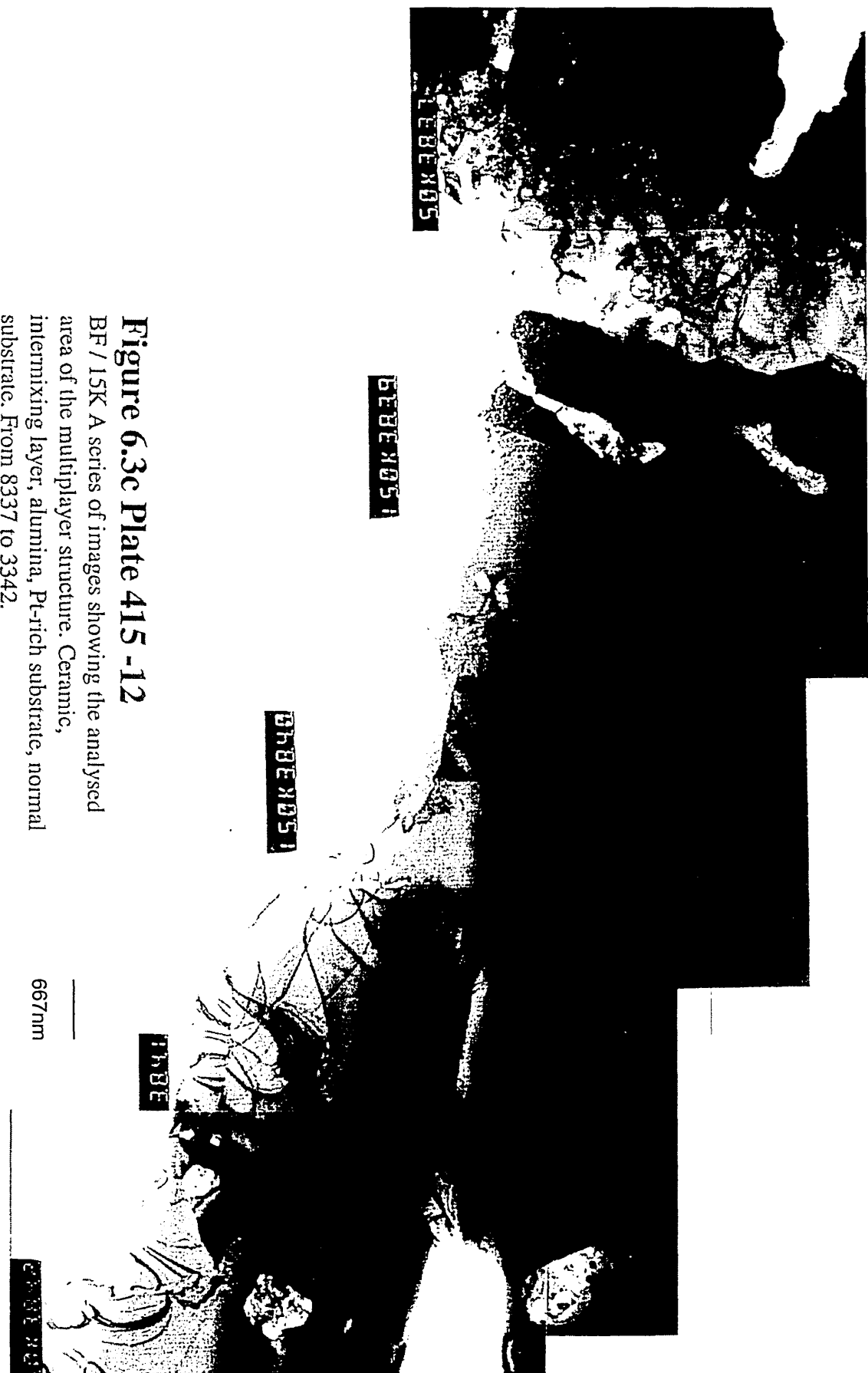


Figure 6.3b: 4 hours ageing (Plate 212-15): BF Image at 150K magnification : Showing  $\text{Al}_2\text{O}_3$  / TBC interface. Very sharp interfacial region without any voids indicating good adhesion.





**Figure 6.3c Plate 415 -12**

BF / 15K A series of images showing the analysed area of the multilayer structure. Ceramic, intermixing layer, alumina, Pt-rich substrate, normal substrate. From 8337 to 3342.

Figure 6.3c: 16 hours ageing (Plate 415-13): (i)BF Image at 27.5K magnification : Alumina interlayer of equiaxial microstructure. The alumina is coarse close to the substrate and becomes fine towards the surface ceramic layer where it presents as an intermixing layer. Also shown (ii) BF Image at 66K : Magnified image of alumina grains and grain boundaries. No voids were involved in the microstructure.

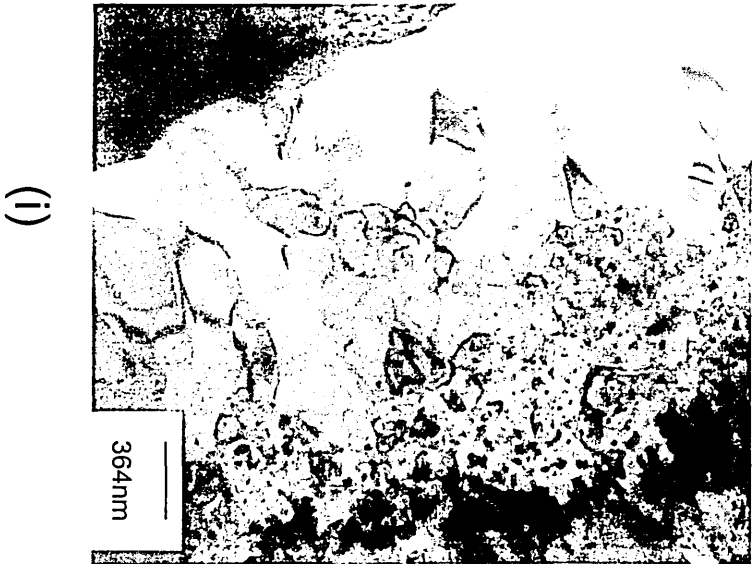


Figure 6.3c: 16 hours ageing (Plate 415-14): BF Image at 88K magnification : Sharp interface between the alumina and bond coat, and also a triple point.

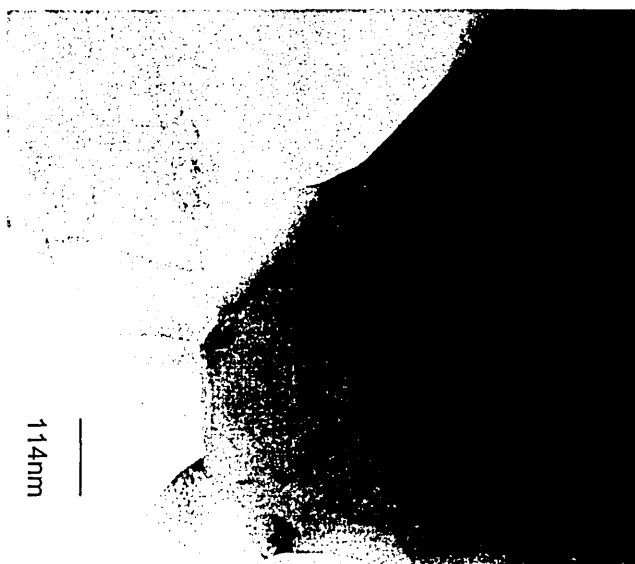


Figure 6.3d: 25 hours ageing (Plate 314-13): BF Image at 27.5K magnification : A series of plates showing TBC/ $Al_2O_3$  and bond coat region.

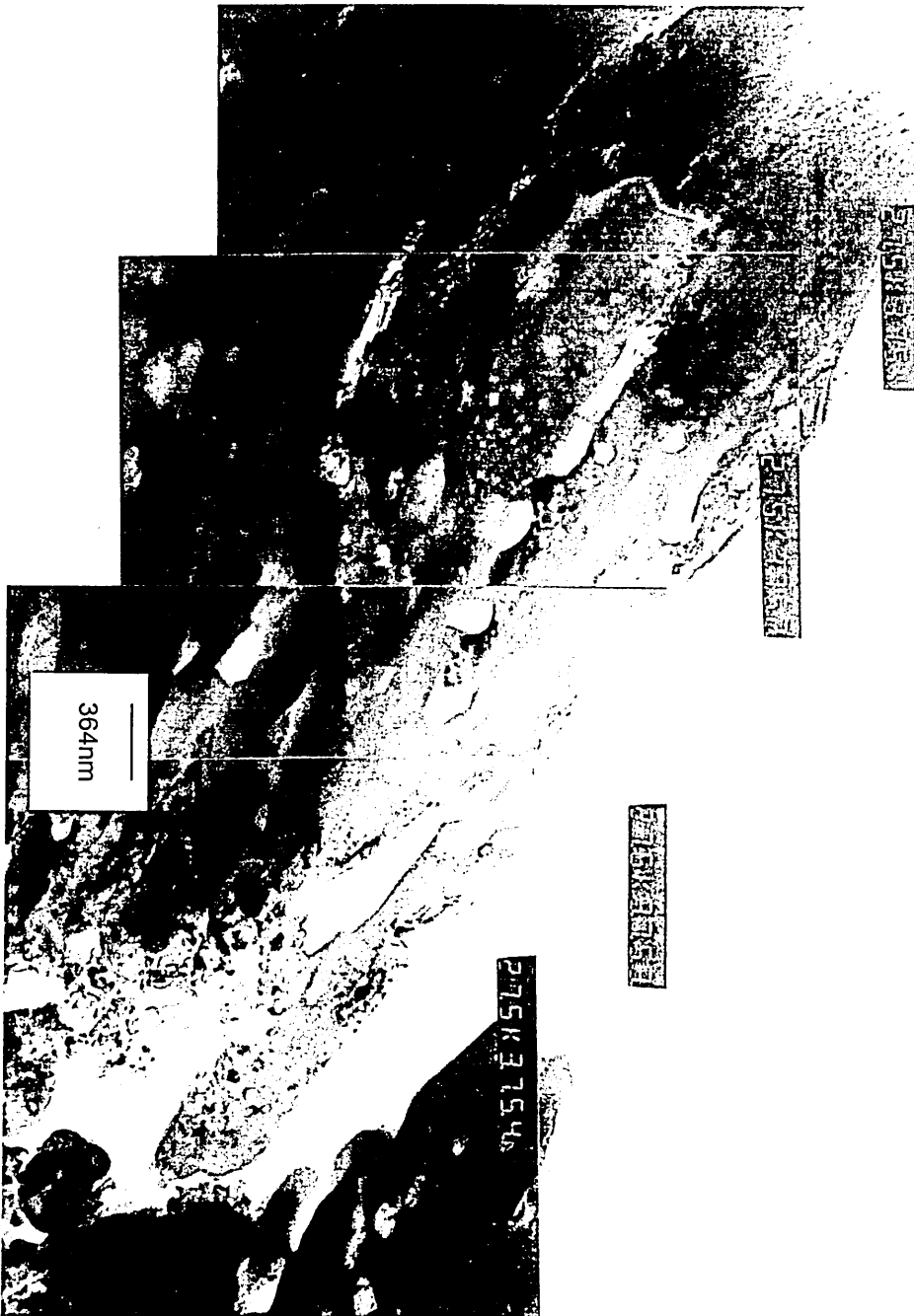


Figure 6.3d (Plate 314-15): BF Image at 27.5K magnification: TBC/Al<sub>2</sub>O<sub>3</sub>/Bond coat regions. Intermixing between the bond coat and alumina, EDX shows that Cr, Ni diffused through, which eventually lead to bond coat degradation. Coarse alumina is still pure, except a little Ni.

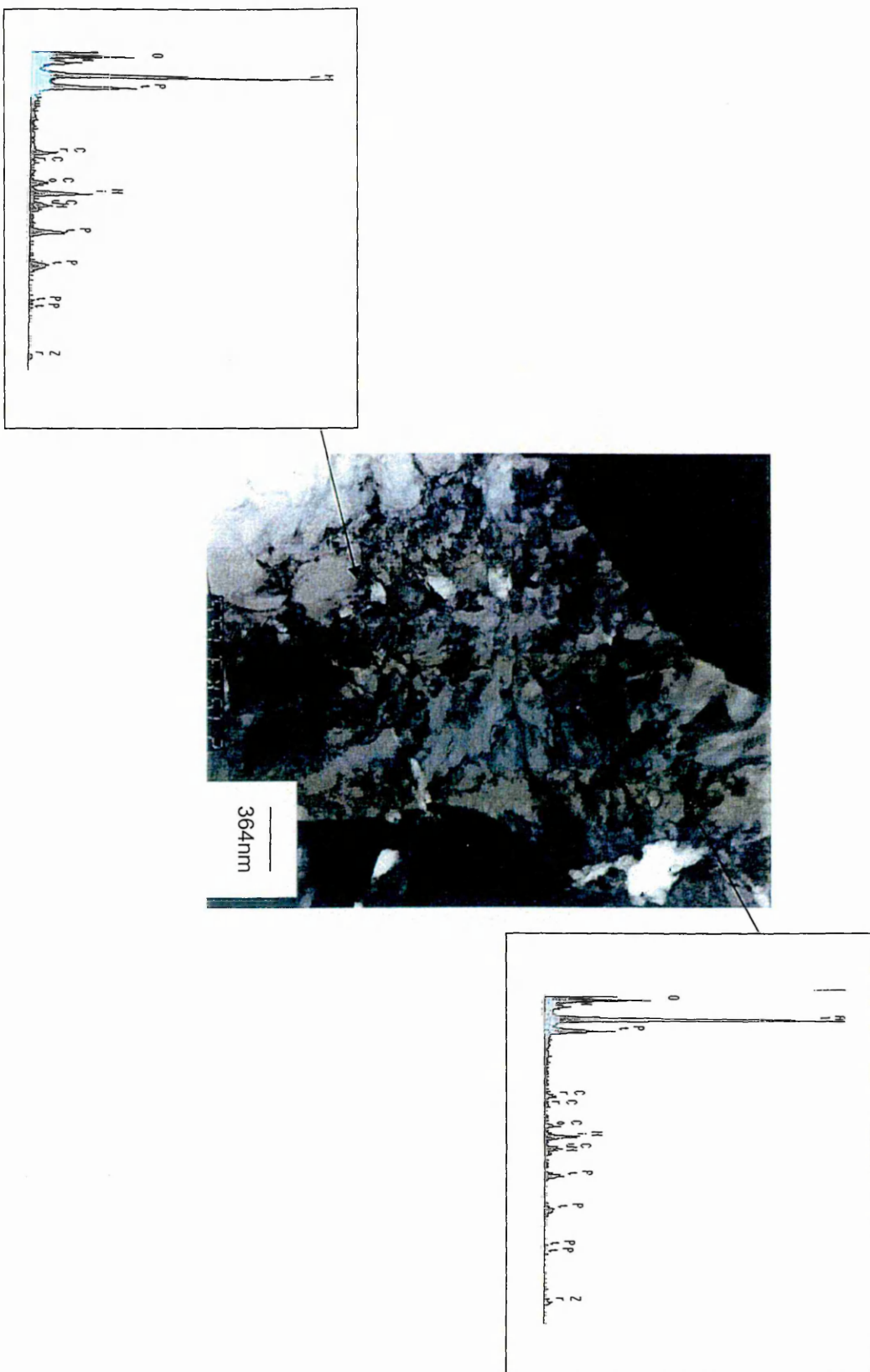
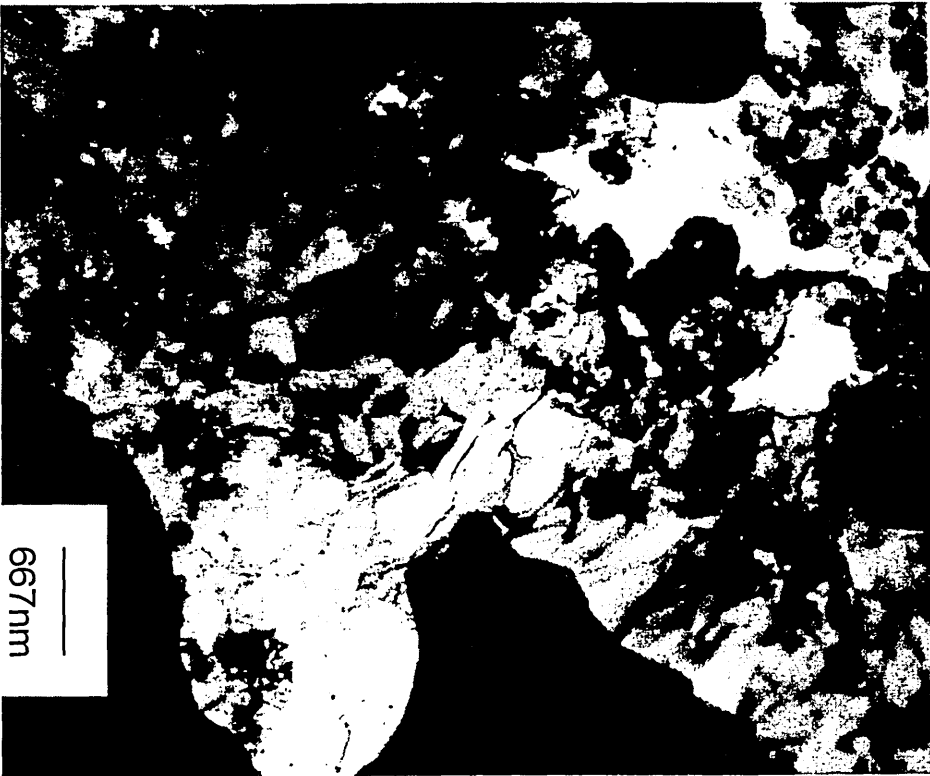


Figure 6.3d (plate 314-17):  $\text{Al}_2\text{O}_3$  layer and projecting peg into bond coat



## References

1. Committee on coatings for High -Temperature Structural Materials, National Research Council, "Coatings for High Temperature Structural Materials: Trends and Opportunities", 1996, National Academies Press.
2. K.D. Sheffler and D.K.Gupta, " Current Status and Future Trends in Turbine Application of Thermal Barrier Coatings", J. Eng. Gas Turbines Power, 1988(110)605.
3. D. Rickerby, H.C Low " Towards Designer Surfaces in the Aero Gas Turbine", 4th European Propulsion Forum, 16-18 June 1993, Bath.
4. Rhys- Jones, High Temp. Technol , 1989, 7(2), 73.
5. T.N. Rhys-Jones, Corrosion Science, 1989, 29(6), 623.
6. R. Jones, "Optimisation of a Bondcoat Designed to Support an EB-PVD TBC for Use Within Gas Turbine Engines", Transfer Report - Rolls-Royce, 1993.
7. R.A. Miller, ASME-Journal of Engineering for Gas Turbines and Power, 111, (1989), 301.
8. T.Schmitt, Surface & Coating Technology, 68/69, 113-115, 1994(Dec).
9. Internet Site <http://www.rolls.royce.com/>
10. Edwin S.Bartlett & H.A.Beale, 'Oxidation Protective Coatings for Superalloys and Refractory Metals', in vol5: surface cleaning , Finishing and Coating, Metals Handbook , 9<sup>th</sup> ed, Oct 1982, ASM.
11. J.A.Sprague & J.L.Cocking, ' M-Cr-Al-X Coatings for Superalloys' in A.K.Koul ed. Advances in High Temperature Structural Materials and protective Coatings, National Research Council, Canada, 1994, pp203-225.
12. T. Barton, 'TBC', Private Communication, Rolls-Royce, 1996.
13. K.D. Sheffler & D.K. Gupta, 'Current status and Future Trends in Turbine Application of Thermal Barrier Coatings', ASME, 1988.
14. Y.C. Tsui & T.W.Clyne, Adhesion of Thermal Barrier Coating Systems and Incorporation of an Oxidation Barrier Layer, Thermal Spray: Practical Solutions for Engineering Problems, ASM Int.1996.
15. J.A.Nesbitt and R.W.Heckel, Modeling of degradation and failure of Ni-Cr-Al Overlay Coatings. Thin Solid Films 119:281-290, 1984.

16. KH.G.Schmitt-Thomas, U.Dietl, Thermal barrier coatings with improved oxidation resistance, *Surface and Coatings Technology*, 68/69 (1994) 113-115.
17. S.R. Levine, R.A.Miller and P.E.Hodge, *SAMPE Quarterly* 20, October 1980.
18. T.E.Strangmann, Engineering for gas turbines and power, *Trans.ASME*, 114 (1992).
19. G..Johner, V.Wilms and K.K.Schweitzer, How to achieve strain tolerant thermal barrier coating by means of varying spray parameters, *ASME 88-GT-313*, 1988.
20. J.H.Wood and E.H.Goldman, in C.T.Sims, N.S.Stoloff and W.C.Hagel(eds), *Superalloy II*, Wiley, New York, 1987, P35.
21. H.M.Tawancy and N.M.Abbas, *Surface and Coatings Technology*, 54/55 (1992),1-7
22. M.C.Thomas, K.Havius,CoST 501 Conference,'Materials for Advanced Power Engineer 1994, October 3-6, 1994.
23. A.Hoque,Bond Coat Review, MRI, Sheffield Hallam University, 1997.
24. D.N.Duhl and C.P.Sullivan, *J-Metals*, July 1971,38.
25. J.E.Dohert,B.H.Kear and A.F.Giamei, *J.Metals*, Nov 1971, 59.
26. P.S.Kotval, J.D. Venables and R.W. Calder, *Met.Trans*, 1972, No.3, 453.
27. M.V. Nathal and L. J. Ebert, *Metallurgical Transactions*, vol. 16A October 1985 p. 1863
28. Chester T. Sims, Norman S. Stoloff, William G. Hagel, *Superalloys II*, John Wiley & Sons, 1987.
29. G.P.Sabal and R.Stickler, *Microstructures of Nickel Based Superalloys*, *Phys.Stat.Sol.* 35,11(1969).
30. L.Pawlowski, *The science and engineering of thermal spray coating*, p.310-318, 1995.
31. B.K.Gupta and I.L.Seige, *Thin Solid Films*, Vol 73, P365 -371, 1980.
32. B.K.Gupta and I.L.Seige, *Thin Solid Films*, Vol 73, P313 -320, 1980.
33. R. Bianco and R.A. Rapp, *Metallurgical and Ceramic Coatings*, P53-54, 1993.
34. L.L Seigle, R. Kossowsky and S.C. Singnal, *Surface Engineering*, P349-369, 1984.

35. S. Shankar and L.L. Seige, Metallurgical and Materials Transactions, P1468-1476, 1978.
36. P. Sahoo and R. Raghuraman, Gator-Gard applied bondcoat for TBC, National Thermal Spray Conference, June 1993.
37. C.C.Berndt & Sanjay Sampath, Thermal Spray Industrial Applications, P64-65, 1994, ASM.
38. W.J. Brindley, Properties of plasma spray bond coats, Metallurgical Transactions 4:83-104,P90, 1997.
39. <http://www.sifco.ie>
40. G.Lehnert and H. Meinhard, Present state and trend of development of surface coating methods against oxidation and corrosion in high temperature, P1, 71-76.
41. P.K. Data and J.S.Gray,'Advances in Surface Engineering, Vol III, P99-120, 1996, The Royal Society of Chemistry.
42. W.Y. Lee, Y. Zhang, I.G. Wright, B.A. Pint and P.K. liaw, Effect of Sulphur Impurity on Scale Addition Behaviour of Desulphurized Ni based Superalloy Aluminized by CVD, in Print 1997.
43. E.C.Dickey,B.A.Pint, K.B.Alexander, and I.G.Wright: High Temperature Surface Engineering, J.Nicholls,ed., Institute of Materials , London,1998 .
44. H.M. Tawancy, N.M. Abbas, T.N.rhys-Jones, Role of Platinum Aluminide in Aluminide Coatings, Surface and Coatings Technology, 49 (1991) , 1-7.
45. H.Hindman & D.P. Whittle, Oxid Met, 18(182) 245.
46. A.Atkinson, in E.Lang(ed), The Role of Active Elements in the Oxidation of High Temperature Metals and Alloys , Elsevier Applied Science, London, 1989.
48. H. L. Tsai and P. C. Tsai, Surface &Coatings Technology (1995), Vol.71, P53.
49. L. Pawlowski, The Science and Engineering of Thermal Spray Coatings, P317, 1994, John Wiley and Sons Ltd.
50. J.H. Westbrook & R.L.Fleischer, Intermetallic Compounds, Principles & Practice, vol.1, p494-495,1994, John Wiley and Sons Ltd.
51. F.H.Stott and G.C.Wood, Materials Science & Engineering (1987), Vol 87, p267
52. W.Y.Lee, Y.Zhang, I.G. Wright, B.A.Pint and P.K.Liaw, Effect of Sulphur ImpurityAdhesion Behaviour of a Desulfurized Ni-Based Superalloy Aluminized by CVD, in print, 1997, ORNL.

53. B.C.Wu,E.Chang,Ch.Chao,m.L.Tsai, Journal of Materials Science, 25(1990),1112-1119
54. C.C. Berndt and S.Sampath, Thermal Spray Industrial Applications Conference Proceeding (1994), p.49,ASM.
55. M.L.Mecartney, J.Ame.Ceram.Soc, 70(1)(1987)p.54-58.
56. B.V.N Rao and T.P Scheneiber, Commun..Amer.Ceram.Soc, 65 {3}(1982) C-44-C-45.
57. Y.Yoshiazawa and T.sakuma, J.Amer.Ceram.Soc, 73 {10}(1990), p.3069-3073.
58. E.P.Butler, R.K.Slotwinski, N.Bonanos, J.Drennan, and B.C.H.Steele, Adv.Ceram,12(1984), p.572-584.
59. F.F.Lannge, B.I.Davis and D.R. Clarke, J.Mat Sci. 15(1980), p.601-610.
60. R.Mcpherson, Thin Solid Films, 83 (1981), p.297-310.
61. H.Herman, Scientific American, Sept (1988), p.112-117.
62. M.V.Zeller, NASA-Lewis Research Center, Informal Report to R.A. Miller, 1988.
63. R.A,Miller, W.J.Brindley, J.G.Goedjen, R.Tiwari and D.Mess, The Effect of Silica on the cyclic life of zirconia-yttria thermal barrier coating, the proceedings of the national thermal spray conference, 1994,ASM.
64. G.M.Ingo & G.Padeletti, Segregation aspects at the fracture surfaces of 8 wt% yttria -zirconia thermal barrier coatings, Surface and Interface Analysis, june-july 1993,vol 21, no.6-7.
65. Y.C.Tsui & T.W.Clyne, Adhesion of Thermal Barrier Coating Systems and Incorporation of an Oxidation Barrier Layer, Thermal Spray: Practical Solutions for Engineering Problems, ASM Int. 1996.
66. J.A. Nesbitt and R.W.Heckel, Modelling of degradation and failure of Ni-Cr-Al Overlay coatings, Thin Solid Films 119:281-290, 1984
67. S.G.Grisaffe, Coating and Protection in Superalloys, 1972, p123-180.
68. E.Y.Lee and R.D. Sison,'The effect of Bond coat oxidation on the failure of thermal barrier coatings, 7th National Thermal Spray Conference Boston, 1994.
69. Ch Meterns-Lecomte, D.Muck, J.Garcia,'Characterisation of a new Aerospace Thermal Barrier Coating, 7th National Thermal Spray Conference Boston, 1994.

70. J.A.Sprague, G.R.Johnston, F.A.Smidt, S.Y.Hwang, F.S.Pettit,'Oxidation of CoCrAlY and Y-Implanted CoCrAl Alloys', Mat.Sci,&Tech.Div,Naval Research Laboratory, washington, D20375,Presented at 112<sup>th</sup> AIME Annual meeting, 1983.
71. B.C. Wu, E.Chang, C.H. Chao, M.L. Tsai, The Oxide Pegging Spalling Mechanism and Spalling Modes of ZrO<sub>2</sub> 8wt% Y<sub>2</sub>O<sub>3</sub> / Ni-22Cr-10Al-1Y Thermal Barrier Coatings under various operating conditions, Journal of Material science 1990, (1112-1119).
72. V.V.Sobolev, J.M.Guilemany, J.Nutting and J.R.Miquel, Development of Substrate adhesion in thermal spraying, International Materials Reviews, 1997, Vol.42, No.3,117.
73. J.Smialek and C.Lowell, Effects of diffusion on aluminum depletion and degradation of NiAl coatings, J.Electrochem Soc, 121 (6), 1974, p300-305.
74. I.P. Wadsworth, D.B.Lewis & G.Williams, Structural Studies of TiN/ZrN Multilayer Coating Deposited by PVD, Journal of Materials Science, Vol.31,1996,pp5907-5914.
75. Surface Science Laboratories, XRF analysis, 1996.Conferences, 20-24, June 1994, Boston.
76. P.J. Goodhew and Humphreys, Electron Microscopy and Analysis, 2nd ed, 1992, Wykeham Publication.
77. .Lawrence E.Mun, Electron and Ion Microscopy and Microanalysis ,'Principles and Applications', second edition, 1991, Marcel Dekker Inc.
78. Ian Wadsworth , Private Communication, 1999, MRI, Sheffield HallamUniversity.
79. J.Nutting, J.M. Guilemany and Z.Dong, Substrate / Coating Interface Structure of WC.Co High velocity oxygen Fuel Sprayed coating on low alloy steel, materials science and technology, 1995, 11(961).
80. S.Yang, 'The structure and control of Ti<sub>2</sub>N phases produced by Unbalanced Magnetron Sputtering', sept 1997, SHU.
81. Alan R.etal, An up-dated ion polishing system for TEM specimen preparation . In preparation for Transmission Electron Microscopy IV, pp263-292.MRS, Symp. Proceedings 480, MRS, Pittsburgh, USA,1997.
82. <http://micron.ucr.edu/public/gatan/pips-691.html>
83. K.Marshall, Glow Discharge Analyses of Materials, Advanced Materials & Processes, 9/97, pp57-59.

84. H.Nickel, D.Guntari, M.Mazurkiewicz & A Naoumidis, Contribution of the Quantification of GLOW Discharge Emission Depth Profiles for Oxide Scales on Ni-based Alloys of Reactor Materials, Sept 1990.
85. F.Bradley, Superalloys , A Technical Guide, ASM international, 1988.
86. J. Donachie,Jr, Superalloys - Source Book, American Society for Metals, 1984.
87. F.Smith, Structure and Properties of Engineering alloys, McGraw-Hill, 1993.
88. Durand-Charre, The Microstructures of Superalloys, Gordon and Breach S Science Publishers, 1998.
89. R.D.Kissinger, D.J.Deye, D.L.Anton, A.D.Cetel, M.V.Nathal, T.M.Pollock and
90. P.K.Wright and Anthony G.Evans 'Mechanisms governing the performance of thermal barrier coatings',PMI-99-11,Feb 1999, princeton materials Institute, princeton University.
91. J.Angeli,K.Haselgrubler,E.M.Achammer and H.Burger, Surface analysis of steel sheets with GDOS and EPMA' Fresenius Journal of Anal Chem (1993) 346:138-143
92. R.Berneron , J.C. Charbonnier (1981), Surf Interf Anal 3:134
93. H M Tawancy et al., Surface and Coatings Technology, 68/69(1994)
94. R. Payling, Delwyn Jones, Arne Bengtson ' Glow Discharge Optical Emission Spectrometry' P309-311,
95. E. Schilbe,'Substrate alloy element diffusion in thermal barrier coatings',Surface and Coatings Technology, 133-134(2000)35-39
96. B.Pint, I.Wright,W.Lee, Y.Zhang, K.Prubner and K.Alexander ORNL,'Substrate and Bond Coat Compositions: Factors affecting alumina scale adhesion'P109, TBC Workshop 1997, sponsored by the TBC Integrity co-ordination committee, NASA Lewis Research Center.
97. R.Streiff and D.H.Boone. J.Mater.Eng.10(1988) 15
98. M.R.Jackson and J.R.Rairden.Metall-Trans.A.8 (1977)1697
99. J.Schaeffer, W.E. White and G.F.Vanderoort, in E.Lang (ed). The role of active elements in the oxidation behavior of metals and alloys. Elsevier applied science, London 1989.P231

100. E.J.Felten and F.S.Pettit, *Oxid.Metal*, 10(3)(1976),189-223.
101. R.Streiff,O.cerclier and D.H.Boone,*Surf.Coat.Tech*,32(1987),111-126
102. H.M.Tawancy and N.M.Abbas,*Surface and Coatings Technology*, 54/55(1992)1-7
103. J.Jedlinski, *Solid State Phenom*,21-22(1992)335
104. M.Huntz,in E.Lang(ed), *The role of active elements in the oxidation behavior of metals and alloys*. Elsevier applied science, London 1989.P81
105. D.P.Moon, *Mater.Sci.Technol*,(1987)251
106. D.P.Whittle and J.Stringer, *Philos.Trans.R.Soc A*,295(1980) 309
107. H.Hindam and D.P.Whittle, *Oxid.Met.*,18(1982)245.
108. T.A.Ramanarayanan, M.Raghavan and R.Petkovic-Luton,*J.Electrochem.Soc.*,131(1984)923.
109. J.Jedlinski, in E.Lang(ed) ), *The role of active elements in the oxidation behavior of metals and alloys*. Elsevier Applied Science, London 1989.P131
110. J.R.Nicholls and P.Hancock, in E.Lang(ed) ), *The role of active elements in the oxidation behavior of metals and alloys*. Elsevier applied science, London 1989.P195.
111. F.H.Stott, in E.Lang(ed) ), *The role of active elements in the oxidation behavior of metals and alloys*. Elsevier Applied Science, London 1989.P3.
112. H.M. Tawancy and N.M. Abbas, *Scr.Met.Mater.*,29(1993)689.
113. C.Guerre, R.Molins and L.Remy, 'Study of the coating stability of a TBC system',*Materials At High Temperatures* 17(2) 197-204.
114. M.S.Ali et al. *Journal of the European Ceramic Society* 22 (2002) 101-107
115. Shillington,E.A.G. and Clarke,D.R.,*Acta Mater.*,1999,47,1297.
116. M.P.Taylor, P.Niranatlumpong, *Materials At High Temperatures* 17(2) 219-224, 2000.
117. J.A.haynes et al. In Press 'Elevated Temperature Coatings:Science and Technology III' Ed J.M.Hampikian (TMS, Warrendale,PA,1998).
118. Prasanna,K.M.N.,Khanna, A.S., Chandra, R.and Quadackers, W.J. Effect of  $\theta$ -alumina formation on the growth kinetics of alumina forming superalloys, *Oxidat. Metals* 46(5/6), 465-480 (1996).

119. Pint, B.A., Treska M. and Hobbs L.W., The effect of various oxide dispersion on the phase composition and morphology of  $\text{Al}_2\text{O}_3$  scales grown on  $\beta$ -NiAl, *Oxidat. Metals* 47 (1/2), 1-20 (1997).
120. Rybicki, B. and Smialek, J.L., Effect of  $\theta$ - $\alpha$ -  $\text{Al}_2\text{O}_3$  transformation on the oxidation behaviour of  $\beta$ -NiAl + Zr, *Oxidat. Metals* 13 (3/4), 275-304 (1989).
121. <http://www.mspusch.de/Ing-Diplomarbeit/2-GeneralBackground.htm>
122. <http://www.mit.edu/people/janos/tbc.htm>
123. K.H.Stern, *Metallurgical and Ceramic Protective Coatings*, 1<sup>st</sup> edition, Chapman & Hall, 1996, P207/P214
124. Jogender Singh, *Multilayer Ceramic/Metallic Coatings by Ion Beam-Assisted Electron Beam Physical Vapor (EB-PVD) Deposition*, The Applied Research Laboratory, 1997, P2, TMS.

# The Application of Glow Discharge Optical Emission Spectroscopy to the Study of Thermal Barrier and Environmental Coatings

A. HOQUE, J. HIGGINS\*, D. RICKERBY\*, J. CAWLEY  
and M. IVES

*Materials Research Institute, Sheffield Hallam University, Sheffield S1 1WB*

*\*Surface and Coatings Technology Group, Rolls Royce Plc, Derby*

## ABSTRACT

Glow discharge optical emission spectroscopy (GDOES) has been developed to investigate thermal barrier and environmental coatings. Qualitative analysis of thermal barrier and environmental coating has shown that this technique exhibits considerable potential. Work has been conducted to quantify the results. This involved the preparation of well documented calibration standards for alloy systems containing up to fifteen elements. The advantages of the technique lies in its ability to analyze up to 44 elements ranging from hydrogen to uranium with a lateral resolution in the order of tens of nanometers.

Results will be presented identifying the elemental distribution across the coating interface which will be compared with results from quantitative analysis conducted using scanning electron microscopy and X-ray fluorescence technique. The results will be discussed in terms of the GDOES technique sensitivity/limitations and elemental interference encountered and possible optimisation in developing this technique for understanding degradation mechanisms involved in thermal barrier and environmental coatings.

## INTRODUCTION

Glow discharge optical emission spectroscopy (GDOES) is a powerful and versatile technique for the bulk analysis of ferrous and non-ferrous alloys with a sensitivity down to approximately 50 ppm; the technique is also capable of quantitative depth profile analysis.<sup>1,2</sup> This paper describes the work currently underway to apply the GDOES technique to understand the oxide bonding mechanisms and degradation modes for thermal barrier and environmental protection coating systems.

Overlay coatings of the MCrAlX type in which M represents a base metal of Ni, Co, Fe or some combination of elements, and X represents either a rare earth element or some other element such as Y or Zr with a high chemical reactivity for oxygen, have many applications in the fields of high temperature and environmental protection. In addition variants of the coatings are used to create the bond between turbine blades and thermal barrier coatings, which are usually stabilised zirconia. The mechanisms

of bonding and the effects on the performance of the blades are not completely understood as yet.

Several analytical methods are available for the analysis of bonding mechanism and degradation process. Electron probe microanalysis is often used to characterise the composition of turbine blade coatings by analysing the cross-section of the specimen. Scanning electron microscopy is used for microstructural assessment and X-ray diffraction for structural analysis. Other more sensitive techniques available include SIMS and AES but they are less convenient due to the high cost and the need to handle the specimen in ultrahigh vacuum. Thus, a more convenient method such as GDOES would be useful for understanding the role of low concentration elements.

## THEORY

### *Glow Discharge Optical Emission Spectroscopy*

Glow discharge spectroscopy is an atomic emission technique that relies on the excitation of atoms within the sample being analysed. It allows both qualitative and quantitative determination of metal and non-metal elemental composition as a function of depth.

If sufficient energy is transferred to an atom from the sample by an argon atom from a glow discharge, an increase in electron energy can occur such that a higher energy level orbital transition takes place to provide an excited state and a lower energy level vacancy. This state is unstable and the atom relaxes back to the ground state by the transition of an electron to fill the vacancy, normally accompanied by the liberation of the excess energy in the form of a photon of wavelength (Fig. 1) defined by the equation:

$$\lambda = hc/E_1 - E_2$$

where;  $E_1$  and  $E_2$  are energy states,  $h$  is Planck's constant,  $c$  is the Speed of light and  $\lambda$  is wavelength.

Each element has different electron orbital energy levels, the wavelength of the photon emissions will therefore be characteristic of the elements present within the sample and the intensities of the emission lines will be proportional to the number of emission quanta and hence elemental concentration.

To produce clean line spectra without significant contribution from continuum energy in the form of thermal radiation or lattice vibrations, the atoms must be in the form of a low pressure gas, volatilised from a solid within a vacuum chamber.<sup>3</sup>

Glow discharge spectroscopy has a number of benefits over the more commonly used analytical techniques:<sup>4</sup>

1. The layer-by-layer removal of sample material allows both qualitative and quantitative depth profile analysis.
2. Very little or no sample preparation is required for bulk solids.

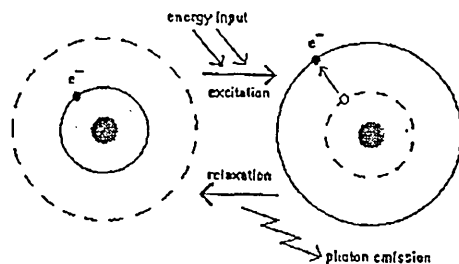


Fig. 1 Principle of excitation and emission.<sup>4</sup>

3. It naturally separates the removal of atoms from the solid surface (atomisation), from the subsequent excitation and ionisation of those atoms, thus reducing matrix effects and normalising sample-to-sample inconsistencies.
4. Due to the small cathode to anode distance, sputtering occurs over a narrow volume resulting in uniform sample erosion over the analysed area giving good resolution when used for depth profiling.
5. The excitation and emission layer is also thin, minimising self-absorption and giving a linear relationship between intensity and concentration, with sharp emission lines.

The glow discharge lamp utilised in this technique is based on a design by Grimm (Fig. 2). Basically, it consists of a small vacuum chamber with a hollow cylindrical anode 4 mm in diameter with the sample to be analysed acting as the cathode at one end. The outside of the anode cylinder is vacuum pumped and bled with a working gas (argon). The other end of the cylinder contains a lens through which the photon emission is detected via a polychromator. Typically operating conditions are -500 to -1500 V and 20 to 200 mA, giving a sputtering rate in the range 10 to 100 nm per second.

#### *Sputtering Process*

The glow discharge sputtering process operates as follows (Fig. 3). The glow discharge lamp provides a low pressure argon environment over the sample. A high negative potential -500V to -1500 V is typically applied to the low pressure environment which causes breakdown of the discharge gas, normally argon, whose ions are then accelerated across the dark space and impact on the cathode (sample) surface, thereby ejecting primarily neutral atoms and electrons, although some ions and polyatomic species are also released. In addition to the ions striking the cathode, the charge-exchange processes in the dark space create fast atoms that also can cause sputter ablation. Through these sputtering steps, the solid sample yields an atom population that diffuses across a thin dark space into the adjacent negative glow, where collisions with electrons metastable atoms and other energetic species cause excitation and ionisation of a fraction of the sample atom, creating species that are analytically useful.<sup>5</sup>

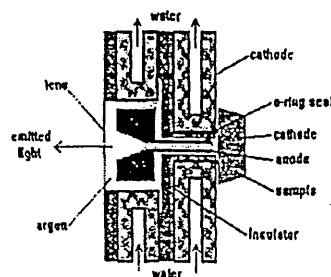
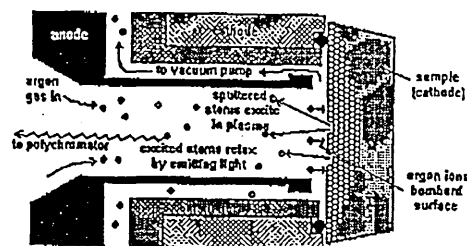
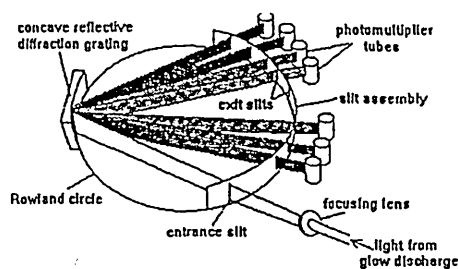
Fig. 2 Glow discharge lamp.<sup>4</sup>Fig. 3 Sputtering in the glow discharge lamp.<sup>4</sup>

Fig. 4 Light emission and measurement.

#### *Light Emission and Measurements*

A polychromator (Fig. 4) based on the Rowland focusing property, separated by a window at the end of a glow discharge lamp is used to detect emitted photons.<sup>4</sup>

The basic arrangement of a polychromator is as follows:

- i a collimator or focusing lens to render the light rays parallel.
- ii an entrance slit that provides a narrow optical image.
- iii a concave reflective diffraction grating to disperse the light.
- iv exit slits at the appropriate locations to isolate particular spectral wavelengths.
- v photomultiplier tubes behind these slits to detect the light, amplify and convert it into an electrical signal for monitoring.

Glow discharge sputtering is strongly dependent on the working gas, sample composition and the applied parameters: current, voltage and pressure. Careful adjustment and monitoring of these parameters is vital for controlling surface analysis or rate of depth profiling and for quantification of collected results.

GDOES can be used to depth profile non-conductive coatings but the main requirements is to have a radio frequency (RF) source.

### EXPERIMENTAL

To assess the capability of the GDOES technique to analyse complex materials, CMSX-4, a nickel-based superalloy used in turbine blade manufacture, and a CoNiCrAlY overlay coating (RT31), used for environmental protection and as a bondcoat for ceramic thermal barriers, were assessed by GDOES, electron probe microanalysis (EPMA) and X-ray fluorescence (XRF).

The glow discharge spectroscopy was carried out on a LECO GDS-750 QDP glow discharge spectrometer. The following optimised operating conditions shown in Table 1 were used. Both qualitative and quantitative studies were performed. Qualitative studies produced a plot of the intensity over time for given elements.

Table 1 Operating conditions for GDOES

Evacuation time	10 sec
Argon flushing time	20 sec
Preburn time	60 sec
Interval delay	0
Burn time	0
Number of repetitions	0
Compensation	5 sec
Integration time	10 sec
GDL operating time	11
Preburn excitation	700 V
Integration excitation	700 V; 30 mA
Flow rate in digits	400
Evacuate until	10E-3 mBar
Anode diameter	4 mm
Profile duration (depends on sample)	300-1000 sec

GDOES quantification was split into two parts: determination of the sputtered depth from the sputtering time and sputter rates of individual elements; and determination of the chemical content from the emission line intensities. The sputter rates can be calibrated from sputter depth measurements. The emission line intensities are dependent on the voltage, current and sputtering rates, as well as the chemical composition. Normally the intensity calibration is performed using certified reference materials of known chemical composition. During depth profile quantification the analysed composition is normalised to 100%. There are quite a number of steps involved in setting up a quantification program. Figure 5 gives an outline of the steps involved for superalloy turbine blade coatings.

A total of 49 calibration standards were used to calibrate the superalloy turbine blade coatings quantitative program covering most of the elements in the coatings. In order to ensure reliable results were obtained, the standards were selected so as to cover the elemental concentration range in the coatings. Table 2 shows an overview of the calibration elements and analytical range with the selected standards.

EPMA using WDS was used to perform chemical analyses on both the CMSX-4 and RT31 samples to enable comparisons to be made with GDOES and XRF results (the XRF results were supplied by Rolls-Royce).

As the substrate alloys and coatings were multiphased systems a straight forward single line scan would contain a lot of scatter as different phase compositions were crossed by the scanning electron beam. In order to reduce this problem a series of 'point' analysis at one micron intervals along a straight line were taken. At each point the beam of the probe was 'rastered' along a 50  $\mu\text{m}$  line normal to the line produced by the series of analyses to form a 'ladder' scan. This enabled an average band (50  $\mu\text{m}$  wide) to be assessed.

## RESULTS AND DISCUSSION

The time-intensity curves and calculated quantification depth concentration profiles for CMSX-4 superalloy substrate are shown in Figs 6 and 7. Only elements Ni, Co, Al (major ones) and Ti, Hf, W (minor ones) have been shown for the sake of clarity. The tendency for the lines to rise as time and depth increases is due to matrix effects resulting from differences in elemental sputtering rates.

The crater produced during the analysis of CMSX-4 after 60 and 1000 seconds are shown in Figs 8(a) and (b), and their measurement by laser profiling is shown in Figs 9(a) and (b). It can be seen that the bottom of the crater in Fig. 8(a) is quite planar, while some re-sputtering of material has created a lip around the rim after 1000 seconds. The laser profile depth measurement shows a good correlation to the calibrated depth values obtained from Figs 7(a) and (b), with errors of the order of 10–15%. The roughness of the bottom of the crater normally increases linearly with time,<sup>6</sup> which is one of the factors limiting the depth resolution. This necessitates a compromise between good depth resolution and high intensity spectral lines when selecting operating parameters.

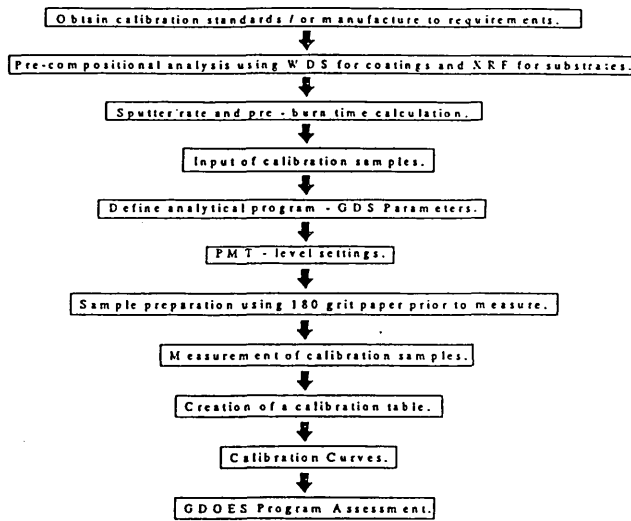


Fig. 5 GDOES quantification program set-up.

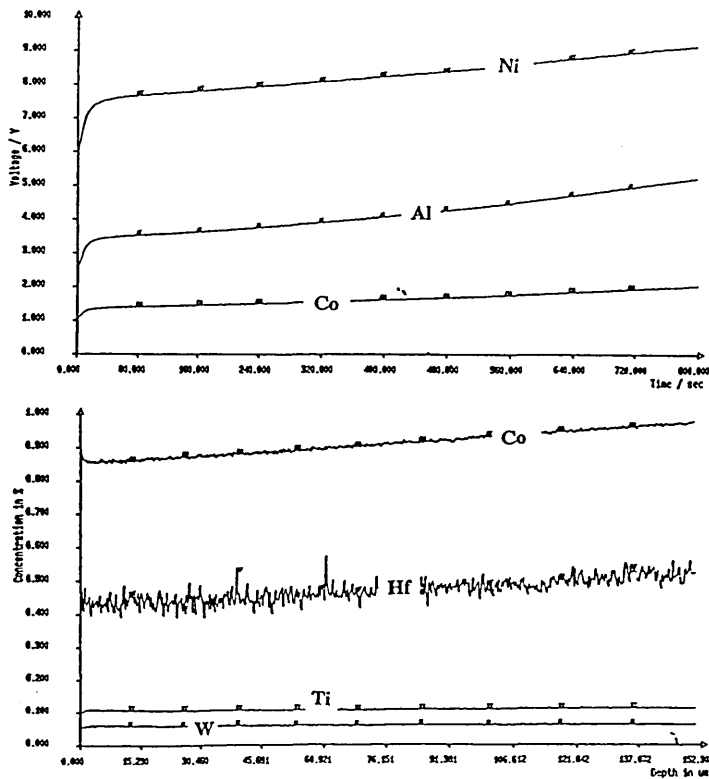


Fig. 6 (a) Time-intensity trace on CMSX-4 showing major elements Ni, Al and Co, (b) Time-intensity trace on CMSX-4 showing Co and minor elements Ti, Hf and W.

Table 2 Calibration standards overview

Analyte	Analytical range	Matrix Element in	Calibration points used
Ni	1.99-64.69%	Ni Fe grades; Aluminide coatings; Pure Ni; MCrAlY	29
Cr	0.23-8.78%	Superalloy: Marmoo2, CMSX-4 Low alloy steel; Pure Co	7
Al	0.00-17.91%	Aluminide coating; Superalloys Pure Al	16
Ti	0.11-1.44%	Superalloys; Aluminide coatings Pure Ti	10
Pt	0.00-99.99%	Pure Pt; Aluminide coatings	4
Y	0.00-99.99%	Pure Y MCrAlY coating	2
Co	0.38-9.42%	Pure Co; High alloy steel; Aluminide coating	19
Mo	0.30-9.41%	Low alloy steel grades High alloy steel grades	11
W	0.20-9.65%	Superalloys Aluminide coatings	9
Ta	1.13-6.48%	Superalloys Aluminide coatings	4
Hf	0.07-1.27%	Superalloy grades	2
Zr	0.00-97.67%	Pure Zirconia	1
Si	0.05-2.69%	Cast iron; High alloy steel Superalloy grades	17
P	45.2-225.8 ppm	Low alloy steel grades High alloy steel grades	13
B	4.27-27.12%	BTiAlN Ni-B	2
S	30.1-378.6 ppm	High alloy steel grades Low alloy steel grades	8
C	0.00-3.35%	Cast iron grades; High alloy grades; Low alloy steel grades	14
O	0.00-26.60%	FeO	1

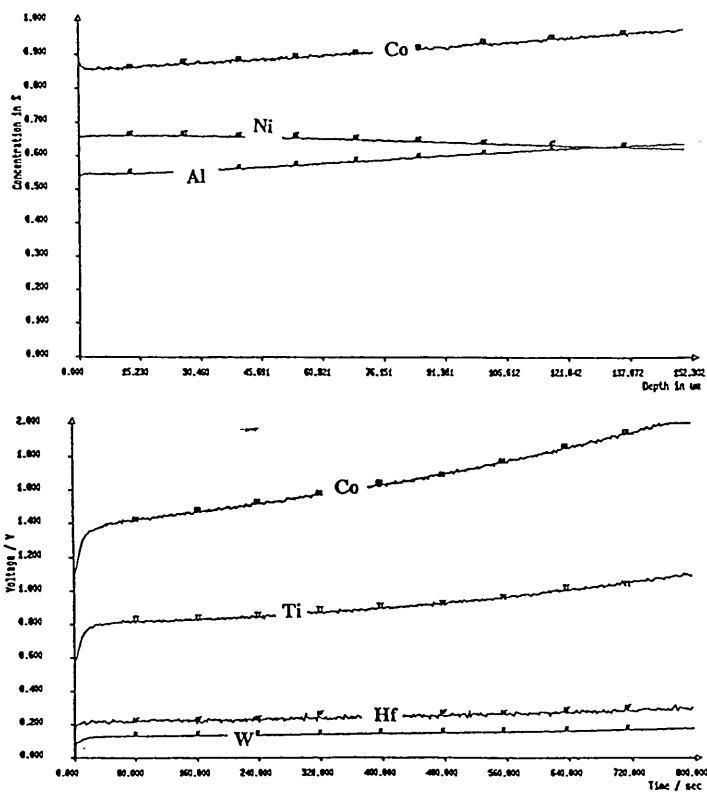


Fig. 7 (a) Depth-concentration profile on CMSX-4 showing major elements Ni, Al and Co, (b) Depth-concentration profile on CMSX-4 showing Co and minor elements Ti, Hf and W.

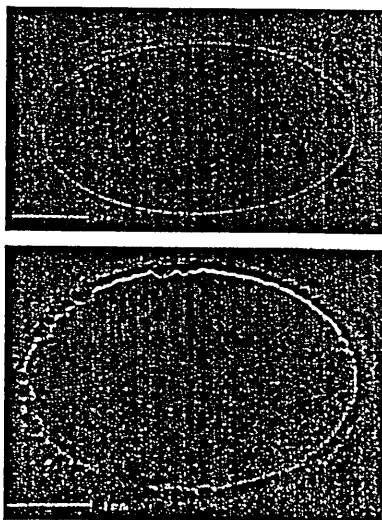


Fig. 8 (a) SEM micrograph of crater at 60 sec, (b) SEM micrograph of crater at 1000 sec.

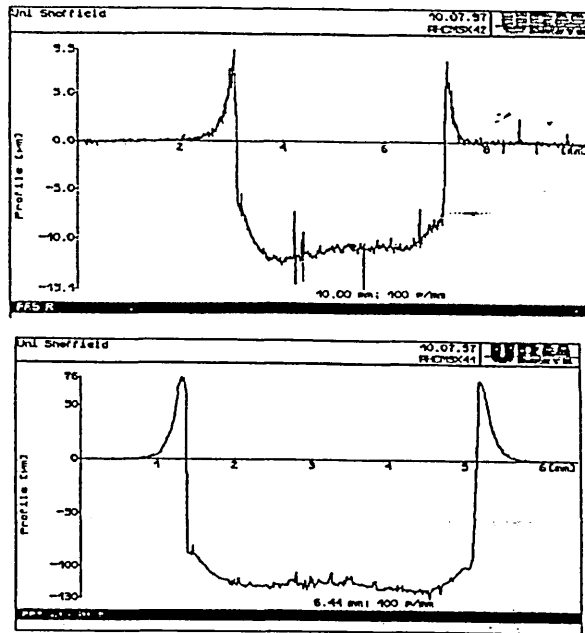


Fig. 9 (a) Laser profile of crater at 60 sec, (b) laser profile of crater at 1000 sec.

Table 3 Comparison of XRT, EPMA and GDOES compositions for CMSX-4.

	Ni	Cr	Al	Ti	Pt	Co	Mo	W	Ta	Hf	Zr	Si	Y	B	O	Re	C	P
XRF analysis	60.82	6.3	5.83	0.98	0.012	9.46	0.6	6.32	6.52	0.1	0.005	0.03				2.71		
EPMA analysis	59.9	6.7	6.3	1.1		9.6	0.6	6.1	6.4	0.1						3.7		
GDOES analysis	64.51	6.39	5.89	1.09	0.431	9.11	0.55	6.07	5.4	0.47	0.009	0.029	0.02	0	0	-	0.001	0.007

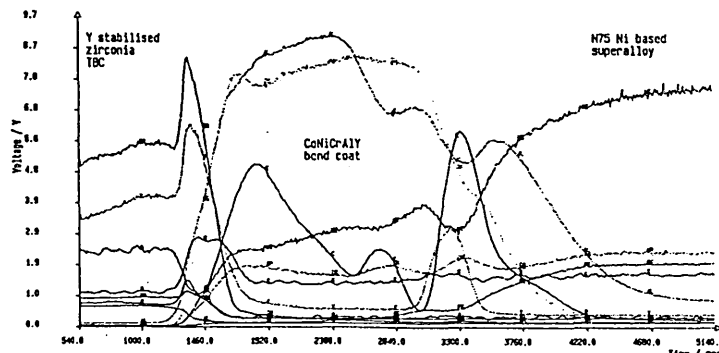


Fig. 10 GDOES depth profile through TBC system.

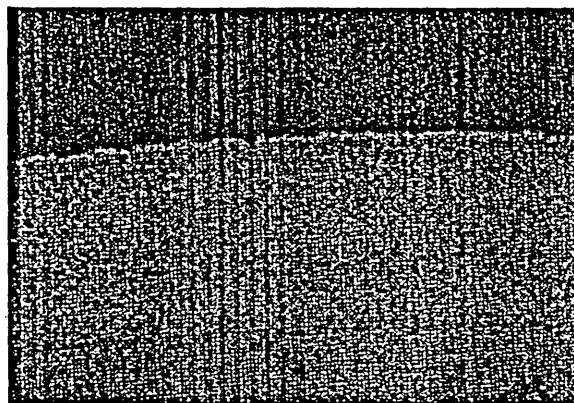


Fig. 11 Cross-sectional view of TBC.

The results of the GDOES and EPMA analyses are compared to the composition determined by XRF in Table 3. Both results showed a good correlation, with the GDOES results generally closer than those of EPMA, although there were some obvious discrepancies which require investigation; the values obtained for nickel, tantalum, hafnium and platinum are inaccurate and may be due to interference between the spectral lines. The GDOES equipment is also not currently able to detect rhenium.

The trace obtained from the thermal barrier system (Fig. 10) clearly distinguishes the different interfacial regions seen in the cross-sectional view (Fig. 11). The elements identified within these regions agree with the EPMA analysis (Fig. 9), with both techniques highlighting the yttrium concentrated at the ceramic/bondcoat and bondcoat/substrate interfaces. GDOES does have the advantage of better sensitivity to very low concentrations of elements such as sulphur, boron, carbon and phosphorus. The results can also be obtained more rapidly with minimum sample preparation.

The current semi-quantitative program set up for turbine blade coating analysis is limited by the number of standards and calibration points used (see Table 2). For example with a minimum of two calibration points it is thus possible to obtain a straight calibration line. It is however, recommended to use a minimum of 3 to 5 calibration samples. The more calibration samples are used, then the easier to detect an inaccurate calibration sample and if necessary to make appropriate correction or deletion. In addition extra elemental channel such as Re and additional elements needs to be installed.

A study was performed on a few selected superalloy turbine blade coatings to assess elemental interference in GDOES traces. Cross-over of emitted wavelengths can result in 'ghost' profiles being produced. Currently further investigations are underway to identify and overcome any interference problems.

The work conducted so far has shown GDOES to be a very useful analytical tool for the characterisation of turbine blade coatings. The large sample area analysis with GDOES, as compared to EPMA, SIMS and AES where microscopic areas are in-

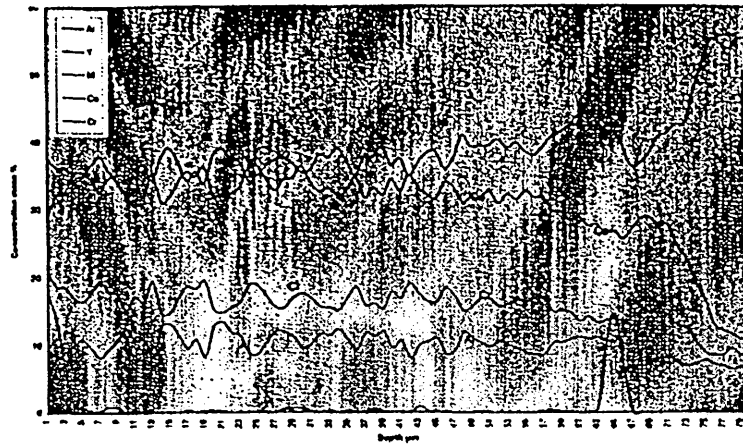


Fig. 12 EPMA analysis of TBC system.

involved is good for obtaining a better representative average result. A semi-quantitative GDOES program has been developed and with further work to resolve the problems seen with elemental interferences, an improved quantitative method will enable a much broader understanding of the role of trace elements in the bonding and degradation mechanisms of both thermal barrier and environmental coating systems.

#### ACKNOWLEDGMENT

The authors would like to thank Mr R. Jones (RR), Dr M.D. Bramhall (SHU), Mr P. Slingsby (SHU) and Mrs C. Shaw (SHU) for their help and advice towards this project.

#### REFERENCES

1. W. GRIMM: *Spectrochimica Acta*, 1968, **23B**, 443.
2. O. DESSENE, A. QUENTMEIER and H. BUBERT: *Fresenius - J. Analytical Chemistry*, 1993, **346**, 340-345.
3. L. A. DONOHUE: *Thesis: Deposition and Characterisation of (Ti,Zr) based hard compound and multilayer pvd films*, Sheffield Hallam University, 1995.
4. M. IVES: *Thesis: Fundamental studies of the PVD technique*, 1994.
5. W. W. HARRISON: *J. Analytical Atomic Spectrometry*, 1992, **7(3)**, 75.
6. R. K. MARCUS: *Glow discharge spectroscopies*, Plenum Press, 1993.

# High Temperature Surface Engineering

*Edited by*  
J. Nicholls and D. Rickerby

Proceedings of the  
Sixth International Conference  
in the Series  
'Engineering the Surface'  
23-25 September 1997  
Edinburgh Conference Centre  
Edinburgh, UK



Book 693  
Published in 2000 by  
IOM Communications Ltd  
1 Carlton House Terrace  
London SW1Y 5DB

© IOM Communications Ltd

IOM Communications Ltd  
is a wholly-owned subsidiary of  
The Institute of Materials

ISBN 1 86125 058 4

Typeset by IOM Communications Ltd

Printed and bound in UK at  
The University Press, Cambridge

**Characterisation of Interfaces on Thermal Barrier Coatings**

A Hoque, J Cawley, MD Bramhall, D Rickerby, J Higgins  
 (Materials Research Institute, Sheffield Hallam University, Sheffield, S1 1WB)  
 (Surface Coatings and Technology, Rolls Royce plc, Derby, DE24 8BT)

Gas turbine blades are protected against high temperature oxidation by thermal barrier coating (TBC) systems, which consists of a low thermal conductivity ceramic coating such as partially stabilised zirconia ( $ZrO_2$ ), deposited onto an oxidation and corrosion resistant bondcoat on a nickel based superalloy substrate. Normally, the adhesion of the TBC to the Ni-based superalloy is poor, so therefore a bond coat which acts as a +glue+ to improve adhesion is provided. The mechanisms of bonding and its effect on the performance of the blade are not completely understood.

**Conclusion**

Preliminary investigations shown here suggest that Glow Discharge Optical Emission Spectroscopy (GDOES) is a fast and economical technique for depth profiling of turbine blade materials. The major advantage of this technique are the ability to analyze up to 44 elements ranging from hydrogen to uranium with a lateral resolution in the order of tens of nanometers, fast speed, simplicity of operation and low cost.

In addition, SEM, EDX, WDS and JTEM combined with GDOES will enable a better understanding of the bonding mechanism at the interface level and hence suggest bond coat design optimisation.

**References**

- [1] A Hoque, J Higgins, D Rickerby, J Cawley, M Ives, High Temperature Conference Abstract, Edinbur 1997.
- [2] O Desene, A Quentmeier and H Bubert, Fresenius Journal of Analytical Chemistry, 1993, 346:340-3.
- [3] R K Marcus, Glow Discharge Spectroscopies, Plenum Press, 1993

**Role of interlayer bonds on optical and conductive properties in layered  $In_2S_3$** 

M Ishikawa, T Nakayama  
 (Chiba University)

Among various multivalent atom combinations, only the In-Se combination shows the layered structure with the stoichiometry of  $In_2Se_3$ . In the present work, we pay attention to the interlayer coupling of this layered  $In_2Se_3$  and theoretically investigate the atom configuration and the optical and conductive properties, by using the ab initio total-energy pseudopotential method in the local density approximation

The following features are clarified:

(1) In order to lower the surface energy of the layer, anions (Se) are located at both sides of the layer such as Se-In-Se-In-Se and have the coordination number of four. As a result, half In atoms have the coordination number of six, while the other In have four. Such multicoordination of In is allowed because the electronegativity difference is large between In and Se, which is also the reason why the layered structure stabilizes only for  $In_2Se_3$ . [1]

(2) The interlayer coupling is produced by the dangling bonds of the layer-edge Se, thus being like the van der Waals coupling. Those dangling bonds induce the strong polarization and the large hole conductivity along the layered direction. [2] These results are discussed in detail with comparing to other III-VI compounds and recent experiments. [3,4]

[1] M. Ishikawa and T. Nakayama: Jpn.J.Appl.Phys 36 Pt2, No.12A, (1997) L1576.

[2] M. Ishikawa and T. Nakayama: Jpn.J.Appl.Phys to be published.

[3] J. Ye, Y. Nakamura and O. Nitono: Philox. Mag. A 73 (1996) 169.

[4] T.Ohno, T.Okamoto, A.Yamada and M.Konagai:  
 Proc 24th International Symposium on Compound Semiconductors, to be published

# Institute of **Physics**

Abstract Booklet

---

**Microscopy of Internal  
Interfaces: Determination  
of Nanochemistry**

Friday 27 February 1998  
The Institute of Physics,  
London

---

Organised by EMAG

The Institute of Physics, 76 Portland Place, London  
W1N 3DH. Telephone +44 0171 470 4800,  
Fax +44 0171 470 4900. Email: [conferences@iop.org](mailto:conferences@iop.org)

The Institute of Physics is a charitable organisation  
and a member of IAPCO (International Association  
of Professional Congress Organisers)

quantitative data obtained with these methods, SEM and with traditional surface analytical techniques are being used to test the topography theories. In the case of semiconductors, most studies have concentrated on Si, GaAs and InP. Recently other electronic materials, such as SiGe have been studied.

#### AS1.FrM.6

##### Comparison of Spring and Autumn Time Collected Outdoor Aerosol Particles Analysed with Depth-Resolving SNMS

J. Goschnick, C. Natzeck, M. Sommer

*Institut für Instrumentelle Analytik, Forschungszentrum Karlsruhe für Technik und Umwelt, Karlsruhe, D-76021, Germany*

Atmospheric aerosol particles are of significant influence to the chemistry of the atmosphere. Emission processes and the interaction with the environment often cause a depth distribution of the chemical compounds within the particles. Thus, the analysis of the chemical composition of the particles as well as the analysis of their depth structure is of great importance for the understanding of atmospheric processes. Moreover the reactivity of elements depends on the current compounds, so the analysis of aerosol particles should give also information on the depth structure of the compounds. To obtain this information Secondary Ion/Neutral Mass Spectrometry (SIMS, SNMS) was applied on aerosol particles collected from outdoor air and deposited on indium foil.

The particles were collected in five size ranges (0.2-10  $\mu\text{m}$ ) with a cascade impactor at the site of the Forschungszentrum Karlsruhe during an autumnal fine weather period. Electron microscopic images were used to determine the particle size distribution of the samples. The finest particles ( $< 0.35 \mu\text{m}$ ) had a nitrogen and sulfur containing shell on a carbon core and originate mainly from traffic soot. The core of the coarse ( $> 2 \mu\text{m}$ ) particles consists of probably geogenic material (Mg, Al, Si- Oxide). Moreover these particles showed an intermediate layer containing Na, covered itself by an organic surfacelayer.

The results agree with the analysis of outdoor particles collected at the same location but in spring time four years ago, where the nitrogen and sulfur containing surface layer was found to be due to ammonium sulfate.

#### AS1.FrM.7

##### GDOES Analysis of Thermal Barrier Coatings for Application in Gas Turbine Blades

A Hoque, J Cawley, MD Bramhall, D Rickerby\*, J Higgins\*

*Materials Research Institute, Sheffield Hallam University, Sheffield, S1 1WB, UK*

*\*Surface Coatings and Technology, Rolls Royce plc, Derby, DE24 8BJ, UK*

Glow Discharge Optical Emission Spectroscopy (GDOES) is a very powerful and rapid analytical technique to determine the concentration distribution in surface-treated materials and coatings. The major advantages of this technique are the ability to analyse up to multiple elements ranging from hydrogen to uranium with a lateral resolution in the order of tens of nanometers.

This paper outlines the potential uses of GDOES in understanding the degradation modes of thermal barrier coating systems, as used in the aerospace industry to extend the life of turbine components. In such systems, TBC performance is very sensitive to the choice of bondcoat (an intermediate layer deposited between the ceramic top coat and underlying substrate) and to chemical interactions between the bondcoat and substrate. Through

understanding of the chemical interactions which occur at the bondcoat/ceramic interface, a number of factors, which are central to TBC performance, have been identified. The underlying mechanisms which govern ceramic/metal bonding will be reviewed.

- [1] W Grimm, *Spectrochimica Acta*, 1968,22B,443
- [2] O Dessene, A Quentmeier and H Bubert, *Fresenius- Journal of Analytical Chemistry*, 1993, 346:340-345
- [3] RK Marcus, *Glow Discharge Spectroscopies*, Plenum Press, 1993

#### AS1.FrM.8

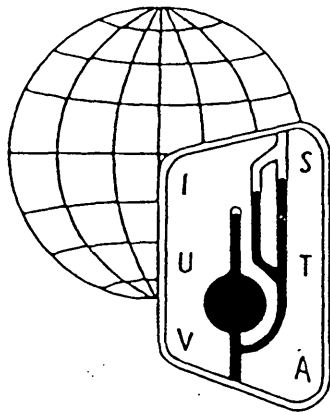
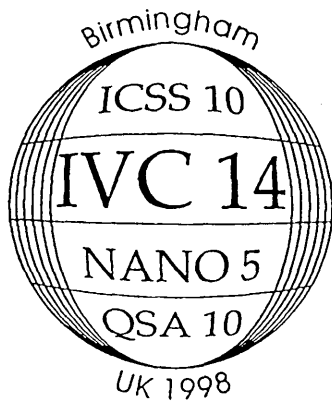
##### Low Energy Nitrogen Ion Bombardment of GaAs.

J Kudjoe, JB Malherbe\*

*Department of Physics, University of the North, Sovenga, 0727, South Africa*

*\*Department of Physics, University of Pretoria, Pretoria, 0002, South Africa*

The nitridation process of the GaAs (100) surface is studied. This is done by low energy (0.5-5.0 keV) nitrogen ion bombardment in an AES system. The extent of nitridation for the different bombardment energies is determined using AES. Auger depth profile of the implanted nitrogen is obtained by subsequent in situ argon bombardment. From these profiles the experimental projected ranges and straggling for the different ion energies have been determined and compared with other theoretical models.



# Abstract Bo

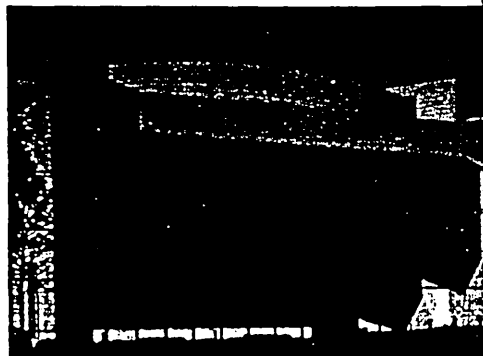
**14th International  
Congress (IVC-14)**

**10th International  
on Solid Surfaces (I**

**5th International C  
on Nanometer-scal  
Technology (NANO**

**10th International C  
on Quantitative Sur  
(QSA-10)**

**International Conve  
Birmingham, UK  
31 August - 4 Septem**



#### Keynote

*Quantitative information from energy dispersive X-ray analysis in the Transmission Electron Microscope.*

J Titchmarsh.

Department of Materials, University of Oxford, UK.

#### Keynote

*Atom Probe characterisation of high temperature materials.*

R Thomson and M K Miller.

Loughborough University, Loughborough, UK.

#### Keynote

*Quantitative aspects of electron energy loss spectroscopy and imaging.*

R Brydson.

University of Leeds, Leeds, UK.

#### Tea/Coffee

*Quantification of precipitates in a 10% chromium steel by means of TEM and EFTEM.*

P Hofer, H Cerjak and P Warbichler.

Technical University Graz, Austria.

*Quantitative evaluation of particle size distributions of different phases in steel P92 exposed at 600°C and 650°C using EFTEM.*

M Hatterstrand and H-O Andrén.

Chalmers University of Technology, Goteborg, Sweden.

*Quantitative analysis of niobium carbo-nitrides in a stabilised stainless steel.*

J Kallqvist and H-O Andrén.

Chalmers University of Technology, Goteborg, Sweden.

*Quantitative mapping and depth profiling of polymeric and ceramic coatings using Raman Spectroscopy.*

J Yarwood.

Sheffield Hallam University, Sheffield, UK.

#### Conference Dinner

## Wednesday 24th November

### SESSION 6

#### Applications

##### Keynote

*Characterisation of microstructural evolution for creep modelling.*

B A Shollock and M McLean.

Imperial College, London, UK.

## Scope

This is the fourth in a series of meetings, planned in association with the High Temperature Materials Performance Committee of the Institute of Materials, concerned with the effects of service exposure on the microstructure and properties of high temperature materials. A knowledge of the microstructural evolution and stability of materials in service is essential in order to assess their full potential operational performance and to assist in the development of new alloys suitable for more advanced service applications.

The first three meetings in this series, have been concerned with the microstructural development and stability of high chromium creep resistant steels for high temperature power plant applications, microstructural stability of high temperature creep resistant steels and nickel based alloys and the modelling of microstructural evolution in creep resistant materials.

R W Vanstone.

ALSTOM Energy Ltd., Rugby, UK.

*Statistical prediction of inclusion sizes in*

H Atkinson.

University of Sheffield, Sheffield, UK

#### Tea/Coffee

*The evaluation of cleanness of advanced*

P N Qusted.

National Physical Laboratory, Teddij

*Statistical assessment of corrosion morph component life prediction.*

J R Nicholls, N J Simms and J E Oal

Cranfield University, Cranfield, UK.

*The development of de-alloyed zones du microstructure and spallation behaviour.*

S Osgerby.

National Physical Laboratory, Teddij

*Microstructure changes of base material heat resistant steel.*

Yu K Petrenya\*, S Ya Mikhailov\* and

\*The Polzunov Central Boiler and T Russia.

\*Lenenergo, St. Petersburg, Russia.

*Electron microscopy and depth profile at turbine blade applications.*

A Hoque\*, J Cawley\*, D S Rickerby

\*Sheffield Hallam University, Sheffield

\*Rolls Royce Plc, Derby, UK.

*Metallography via deformation simulat*

E J Palmiere.

University of Sheffield, Sheffield UK

#### Lunch

### SESSION 7

#### Future Prospects

*Discussion on future developments and x-ray microanalysis and image analysis*

*Close of conference*

The focus of this fourth meeti microscopy and will concentra microstructure and properties measure microstructural para

Along with a call for papers, k by international experts on hig applications.

This important conference wi engineers and metallurgists fro is anticipated that through a fo the industry relating to the co properties of materials which be highlighted and discussed.

Sheffield, United Kingdom

*International Conference*

# QUANTITATIVE MICROSCOPY OF HIGH TEMPERATURE MATERIALS

**22-24 November 1999**

## Registration Form

### Organised by

Materials Research Institute  
Sheffield Hallam University

The Institute of Materials

Department of Engineering Materials  
University of Sheffield

The Royal Microscopical Society

### Conference organiser

Helen Kelly

Materials Research Institute  
Sheffield Hallam University  
Room 501 Norfolk Building  
City Campus

Howard Street

Sheffield S1 1WB

Tel 0114 225 2188

Fax 0114 225 3501

E-mail [mri@shu.ac.uk](mailto:mri@shu.ac.uk)

